PETROGENESIS AND POTENTIAL FOR MAGMATIC MINERALISATION OF THE MAFIC DYKES OF THE NORTHEASTERN PART OF THE IRUMIDE FOLD BELT OF NORTHEASTERN ZAMBIA

By

Sakwiba Musiwa, B.Min.Sc., M.Sc.

A thesis submitted to the University of Zambia in fulfilment of the requirements for the degree of Doctor of Philosophy in Geology

THE UNIVERSITY OF ZAMBIA
LUSAKA

2023

DECLARATION

I, **Sakwiba Musiwa**, do hereby declare that this has been written in accordance with the rules and regulations governing the award of the Degree of Doctor of Philosophy of the University of Zambia.

I further declare that this thesis is the result of my own work, where use has been made of the work of others, it has been duly acknowledged. This thesis has not been submitted for the award of any other degree, diploma or other qualification at the University of Zambia or in any other University.

Signed ……

This ……..day of…….2023

CERTIFICATE OF APPROVAL

This thesis of **Sakwiba Musiwa** has been approved as fulfilling the requirements for the award of the Doctor of Philosophy in Geology by the University of Zambia.

	Name	Signature	Date
Supervisor	……..		
External Examiner	……		
Internal Examiner (1)	……		
Internal Examiner (2)	…….		
Thesis Chairperson	……..		

ABSTRACT

The area of northeastern Zambia, between Chama and Lundazi towns, is underlain by rocks belonging to the Irumide Fold Belt, a Mesoproterozoic orogenic belt whose geology is dominated by biotite gneisses, which often show incipient migmatisation, that belong to the Kampemba Group. Less common unmigmatised rocks types are schists, quartzo-feldspathic gneisses, calc-silicates, quartzites and metamorphosed basic and aplitic sills. Porphyroblastic leucogneisses are represented as narrow strips and these have general NE-SW trending foliations, the general Irumide structural fabric, and dipping to the NW. A complex of a mafic dyke swarm that occupies a NE trending fracture zone, occurs mainly between Chama and Lundazi. Individual dykes vary in size from about 100s of metres long by a few 10s of metres wide, to about 4 km long and about 100 metres wide. By nature of their emplacement, the dykes could contain potential for economic magmatic mineralisation. This study, therefore, looked at the petrogenesis of the mafic dyke swarm, through the application of whole rock geochemistry, geochronology and isotope geochemistry. The study also made an assessment of the potential for Cu-Ni-PGE sulphide mineralisation of the dyke swarm by applying chemical data and empirical evaluation methods. Fifteen fresh samples were sent to Actlabs in Canada for whole rock geochemical analysis. Three of the fifteen samples were analysed for Rb-Sr and Sm-Nd isotope geochemistry; and the same three samples were used in the K-Ar age determination of the rocks. The results received on age determination gave the ages, 1522 ± 90 Ma, 1067 ± 55 Ma and 608 ± 35 Ma. Sm and Nd concentrations range from 1.99 – 3.112 ppm and 6.666 – 9.88 ppm respectively. $_{E}$Nd were calculated by the laboratory at -5.23, -8.23 and -9.73. $^{87}Sr/^{86}Sr$ returned values of 0.710886, 0.714503 and 0.719612. From the study of the thin sections and photomicrographs, it has been concluded that the dykes studied are gabbroic in composition and exhibit differences in composition, textures, alteration and microstructures. They are composed mainly of plagioclase, clinopyroxene, hornblende with subordinate olivine, quartz, sericite, epidote and opaque phase minerals. The dyke rocks occur mainly in coarse and medium grained varieties as only two of the twelve samples examined, are fine grained. Several diagrams which have been applied in the evaluation of crystallisation fractionation of both types of rocks have revealed that fractional crystallisation affected the magma of both types of rocks studied, tholeiitics and calc-alkalics. This is further supported by the wide ranges of Mg#, MgO, Ni and Cr in both rock types, which indicate significant crystallisation fractionation either in magma chambers or during ascent. The low Mg# (29.7-58.0), Ni (80-720 ppm) and Cr (150-1400 ppm) are suggestive of evolved magmas that underwent fractional crystallisation. Since no two samples came from the same dyke, it can also be concluded that all the mafic dykes in the Study area experienced various levels of fractional crystallisation. Both types of dykes show enrichment of the source magma by

addition. The enrichment must principally have come from the terrigenous felsic sediments rich in HFSE and LILE which were subducted at the mantle wedge. From the analysis of all the available information that would be critical to sulphide mineralisation and possible occurrence of deposits of Cu-Ni in the mafic dykes of the study area, it is concluded that the dykes exhibit no parameters that would have allowed such mineralisation to take place. Whilst the study has revealed, from age dating perfomed on three samples, that the mafic dykes of the northeastern part of the Irumide Fold Belt of northeastern Zambia were emplaced in at least three pulses, it is still recommended that high precision and more expensive age dating methods such as U-Pb Zr are carried out.

ACKNOWLEDGEMENTS

First and foremost, I would like to extend my heartfelt gratitude to my Supervisor, Dr Osbert N. Sikazwe (late) for guiding me so ably throughout this Ph. D research. His tireless efforts in guiding the writing of the thesis and bringing out sense from muddled up original drafts are greatly appreciated. Dr Sikazwe endured gruelling field work with me and this supervision in the field is sincerely acknowledged. Professor A. F. Kamona, the research co-Supervisor, is greatly appreciated for his immense guidance from the fine tuning of the research proposal up to the final product, this thesis.

I thank all the academic staff in the Geology Department of the School of Mines, University of Zambia, in particular, for all the support in different ways and for encouraging me to keep on with the task at hand. The technical staffs in the Department were so helpful when I needed their help of various forms and these are highly appreciated.

The academic staff of the School of Mines, University of Zambia, in general who kept on encouraging me to keep on with it, especially my fellow Ph D student, Dr S. Kangwa for his companionship in this academic journey of two old men, are highly appreciated. Dr Sam Kangwa always gave me the strength to soldier on.

The support from my wife Penelope has no measure. She is the one who encouraged me most to start this study program despite my very advanced age. All along, she has given me all the support and encouragement, especially when I showed tiredness and ready to give up. She gave me no pressure on my shifting dates of completing the thesis, always giving me enough space to do my work with negligible disturbances. I thank my family at large for all the support and encouragement they gave me.

Last but not least, I thank the University of Zambia Management for securing the scholarship. The financial support was provided by AfDB through the Ministry of Higher Education. Thank you to AfDB and the Ministry of Higher Education, Republic of Zambia.

TABLE OF CONTENTS

LIST OF FIGURES

LIST OF TABLES

List of Abbreviations

AfDB – Africa Development Bank

CAB – Calc-alkaline basalt

CFB – Continental flood basalt

CIPW – Cross, Iddings, Pirsson and Washington (rock classification method invented by these four people)

E-MORB – Enriched Mid-oceanic Ridge basalt

Ga – Billion years

GPS – Global positioning system

HFSE – High field strength element

HREE – Heavy rare earth element

K_d – Element distribution coefficient

km – kilometre

LILE – Large ionic lithophile element

LREE – Light rare earth element

Ma – Million years

ME – Multi-element

MORB – Mid-oceanic Ridge basalt

N-MORB – Normal Mid-oceanic Ridge Basalt

OIB – Oceanic island basalt

PGE – Platinum group of elements

ppm – parts per million

REE – Rare earth element

SIB – Southern Irumide Belt

TAS – Total alkaline silica

UTM – Universal Transverse Marcator

VAB – Volcanic arc basalt

WPB – Within plate basalt

WPT – Within plate tholeiites

wt% - Weight percent

1 INTRODUCTION

1.1 Background

This section discusses the importance of mining to the economy of Zambia and the need for new discoveries. The problem of the study is introduced and section further highlights: the significance of dyke swarms in petrogenetic studies; the application of isotopes in petrogenetic studies of igneous rocks; and the use of trace and rare earth elements in petrogenetic studies.

1.1.1 General

Zambia is endowed with substantial mineral resources in economic or potentially economic quantities and its mining history dates as far back as the beginning of the 20th century. Copper, by far, is the most important mineral commodity in terms of proved reserves and production. The country produced about 860,000 tonnes of copper in 2018 (Zambia Chamber of Mines, 2020). All the Country's copper and cobalt production come from the Lufilian Arc, a mineral rich Neoproterozoic tectonic province that straddles part of the border between Zambia and Democratic Republic of Congo (Figure 1.1).

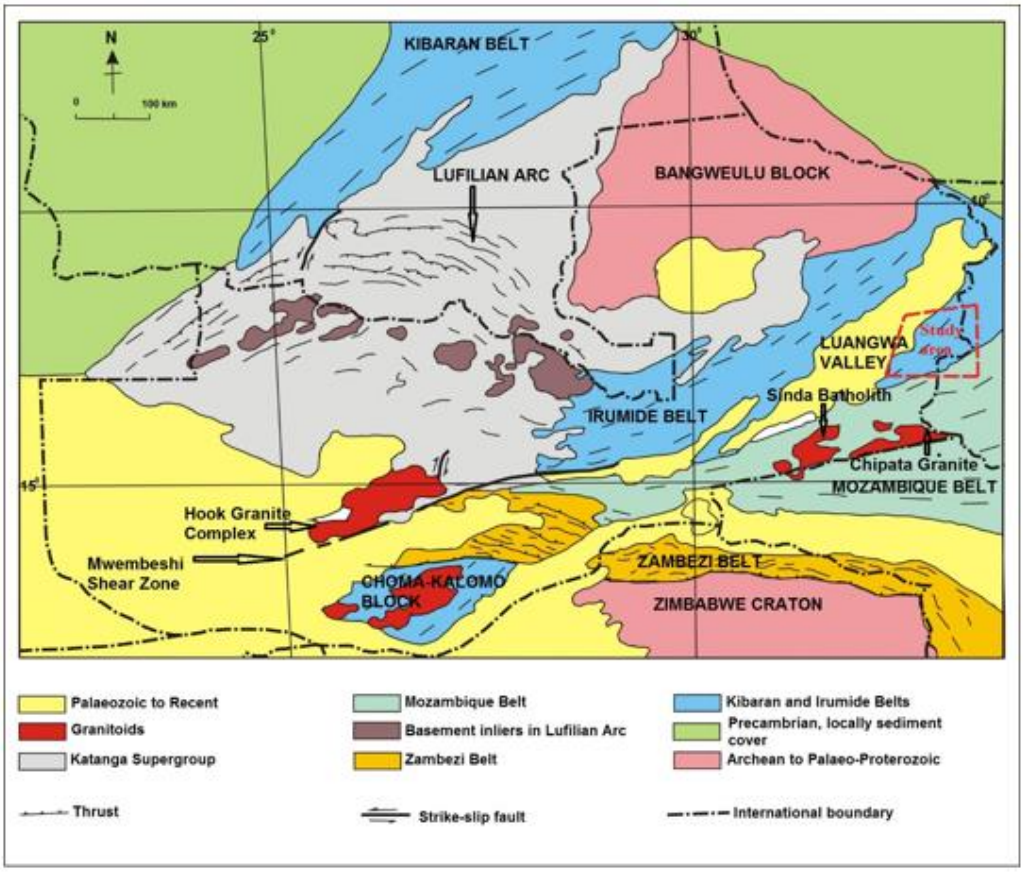

Figure 1.1: The geological and tectonic map of Zambia (modified after Porada, 1989)

Zambia is one of the few countries in the World whose economies depend almost exclusively on a single mineral commodity. Zambia's economy is highly dependent on the mining industry, which generates about 80% of the country's foreign exchange earnings (Sikamo et al., 2016). This dependence on copper is likely to last for most parts of the 21st century thereby prolonging the precarious economic position the country is in. Whilst the copper mining industry is striving to maintain an optimum level of output, the ore grades and reserves are heading for subsequent decrease. In view of this and the country's dependence on copper, there is more need now than ever before to broaden the base of the mining industry by finding more economic deposits of copper and other metal commodities. The discovery and development of any substantial deposits would contribute significantly to the socio-economic security of Zambia through job creation, enhanced foreign exchange revenue and to the growth and sustainability of a more vibrant mining industry. However, like the rest of the World, Zambia is faced with the harsh reality of discovery depletion, meaning the ease to find metal mineral deposits have significantly become difficult. The current search for ore minerals in the country as a whole, has to be for blind or concealed deposits, which show no surface expressions of their existence. The search for blind deposits is complex and requires research into predictive mineral deposit models for use in exploration.

1.1.2 Statement of the Problem

Exploration cannot be effectively executed and achieve desired results, especially in the case of concealed deposits, without basic knowledge of ore genesis. To understand why ore deposits form where they do, it is first necessary to understand the ways in which they form and the role of geological events and related physio-chemical dynamics which lead to specific mineral systems (Pirajno et al., 2009).

Zambia's complex geology has led to speculated significant mineral potential beyond what is already known and discovered, amidst the possible diverse mineral endowment of the country. The mineral endowment is mainly a function of the variety of geological terrains and the multiplicity of thermal and tectonic events which have overprinted and shaped the same terrains. The resulting are geological domains, each with specific metallogenic characteristics of possible mineral occurrences that can be successfully utilised to direct exploration. The more complex geology is hosted in rocks that belong to mobile belts, of which the Irumide Mobile Belt is one of them, and orogenic environments that range in age from Archean to Neo-Proterozoic.

The Neo-Proterozoic Lufilian Arc, which occupies the northwestern, and central parts of Zambia, has experienced sustained geological investigations from the time copper

mineralisation was discovered, in the early 20th century, in the present day Copperbelt Province (e.g. Unrug, 1988; Sweeney and Binda, 1989; Hitzman, 2000; Master et al., 2005;). In recent years, geological investigations have accelerated in the Northwestern Province, to the west of the Copperbelt Province, which is underlain by rocks that belong to the Katanga Supergroup of the Lufilian Arc. This intensity in exploration is mainly due to discoveries of huge copper deposits at Kalumbila and Lumwana in the last 10 to 20 years (e.g. Arc Minerals Ltd, 20202). The rest of the country has received comparatively little exploration activities due to lack of known mineral deposits. Consequently, the geology of these parts of the country, which are generally believed to be economically uninteresting in terms of mineral endowment, is very poorly understood. One such geological terrain that has received no particular interest in terms of mineral exploration, is the Irumide Mobile Belt, which is Mesoproterozoic in age. The Irumide Fold Belt occupies parts of central and northeastern Zambia. The Belt, which hosts mafic dyke swarms in its northeastern parts, has not received deserving mineral exploration attention despite its complex geology that, conceptually, may have good potential for economic mineral deposits. Consequently, the fold belt's geology is still just marginally known.

This study aims at investigating the petrogenesis of the dyke swarms of the northeastern part of the Irumide Fold Belt, and their potential for magmatic mineralisation. Being the first of its kind, findings of this pioneering study will create a firm foundation of the geology, on which models for future mineral exploration in the area will be based, and possibly stimulate interest for similar studies for other parts of the country outside the known mineralised Lufilian Arc of Zambia.

1.1.3 Significance of dyke swarms in petrogenetic studies

Dykes are believed to be the main conduits for magmas from great depths to shallower levels in the crust (Costa et al., 2007; Munteanu et al., 2017). Occasionally, dykes provide suitable environments for sulphide mineralisation of selected metals especially Cu, Ni and PGE, which accumulate when the dyke section increases, resulting in slowing of magma movement (Munteanu et al., 2017 and references therein). The individual dyke's generally limited volume and space are conducive for flow differentiation which may separate the solid phases from the transporting melt thereby forming cumulate rocks (Munteanu et al., 2017 and references therein). As the mantle melt ascends through the crust, differentiation, mainly by fractional crystallisation, takes place in staging chambers. With the possibility of crustal assimilation, in addition to fractional crystallisation, it is common that only the evolved fractions of the primary mantle melts reach shallow levels in the crust or erupt on the surface (Munteanu et al., 2017).

Study of dyke swarms may provide invaluable information on the geodynamics of a particular geological environment in which they occur (Halls, 1982; Fahrig, et al., 1986; Sial, et al., 1987; Sheraton and Sun, 1997; Maurice et al., 2009; Srivastava et al., 2014). Mafic dykes in North America and India have been used to highlight certain structural features that may provide further insight in the origin and geodynamic significance of dyke swarms, particularly those of Pre-Cambrian age (Halls, 1982). Structural aspects within one dyke swarm include regional variations in dyke attitude, preference in direction of dyke branching, radiating dyke patterns and orthogonality of dyke trends with the structural fabric of the enclosing host rock (Halls, 1982). Sub-horizontal magma flow is a common feature of dyke intrusion and thus, changes in petrology, geochemistry and flow-induced fabric along the length of the swarm may be expected (Halls, 1982; Sreenivasulu, et al., 2014, Munteanu et al., 2017). These features may be used to identify magma sources and processes of magma injection. Sheraton and Sun (1997) observed that emplacement of several suites of mafic dykes commonly define periods of crustal extension and form useful stratigraphic markers and that their composition provides information on compositional variations with time and mantle origin. Halama et al. (2004 and references therein), stated that mafic dyke swarms of Proterozoic age are widespread in many Precambrian cratons and their intrusion indicates considerable extension of the continental crust. Studies of rift-related mafic dyke swarms are essential for understanding the generation of such extensive mafic magmatism, and that these may be used to identify mantle plumes (Halama et al. 2004).

1.1.4 Application of isotopes in petrogenetic studies of igneous rocks

Isotope compositions of igneous rocks can provide a wealth of information about processes and timescale involved in their formation (Faure, 1986; Hoefs, 1978; Sun and Mc Donough, 1989; Phinney and Halls, 2001; Petersson et al., 2015). Some of the most important applications of isotopes to geological problems, include those that concern igneous petrogenesis where they have been fundamental in understanding both the timescale and processes operating in igneous systems. Use of radiogenic isotopes in dating crystallisation of igneous rocks is one of the most important applications (De Paolo, 1988; Arndt and Goldstein, 1987; Petersson et al., 2017). Radiogenic, stable and cosmogenic isotope systems also play critical roles as tracers of diverse geological processes. This is because the isotopes of such elements like Sm, Nd, Sr, and Rb generally undergo minor or undetectable fractionation during igneous processes. Whilst trace elements provide information on abundance ratios, which can be affected by recrystallisation and melting processes, radiogenic isotope ratios directly record the source and composition of the rock (Ciborowski, 2013). The isotope differences that exist among the crust, mantle and core are applied in tracing the sources involved in magmatic processes. The recent combined use of radiogenic

and stable isotope systems, such as Sm-Nd and Rb-Sr, among others, have been critical in the understanding of the processes that affect shallow magmatic systems and the importance of open system versus close-system fractionation (De Paolo, 1988).

1.1.5 Use of Trace and Rare Earth Elements in Petrogenetic studies

Trace elements, which include Rare Earth Elements, have been applied with a lot of success, in petrogenetic studies of igneous rocks (Gast 1968; Banno et al., 1973; Kay and Gast, 1973; Drake and Weill, 1976; Allegre, et al, 1977; Allegre and Minster 1978; Hanson, 1980; Srivastava et al., 2014; Petersson et al., 2017). Gast (1968) stated that trace element modelling of basic rocks has been widely and successfully applied to constrain the degree of partial melting of basalts from their source and to quantify the subsequent fractionation of the melt. Hanson (1980) documented that, the development of precise analytical techniques for the analysis of individual REE as well as the development of quantitative trace element modelling using single element distribution coefficients (K_d) in mineral-melt systems, have made the REE particularly valuable for placing limits on the applicability of proposed petrogenetic models.

Sreenivasulu et al. (2014) reported that different basaltic magmas are produced independently at different depths. According to Yoder and Tilley (1962), olivine-tholeiite, which is slightly poorer in silica than normal tholeiites, is produced by partial melting of garnet-peridotites of the mantle at greater depth. Sreenivasulu et al. (2014) were of the view that, if this magma fractionates at shallow depth, it evolves into an oversaturated tholeiite and if the same magma undergoes fractional crystallisation at great depth, it gives rise to alkali-olivine magma. Sreenivasulu et al. (2014) stated that in both hypotheses, the depth of magma generation and fractionation are important factors in controlling the composition of the magma.

Roberts (1990) concluded that the tholeiitic metadolerite rocks show chemical traits which indicate Transitional-MORB (T-MORB) basalts that have affinities, with fairly flat, chondrite-normalised REE patterns and a $(La/Nb)_N$ of just over 1. The low initial $^{87}Sr/^{86}Sr$ ratio, 0.7030, and lack of enrichment suggest that the magma was not contaminated to any extent during its upward passage from a secondarily slightly LIL element-enriched but primarily depleted mantle source (Roberts, 1990).

1.2 Study Area

This section brings out information which is laid out in the following order: general geological setting of the Study area; Study area selection (29^{o} to 32^{o} E and 11^{o} to 13^{o} S); Objectives; and thesis lay out.

1.2.1 General Geological Setting of the Study area

The geology of the Irumide Belt, between 11^{o} and 13^{o} south, and 29^{o} and 32^{o} east; where this study is located and hereinafter referred to as the Study area (Figure 1.2), is described, in parts, by Page (1973), O'Connor (1976) and Lewington (1987). Their works cover almost the whole area that extends over 8,000 km^{2}. The geology of the study area is dominated by biotite gneisses, which often show incipient migmatisation, that characterise the Kampemba Group (Page, 1973; Lewington, 1987). Less common and unmigmatised rock types are schists, quartzo-feldspathic gneisses, calc-silicates, quartzites, metamorphosed basic and aplitic sills and dykes (Lewington, 1987). Porphyroblastic leucogneisses are represented as narrow strips and these have general NE-SW trending foliations, the general trend of the Irumide structural fabric, and dipping to the NW (Page, 1973). Page (1973) indicated that the age relationships of the different gneisses are not clear but that they all seem to have been affected by the same deformation episodes as they exhibit similar structures.

Two sets of mafic and ultramafic dykes have been reported in the three Geological Survey of Zambia reports mentioned above. Page (1973) made a more concise record of the dykes that are found in the area he mapped. He reported that an earlier set of basic dykes was intruded into the Kampemba Group just before the end of tectonic activity and that the dykes were mildly metamorphosed to metagabbro, and deformed into large open folds. According to Page (1973), the metagabbro dykes occur as narrow ridges and that in their centres, the only sign of alteration is the mantling of the original clinopyroxene successively by a thick rim of uralite and a thin rim of hornblende. The margins of the dykes are more strongly metamorphosed and the pyroxene is completely replaced by hornblende and quartz (Page 1973). He described microcline as usually occurring as inclusions in the hornblende poikiloblasts.

Page (1973) stated that the second set of dykes post-date the Karroo faulting and are undeformed and unmetamorphosed. The post Karroo dykes also have a general NE-SW trend. The mineralogy of these post-Karoo dykes has not been well documented although they have been classified as gabbroic and doleritic.

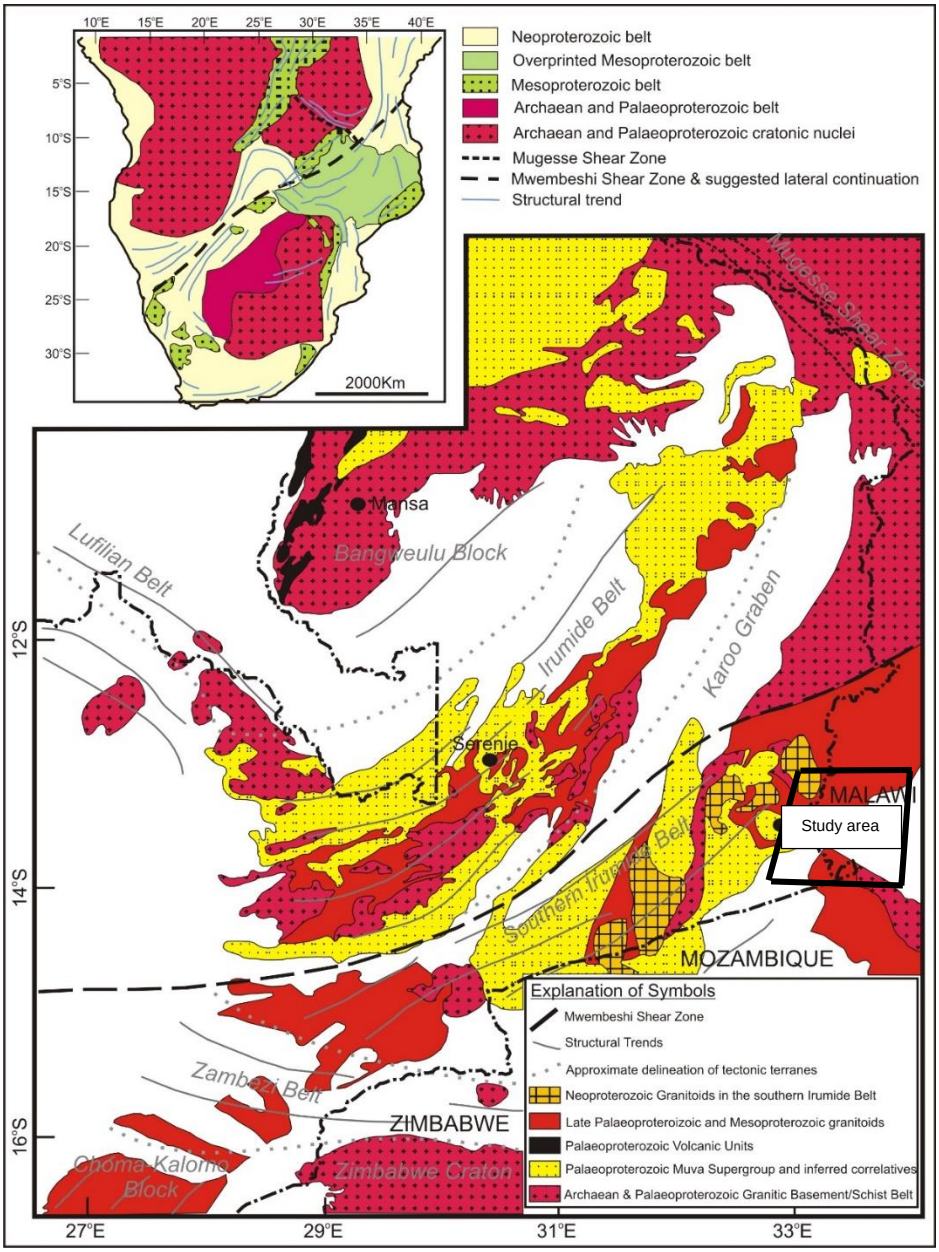

Figure 1.2: The geology and tectonic map of the eastern part of Zambia, showing the Study Area (modified from De Waele and Fitzsimons, 2007).

1.2.2 Study area selection (29º to 32º E and 11º to 13º S)

The mafic dykes, which have been described by Page (1973) and other geologists mentioned above, have not been studied in detail in terms of distribution, petrology, chemical composition, age and possible geodynamic evolution. However, in 2015, Zawar Natural Resources Limited, a company engaged in mineral exploration in Zambia, carried out a regional soil geochemical sampling programme over an area covering about 800 km^2 in the northern parts of the Irumide Belt, Northeastern Zambia. The area of the exploration is located in the northern parts of the Study Area (Figure 1.2 above). The exploration programme

involved a regional 500x500m grid soil sampling exercise that was followed by a tighter 100x100m follow up soil sampling survey over areas identified as anomalous for Ni-Cu. Subsequent preliminary geological mapping, by the author and another geologist, of some of the anomalous target areas, revealed a complex of a dyke swarm that extends beyond previously mapped and known areas. The rough extent and distribution of the areas occupied by mafic rocks of the dyke swarm in the 800 km^2 area covered by soil geochemical sampling was outlined through the anomalous distribution patterns of Ni-Cu-Cr-Fe (Figure 1.3) (Musiwa and Shanzambwa, 2015). The swarm extends further north and south of the mineral exploration licence area.

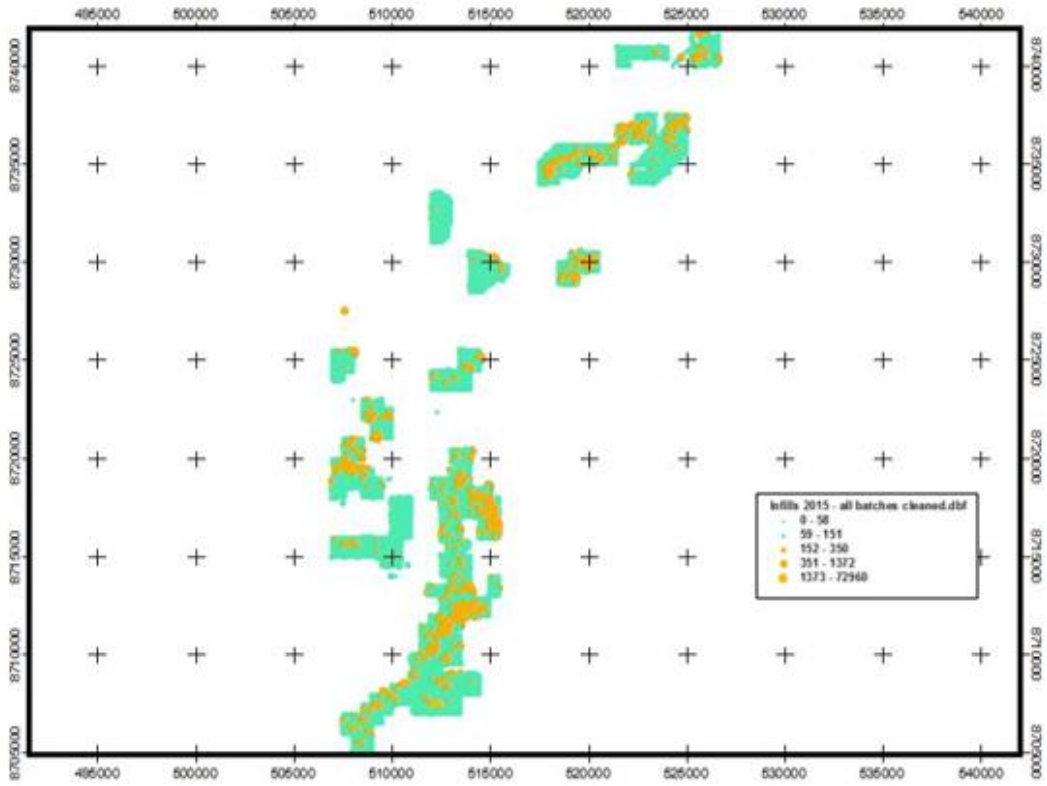

Figure 1.3: Spatial distribution of Nickel Anomalies in the Chama-Lundazi license Area – UTM Projection (after Zawar Natural Resource 2015 exploration report).

The previous works which have so far been carried out over this part of the Irumide Fold Belt, paid little attention to the mafic dykes, with clear absence of systematic studies on their petrogenesis, source characteristics, age and possible number of emplacement phases. This information is so far missing. This research work has been, in fact, primarily stimulated by the presence of the dyke swarm and the high potential for base metal and PGE mineralisation which has been indicated by anomalous values of Cu-Ni and PGE in soil samples. It seeks to carry out studies which will lead to the documentation of petrological, geochronology and geochemical information of the rocks of the mafic dykes of the study area. The generated and

documented information will contribute to the better understanding of the geodynamic evolution of the mafic rocks (petrogenesis) of the dyke swarm and aid in possible exploration for economic mineral deposits over the area. Furthermore, through the study, the geodynamics of the processes of the evolution of this part of the Irumide Mobile Belt in general, may be better understood (e.g. Halls, 1982; Sial et al., 1987; Sheraton and Sun, 1997; Maurice et al., 2009).

1.2.3 Objectives

The main objectives of the study were to:

a) establish the evolution and possible number of emplacement pulses of the mafic dyke swarm rocks of the Study area;

b) develop a genetic model of the mafic rocks of the dyke swarm of the Study area, and;

c) determine the potential for magmatic mineralisation of the mafic rocks of the dyke swarm for Cu-Ni-PGE.

1.2.4 Thesis Layout

This thesis is structured in 6 chapters as follows:

Chapter 1: Introduction – this gives the background information to the research, its importance, main objectives and main methods applied in execution. It also describes the study area (see 1.2).

Chapter 2: Overview of the geology and literature review – this brings out the summary of the regional geology of the northeastern part of the Irumide Fold Belt where the Study area is located.

Chapter 3: Methodology – this addresses in detail, the steps which were followed during the study from field data acquisition up to conclusion.

Chapter 4: Results – this chapter documents the results obtained from analytical work and interpretations. The results include; petrographic, geochemistry, isotope geochemistry, age dating, petrogenetic interpretations, and assessment of potential for magmatic mineralisation.

Chapter 5: Discussion – this chapter discusses the findings of the study against the background of known concepts and theories of the subject of study.

Chapter 6: Conclusions and recommendations – in this chapter, the conclusions of the study and recommendations for future works are presented.

2 LITERATURE REVIEW

2.1 Regional Geology

The Irumide Belt is a northeast-trending Mesoproterozoic orogenic fold and thrust belt that stretches for about 700 km from central Zambia in the southwest, into northern Malawi and Tanzania, in the northeast, figure 2.1, (Daly, 1986; Daly,1988; Poranda, 1989; De Waele and Mapani, 2002; Johnson et al., 2005; De Waele et al., 2006, De Waele and Fitzsimons, 2007). It is bounded by the Neoproterozoic orogenic Lufilian Arc to the west, and by the Paleoproterozoic Bangweulu stable cratonic block to the north. To the east, the Irumide Belt passes into the high-grade gneisses of the southern parts of the Neoproterozoic orogenic Mozambique Belt. Mapani et al. (2001) were of the view that eastern Zambia is underlain by a series of tectonic terrane stacks, including the Serenje, Luangwa and Nyimba terranes, which they regard as part of the Irumide Orogenic Fold Belt. Johnson et al. (2005) referred to the region as Southern Irumide Belt (SIB) (Figure 1.2 above). This current study was carried out over an area, to the north of SIB that lies to the north of the 13^{o}S latitude, which is characterised by mafic dykes. To this writer, this part of the Irumide Belt may not necessarily be part of the SIB genetically due to significant differences in the lithotype suites and structural fabric. He believes that this is part of the main Irumide Fold Belt, to the northwest, that is separated from it by the Luangwa Rift Valley. The geological province referred to, by Johnson et al. (2005) as SIB is part of the orogenic environment that is generally referred to as the Mozambique Fold Belt (see Figure 1.2 above).

The major rock types of the Irumide Fold Belt include: gneisses, granites, schists, migmatites, quartzites and amphibolites. Johnson et al., (2005), noted that the Irumide Belt displays overall northwesterly tectonic vergences, placing rocks affected by its orogenic deformation on top of undeformed Palaeoproterozoic rocks of the Bangweulu Block in northern Zambia. As regards metamorphism, Johnson et al. (2005), stated that, within the Irumide Belt, metamorphic grade changes rapidly across strike. They observed that this is characterised by an increase of metamorphic grade, from sub-greenschist to greenschist facies in the foreland to the northwest, to amphibolite facies and localised granulite facies in the internal zone of the belt to the southeast.

2.2 Mafic dyke distribution and field relationships

Detailed mapping of Musolomoka area, (Figure 2.1a) (Musiwa and Shanzambwa, 2016), which is within the Study area, revealed existence of mafic dykes with varying dimensions which have a general NE-SW trend, in agreement with the findings by the earlier workers. Mafic rocks in the area are restricted to the dykes. The orientation of the dykes is sub-parallel

to the structural fabric of the Irumide Fold Belt. They are generally exposed as large fractured pieces of rocks with sharp edges (Figure 2.1b), evidently with no sign of movement from the original positions of emplacement. They do not form any noticeable relief features although in some places the dykes tend to form very low ridges which rise to only about one metre above the surrounding areas. The dyke swarm occurs in clusters which vary both in length and width. Individual dykes range in size from a few hundreds of metres to about 4.5 kilometres in length, and a few tens of metres in width. Larger individual dykes have very little vegetation on them and exhibit unnoticeable weathering in the field. Reaction zones between the dykes and the intruded metamorphic rocks are not easily noticeable in the field maybe due to a lot of rubble and soil cover at the contacts. The dyke swarm extends far beyond the detailed mapped area, which was among the many such clusters that were identified more clearly by soil geochemical sampling (Musiwa and Shanzambwa, 2016). The actual extent of the area occupied by the dyke swarm in this part of the Irumide Fold Belt is not very clear and one may just have to rely on the reports of the Geological Survey of Zambia referred to in above.

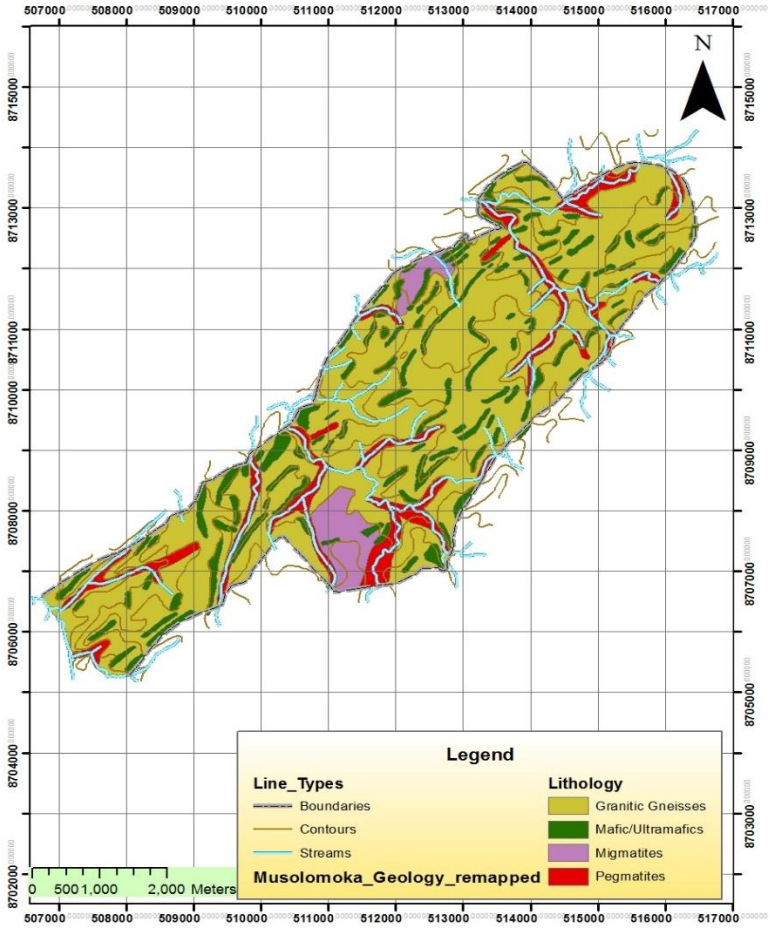

Figure 2.1a: Detailed geological map of Musolomoka Area, between Chama and Lundazi, which is within the study area and which was covered by tight 100x100m soil sampling (from Zawar Natural Resources 2015 exploration report)

Figure 2.1b: Typical exposure of a mafic dyke in the northeastern part of the Irumide Fold Belt, Northeastern Zambia.

2.3 Magmatic Mineralisation Potential Assessment

2.3.1 Factors critical for Ni-Cu-PGE magmatic mineralisation

Effective exploration for magmatic Ni-Cu-PGE, in particular, starts with understanding the critical factors that lead to host rock emplacement and mineralisation. Magmatic Ni-Cu-PGE sulphide deposits are formed by the segregation and accumulation of immiscible sulphide liquid from mafic or ultramafic magmas (Maier et al., 2008; Barnes et al., 2016). These deposits form when mantle derived suitable parent magmas become saturated in sulphide and segregate immiscible sulphide liquid commonly following interaction with crustal rocks (Arndt, et al., 2005). Arndt et al. (2005) stated that, it is important to know that although the metal contents of the primary magmas influence ore composition, they do not control ore genesis because the metals partition strongly in sulphide liquid and most magmas that are capable of segregating sulphide liquid contain sufficient abundances of ore metals. Arndt et al. (2005) observed that the most important factors that govern mineralisation include: a) temperature; b) viscosity; c) volatile content; and d) mode of emplacement of the magma. These control the dynamics of emplacement and the degree of interaction between the

magma and the crustal rocks. In this regard, high temperature, low viscosity komatiites and tholeiitic picrites are more cable of forming Ni-Cu-PGE deposits (Huppert and Sparks, 1985; Lesher and Keays, 2002; Arndt et al., 2003; Arndt et al., 2005). Naldrett (2004) observed that there are four critical phases in the formation of magmatic Fe-Ni-Cu ± platinum-group element (PGE) sulphide deposits. He listed them as follows: 1) a metal-bearing, mafic or ultramafic parental magma forms by partial melting of the mantle, separates from the solid residue, ascends through the asthenospheric and lithospheric mantle, and intrudes into the crust or erupts on the surface; 2) the magma interacts with its wall rocks, losing heat, forming a hybrid or contaminated magma, and commonly incorporating crustal sulphur, processes that result in the generation or segregation of an immiscible sulphide melt; 3) the sulphide melt interacts dynamically with a much larger mass of silicate magma, a process that increases the tenors of ore metals, especially for highly chalcophile elements and; 4) finally, the metal-rich sulphide liquid accumulates in sufficient quantity to form an economic deposit (Fgure 2.2). Low temperature, high volatile magmas are less likely to form these ores. Ore formation, on the other hand, is directly linked to the incorporation of sulphur-rich country rocks and indirectly through contamination by felsic crust. Campbell and Naldrett (1979) were of the view that, bulk compositions of magmatic ore deposits are determined by two major factors: the composition of the associated silicate magma, and the relative volumes of silicate and sulphide liquid that equilibrate with one another.

Lamberg (2005 and references therein), stated that the formation of Ni-Cu sulphide deposit requires 1) hot, primitive, high-magnesium magma, 2) a mechanism to achieve sulphur saturation and immiscibility of sulphide melt, 3) mechanism to enhance reaction between sulphides and sufficient amount of magma to concentrate chalcophile elements to an economic level, and 4) magma dynamics and physical traps to concentrate magmatic sulphides in a restricted locality where their abundance is sufficient to constitute an ore. Lamberg (2005) further stated that, the most magmatic Ni-Cu-(PGE) sulphide deposits are interpreted as having been formed from the magmas that were originally sulphide-undersaturated. He noted that crustal contamination has been proven to be the key process in the formation of the ores in almost all the studied Ni deposits. He was of the view that, contamination causes sulphide segregation either directly by incorporation of crustal sulphur and increasing the sulphur content of magma or indirectly by decreasing the sulphur solubility by changing the magma composition.

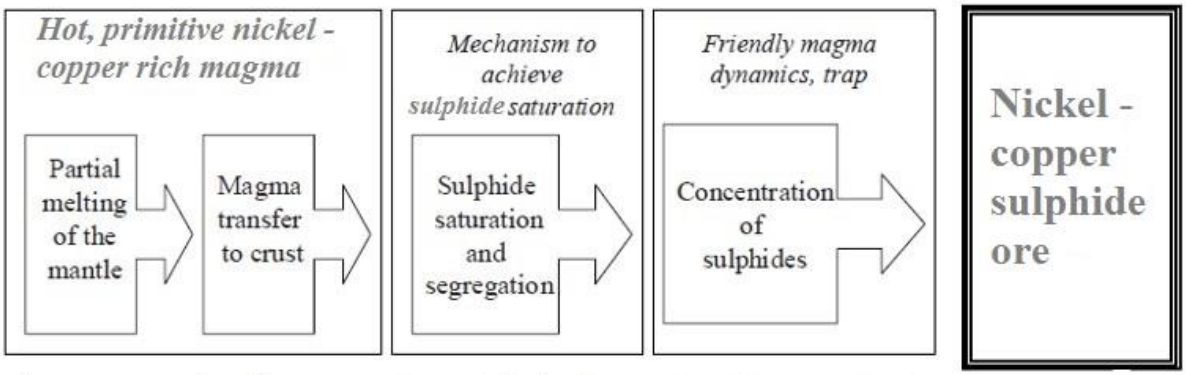

Figure 2.2: Stages and requirements of Cu-Ni sulphide ore formation, modified after Barnes et al. (2016).

2.3.2 Tectonic setting and geodynamic history

The importance of tectonic setting as a targeting criterion for Ni–Cu–PGE sulphide deposits has been recognised for many decades (Thakurta et al., 2008; Barnes et al., 2016). Thakurta et al. (2008) stated that magmatic Cu-Ni-PGE sulphide mineralisation associated with mafic to ultramafic igneous rocks is rare in convergent plate settings, but Barnes et al. (2016) pointed out that this picture is too restrictive, and does not account for the tectonic settings of many of the world's major camps and deposits. Barnes et al. (2016) observed that, whereas magma emplacement into rift basins containing abundant crustal sulphur, such as the Pechenga Belt of NW Russia and the Duluth Complex deposits of the Mid-Continent Rift of the USA, this association is unclear in many cases that include several major Ni–Cu–PGE camps. Barnes et al. (2016) further stated that the ore-forming magmatic episodes in the Cape Smith Belt formed 150 Ma after the initiation of a rifted passive margin, and that the tectonic setting at Voisey's Bay has been characterised as transtensional with no obvious evidence of a large scale syn-intrusive rift basin. Thakurta et al. (2008), and references therein, are of the view that the Noril'sk-Talnakh type, however, appears to be associated with the changeover from localised graben-controlled rift related basaltic volcanism immediately preceding ore formation to a main ore-associated phase of regional flood basalt volcanism with a different depocentre.

2.3.3 Source and composition of ore forming magmas

Barnes et al. (2016) drew the attention of the readers to the debate on the source of the predominantly aqueous fluids that carry and deposit metals in hydrothermal systems. They stated that these fluids are characteristically younger than the host rocks to the ore, and substantially out of equilibrium with them, giving rise to alteration haloes that extend well beyond the boundaries of the orebody itself. In magmatic systems, the ores and immediate host rocks are derived from the same fluid source, the transporting silicate magma (Baumgartner et al., 2015; Barnes et al., 2016). The metals in magmatic ores are sourced

from the transporting fluids themselves, the magma and hence originate from the mantle source (Lamberg, 2005; Barnes et al., 2016). Barnes et al. (2016) are of the view that most of the cases stated above, magma sources are generally held to be sub-lithospheric and derived from deep seated mantle plumes. They further pointed out that available evidence is that, mineral provinces are commonly associated with magmas that are higher in MgO, and hence hotter, than typical ambient mantle melting products such as MORBs. Consequently, where multiple magma suites are found within the same province, Ni–Cu–PGE ores are characteristically associated with the suite formed by the highest degree of partial melting, which are higher in MgO and low Ti (Zhou et al., 2008; Godel et al., 2011, Barnes et al., 2016).

According to Barnes et al. (2016) the composition of the ore-forming magma can, in some cases, be determined directly from the chilled margins of the magma bodies that host the ore deposits. They gave the examples of komatiite flow hosted deposits, where samples of magma bearing the imprint of ore forming processes can be found in spinifex-textured margins of the host flows, e.g., at Kambalda. Barnes et al. (2016) noted that in most cases, including komatiites, host rocks are predominantly cumulates: rocks formed by accumulation of liquidus crystallisation products. In this regard, the composition of cumulates differs significantly from the composition of the parent magma itself, having higher MgO and lower contents of incompatible elements. Arndt et al. (2005), and Barnes et al. (2016) noted that the compositions of ore-forming magmas may range from highly magnesian komatiites with MgO contents as high as 30% through to komatiite-derived basalts (MgO 12–18%) to relatively fractionated tholeiites with MgO contents well below 10%.

2.3.4 Sources of sulphur and transport of sulphide liquid

According to Ripley and Li (2013); Keays and Lightfoot (2010); Barnes et al. (2016), in almost all magmatic Cu-Ni-PGE sulphide deposits, with an exception of just a few, sulphur isotopic evidence strongly suggests the role of assimilated crustal sulphur in their formation. Lesher and Groves (1986) presented evidence that showed that a sulphur-rich crustal source is required to form major Ni-Cu sulphide deposits associated with komatiites and komatiitic basalts such as those in Western Australia (e.g., Kambalda) and Canada (e.g., the Thompson Ni belt, the Cape Smith Fold belt, and the Abitibi Greenstone belt) (Keays and Lightfoot, 2010). Bekker et al. (2009) observed that this is more evident in the case of deposits associated with high temperature magmas such as komatiites whose sulphur content at source in the deep mantle is well below the sulphur content at sulphide liquid saturation (SCSS).

Barnes et al. (2016) are of the view that the mechanisms by which sulphide liquid is transported from a site of assimilation remain poorly understood. They state that the current models for a number of important deposits attribute the initial segregation of sulphide liquid to

deep seated processes, occurring in the lower crust well below the eventual level of formation of the actual deposits, followed by entrainment, upward transport and mechanical deposition. They give some of the model type examples, with their references, as: Voisey's Bay (Lightfoot et al., 2012; Saumur et al., 2013); Jinchuan (Tang, 1991; Song et al., 2012); Eagle (Ding et al., 2012b); and Norils'k-Talnakh (Arndt et al., 2003; Li et al., 2009) (Figure 2.3). In some deposits, the sulphur isotopic composition of the ores coupled with a lack of matching crustal sulphur in adjacent country rocks, require that the sulphide liquid component be introduced from a distal source on a scale of kilometres. This then means that ore formation requires some process of initial segregation of the ore component, followed by remobilisation and mechanical transport to the site of ore deposition (Barnes et al., 2016). Barnes et al. (2016) suggested that if there is a single unifying factor among all Ni–Cu–PGE sulphide deposits, it is that they are hosted within environments of protracted flow through of magma. They further indicated that high magma fluxes and prolonged flow within magma conduits are advantageous for several reasons which include: a) they provide ideal environments for extensive assimilation of wall rock and crustal sulphur; and b) they allow for significant conduit geometry modification by thermal-mechanical erosion; c) they potentially concentrate large volumes of originally dispersed sulphide droplets into a small space of potential ore grade and tonnage and; d) they facilitate the reaction of transported sulphide with large volumes of magma giving rise to high magma to sulphide melt ratios and hence high ore tenors.

Keays and Lightfoot (2010), stated that commonly used tools to determine whether or not a magma has been sulphur saturated are Ni/MgO and Cu/Zr ratios and that this is because Ni and Cu are lost from the magma to segregating magmatic sulphides. They are of the view that whether or not a magma becomes sulphur saturated during partial melting of the mantle depends on a number of factors, including the sulphur content of the mantle reservoir from which the partial melt was extracted, the degree of partial melting, the temperature and pressure at which partial melting occurred, the sulphur capacity of the partial melt being extracted, and the FeO content of that melt. Keays and Lightfoot (2010) advanced the following evidence which was presented by Lesher and Groves (1986) on the involvement of crustal sulphur source in Cu-Ni-PGE sulphide mineralisation as follows: 1) there is a strong spatial association between the mineralised ultramafic rocks and sulphur rich sediments in all cases; 2) due to their high temperatures (>1,600°C) and the fact that they were formed by high degrees of partial melting, the parental magmas to these rocks would have been strongly sulphur undersaturated; an external sulphur-rich source was necessary to bring them to sulphur saturation; 3) due to the pressure drop during ascent from the mantle, magmas which are sulphur saturated at depth become sulphur undersaturated; an external sulphur rich source is required to bring the magma to sulphur saturation; 4) although the sulphur isotopic

composition of the ores varies from ore deposit to ore deposit, the $\delta^{34}S$ of each ore deposit matches that of the local sulphur-rich sedimentary country rocks; and 5) whereas there is a narrow range in the isotopic composition of the parental magmas to the ultramafic host rocks, different ore shoots in the same ore system often display different metal tenors; this is best explained by assimilation of different quantities of sulphur in the local sulphur-rich country rocks.

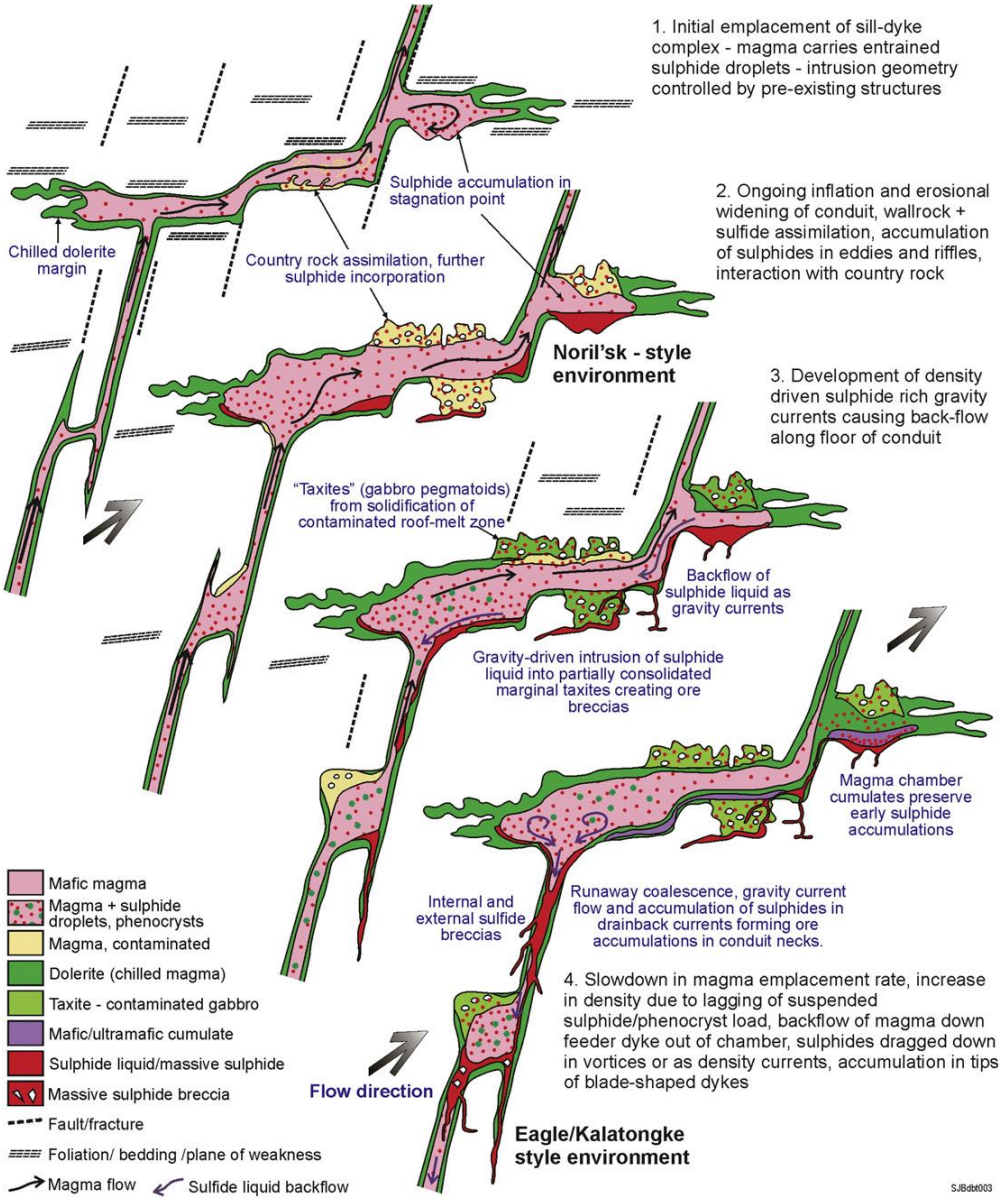

Figure 2.3: Schematic illustration of components of the crustal portion of an idealised magmatic plumbing system, showing a hypothetical sequence of events leading to the development of Norils'k style, Eagle–Kalatongke style and Voisey's Bay style settings for mineralisation (adapted from Barnes et al., 2016).

2.3.5 Geometries of mineralised intrusions

Ore-hosting magmatic bodies come in a wide variety of shapes and sizes (Barnes et al., 2016). Barnes et al. (2016) summarised the examples of these, which vary from feeder channels to vast komatiite flow fields such as: Kambalda deposit, Perseverance and Mt Keith (Lesher et al., 1984; Barnes et al., 2011a); channelised subvolcanic sills such as Noril'sk and Nkomati/Uitkomst (Fedorenko et al., 1996; Gauert et al., 1996; Naldrett and Lightfoot, 1999; Maier et al., 2004) (Figure 2.5).

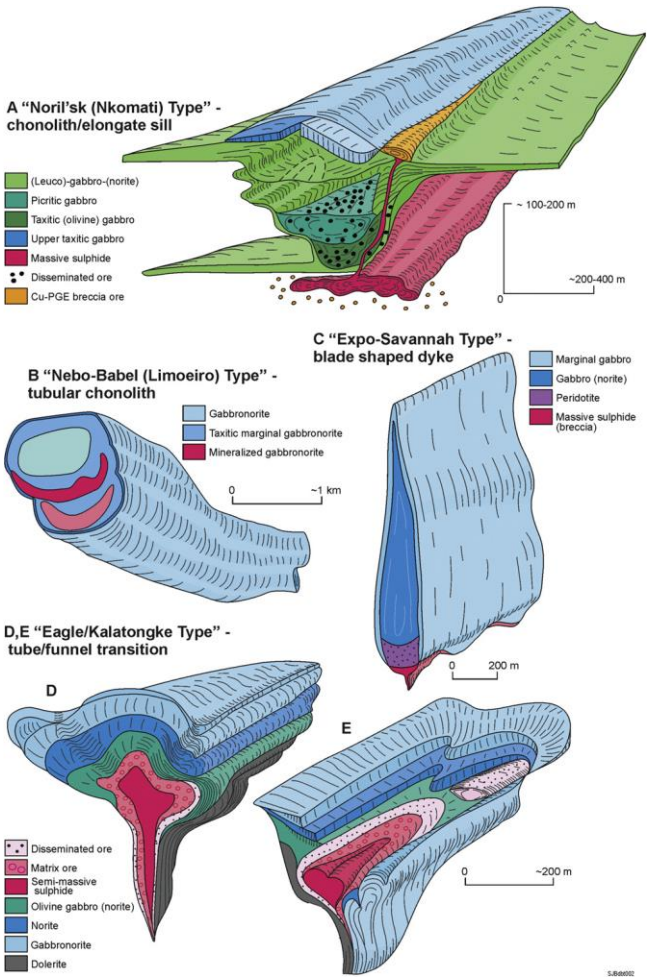

Figure 2.4: Schematic illustration of the spectrum of characteristic geometries of composite mafic and mafic–ultramafic intrusions known to host magmatic Ni–Cu–PGE sulphide mineralisation. A. Noril'sk type from Naldrett (2004). B. Chonolith type based on Nebo–Babel (accepting the interpretation that this deposit and host intrusion is structurally overturned) and Limoeira (Seat et al., 2007; Mota-e-Silva et al., 2013). C. Blade-shaped dyke type based on Savannah (formerly Sally Malay, Western Australia, unpublished) and Mesamax and other intrusions of the South Raglan tend, northern Quebec (Mungall, 2007a, 2007b, 2007c). D, E. Eagle–Kalatongke type based on interpreted geometries of these two intrusions, and other

elongate dyke–keel complexes in China including Huangshangdong, Limahe and Jingbulake, from various authors (Zhou et al., 2002; Song et al., 2011; Ding et al., 2012a; Lightfoot and Evans- Lamswood, 2015) (adapted from Barnes et al., 2016).

2.3.6 Significance of the size of the intrusive body to mineralisation

Small bodies of mafic-ultramafic rock can contain exceptionally large economic Ni sulphide deposits; examples include the Jinchuan Intrusion which has a projected surface outcrop area of less than 1.4 km^2, yet contains a historic and present reserve and resource of over 500 Mt of mineralised ultramafic rock (Chai and Naldrett, 1992; Lightfoot, 2007). At Sudbury, the 20-60 m wide by 14 km long Copper Cliff Offset Dyke is composed of weakly magnetic quartz diorite. This dyke contains a historic and current resource and reserve in excess of 240 Mt of mineralization (Lightfoot, 2007).

At Noril'sk, the Kharaelakh Intrusion is only 100-250 m wide, yet the enormous Oktyabrysk, Taimyrsk, and Komsomolsk deposits are all contained in an intrusion that has a volume of little more than 2-3 km^2 (Lightfoot and Zotov, 2007). A number of the very small producing or past-producing mines in China are associated with intrusions that are volumetrically trivial and have surface areas of less than 0.5 km^2 (Tang, 1991). Many of these intrusions have very high ratios of sulphide/silicate rock, but few are as extreme as the Ovoid Deposit at Voisey's Bay where, with the exception of a narrow dyke and a series of breccias at the contact, the entire body consists of massive pyrrhotite, chalcopyrite, pentlandite, and magnetite (Lightfoot, 2007).

3 METHODOLOGY

3.1 Field data collection

The samples were collected against the backdrop of extracting information which is representative of all the mafic rocks of the dyke swarm. Consequently, attention was paid to: a) the spread of the sampling points over the study area; and b) collecting fresh samples which were massive (homogeneous) and devoid of any veins, alterations or any visible contaminations. Samples were collected as close to the centre of each individual dyke that was sampled, as possible to eliminated possible magma contamination. Accessibility played a significant role in the final determination of the spread of the samples which were finally collected, as some of parts of the Study area are very difficult to access.

Initially, 62 samples were collected over a distance of about 75 kilometres along the NE-SW general strike of the dyke swarm and about 4 kilometres across the strike. There was no particular pattern or sample spacing interval that was followed. Two samples, each weighing about 1.5 kg on average, were collected from each sampling site whose coordinates were recorded in UTMs using a Garmins hand held GPS set. Fifteen (15) samples, CH-WHR-01 to 12 and CH-ISO-01 to 03, were selected from the sixty two, for geochemical analysis and out which, twelve (12) (CH-WHR-01 to 12) were also subjected to petrographic studies (Figure 3.1). All the geochemical analyses, which included:

a) whole rock geochemistry;

b) isotope geochemistry; and

c) geochronology,

were carried out at Activation Laboratories, Lancaster, Canada. Only three of the fifteen samples, CH-ISO-01 to CH-ISO-03 (Figure 3.1), were used for age dating and isotope geochemistry. Budgetary constraints limited the number of samples which were subjected to geochemical analyses.

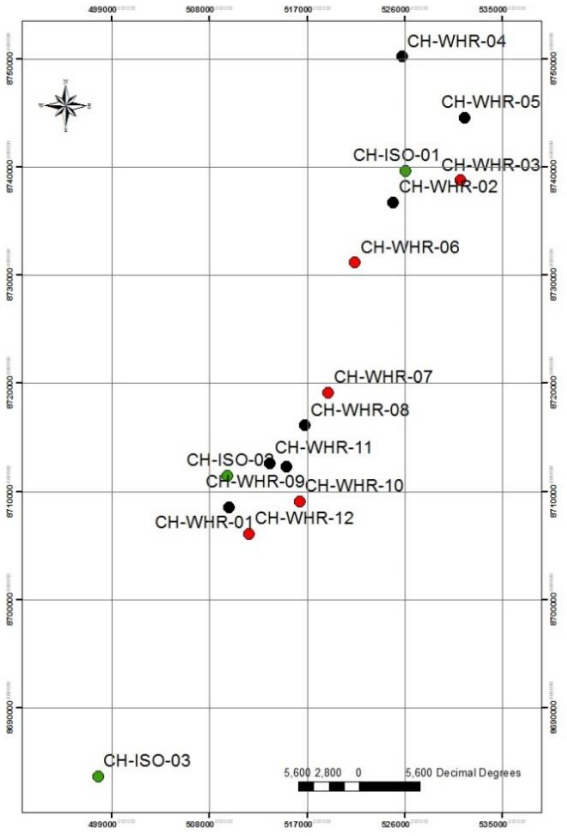

Figure 3.1: Sample locations for 15 samples which were sent for geochemical analysis; green = samples analysed for age dating and isotope geochemistry, red = samples which turned out to be of tholeiitic rocks, and black = samples which turned out to be of calc-alkalic rocks (UTM Projection, Zone 36L)

3.2 Petrography

Twelve samples which were selected for both petrographic and whole rock geochemistry studies had thin sections made from portions of them in the School of Mines, University of Zambia, laboratories. Detailed petrographic descriptions of the thin sections were made. Stable mineral parageneses were noted, as were textural features of minerals indicating overprinting events (e.g., coronas, overgrowths, and pseudomorphs). Secondary mineral assemblages and replacement relations to primary phases were described. The nature of minor and trace phases as well as the extent of alteration were also described. The modal estimates, which allowed characterisation of the intensity of metamorphism, were made as well as extraction of microtextural information. The dykes were petrologically classified on the basis of the information gathered form the above stated examinations.

3.3 Geochemistry

Geochemistry covers all activities and products of wet chemical analysis which include:

a) whole rock geochemistry;
b) Isotope geochemistry and dating;
c) Petrogenetic evaluations; and
d) Magmatic mineralization potential assessment.

3.3.1 Whole rock geochemistry

Rock samples used in this study were analysed at Activation Laboratories Limited, Ancarster, Ontario, Canada. Major elements and some trace elements, Sc, Be, V, Ba, Sr, Y and Zr, were analysed by FUS-ICP. The rest of the trace elements and REE that include: Cr, Co, Ni, Cu, Zn, Ga, Ge, As, Rb, Nb, Mo, Ag, In, Sn, Sb, Cs, La, Ce, Pr, Nd, Sm, Eu, Gd, Tb, Dy, Ho, Er, Tm, Yb, Lu, Hf, Ta, W, Tl, Pb, Bi, Th and U were analysed by FUS-MS.

The calculation of $FeO_{(T)}$, $FeO_{(EST)}$ and Mg# are adapted from Gill, 2011 as follows:

1) $FeO_{(T)} = Fe_2O_{3(T)} \times 0.8998$
2) $FeO_{(EST)} = 0.9 \times FeO_{(T)}$
3) $Mg\# = 100 \times [MgO/(MgO+FeO_{(T)})]$

The X and Y variables for element linear relationships were calculated using the free online Pearson correlation coefficient factor computation. The coefficient factor (R) indicates how the level of variation in variable Y is due to the variable X in percentage terms (e.g. Ciborowski, 2013). The value of R, defines the strength of correlation whereby the values approaching 1, indicate good correlation whilst those approaching 0, indicate poor correlation. In this study, this approach has been adopted for the following indices as X variables where they have been applied: SiO_2, MgO and Zr. Linear relationships can be positive, increase of both variables relative to each other, or negative, with one variable degreasing relative to the increase of the other. In the case of it being negative, the correlation coefficient (R), appears with a negative sign. The general principle that is adopted in this study is that, elements with coefficient factor values of $R \geq 0.75$ reflect good correlation, elements with coefficient factor values of $0.75 > R \geq 0.5$, are considered as moderately correlated and elements with coefficient factor values of $R < 0.5$, are considered as poorly correlated (e.g. Ciborowski, 2013).

Major and trace element geochemistry are discussed both qualitatively and quantitatively. Effects of post magmatic or sub-solidus alteration and element mobility are assessed by plotting selected elements against Zr, an incompatible and immobile element. Elements which

show good linear correlation with Zr are deduced to have been immobile since solidification of the magma and are considered as strong candidates for petrogenetic interpretations. Elements which show unexplainable scatter are considered to have been remobilised and therefore unsuitable in petrogenetic interpretations. Both major and trace elements are plotted against different fractionation indices for interpretations of crystallisation history of the mafic rocks of the dyke swarm. Plots of both major and trace element discrimination diagrams, element ratios, as well as chondrite normalised diagrams are used in the interpretation of tectonic settings and source composition (e.g. Song et al., 2008; Shellnutt and Jahn, 2011; Ciborowski, 2013; Sheth et al., 2013). The normalised chondrite plots are also used for the establishment of the enrichment and/or depletion of each individual rare earth and trace element as applicable. CIPW norm is applied to reveal normative mineral concentrations of the sampled dykes and normative quartz saturation or under-saturation.

The assessment of possible alteration was done by plotting the highly mobile elements under secondary alteration, Sr, Ba, K and Rb against Zr. They were chosen for their high mobility under liquid environments as opposed to the HFSE which are generally immobile under similar conditions.

3.3.2 Isotope geochemistry and dating

In petrogenetic studies, radiogenic isotopes are applied mainly to provide an absolute age of a sample, and to trace the origin of the rock (e.g. Kay and Gast, 1973; Hanson, 1980; De Paolo, 1981, 1988; Kerr, 2015) (also see section 1.1.2 above). In the present study, three samples were selected for isotopic studies for age dating and for aiding in the tracing of the origin of the magmatic components.

Rb-Sr and Sm-Nd isotope composition analyses were aimed at tracing the origin of the magma whilst K-Ar was applied in age dating. The selection of the samples from the sixty two collected from the Study area was based on the spread along the NE-SW strike, that would give as much representation of the dyke swarm as possible (Figure 3.1 above) and also on the homogeneity and freshness of the samples. The aim of the isotopic study was to generate useful data that would help in interpretation and better understanding of the mantle sources and material responsible for the magmatism of mafic dyke swarm, in the northeastern part of the Irumide Fold Belt, northeastern Zambia. The other reason for the isotopic studies was to determine the age(s) of the mafic rocks of the dyke swarm.

Rb-Sr methodology

The Rb and Sr concentrations as well as the $^{87}Sr/^{86}Sr$ and $^{87}Rb/^{86}Sr$ isotopic ratios were determined in the studied rocks using an isotope dilution technique with a mixed ^{85}Rb-^{84}Sr

spike, which were added to the samples immediately before their chemical decomposition. Sample was dissolved in the $HF+HNO_3$ mixture under atmospheric pressure and a temperature of 80°C. Rb and Sr were separated using common chromatographic technique. Extraction of the elements was carried out in 2.4 M HCl using the ion-exchange column filled with 3 mL of BioRad W50x8 (200–400 mesh) resin. Isotope ratios were measured on a Micromass Sector 54 multicollector TIMS (Thermo Scientific). The precision of results was controlled by the systematic analysis of SRM-987 International standard (average measured value was $^{87}Sr/^{86}Sr=0.710249\pm9$ (2SD, n=5) during the period of the analysis). The $^{87}Sr/^{86}Sr$ and $^{87}Rb/^{86}Sr$ isotope ratios in the studied samples were measured with accuracy better than 0.002 and 0.5 rel. %, respectively (Activation Laboratories, 2020).

Sm-Nd methodology

Nd isotope ratios were measured on a multi-collector Triton Plus TIMS (Thermo Fisher Scientific). $^{147}Sm/^{144}Nd$ ratios were determined additionally by isotope-dilution method using ^{149}Sm-^{150}Nd mixed spike. About 100 mg of rock powder was dissolved in HF-HNO_3 mixture in microwave oven with addition of ^{149}Sm-^{150}Nd spike prior to dissolution for precise determination of $^{147}Sm/^{144}Nd$ in the samples. For Nd isotopic analysis, the REE were initially separated from major elements and Ba by cation exchange using Re resin (Eichrom Industries, Illinois, USA), before isolation of Nd and Sm according to Misawa et al.(2000). Ln resin (Eichrom Industries, Illinois, USA) was used for Nd and Sm isolation following procedures of Mikova and Denkova (2007). Nd isotope ratios were measured in multidynamic collection mode. Isotope ratios were normalized to $^{146}Nd/^{144}Nd=0.7219$ (O'Nions et al., 1977). Measured values in the International standard sample JNdi-1 (Tanaka et al., 2000) ($^{143}Nd/^{144}Nd=0.512115$) were $^{143}Nd/^{144}Nd=0.512094\pm10$ (2SD, n=4) during the measurement period.

K-Ar methodology

Aliquots of the samples were weighed into Al containers, loaded into sample system of extraction unit, degassed at ~100°C during 2 days to remove the surface gases. Argon is extracted from the sample in double vacuum furnace at 1700°C. The determination of radiogenic argon content was carried out twice on MI-1201 IG mass-spectrometer by isotope dilution method with ^{38}Ar as spike, which is introduced to the sample system prior to each extraction. The extracted gases were cleaned up in two step purification system. Then pure Ar is introduced into custom built magnetic sector mass spectrometer (Reinolds type). It sHalls be noted that the test was done twice per sample to ensure the consistency of the result. Two globally accepted standards (P-207 Muscovite and 1/65 "Asia" rhyolite matrix) were measured for ^{38}Ar spike calibration. For age calculations the international values of constants were used

as follow: λK=0.581*10-10y-1, λβ-=4.962*10-10y-1, 40K=0.01167 (at.%) (Activation Laboratories, 2020).

3.3.3 Petrogenetic evaluations

The rare earth element ratios and their trends are applied in this study in the evaluation of melting conditions and nature of mantle compositions. Models of Gribble et al., (1998) and Sayıt et al., (2016) of TiO_2 vs Yb and Sm vs Sm/Yb diagrams respectively, as adapted by Cimen (2016), are applied in the evaluation of the melting systematics. The method applied by Cimen (2016), of only using samples with MgO concentrations higher than 8 wt% to avoid effects of fractional crystallisation, is adopted. In this regard, the models could not be applied on the tholeiitic rocks as all the samples of this type of the dykes studied, apart from one, show MgO concentration values which are less than 8 wt%. Consequently, the data used in Figure 4.66 (Chapter 4), is for the calc-alkalic rock samples, which all but one, have MgO values greater than 8 wt%. Cimen (2016) outlined the calculations he applied, which this study has adopted, and their sources in the extract below. In addition the samples are also evaluated using PRIMELT3 MEGA.XLSM software for primary magma calculation (Herzberg and Asimow, 2015).

3.3.4 Magmatic mineralization potential assessment

In this study, the mafic dykes of the Study area are assessed, both geochemically and empirically, for their magmatic mineralisation potential in Cu-Ni-PGE. The method of assessment involves:

i) a literature review on the Ni-Cu-PGE magmatic mineralisation particularly as it relates to mafic dykes; and

ii) a comparative analysis between the mineralisation information obtained from the literature and the geological-geochemical parameters of the studied dykes.

Reasons for carrying out this type of assessment, as reflected in the literature, are presented. From the literature review, key information on mafic magma mineralisation is extracted and this includes:

i) Physio-chemical factors critical for Ni-Cu-PGE magmatic mineralisation;
ii) Tectonic setting and geodynamic history;
iii) Source and composition of ore forming magmas;
iv) Sources of sulphur and transport of sulphide liquid;
v) Geometries of mineralised intrusions; and
vi) Significance of the size of the intrusive body to mineralisation.

In addition, chemical plots are generated from the geochemical data of the Study area dykes samples and these are also used in the assessment of the mineralisation potential.

4 RESULTS

4.1 Petrography

This section documents the petrographic observations arrived at after examining the thin sections of the twelve dyke samples whose other portions were sent for geochemical analysis. Based on the information deduced from the examination, rock names and interpretations of the processes which may have affected the rocks during and after emplacement are attempted. The dykes occur and are described in three different grain sizes; fine, medium and coarse. The petrographic descriptions mainly address mineralogy, alteration and texture.

4.1.1 Fine-grained variety dykes

Petrographically, the fine grained variety is equigranular and granoblastic with intergranular textures (Figure 4.1). This type is mineralogically dominated by plagioclase, orthopyroxene, clinopyroxene and hornblende with minor quantities of olivine and biotite. Plagioclase is the most dominant (45-50%). More than 50% of the mineral grains are very small, which may be as a result of grain boundary recrystallisation. Medium size grains may probably represent first phase of recrystallisation. The observed twins may be due to growth, whilst those displaying tapered boundaries indicate that they are most likely deformation related. Relict grains have many tiny dot-like inclusions. The plagioclase shows very limited to no alteration with most crystals exhibiting good quality twinning.

Clinopyroxene forms about 30% of the examined fine grained dyke samples, with large relict grains being less than 0.5mm. Recrystallised and equant grains are markedly larger but these are much fewer. Slightly bent cleavage is observed in some of the larger grains. Some of the larger grains appear to have been fractured into smaller grains. Most smaller grains are quite equant with granoblastic texture. Minor bleb inclusions of brown amphibole occur where clinopyroxene retains igneous boundaries. Most grains are curvilinear and have very narrow rims of brown hornblende.

Hornblende forms about 10-15% of the examined fine grained variety. It occurs in different colours, but primarily reddish-brown, brown and green. It characteristically rims around pyroxene and pseudomorphs usually with very irregular boundaries. It also occurs as massive in plagioclase matrix where it displays fairly regular boundaries. It may contain small Inclusions of apatite and often associated with minor amounts of epidote and irregular grains of opaques. Occasionally, it is found as small grains interstitial to plagioclase and clinopyroxene. In places, hornblende displays some mottled appearance due to being replaced by some opaque minerals.

Olivine forms less than 2% of the fine grained examined samples and much is already altered to tremolite and talc plus opaque. Originally, it might have been slightly higher in quantity. Grains are anhedral with very curvilinear outlines. Larger patches of olivine are aggregates, but individual grains show strain features. Blue-green hornblende and colourless amphibole are coarsely mixed in rims around some olivine grains. Alteration products do not appear to be in a particular order, though blue-green tends to be outside the colourless amphibole.

In these fine grained dykes, the opaque minerals represent about 5% of the rocks. They occur as small grains or blebs along plagioclase-clinopyroxene boundaries and may approach euhedral outlines if enclosed in hornblende. They are interstitial in plagioclase domain and display exsolved rectangular grains in clinopyroxene. Late cracks in plagioclase and a few pyroxene are filled with sericite, chlorite and lesser in amphibole. Cracks appear to be crystallographically controlled in many plagioclase grains. Where it is present, quartz is unevenly distributed and the crystals are subhedral.

In terms of texture, it appears the original texture is probably that of plagioclase with interstitial pyroxene and olivine, with static recrystallisation and growth of brown hornblende, apatite and epidote. Relict igneous textures indicate plagioclase was preferentially subhedral.

A

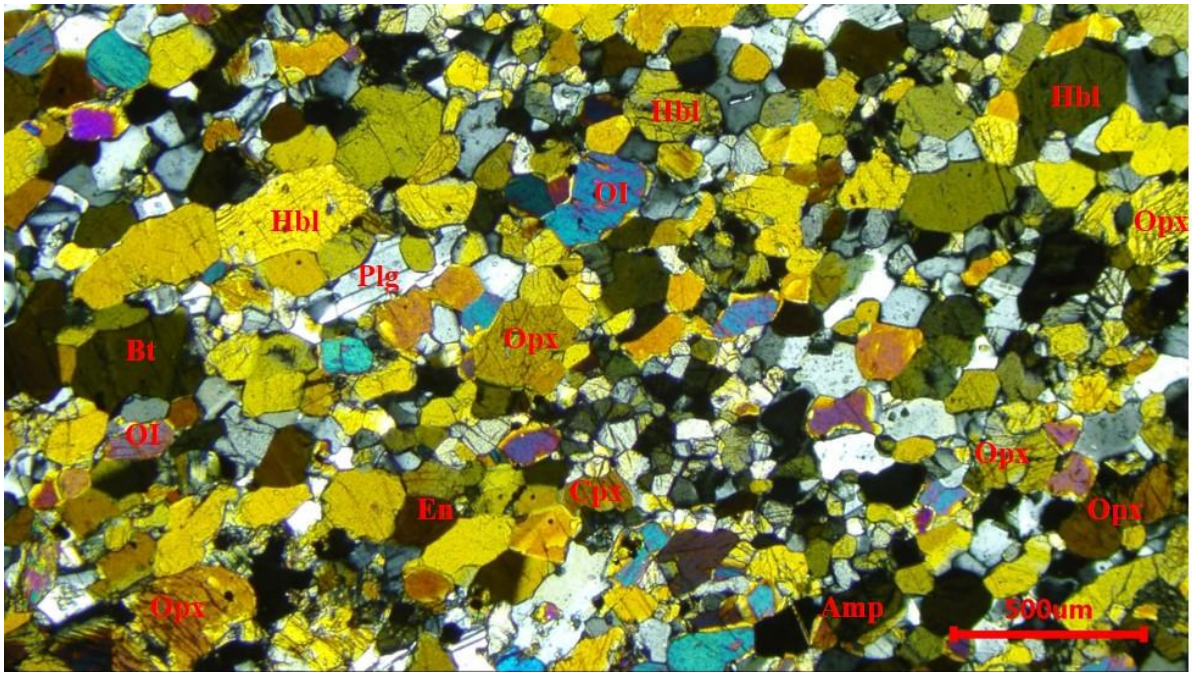
Hbl
Hbl
Hbl
Ol
Opx
Plg
Opx
Bt
Ol
Opx
Cpx
En
Opx
Opx
Amp
500um

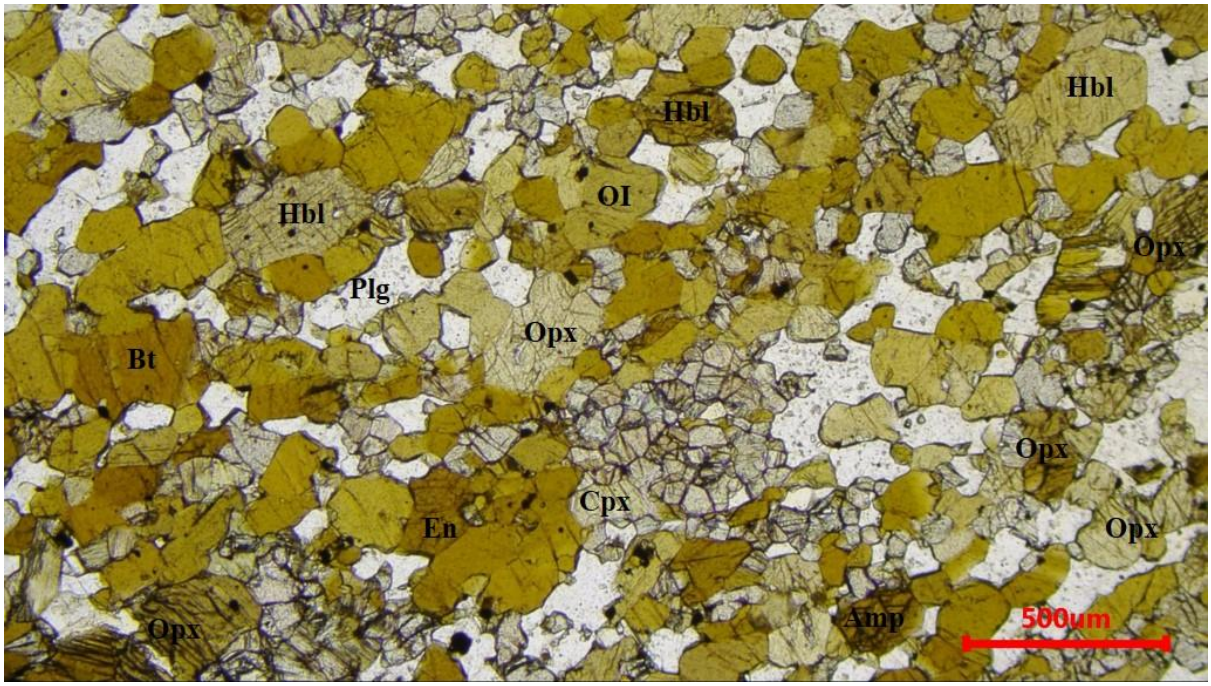
Hbl
Hbl
Hbl
Ol
Opx
Plg
Opx
Bt
Opx
Cpx
En
Opx
Opx
Amp
500um

B

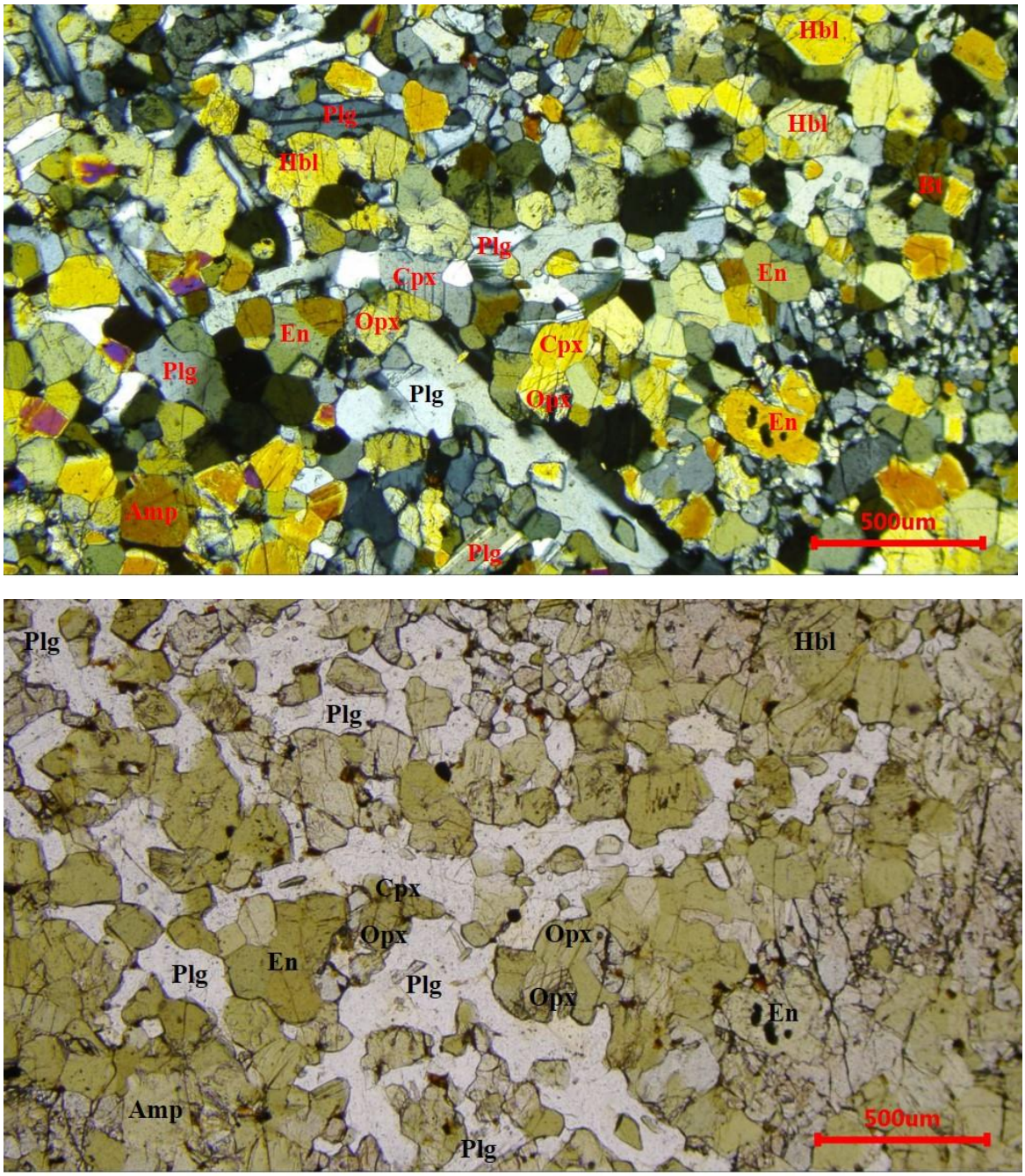

Figure 4.1: Photomcrographs (XPL & PPL) showing typical mineralogy and texture of the fine grained mafic dykes of the northeastern part of the Irumide Fold Belt, Northeastern Zambia. Cpx – clinopyeroxene, Opx – orthpyroxene, Hbl – horblende, Amp – amphibole (unclassified), Plg – plagioclase, Bt – biotite, Ol - olivine and En – enstatine.

4.1.2 Medium grained variety dykes

The medium grained sampled dykes have similar mineralogy to the fine grained variety in that they are also dominated by plagioclase, clinopyroxene, orthopyroxene and hornblende with subordinate olivine, quartz, epidote and sericite (Figure 4.2). Plagioclase is noticeably less in

this type than in the fine grained variety (about 40%). It predominantly occurs as lath-like micro-phenocrysts with ragged grain boundaries and a few phenocrysts. Many grains exhibit simple twinning, although some show polysynthetic twinning within a simple twin. Mechanical twinning is common in large grains. Both zoning and undulose extinction are common. In some grains, inclusions may be abundant in the centres, sparse in the rims. Yet in other grains, randomly oriented lines of tiny inclusions which are preferentially altered are observed. Some grains show sutured boundaries and subgrain development. Minor sericitic alteration is present, possibly crystallographically controlled. Most relict grains, less 0.5mm in size, are irregular but elongate. Occasionally, relict plagioclase-clinopyroxene grain boundaries, subhedral shapes, are preserved in parts. Small plagioclase grains are less than 0.25mm in size and these are recrystallised and equant (Figure 4.2A). Perhaps 60% of the mineral is very fine-grained, a result of cataclastic strain. Some small grains do not have undulose extinction (suggesting some recovery or grain growth). Much of plagioclase has heavy dusting of fine opaques. Alteration to sericite and oxide stains along grain boundaries are quite common; alteration to yellowish green layer silicate, probably smectite, is common around mafic minerals, both as “veins”, parallel foliation and along grain boundaries across foliation.

Clinopyroxene ranges from about 15 to 30% in the examined medium grained dyke samples. The original grain size could have been an averaged of about 1mm, but the present grain size, resulting from recrystallisation and alteration, is less than 0.5mm. A few relict grains show clear zoning, possibly manifesting recrystallisation. The interiors of the grains are mostly preserved although they are often bent and sheared along cleavage planes. Larger grains display slightly bent cleavage and appear to have been fractured into smaller pieces (Figure 4.2B. Most smaller grains are quite equant with granoblastic texture. The boundaries are mostly curvilinear and have very narrow rims of brown hornblende and opaques. Most clinopyroxene grains are badly stained in reddish-yellow and therefore identification is based on internal texture. Cleavage, fine exsolution lamellae and minor alteration along cracks are prominent features of the clinopyroxene. Vermicular to mottled intergrowths of clinopyroxene and brown hornblende are common. It is possible that much of the pyroxene is now epidote, as birefringence is quite high, whilst plagioclase shows normal colours. Tiny opaque inclusions are also common. Minor bleb inclusions of brown amphibole where clinopyroxene retains igneous boundaries are observed. Almost all orthopyroxene is altered to opaques or pale amphibole whose outside rims are usually bluish green in colour, whilst chlorite may form at far outer rims.

Hornblende ranges between about 5 to 10% in the studied medium grained dykes. It occurs as brown blebs in clinopyroxene and as cores to green hornblende either replacing a mafic

mineral or rimming it. Green hornblende is much more common than brown. Greenish brown hornblende usually rims around pyroxene and often has very irregular boundaries. Hornblende is massive in plagioclase matrix where it occurs with regular boundaries. It may contain small Inclusions of apatite and often associated epidote which displays prismatic grains. It is also associated with minor opagues.

Olivine forms about 2% of the medium grained variety dykes studied. Original preserved olivine crystal grains are among the largest, meausuring up to about 1 mm across (Figure 4.2A). These large olivine crystals are characteristically altered to clinopyroxenes or hornblende at the rims giving them ragged edges. Granoblastic recrystallisation is masking original textural relationship, probably interstitial to pyroxene and plagioclase. In places, it is rimmed by clinopyroxene. Some alteration to opaques is seen, mostly to brownish fibrous minerals mimicking cleavage. Undulatory extinction and cracks are common and deformation lamellae are visible. Blue-green hornblende and colourless amphibole are coarsely mixed in rims around olivine.

Epidote, 2 – 5% by volume, is markedly more in two of the four medium grained samples and exhibits subhedral to euhedral crystals, where it appears to have totally replaced hornblende (Figures 4.2C & D). The crystal contacts of the two minerals are sharp, giving the impression that epidote was not replacing hornblende from the edges.

Opaques and probably apatite (about 3-5%) are concentrated together in zones occurring in anhedral grains as veins or fillers parallel to foliation. Minor amounts of opaques occurring as small anhedral to subhedral grains which found within pyroxene or hornblende or are closely associated with these minerals and alteration aggregates.

Quartz is colourless to white in colour and occurs in euhedral to subhedral crystals. It is identified both as open space (vesicle) fillings and vein filling mineral. Alteration minerals form up to 10% of the medium grained variety dykes. They may occur as patches of fibrous amphibole mimic pyroxene cleavage, usually pale and cloudy. Some patches suggest alteration after recrystallisation, whilst patches of serpentine are pseudomorphing orthopyroxenes (Figure 4.2C). Kinking of some of fibrous minerals indicates some deformation after alteration. Alteration may be of static nature, but maybe fracture-related, serpentine comes after sericite as deduced from crosscutting relationships.

The igneous texture of the medium grained variety of the examined dykes is clearly sub-ophitic, which is still well preserved. Original texture probably plagioclase with interstitial pyroxene and olivine. Subsequent deformation with some mortar texture developed.

Cataclastic deformation produced good foliation and well-developed gneissic texture. Grain size was greatly reduced whilst much of the mineralogy and mineralogical relationship are obscured by heavy oxidation. Little polysynthetic twinning of plagioclase and lack of other deformation textures may indicate insignificant deformation. Granoblastic texture has obscured some primary textures, although zoning in clinopyroxene is still observed. Some of the slightly larger grains suggest primary prismatic shapes.

A

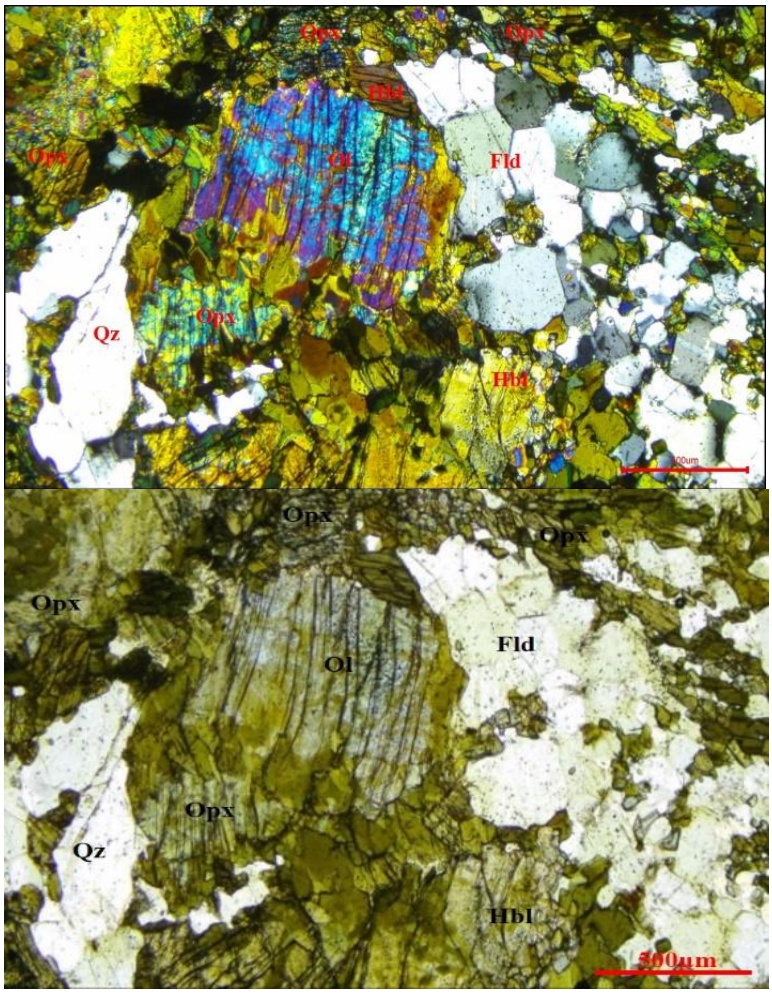

B

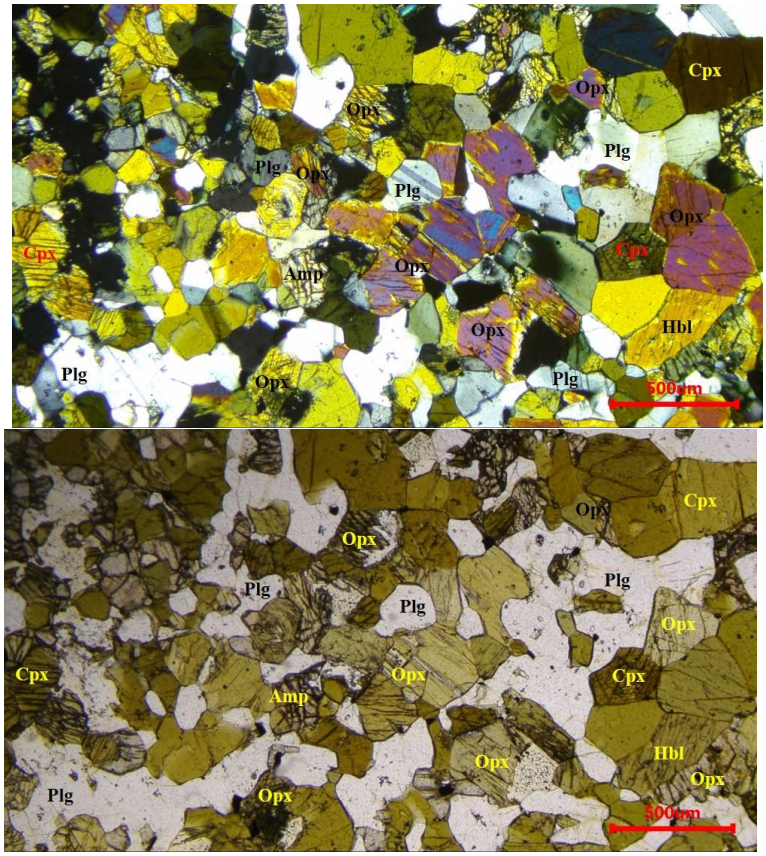
Cpx
Opx
Opx
Plg
Plg
Opx
Plg
Opx
Cpx
Cpx
Amp
Opx
Opx
Hbl
Plg
Opx
Plg
500um
Opx
Cpx
Opx
Plg
Plg
Opx
Cpx
Amp
Opx
Cpx
Opx
Hbl
Opx
Plg
Opx
500um

C

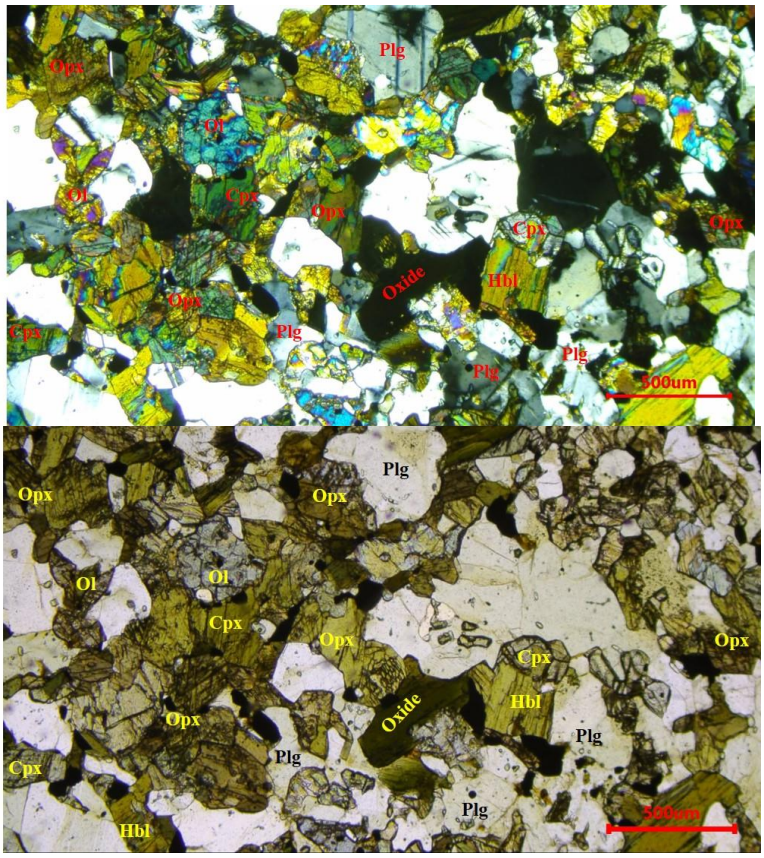
Plg
Opx
Ol
Ol
Cpx
Opx
Cpx
Opx
Oxide
Hbl
Opx
Cpx
Plg
Plg
Plg
500um
Plg
Opx
Opx
Ol
Ol
Cpx
Opx
Cpx
Opx
Oxide
Hbl
Opx
Plg
Cpx
Plg
Plg
Hbl
500um

D

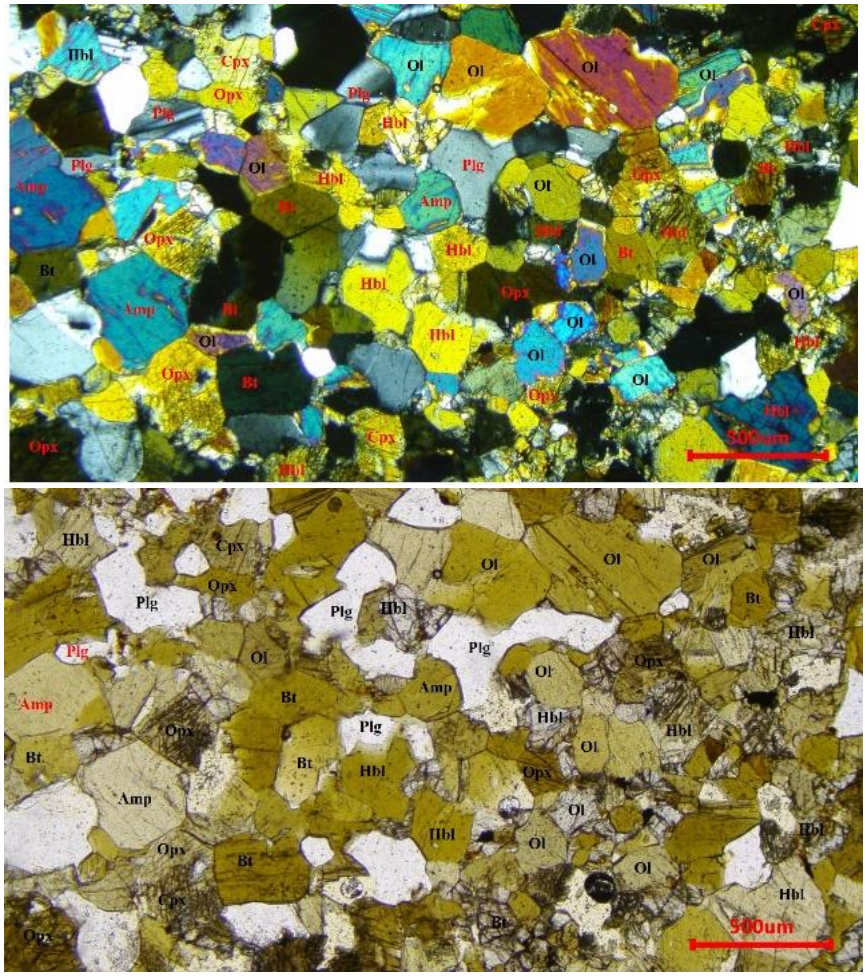

Figure 4.2: Photomicrographs (XPL & PPL) showing typical mineralogy and texture of the medium grained mafic dykes part northeastern part of the Irumide Fold Belt, Northeastern Zambia. Cpx – clinopyeroxene, Opx – orthpyroxene, Hbl – horblende, Amp – amphibole (unclassified), Ol – olivine, Bt – biotite, and Pl - plagioclase.

4.1.3 Coarse grained variety dykes

The coarse grained sampled dykes form half (6) of the rock samples examined. Their mineralogy is dominated by plagioclase, clinopyroxene and hornblende, with subordinate sericite, opaques and epidote (Figure 4.3).

Plagioclase (40 to 60%) is moderately to well-developed granoblastic in texture, with tapered polysynthetic twins in greater than 75% of the grains. Most grains are of subhedral and subequant shape, elongate to granular, generally showing sharp and straight to very curvilinear and muted boundaries with other plagioclase/microline grains (Figures 4.3B, C & D). Much of the grains are fractured with some of the large fractures containing alteration phases such as sericite. The boundaries with mafic phases are obscured by incipient sericite

alteration. Most grains are >1mm equant to stubby-elongate, with smooth to irregular grain boundaries. Some of the larger grains consists of sub-grain or form broken aggregates. Almost all grains show twinning, infrequently in two directions, and of both mechanical and growth type. Medium size grains are probably as a result of first phase of recrystallisation. Optical zoning under crossed polars is sometimes associated with cloudy cores but not all the time. Twinning is either tapered, bent or, in a few cases, kinked. Few of the largest grains show bent twinning and some show zoning, with greyish cores under plane light. Most grain boundaries and intragranular cracks contain pale green chlorite and sericite (Figures 4.3E & F). Some samples examined show that some crystals are mottled by hornblende and some opaque phases (Figures 4.3B, D & F).

Clinopyroxene (25 to 35%) occurs in grains which are predominantly 1mm and above, poikilitic and may have been interstitial to plagioclase. Large grains show little exsolution in areas where they have recrystallised to semi-granoblastic texture. Some of the larger “relict grains” show intergrowth texture and/or blebby exsolution. Bent cleavage is seen in some larger grains. There has been some minor recrystallisation along a few grain boundaries. The new pyroxene is much clearer and may contain inclusions of opaques and brown hornblende (Figure 4.3A). Minor bleb inclusions of brown amphibole are common within the clinopyroxene grains. In some cases, the clinopyroxene appears to have been fractured into smaller pieces. Narrow rims of reddish brown, brown and green hornblende are almost ubiquitous, exhibiting irregular edges. In places, alteration to brown and brown-green hornblende has created wider, irregular rims which may be gradationally zoned (laterally and from rim to core). Internal texture is either finely cleaved or with numerous blebby lamellae of brown hornblende. It often encloses opaques with plagioclase in rims as myrmekitic or bladed intergrowths and as separate grains in recrystallised plagioclase.

Hornblende, about 20% by volume, often occurs in aggregates measuring 4 mm or more; it is subhedral and slightly elongated. Brown hornblende occurs primarily as rims to green hornblende, apparently as pseudomorphs after clinopyroxene. Grain boundaries are spikey where amphibole has grown into plagioclase. There are small inclusions of euhedral plagioclase. Aggregates of green hornblende are of equant and interlocking grains. There is very little deformation of hornblende pseudomorphs. About 15-20% of hornblende is massive in a plagioclase matrix and may contain small inclusions of apatite. Green and brown hornblende partially rims clinopyroxene in discrete grains and pseudomorphs of clinopyroxene. Patches of felted mat of actinolite, less than 1 mm, are rimmed by green hornblende. Actinolite is bladed and colourless to pale green or brown. In a few places, hornblende is marginally altered to epidote (Figure 4.3C).

Olivine is less than 2% in the coarse grained dykes examined. It is medium grained, subhedral and granoblastic, mainly interstitial to plagioclase and in some places, it includes clinopyroxene or inter-grown with it. It is ubiquitously cracked, with opaques and/or alteration phases filling these cracks in clusters of grains.

Opaque and other minor minerals comprise about 2% of the coarse grained examined dyke samples. They generally occur as anhedral grains in brown hornblende and as interstitial grains in mafic aggregates and also in cracks of olivine as anhedral blebs. In addition, they also occur as tiny subhedral inclusions in clinopyroxene and as a few tiny interstitials in plagioclase. Apatite, which is in very small proportions, is a secondary mineral, anhedral and subequant grains in narrow zones associated with opaque and brown hornblende. Opaques may represent several unidentified alteration phases. Where opaques and sphene occur together, sphene rims opaques. Epidote occurs as discrete grains in hornblende and plagioclase, with ragged boundaries (Figures 4.3C and E).

Alteration and texture: Igneous plagioclase texture is dominant with some characteristic poikilitic inclusions by clinopyroxene (Figures 4.3B, C & F). Maximum grain size is probably about 2cm and all minerals are affected by strain, plagioclase the most. Recrystallisation appears to have taken place during and after deformation, but most alteration probably happened after deformation. Deformation is predominantly brittle and plagioclase is more cracked than clinopyroxene. Recrystallisation to granoblastic textures is quite widespread. Grain boundaries between plagioclase and clinopyroxene are usually cuspate and irregular. Alteration is primarily along cracks in plagioclase grains and perimeter of mafic phase groups. This is reasonably static and postdates deformation that destroyed most of original plagioclase textures and created subgranoblastic texture and mechanical twins. There is little apparent deformation after alteration. Only minor alteration occurs within a cluster of mafic minerals, and that which exists is usually confined to a crack or vein originating in the plagioclase. There is no clearly defined foliation. Mafic grain shape suggest they were subpoikilitic, with about subhedral plagioclase laths. Brown hornblende and opaques are interstitial to clinopyroxene. Chlorite and serpentine are scarce but these filled fractures which are now almost non-existent. Clinopyroxene is considerably more resistance to deformation than plagioclase, preserving some primary texture.

A

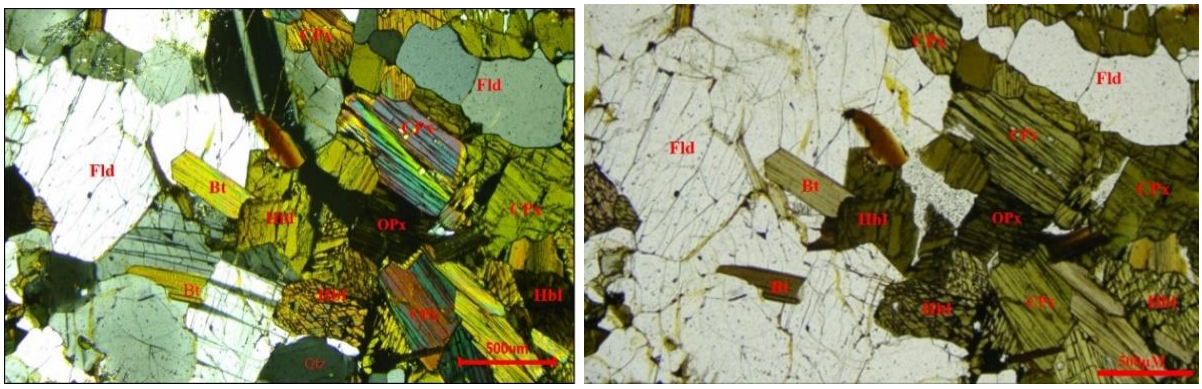
CPx
Fld
CPx
Fld
Bt
Hbl
OPx
CPx
Bt
Hbl
Hbl
Qz
500um
CPx
Fld
Fld
CPx
Bt
CPx
Hbl
OPx
Bt
Hbl
CPx
Hbl

B

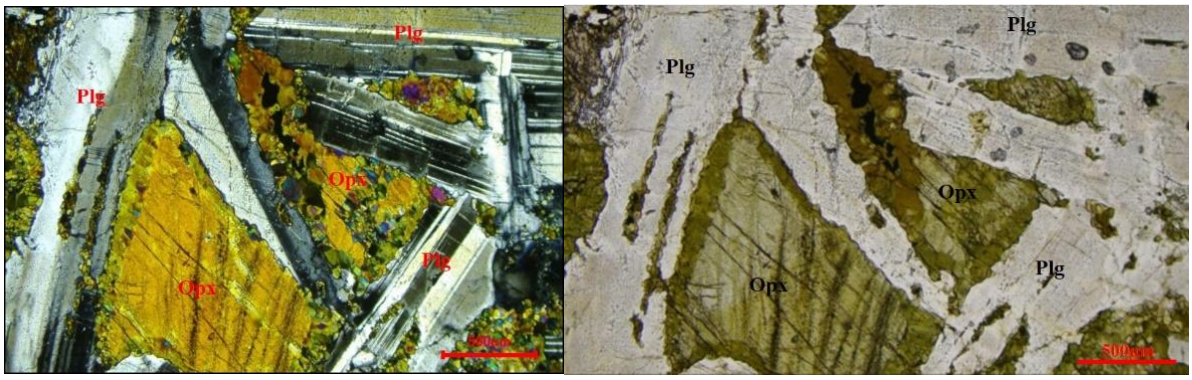
Plg
Plg
Opx
Opx
Plg
Plg
Plg
Qpx
Opx
Plg
500um

C

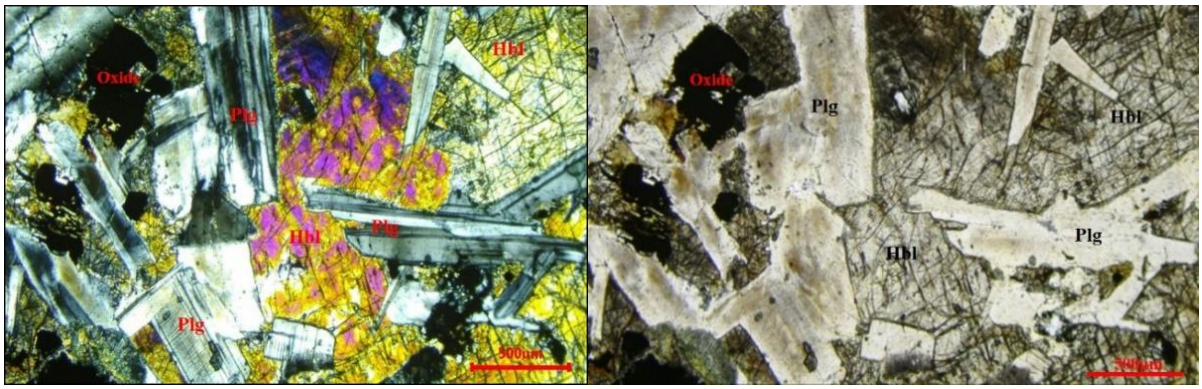
Hbl
Oxide
Plg
Hbl
Plg
Plg
500um
Oxide
Plg
Hbl
Hbl
Plg

D

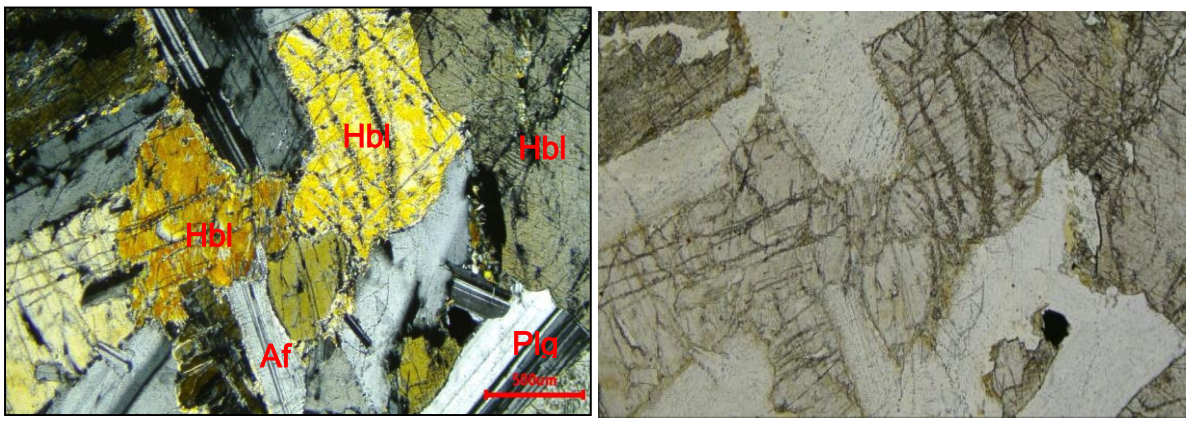
Hbl
Hbl
Hbl
Af
Plg
500um

E

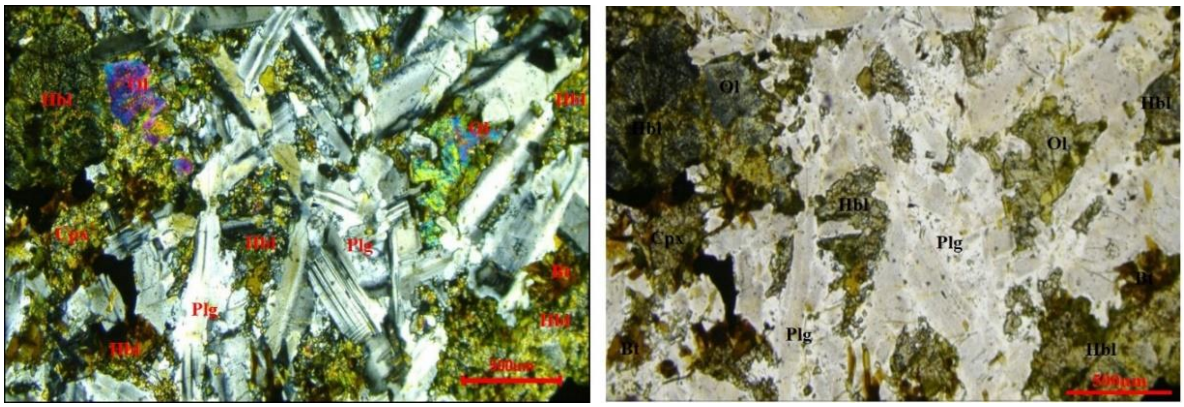

F

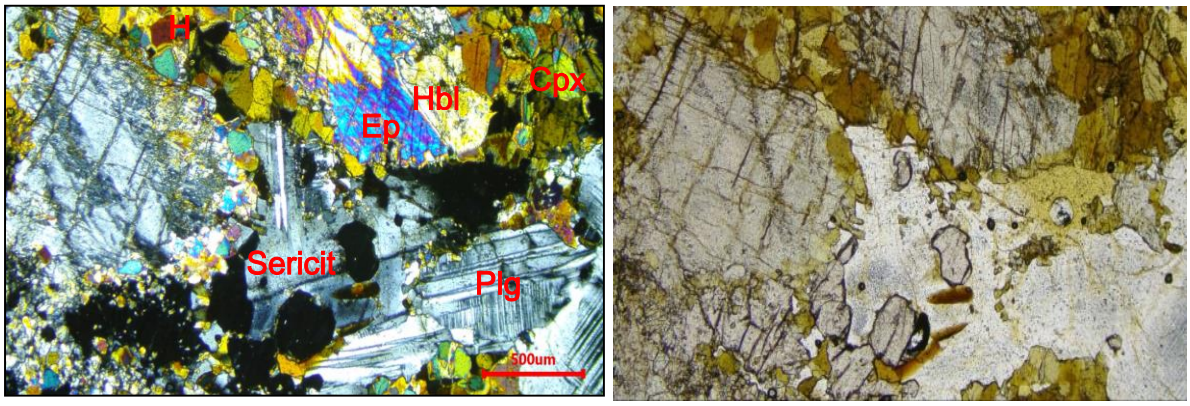

Figure 4.3: Photomicrographs (XPL & PPL) showing typical mineralogy and texture of the course grained mafic dykes of the northeastern part of the Irumide Fold Belt, Northeastern Zambia. Cpx – clinopyeroxene, Opx – orthpyroxene, Hbl – horblende, Bt – biotite, and Plg – plagioclase.

4.2 Application of CIPW norms on the oxides

The CIPW norm, is a means of converting the chemical composition of an igneous rock to an ideal mineral composition (Verma et al., 2002; Gonzalez-Guzman, 2016). The normative analysis is based on the calculation of a theoretical assemblage of standard minerals for a rock that can result from the whole rock chemical composition that has been determined by analytical techniques (Cucciniello et al., 2015; Gonzalez-Guzman, 2016). The method allows for the grouping of rocks with similar bulk chemical composition irrespective of their mineralogy – classification based on normative mineral percentages. Some similarities are at times observed in rocks with different modes due to several factors that may include: disequilibrium (for example, zoned minerals or reaction rims isolating the interiors of grains), temperature, pressure, alteration, water content and other minor constituents. The CIPW norm is calculated under the basic principle assumption that the magma crystallizes under anhydrous conditions

so that no hydrous minerals such as hornblende and biotite are formed, and that the magma crystallises perfectly.

The CIPW norms were performed on the oxide results of the mafic dyke swarm rock samples of the present study, using a programme which was written by Gonzalez-Guzman (2016). The results and interpretations are presented here below (Table 4.1).

Table 4.1: CIPW normative computations for the rock samples of the Study area

Sample CH-WHR-01

Normative minerals	weight %	Volume %
Plagioclase	46.4	53.39
Orthoclase	1.24	1.51
Diopside	10.52	10.19
Hypersthene	16.55	16.08
Olivine	6.19	6
Ilmenite	0.46	0.3
Hematite	15.4	9.15
Apatite	0.25	0.25
Sphene	3.38	3.01
	100.39	

Sample CH-WHR-02

Normative minerals	weight %	volume %
Quartz	0.13	0.15
Plagioclase	54.86	61.36
Orthoclase	2.07	2.44
Diopside	13.69	12.87
Hypersthene	13.60	12.82
Ilmenite	0.40	0.25
Hematite	12.66	7.29
Apatite	0.28	0.26
Sphene	2.83	2.44
	100.52	

Sample CH-WHR-03

Normative minerals	weight %	Vol. %
Quartz	5.70	6.49
Plagioclase	48.80	54.69
Orthoclase	6.15	7.24
Diopside	5.43	5.08
Hypersthene	11.93	11.21
Ilmenite	0.44	0.28
Hematite	15.23	8.75
Apatite	0.83	0.79
Sphene	6.23	5.37
	100.74	

Sample CH-WHR-04

Normative minerals	weight %	Vol %
Quartz	1.06	1.22
Plagioclase	52.01	58.54
Orthoclase	2.48	2.96
Diopside	11.37	10.77
Hypersthene	16.25	15.43
Ilmenite	0.42	0.27
Hematite	13.46	7.82
Apatite	0.25	0.24
Sphene	3.04	2.65
	100.34	

Sample CH-WHR-05

Normative minerals	weight %	Vol %
Quartz	6.24	7.07
Plagioclase	52.65	58.23
Orthoclase	3.78	4.44
Diopside	13.77	12.84
Hypersthene	10.93	10.22
Ilmenite	0.35	0.22
Hematite	9.57	5.47
Apatite	0.19	0.17
Sphene	1.43	1.23
	98.91	

Sample CH-WHR-06

Normative minerals	weight %	Vol %
Quartz	5.67	6.52
Plagioclase	47.06	53.19
Orthoclase	2.72	3.24
Diopside	12.14	11.50
Hypersthene	10.79	10.25
Ilmenite	0.44	0.28
Hematite	14.83	8.61
Apatite	0.63	0.60
Sphene	6.55	5.71
	100.83	

Sample CH-WHR-07

Normative minerals	weight %	volume %
Quartz	5.00	5.79
Plagioclase	47.98	54.61
Orthoclase	2.48	2.98
Diopside	14.18	13.51
Hypersthene	9.47	9.05
Ilmenite	0.44	0.28
Hematite	14.23	8.32
Apatite	0.49	0.47
Sphene	5.57	4.88
	99.84	

Sample CH-WHR-08

Normative minerals	weight %	volume %
Plagioclase	45.82	53.41
Orthoclase	1.71	2.12
Diopside	8.50	8.34
Hypersthene	22.04	21.70
Olivine	2.76	2.71
Ilmenite	0.44	0.29
Hematite	14.22	8.56
Apatite	0.23	0.23
Sphene	2.79	2.52
	98.51	

Sample CH-WHR-09

Normative minerals	weight %	volume %
Plagioclase	56.27	63.05
Orthoclase	2.90	3.43
Diopside	9.12	8.59
Hypersthene	16.05	15.16
Olivine	0.50	0.47
Ilmenite	0.40	0.25
Hematite	12.25	7.07
Apatite	0.21	0.20
Sphene	1.94	1.68
	99.64	

Sample CH-WHR-10

Normative minerals	weight %	volume %
Quartz	5.77	6.56
Plagioclase	51.63	57.66
Orthoclase	5.97	7.03
Diopside	9.20	8.61
Hypersthene	9.78	9.19
Ilmenite	0.42	0.26
Hematite	12.47	7.16
Apatite	0.37	0.35
Sphene	3.58	3.09
	99.19	

Sample CH-WHR-11

Normative minerals	weight %	volume %
Plagioclase	41.36	48.28
Orthoclase	1.42	1.76
Diopside	10.03	9.90
Hypersthene	24.45	24.19
Olivine	6.47	6.38
Ilmenite	0.42	0.28
Hematite	12.38	7.49
Apatite	0.16	0.16
Sphene	1.60	1.45
	98.29	

Sample CH-WHR-12

Normative minerals	weight %	volume %
Plagioclase	44.67	51.86
Orthoclase	2.48	3.04
Diopside	17.23	16.78
Hypersthene	12.07	11.79
Olivine	5.86	5.71
Ilmenite	0.42	0.28
Hematite	12.45	7.44
Apatite	0.35	0.34
Sphene	2.97	2.66
	98.50	

The CIPW norm calculations on the studied samples have revealed two groups of rocks in terms of silica saturation, the saturated and the under-saturated. All the samples of rocks that are classified earlier as tholeiitic (see Figure 4.15) are silica normative saturated with normative quartz averaging 5.34 vol%. Samples of calc-alkaline rocks are all normative quartz under-saturated with two being at the margin with 0.13 and 1.22 vol% normative quartz. Normative hypersthene is higher in the calc-alkali rocks averaging 18.24 vol%, whilst in the tholeiitic rocks, it averages 10.49 vol%. Normative sphene or titanite is characteristically higher in the tholeiitic rocks with an average of 5.48 vol%, whilst in calc-alkalic rocks, it averages 2.83 vol%. Normative plagioclase ($CaAl_2Si_2O_8$ – $NaAlSi_3O_8$) is dominant, ranging between 41.36 to 56.27 vol%. The range of normative hypersthene $(Mg,Fe)SiO_3$) for all the samples is 9.47 to 24.45 vol%, whilst normative sphene or titanite ($CaTiSiO_5$) ranges between 1.43 to 6.55 vol%, and normative diopside ($MgCaSi_2O_6$) ranges between 5.43 and 17.23 vol%. As expected, olivine is absent in saturated samples but ranges between 0.5 and 6.47 vol% in the unsaturated type. Normative hematite (Fe_2O_3) ranges between 9.57 and 15.4 vol%. Apatite and ilmenite normative values all fall below 0.5 vol% whilst orthoclase ($KAlSi_3O_8$) normative values range between 1.25 and 6.15 vol%.

4.3 Whole rock Geochemistry

The whole-rock elemental geochemical results of the samples collected and analysed, from the Study area, are shown in Table 4.2. The results show the concentrations in respective samples in weight percent (wt. %) in the case of the oxides, and parts per million (ppm) in the case of the trace elements, which include rare earth elements.

Table 4.2: Whole rock elemental chemistry of the samples of the Study area (major element oxides are in wt.%, trace elements are in ppm)

Sample	WHR-01	WHR-02	WHR-03	WHR-04	WHR-05	WHR-06	WHR-07	WHR-08	WHR-09	WHR-10	WHR-11	WHR-12	ISO-01	ISO-02	ISO-03
SiO2	44.3	47.2	48.8	46.8	50.3	48.2	48	44.7	47.1	49.6	45.1	45.8			
Al_2O_3	14.5	16.9	15	16.3	17.1	14.3	14.4	14.5	17.5	16.3	13.5	13.7			
Fe_2O_3(T)	15.4	12.7	15.2	13.5	9.57	14.8	14.2	14.2	12.3	12.5	12.4	12.5			
MnO	0.2	0.17	0.19	0.18	0.15	0.19	0.19	0.19	0.17	0.18	0.18	0.18			
MgO	12.2	8.01	5.8	8.64	6.95	6.59	6.44	12	8.43	5.64	15.4	11.4			
CaO	10	11.3	8.81	10.7	11.3	10.8	10.9	9.3	10.1	9.61	9.2	10.8			
Na2O	1.85	2.49	2.74	2.18	1.97	2.4	2.52	1.79	2.53	2.58	1.33	2.18			
K2O	0.21	0.35	1.04	0.42	0.64	0.46	0.42	0.29	0.49	1.01	0.24	0.42			
TiO2	1.62	1.36	2.77	1.46	0.77	2.9	2.5	1.37	1	1.68	0.87	1.43			
P2O5	0.11	0.12	0.36	0.11	0.08	0.27	0.21	0.1	0.09	0.16	0.07	0.15			
LOI	0.1	0.07	-0.31	0.28	0.27	0.01	0.12	0.53	0.64	0.32	0.5	1.06			
Total	101	101	100	101	99.2	101	99.9	99	100	99.5	98.8	99.5			
Sc	34	35	28	34	34	34	34	35	39	31	30	34			
Be	1	1	2	1	1	1	1	1	1	1	1	1			
V	344	278	341	302	212	351	335	294	244	325	236	268	256	275	206
Cr	760	380	210	500	240	260	160	430	190	150	1140	530	1400	640	760
Co	84	58	55	61	45	53	48	72	59	43	80	63	73	77	75
Ni	520	170	230	210	150	120	100	440	290	80	720	280	520	410	530
Cu	130	130	110	140	110	180	170	130	130	100	110	90	560	150	170
Zn	100	90	140	100	70	130	100	90	80	90	70	90	90	90	80
Ga	19	20	23	20	18	22	20	19	18	23	16	18	15	17	15
Ge	2	2	2	2	2	2	1	2	2	2	1	2	1	1	2
As	4	4	4	4	4	4	4	4	4	4	4	4	4	4	4
Rb	6	11	35	14	25	12	11	9	16	41	9	9	12	14	16
Sr	198	217	325	218	154	317	312	202	171	300	135	259	97	144	91
Y	20	17	29	19	18	26	27	21	25	21	17	17	23	22	18
Zr	88	68	174	82	59	151	132	80	70	80	53	78	53	72	43
Nb	2	2	17	2	3	23	16	3	3	9	2	13	2	2	2
Mo	1	1	1	1	1	1	1.5	1.5	1.5	1.5	1.5	1.5	3	1	1
Ag	0.4	0.4	0.8	0.4	0.4	0.7	0.4	0.4	0.4	0.4	0.4	0.4	0.4	0.4	0.4
In	0.1	0.1	0.1	0.1	0.1	0.1	0.1	0.1	0.1	0.1	0.1	0.1	0.2	0.1	0.1
Sn	1	1	2	1	1	2	1	1	1	1	1	1	120	27	5
Sb	0.4	0.4	0.4	0.4	0.4	0.4	0.4	0.4	0.4	0.4	0.4	0.4	0.4	0.4	0.4
Cs	0.4	0.4	0.9	0.4	0.6	0.4	0.4	0.4	0.4	0.4	0.4	0.4	0.5	0.4	0.4
Ba	86	165	271	139	193	128	166	162	415	278	203	112	129	109	85
La	5.2	4.9	27.2	6.8	10.3	19.7	13.2	5.8	11.5	14.2	4.8	11.1	8.9	7.2	5.7
Ce	11.6	11.3	58.6	15.3	20.8	45.7	30.1	14	22.7	31.1	10.7	24	13.1	15	12
Pr	2.08	1.71	7.62	2.24	2.54	6.06	3.94	1.97	2.64	3.87	1.44	3.01	2.09	2	1.5
Nd	11.3	8.6	32.2	11.4	10.3	26.6	19	10.5	11.8	17.6	7.7	13.5	8.9	10	6.6

Sm	3.9	3.2	7.4	3.6	2.6	6.6	5.1	3.4	3.1	4.4	2.3	3.3	2.6	3.2	2.1
Eu	1.39	1.27	2.3	1.33	0.87	2.25	1.88	1.19	1.13	1.38	0.87	1.21	0.9	1.2	0.7
Gd	4.6	3.9	6.9	4.2	3.2	6.5	5.4	4	3.9	4.7	2.8	3.5	3.5	3.9	2.6
Tb	0.7	0.7	1.1	0.7	0.6	1	0.9	0.6	0.6	0.8	0.5	0.5	0.6	0.7	0.5
Dy	4.3	3.8	6	4	3.5	5.7	4.9	3.9	4.3	4.3	2.8	3.2	3.8	4.2	3.1
Ho	0.8	0.7	1.1	0.8	0.7	1	0.9	0.8	0.9	0.8	0.6	0.6	0.8	0.8	0.6
Er	2.1	2	3.1	2.1	2	2.7	2.5	2.1	2.6	2.1	1.6	1.7	2.3	2.2	1.8
Tm	0.29	0.28	0.44	0.28	0.29	0.38	0.34	0.3	0.38	0.29	0.23	0.24	0.33	0.3	0.3
Yb	1.9	1.7	2.7	1.8	2	2.3	2	1.9	2.5	1.8	1.5	1.4	2.1	1.9	1.8
Lu	0.29	0.25	0.4	0.27	0.29	0.35	0.3	0.28	0.39	0.27	0.21	0.21	0.3	0.3	0.3
Hf	2.6	2	4.4	2.5	1.8	4.2	3.4	2.3	2	2.3	1.5	2.2	1.6	2.2	1.3
Ta	0.1	0.1	1.3	0.1	0.2	1.6	1	0.1	0.1	0.6	0.1	0.7	0.1	0.1	0.1
W	1	1	1	1	1	1	1	1	1	1	1	1	1	1	1
Tl	0.1	0.1	0.1	0.1	0.1	0.1	0.1	0.1	0.1	0.1	0.1	0.1	0.1	0.1	0.1
Pb	5	4	5	4	4	4	4	4	4	6	4	4	4	4	4
Bi	0.3	0.3	0.3	0.3	0.3	0.3	0.3	0.3	0.3	0.3	0.3	0.3	0.3	0.3	0.3
Th	0.8	0.9	4.1	1.4	2.2	1.9	1.2	1.2	2.7	3.3	1.1	1.1	1.7	1.4	1.6
U	0.1	0.1	1	0.1	0.3	0.5	0.3	0.1	0.2	0.3	0.1	0.3	0.3	0.1	0.3

4.3.1 Alteration and Element Mobility Analysis

The alteration of the studied rocks is assessed by plotting the highly mobile elements under hydrous liquid environment, strontium, rubdium, barite and potassium, against zircon for linear correlation. The plots are presented here in Figure 4.4.

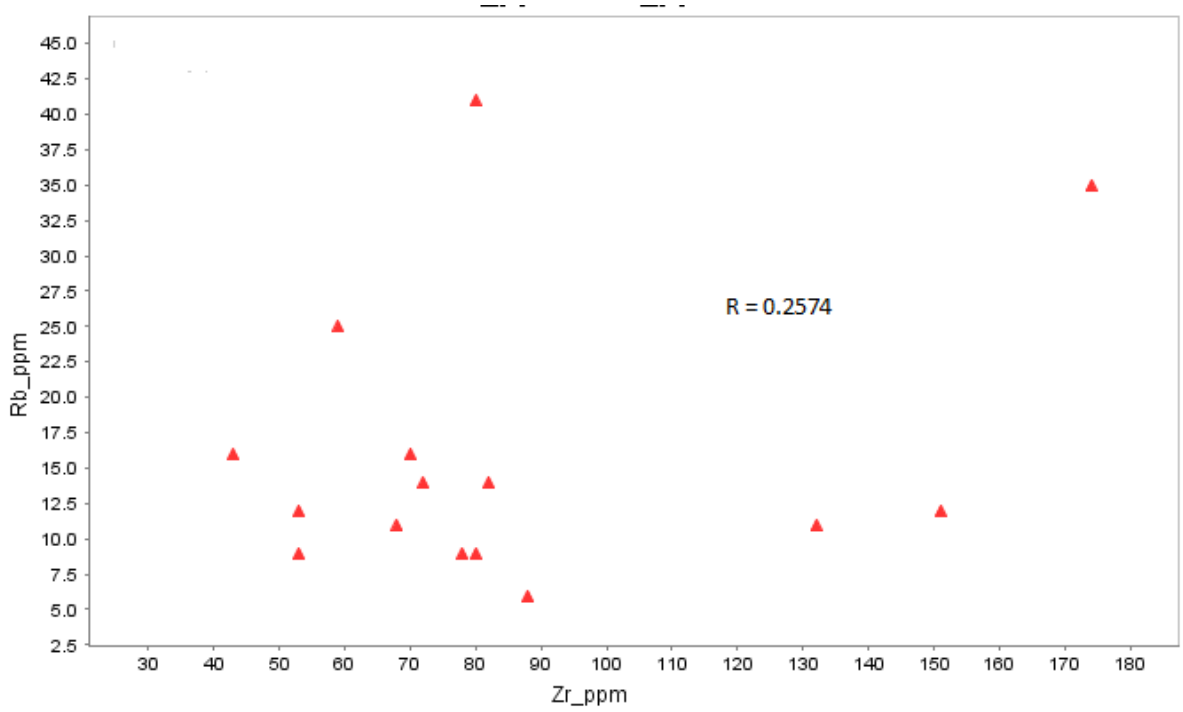

(a)

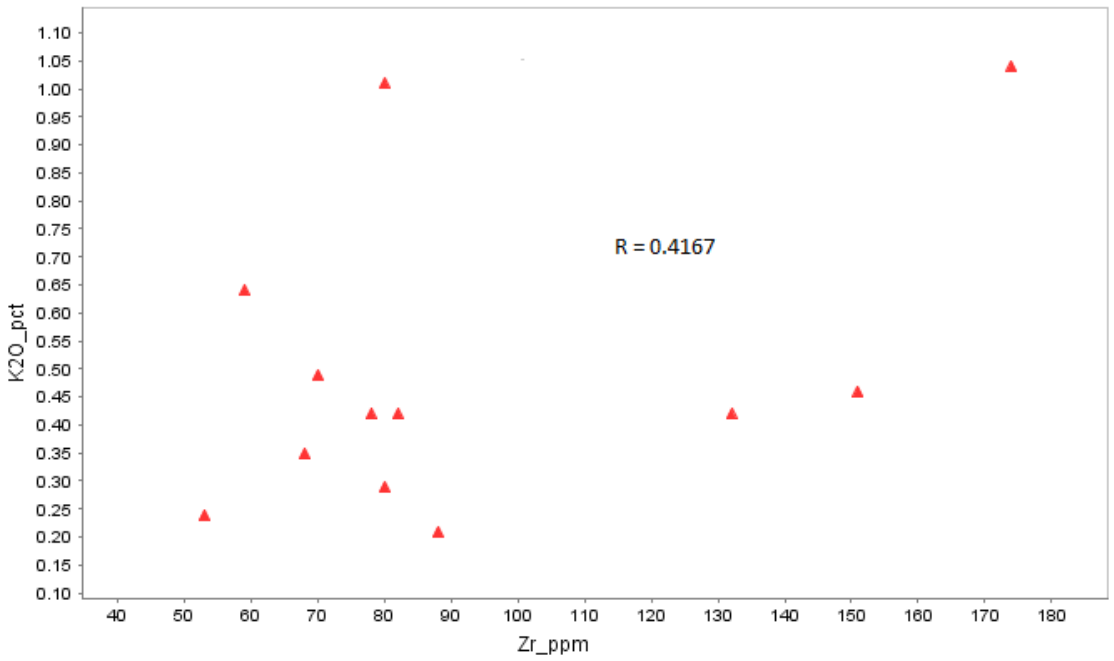

(b)

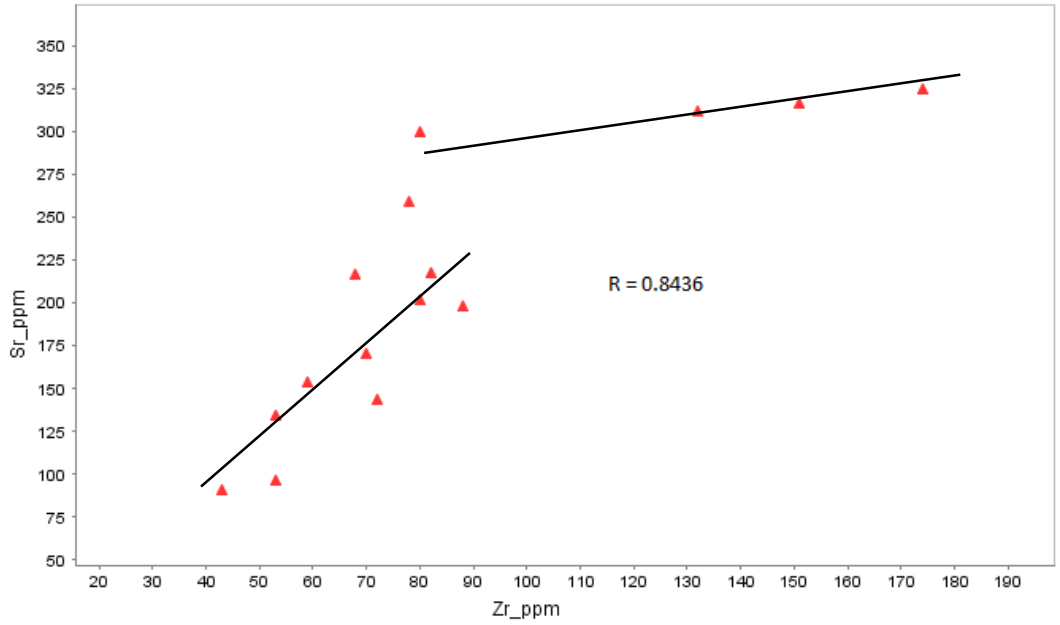

(c)

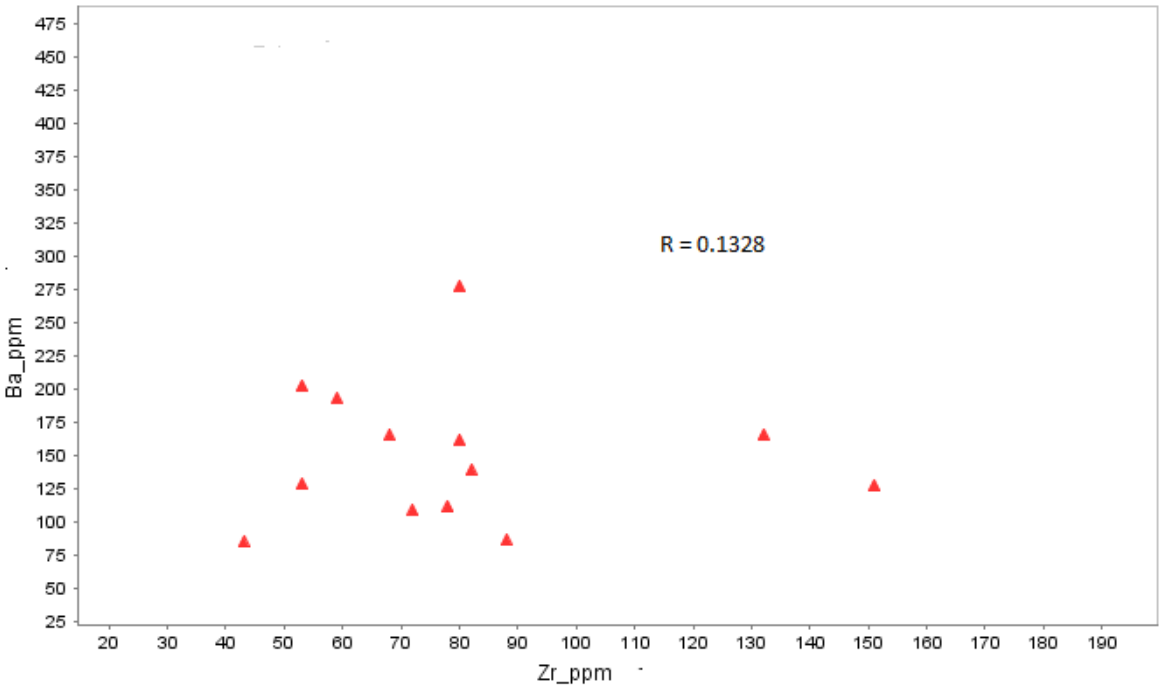

(d)

Figure 4.4: Zr variation plots with some highly mobile elements where: (a) = Zr vs Rb; (b) = Zr vs K_2O; (c) = Zr vs Sr; and (d) = Zr vs Ba (R = Pearson linear correlation factor).

The plots of the four elements above have revealed that only Sr, which is the least mobile of the lot, has good correlation with Zr, whilst K is weakly correlated. This could mean that there is some degree of alteration that has affected the sampled mafic dykes of the Study area, from the geochemical point of view. Ba is completely uncorrelated with Zr, suggesting that it is a supracrustal element not associated with Zr in the magmatic processes. Similar to Ba, the none correlation altogether of Rb with Zr could also be a result of contamination of the mafic magma by felsic crustal rocks on its way up before emplacement.

The loss on ignition (LOI) values, which are reported together with whole rock geochemical results, also give an indication of possible levels of post magmatic alterations the rocks might have under gone. LOI values for the samples used in the present study range between -0.31 and 1.06 wt%. These values are relatively low and may suggest that the sampled rocks have undergone very little, if any, alteration. Very low LOI values indicate very little or no post magmatic alteration affected the concerned rocks (Cimen, 2016).

4.3.2 Major Element Variations

Chemical variation diagrams are basically displays of element differences and trends which are shown by a related suite of rocks. One of the most common of these is a Harker diagram which a plot of SiO_2 versus other oxides, useful for felsic and basic rocks, and oxides versus

MgO, useful for basic rocks. In this study, major elements are plotted against SiO_2, MgO and Mg#. The Mg# is used as an index to monitor the degree of fractional crystallisation that the magma exhibits, as it is insensitive to contamination (Cox, 1980). Higher values of Mg# indicate least evolved nature while the lower values are suggestive of fractionated nature of the concerned rocks (Karmalkar et al., 2016). In the sampled rocks used in the study, SiO_2 shows a narrow variation content range of 44.28 to 50.32 wt%, whilst MgO content shows a wide variation ranging between 5.64 to 15.39 wt%. Calculated Mg# also shows a wide variation with values ranging between 29.7 and 58.0. These Mg-numbers are much lower than the Mg# of 70 estimated for primitive mantle-derived basaltic magmas (Halama et al., 2004; Talusani, 2010; Cucciniello et al., 2013). Total alkali content ranges between 1.57 and 3.78 wt%. The Al_2O_3 content ranges between 13.48 to 17.47 wt%, whilst the TiO_2 content also shows wide variation of values ranging between 0.766 to 2.903 wt%. The other oxides exhibit the following ranges: $Fe_2O_{3(T)}$, 13.48 to 17.47 wt%; MnO, 0.148 to 0.2 wt%; CaO, 8.81 to 11.37 wt%; Na_2O, 1.33 to 2.74 wt%; K_2O, 0.21 to 1.04 wt%; and P_2O_5, 0.07 to 0.36 wt%. Loss on ignition (LOI) ranges between -0.31 to 1.06. Total alkalis range between 1.57 and 3.78 wt%.

Major elements which show good linear correlation with SiO_2 of $R \geq 0.75$ are MgO (-0.8723) and K_2O (0.7751) (Figures 4.5 a & b), whilst those which show moderate linear correlation with SiO_2, of $0.75 > R \geq 0.5$ are Na_2O (0.6141) and Al_2O_3 (0.5215) Figures 4.5 c & d). The rest that include; Fe_2O_3 (-0.3948), P_2O_5 (0.3931), CaO (0.2708), and TiO_2 (-0.2502) (Figures 4.5 e, f, g & h), exhibit poor linear correlation with SiO_2. The reduction of MgO in relation to SiO_2 is due to the fractional crystalisation of olivine and pyroxenes (Figure 4.5 a).

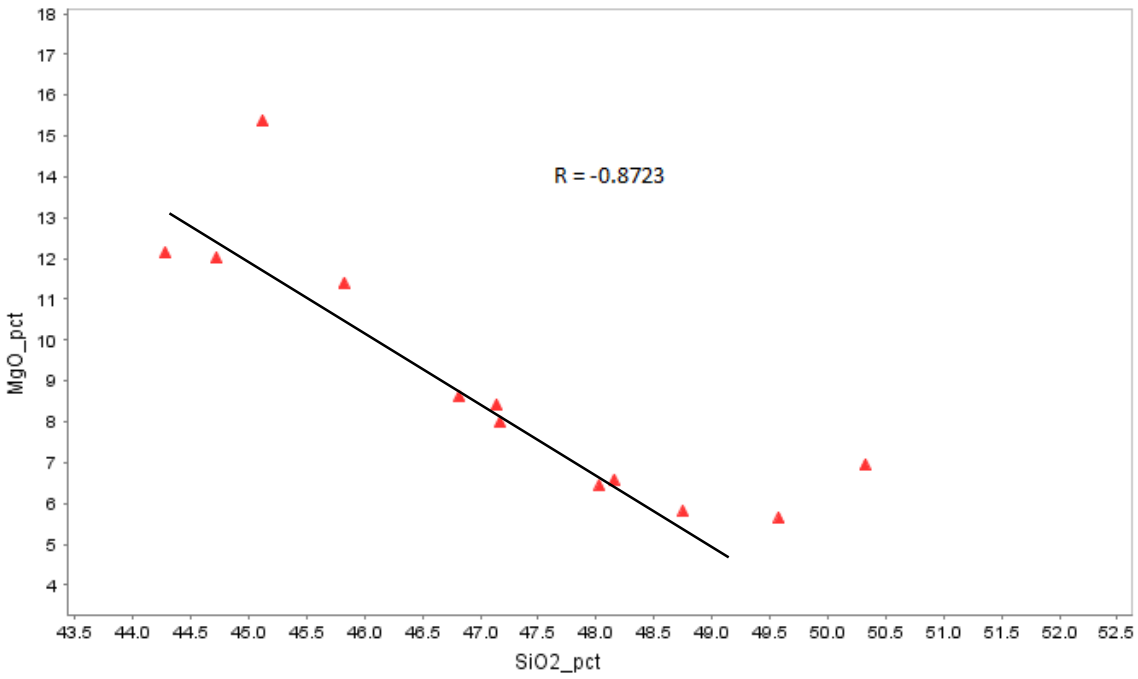

(a)

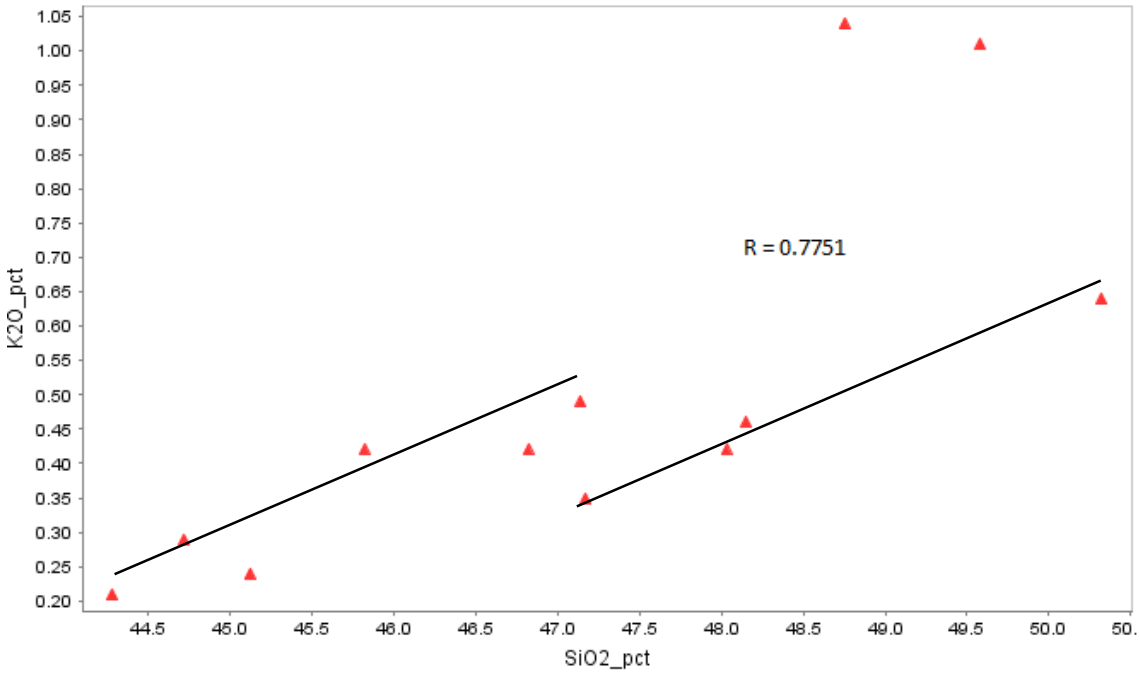

(b)

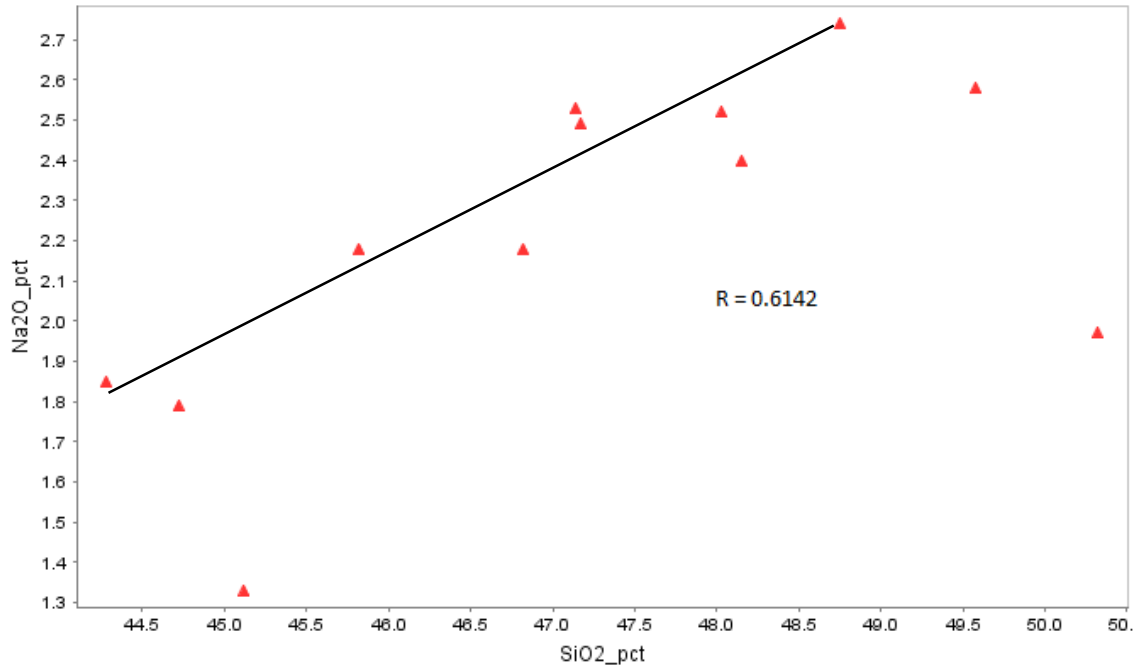

(c)

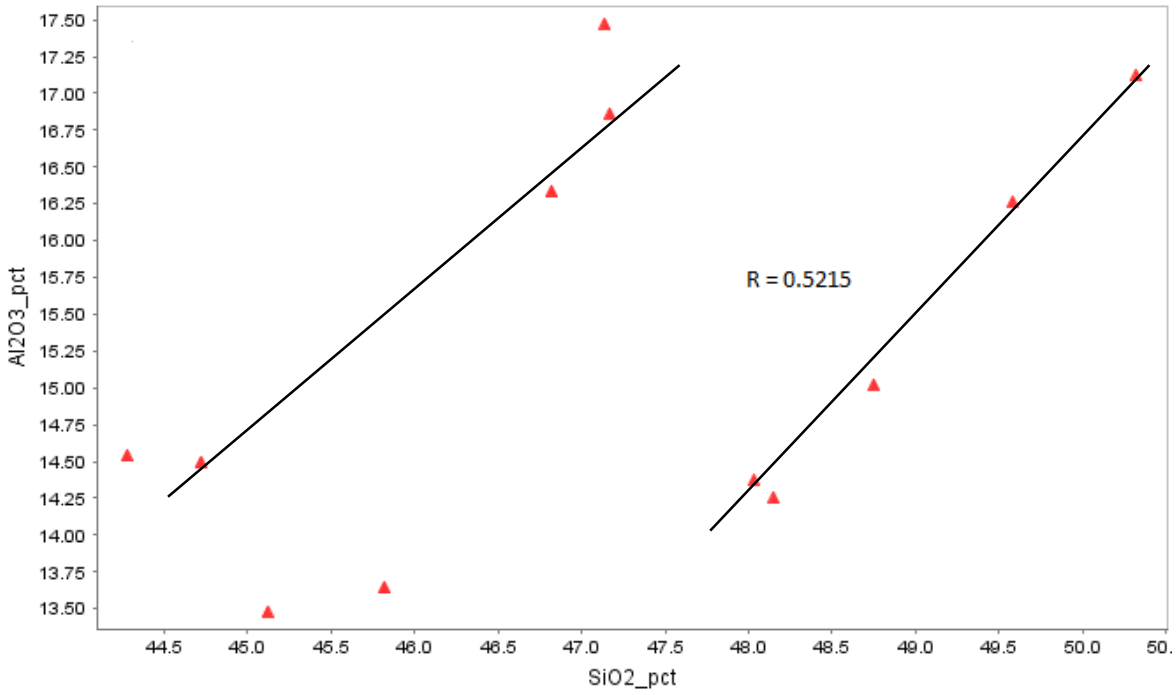

(d)

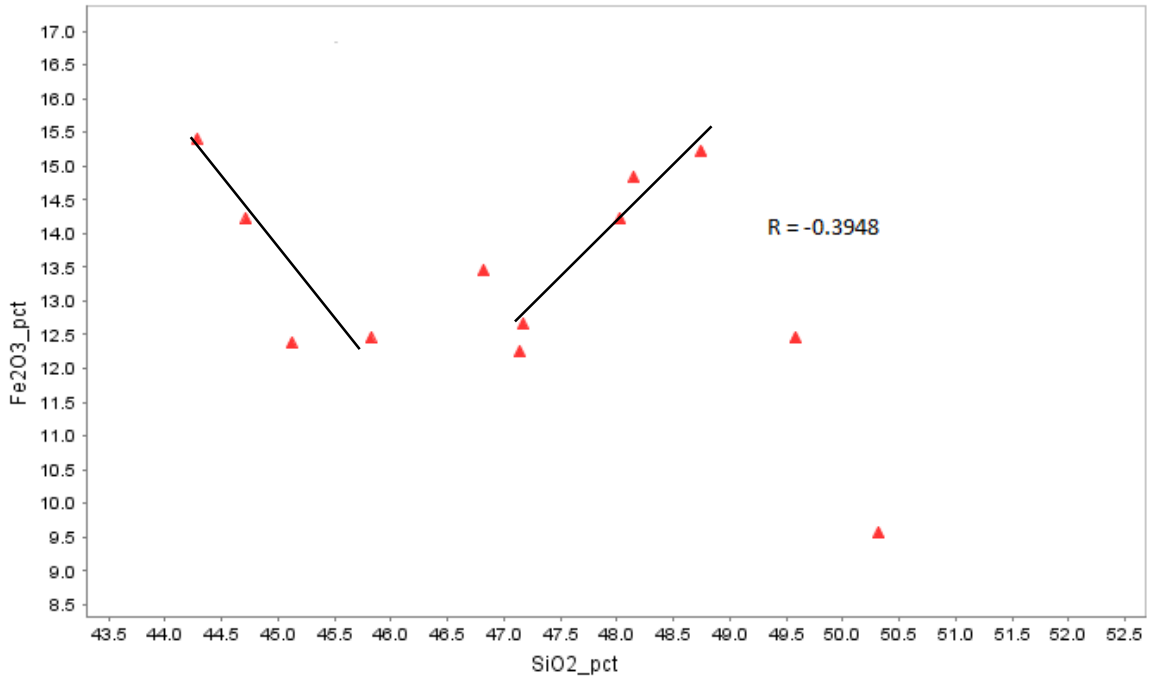

(e)

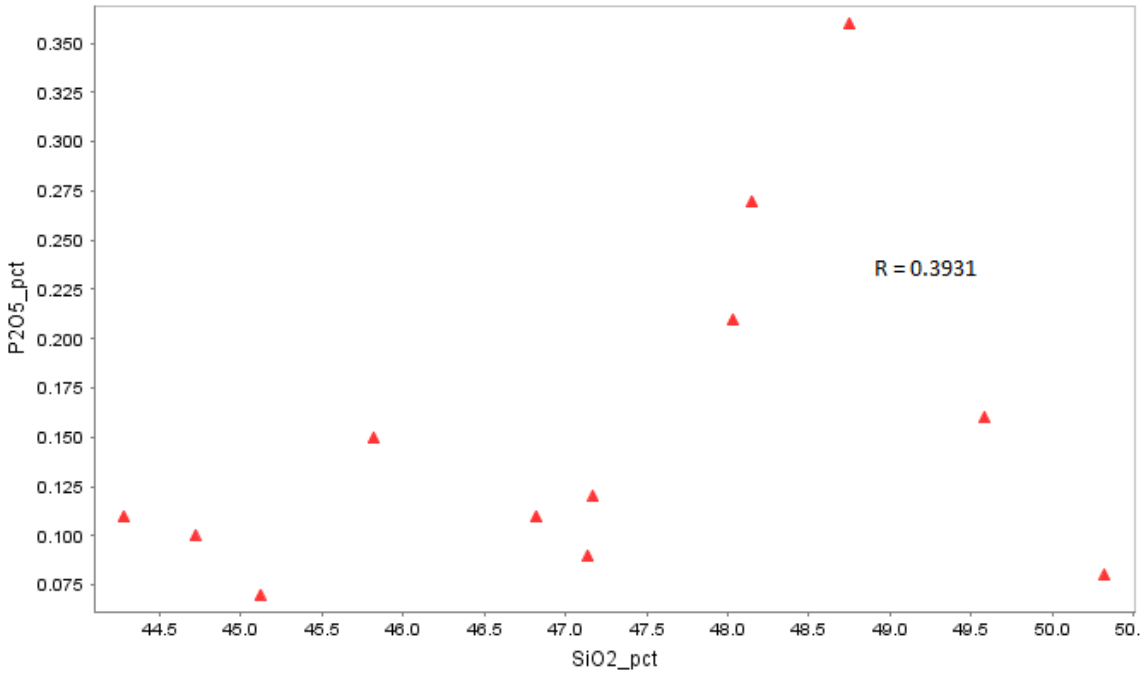

(f)

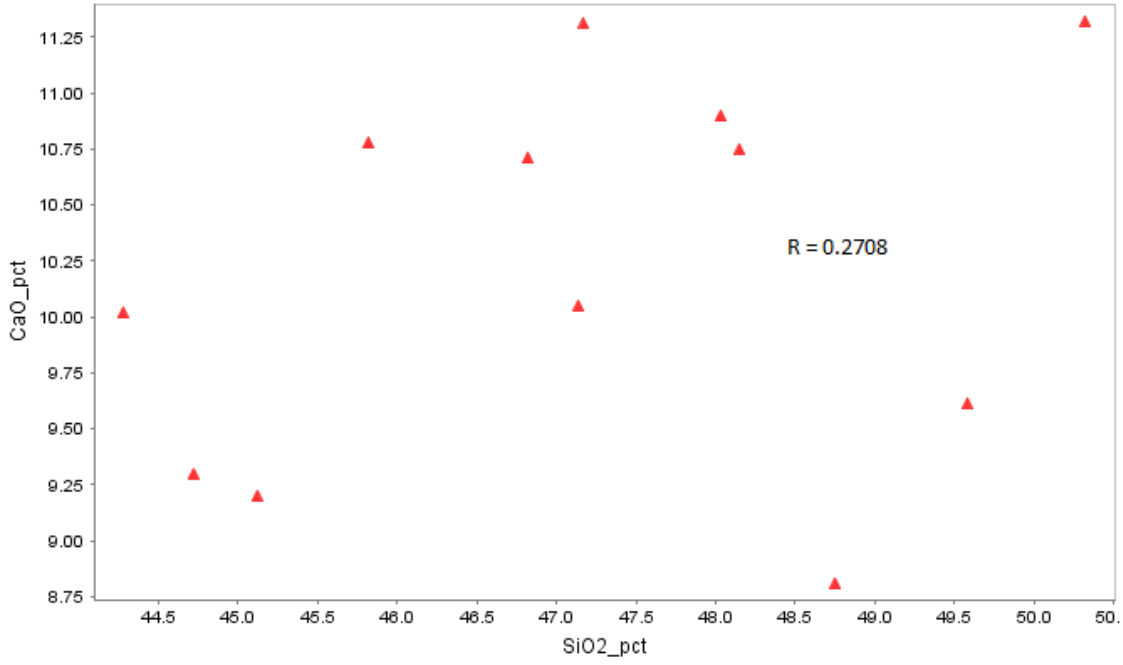

(g)

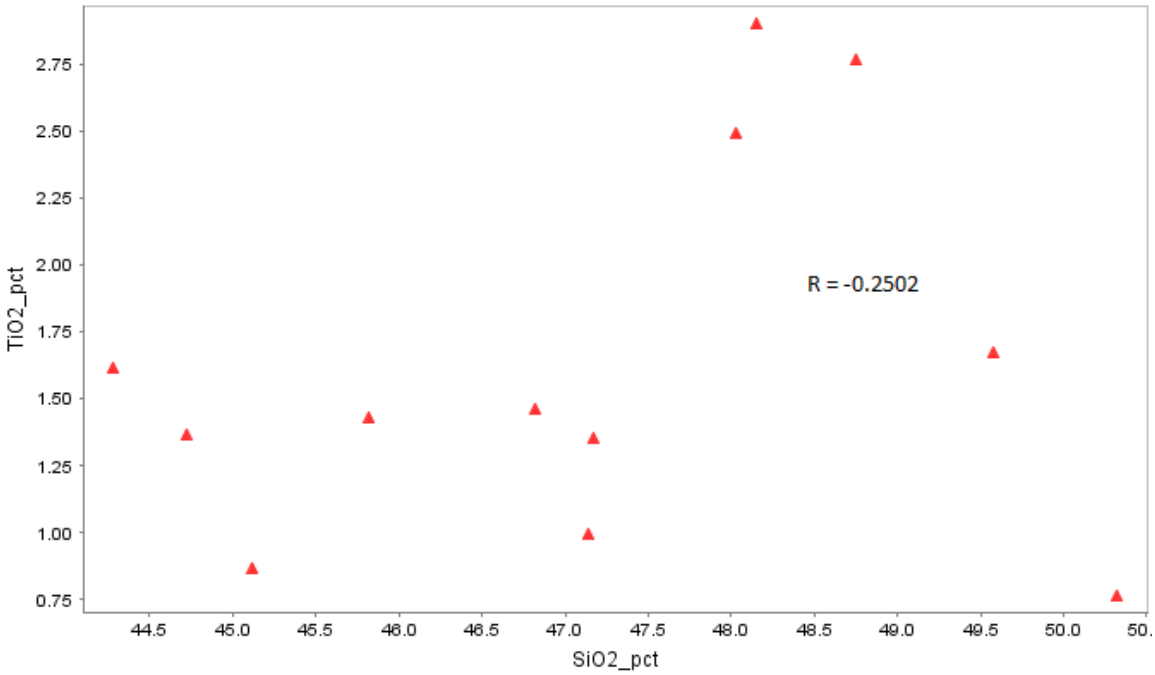

(h)

Figure 4.5: SiO_2 variation plots for major oxides in percentage weights; where (a) = SiO_2 vs MgO; (b) = SiO_2 vs K_2O; (c) = SiO_2 vs Na_2O; (d) = SiO_2 vs Al_2O_3; (e) = SiO_2 vs Fe_2O_3; (f) = SiO_2 vs P_2O_5; (g) = SiO_2 vs CaO; and (h) = SiO_2 vs TiO_2 (R = Pearson linear correlation coefficient factor).

Major elements which show good linear correlation with MgO (+ve and –ve) of $R \geq 0.75$ are K_2O (-0.7198) and Na_2O (-0.8728), whilst those which exhibit moderate correlation of $0.75 > R \geq 0.5$ are Al_2O_3 (-0.5166), TiO_2 (-0.5265) and P_2O_5 (-0.5777). The rest, apart from SiO_2 which is already reported above, that include; Fe_2O_3, MnO and CaO show no correlation (Figure 4.6). The good to moderate correlation of Na, K and Al to with SiO_2 and MgO indicates that the elements experienced insignificant post solidus mobility.

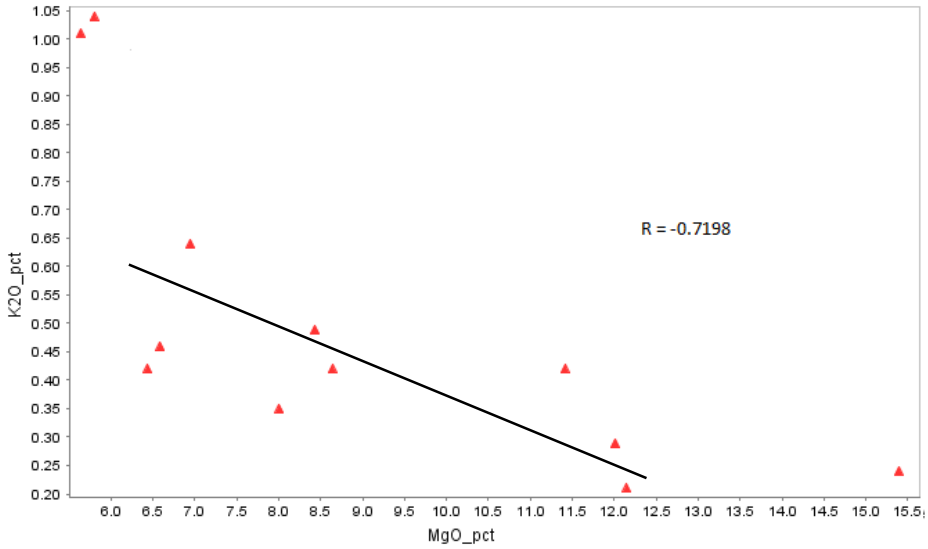
R = -0.7198
K2O_pct
MgO_pct

(a)

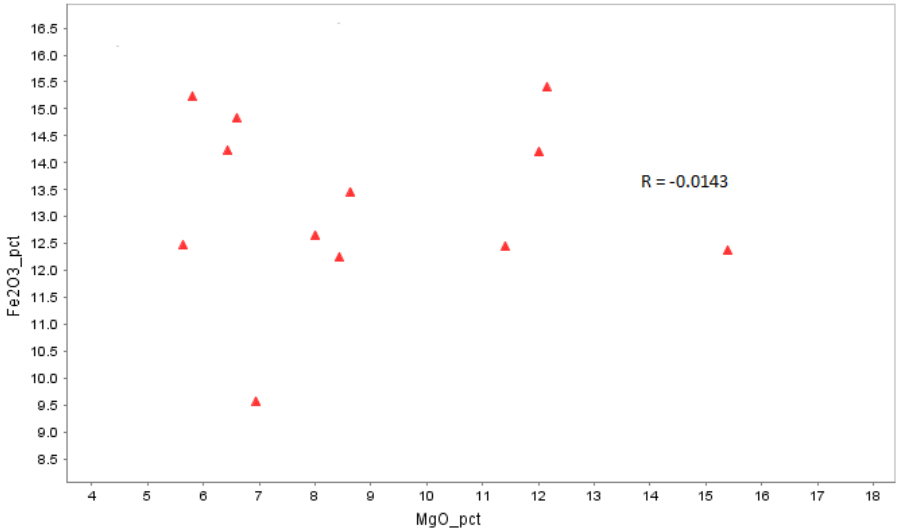
R = -0.0143
Fe2O3_pct
MgO_pct

(b)

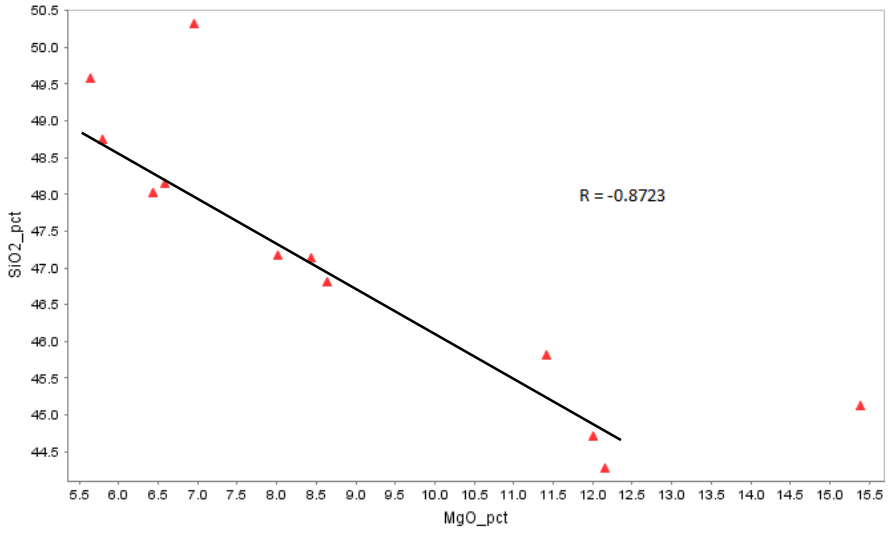
R = -0.8723
SiO2_pct
MgO_pct

(c)

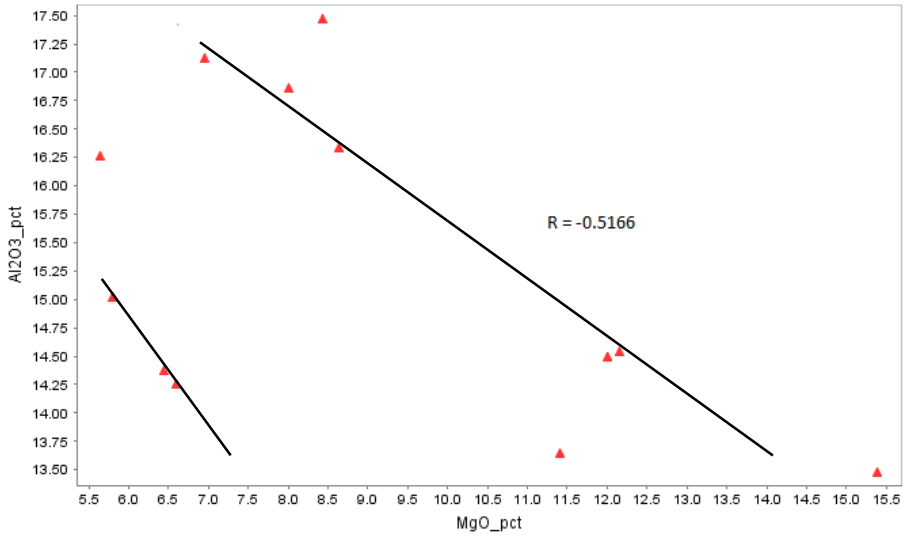
Al2O3_pct
MgO_pct
R = -0.5166

(d)

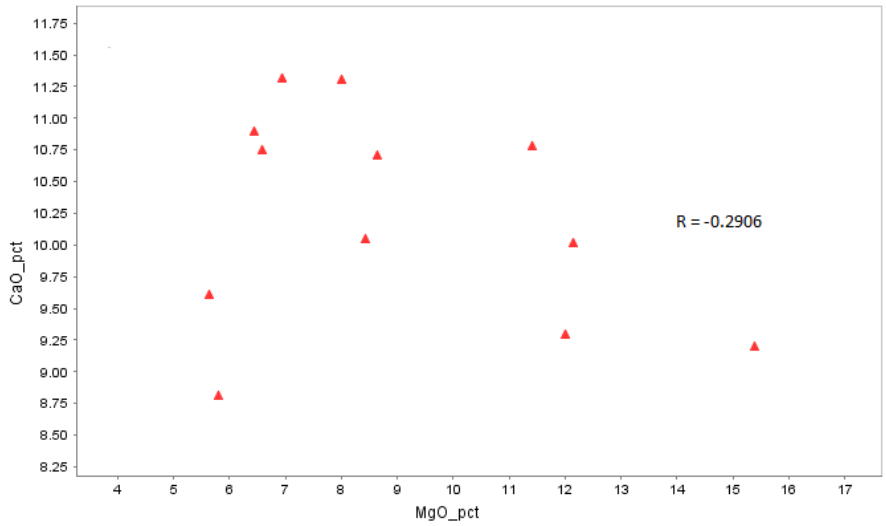
CaO_pct
MgO_pct
R = -0.2906

(e)

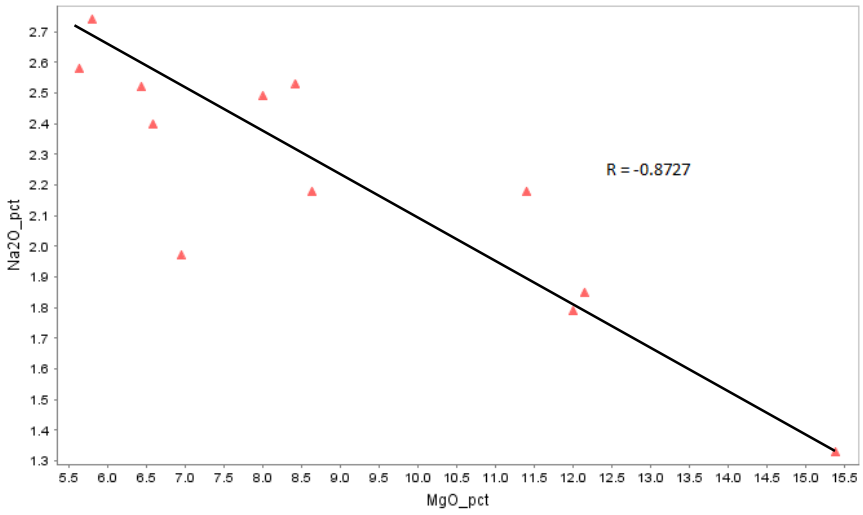
Na2O_pct
MgO_pct
R = -0.8727

(f)

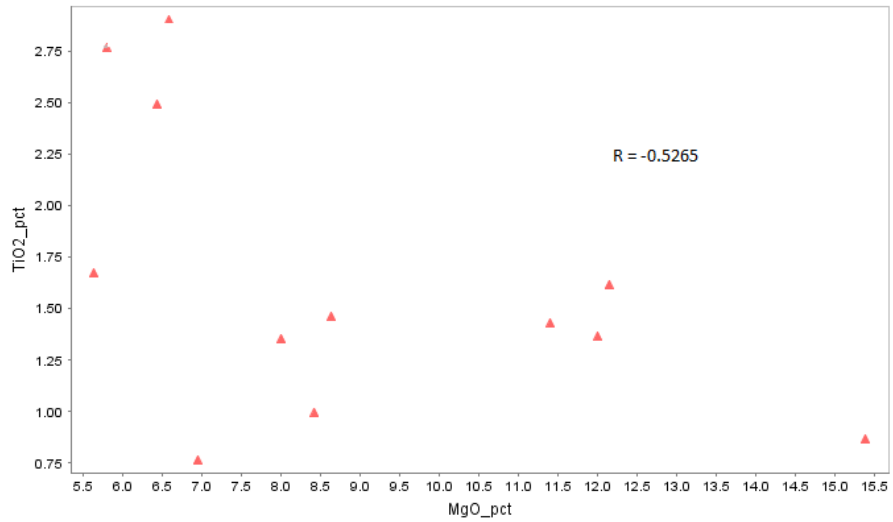

(g)

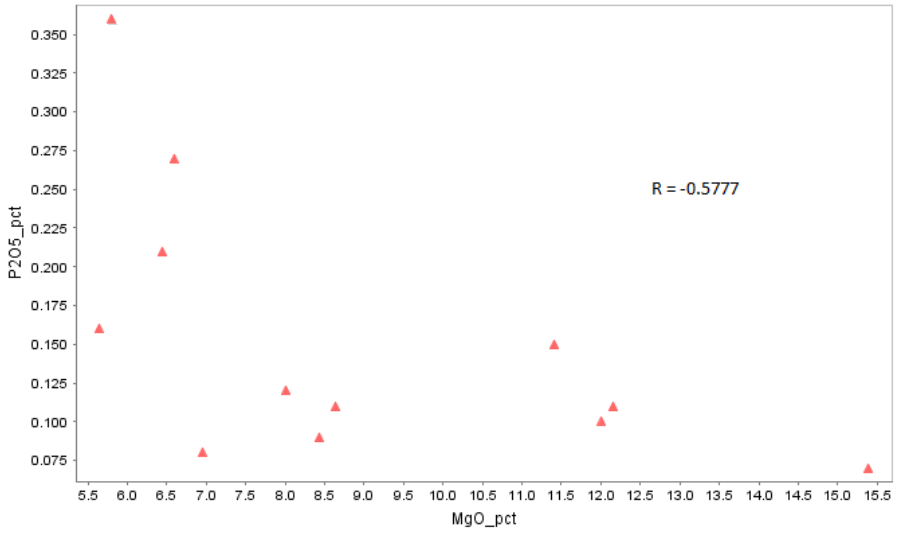

(h)

Figure 4.6: MgO variation plots for major oxides in percentage weights; where (a) = MgO vs K_2O; (b) = Mg vs Fe_2O_3; (c) = MgO vs SiO_2; (d) = MgO vs Al_2O_3; (e) = MgO vs CaO; (f) MgO = Na_2O ; (g) = MgO vs TiO_2; and (h) MgO vs P_2O_5 (R = Pearson linear correlation coefficient factor).

4.3.3 Trace Element Variations

Selected trace elements, which are compatible or incompatible during fractionation of mafic melts including some REE, are plotted against Zr and MgO. For trace element variations, Zr has been chosen as an index of evolution because it; (a) shows large variation in the sample results (43 to 174 ppm), (b) is one of the elements which are least likely to be affected by alteration, and (c) is one of the most incompatible trace elements in a partial melting or crystal

fractionation process of basalt (Talusani, 2010). Three main compatible trace elements, Ni, Cr and Co, exhibit wide content variation as follows: Ni, 80 to 720 ppm; Cr, 150 to 1400 ppm; and Co, 43 to 84 ppm. Selected incompatible trace elements also show wide content variation and these include: Sr, 91 to 325 ppm; Rb, 6 to 41 ppm; Nb, 2 to 23 ppm; Y, 17 to 29 ppm; Hf, 1.3 to 4.4 ppm and Th, 0.8 to 4.4 ppm. The compatible trace elements show good correlation with MgO; with R values of 0.931, 0.9115 and 0.9039 for Ni, Cr and Co respectively (Figure 4.7). MgO is moderately negatively correlated (0.75 > R ≥ 0.5) with incompatible trace elements; Rb, Sr, Zr, Nb, Y, Nd and Sm. It is poorly negatively correlated with V (R=-0.3531) (Figure 4.8). The positive colleration between Mg and the three compatible elements; Ni, Cr, and Co; indicates that the magma evolved and that these were used in the early phases of olivines and pyroxenes. The none compatible elements were enriched in the later phases depleted of Mg as they were not used in the earlier crystalised phases of olivines and pyroxenes.

Zr shows good correlation (R>0.75) with incompatible trace elements, Hf, Nb, Y, La, V, Nd, Sm and Ce. It shows a moderate correlation (0.75 > R ≥ 0.5) with Yb and Lu, whilst it exhibits poor correlation with Th (R=0.4294) and Cu (R=0.1838) (Figure 4.9).

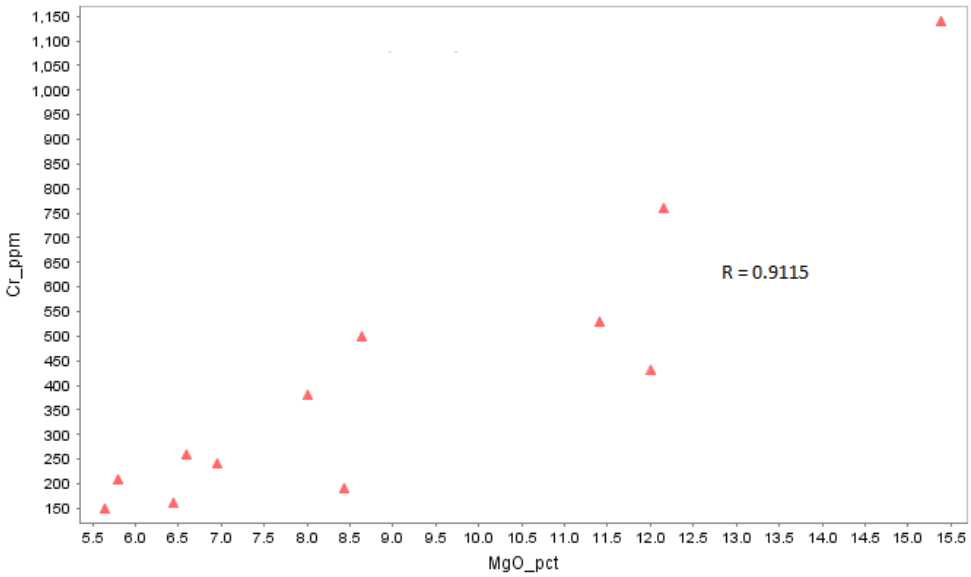

(a)

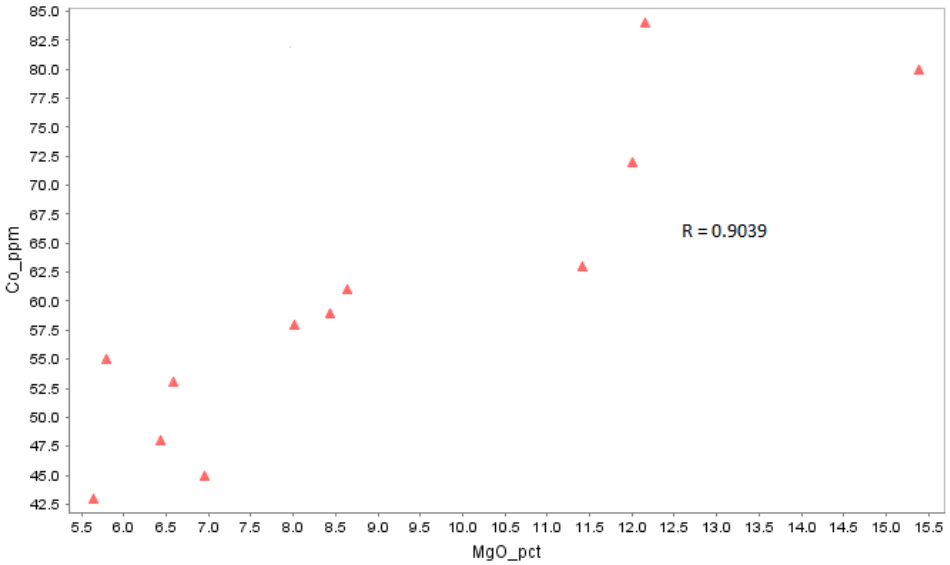

(b)

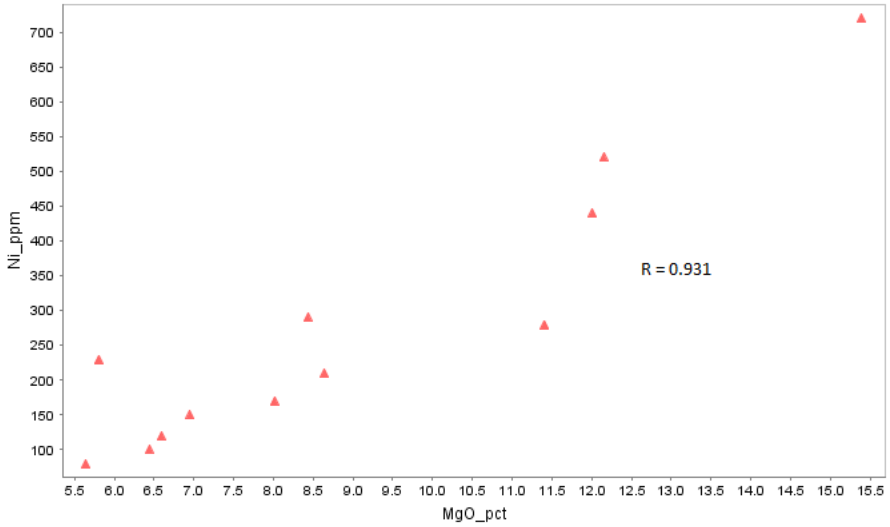

(c)

Figure 4.7: MgO variation plots with some compatible trace elements where (a) = MgO vs Cr; (b) = MgO vs Co; and (c) = MgO vs Ni (R = Pearson linear correlation coefficient factor).

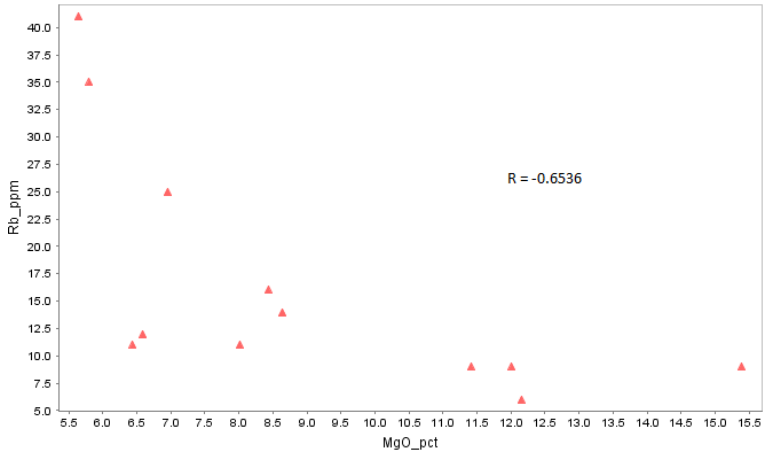

(a)

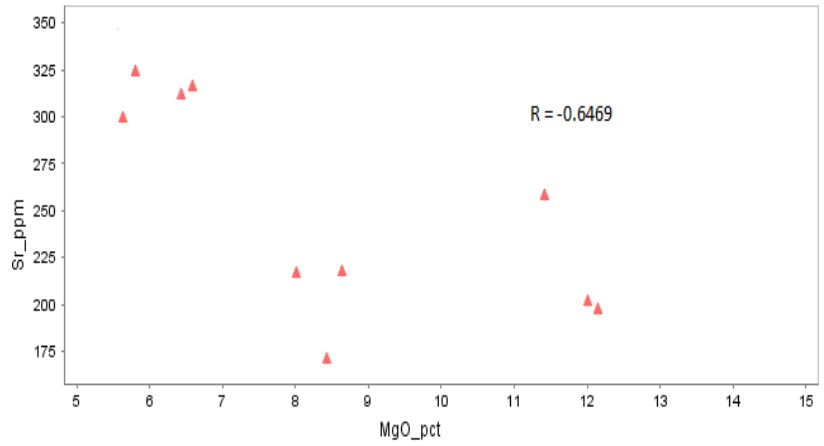
R = -0.6469
Sr_ppm
MgO_pct

(b)

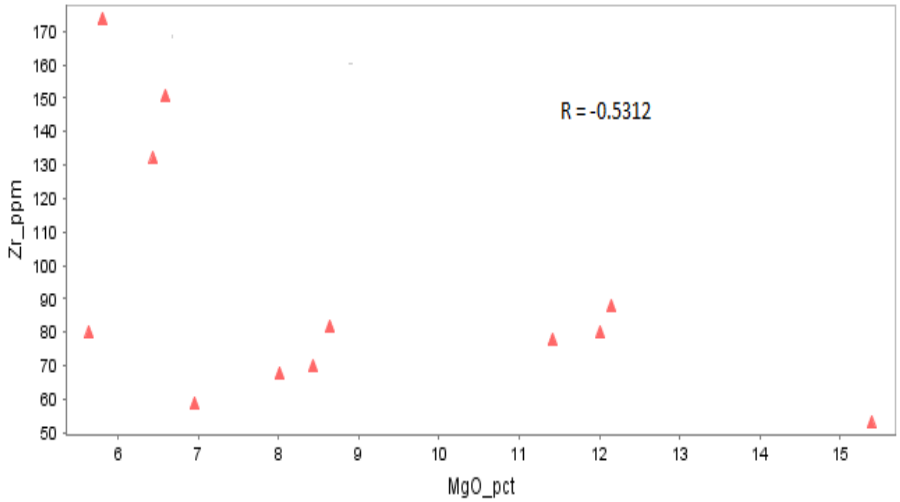
R = -0.5312
Zr_ppm
MgO_pct

(c)

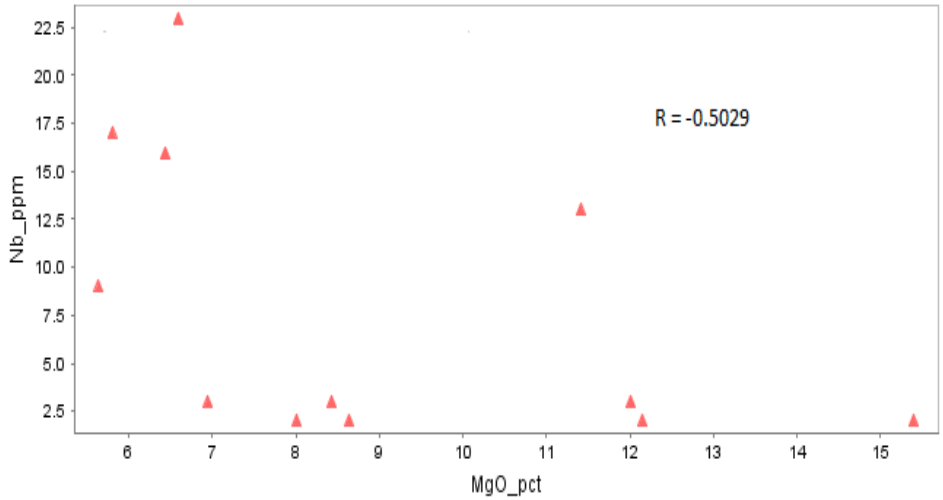
R = -0.5029
Nb_ppm
MgO_pct

(d)

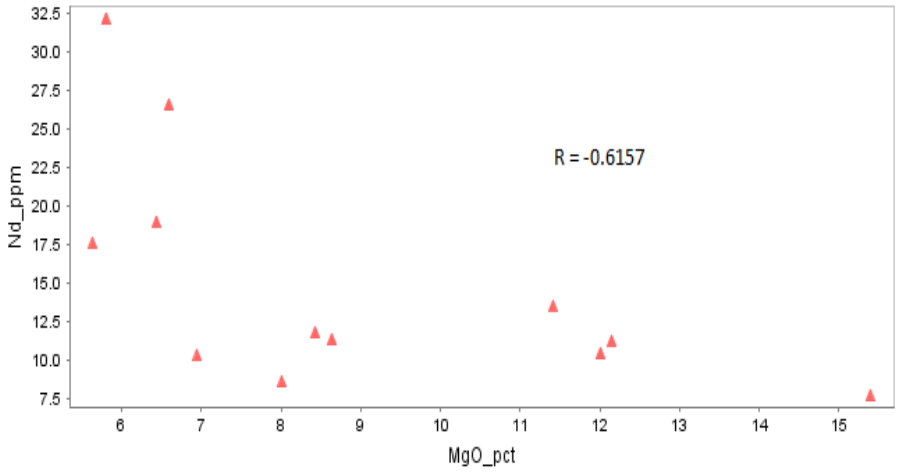

(e)

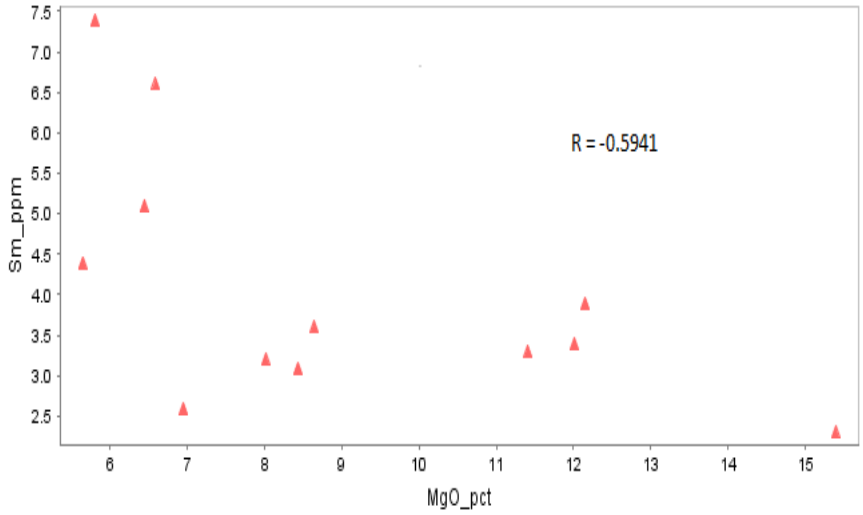

(f)

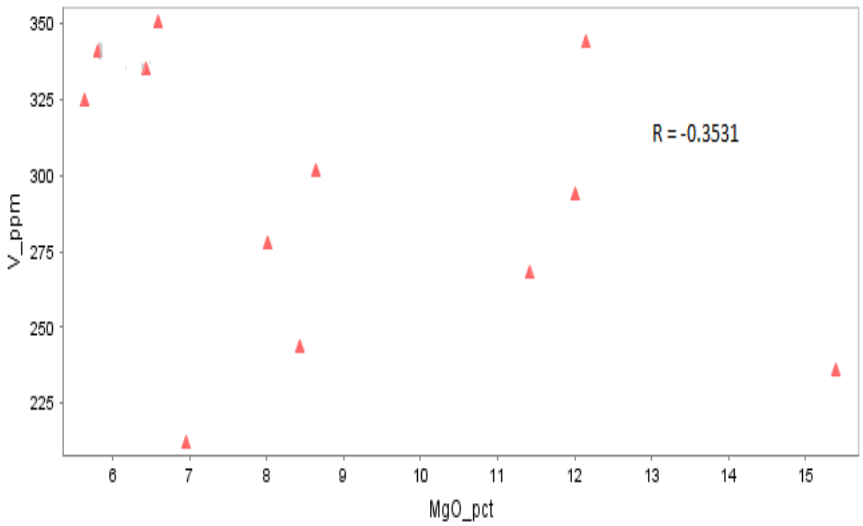

(g)

Figure 4.8: MgO variation plots with some incompatible elements where (a) =MgO vs Rb; (b) MgO vs Sr; (c) = MgO vs Zr; (d) MgO vs Nb; (e) MgO vs Nd; (f) MgO vs Sm; and (g) MgO vs V (R = Pearson linear correlation factor).

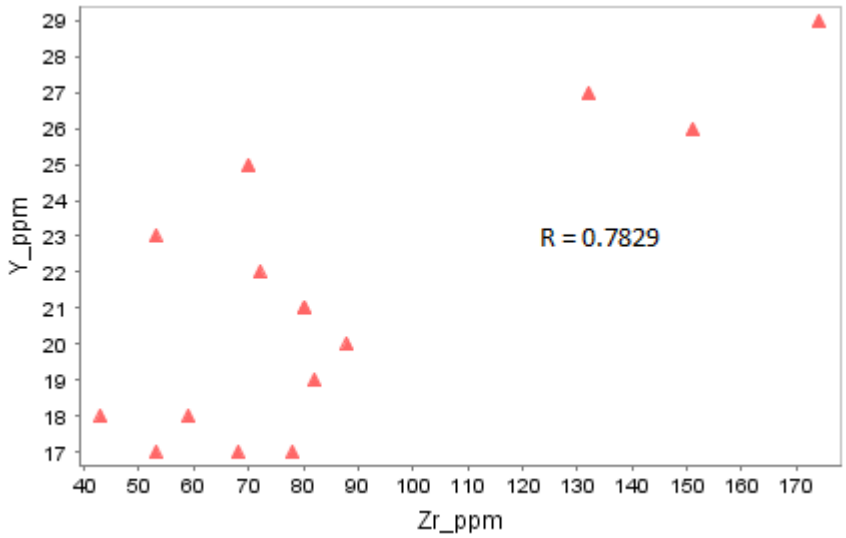

(a)

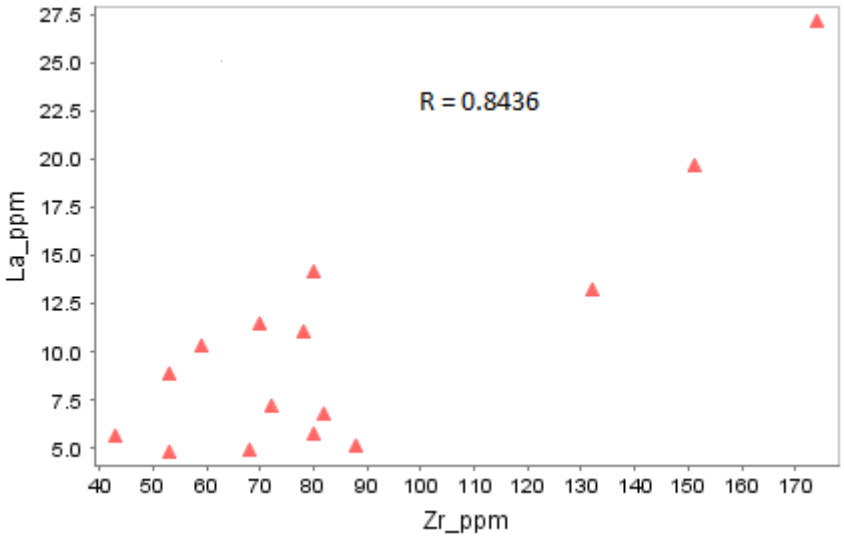

(b)

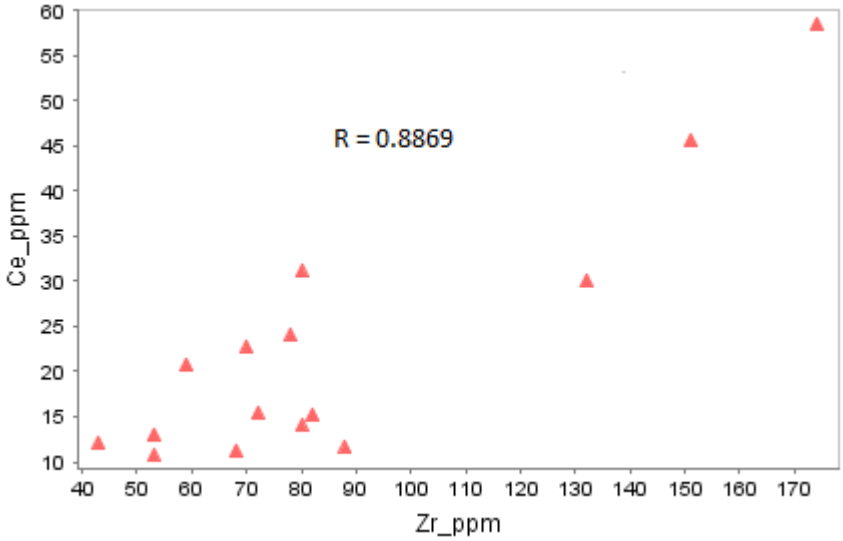

(c)

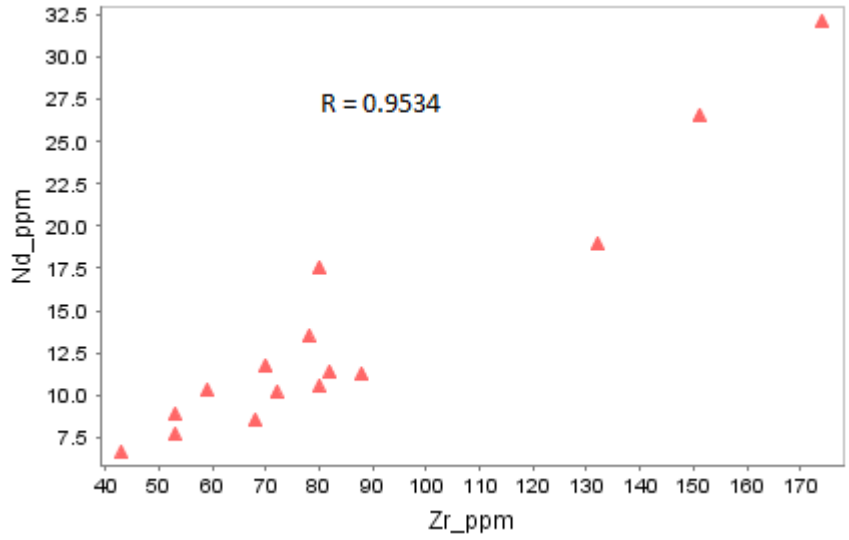

(d)

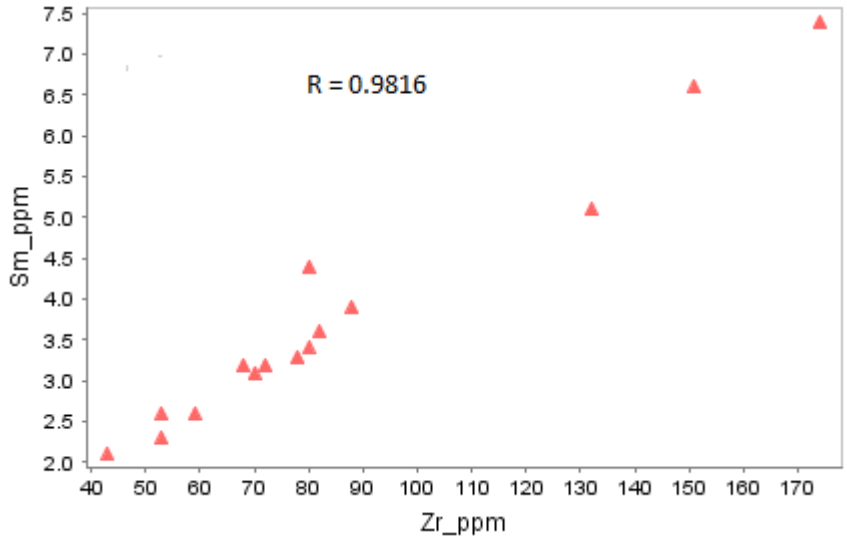

(e)

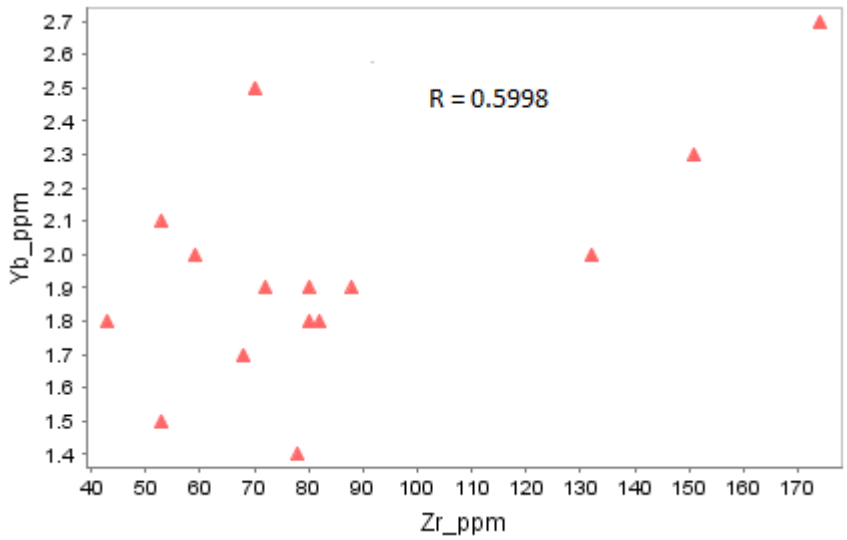

(f)

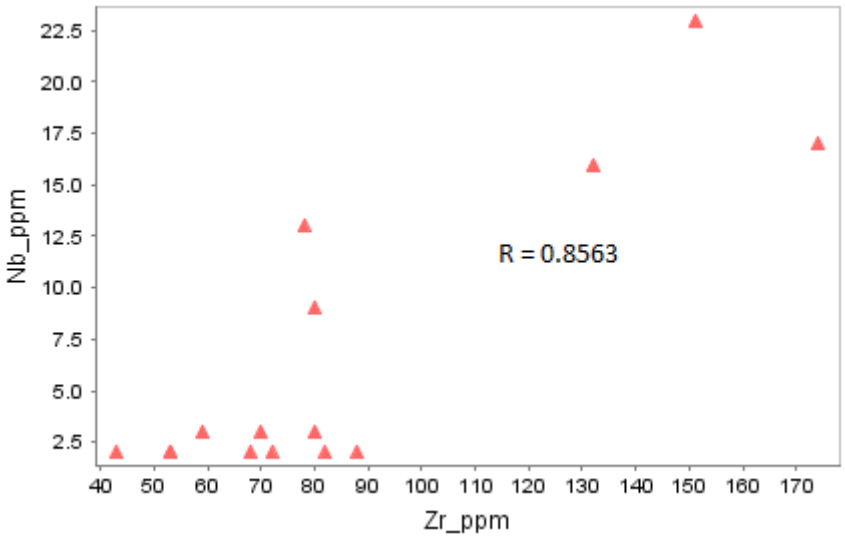
Nb_ppm
Zr_ppm
R = 0.8563

(g)

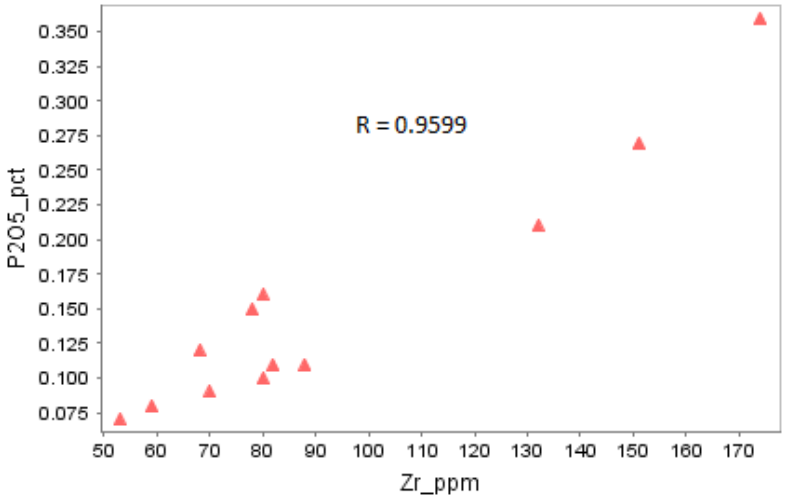
P2O5_pct
Zr_ppm
R = 0.9599

(h)

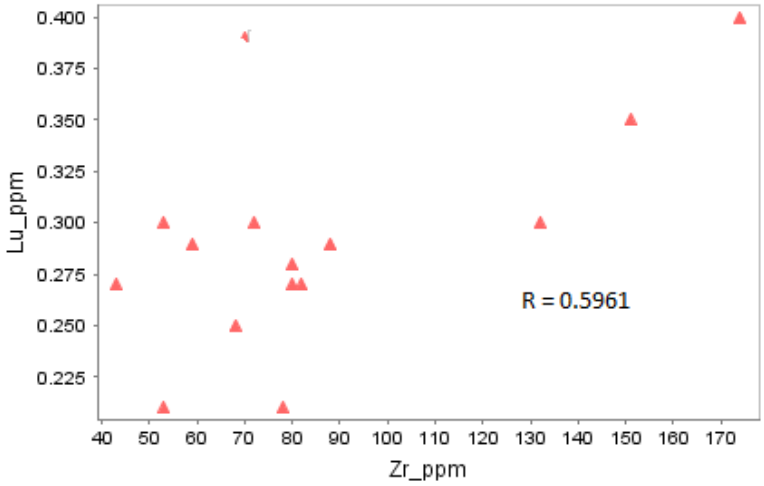
Lu_ppm
Zr_ppm
R = 0.5961

(i)

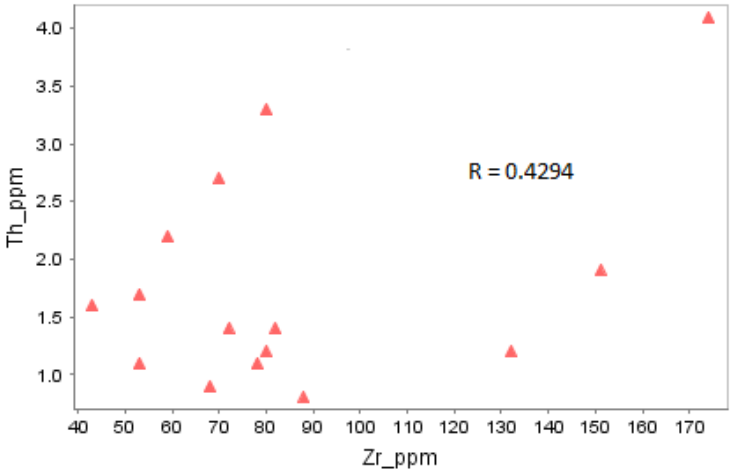

(j)

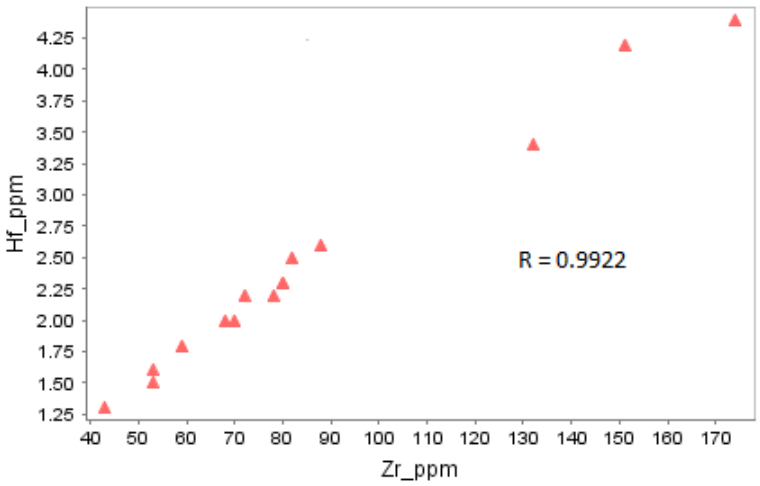

(k)

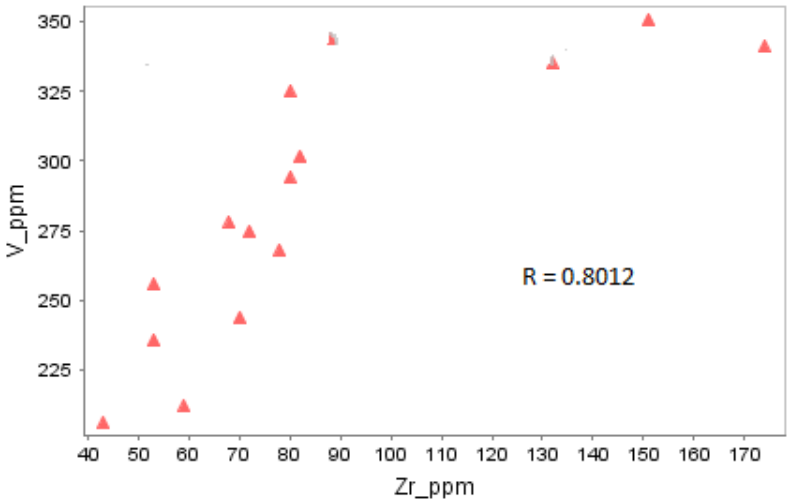

(l)

Figure 4.9: Zr variation plots with some immobile elements where (a) = Zr vs Y; (b) = Zr vs La; (c) = Zr vs Ce; (d) = Zr vs Nd; (e) = Zr vs Sm; (f) = Zr vs Yb; (g) = Zr vs Nb; (h) = Zr Vs P_2O_5; (i) = Zr vs Lu; (j) = Zr vs Th; (k) = Zr vs Hf; and (l) = Zr vs V (R = Pearson linear correlation factor).

In general, High Field Strength Elements (HFSE) and rare earth elements (REE), exhibit good correlations with fractionation indices, MgO and Zr, further indicating their immobile characteristic under secondary processes, or that in this particular study, there is insignificant effect from secondary processes.

4.3.4 Geochemical Classification of Rocks

The rocks are classified according to the total alkali-silica (TAS) model diagrams of Cox et al. (1979, adapted by Wilson 1989) and Middlemost (1984); and other discrimination digrams, e.g. $FeO_{(T)}$/MgO vs $FeO_{(T)}$ and $FeO_{(T)}$/MgO vs SiO_2 (Miyashiro 1974). The good to moderate correlation of key elements which are used in TAS plots, Na and K, with index of SiO_2 and MgO, indicates that these elements experienced no or insignificant post solidus mobility. Therefore the same elements could be used with confidence in the TAS plots. On the TAS model diagram of Cox et al. (1979), all the samples plot in the gabbro field apart from one outlier that has the lowest total alkalis (Figure 4.10). On the TAS of Middlemost (1984), almost all the samples plot along the transition of alkali gabbro and gabbro fields with three samples plotting along the transition of gabbro and peridogabbro (Figure 4.11).

Mineralogically, the rocks are classified according to the IUGS model diagrams of Streckeisen (1976) using modal abundances of plagioclase, pyroxenes and hornblende. On the Streckeisen (1976) Classification and Nomenclature of Igneous Rocks for plagioclase-pyroxenes-hornblende, and plagioclase-orthopyroxene-clinopyroxene models (Figure 4.12), all the samples plot in the gabbroids field apart from one outlier with higher anorthosite content.

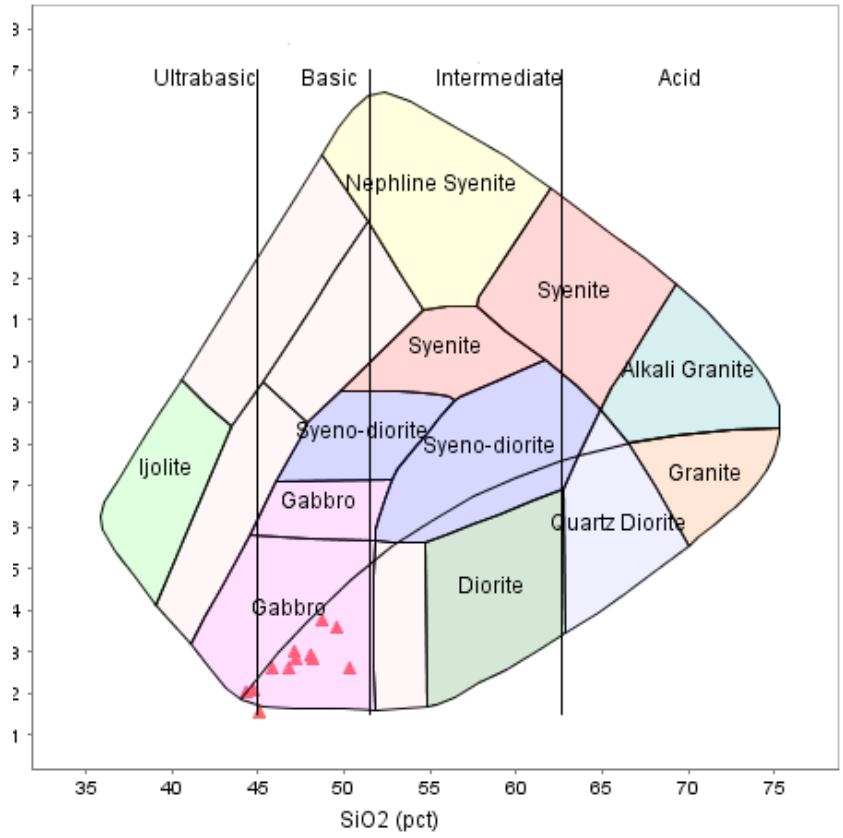

Figure 4.10: TAS Plutonic Igneous Rocks Plot (Cox et al. 1979 adapted by Wilson 1989).

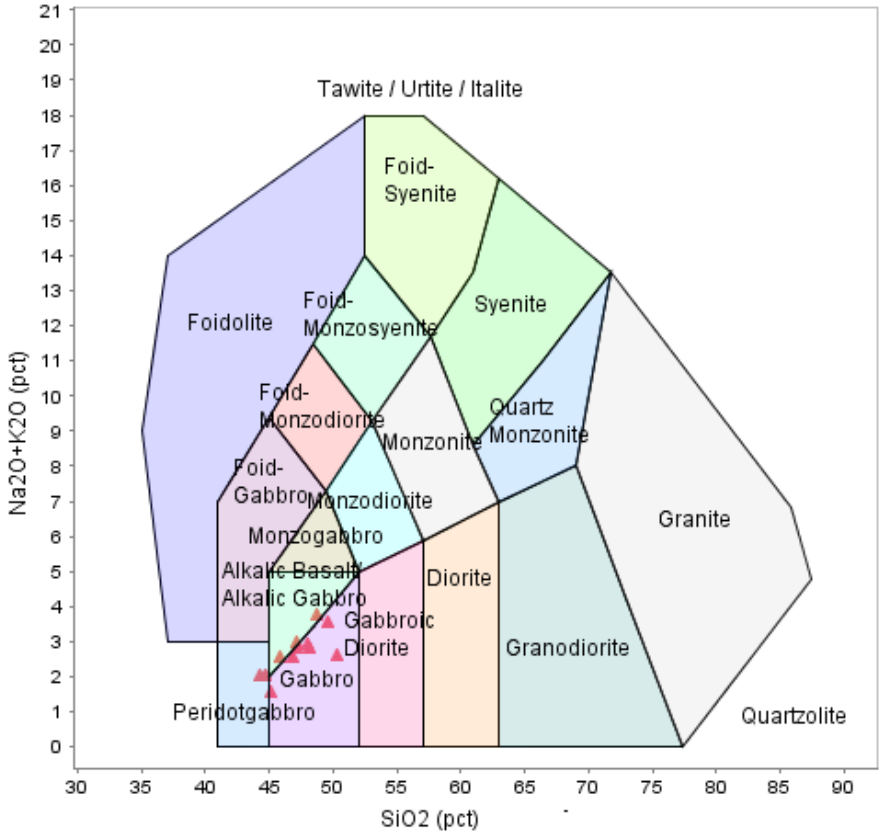

Figure 4.11: TAS Plutonic Igneous Rocks Plot (Middlemost, 1994).

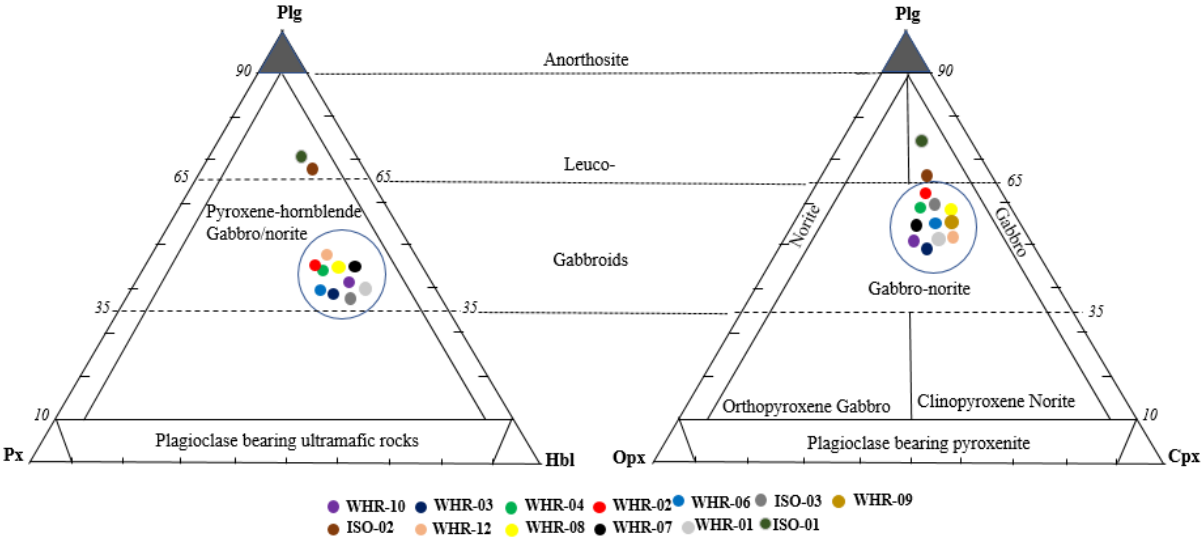

Figure 4.12: Plots of the dyke rock samples on the IUGS models, Plg-Px-Hbl and Plg-Opx-Cpx, of Streckeisen (1976) for Classification and Nomenclature of Igneous Rocks.

The mafic rocks of the dykes studied are of sub-alkalic affinity with Nb/Y ratios ranging between 0.09 and 0.88 (Pierce, 1996) (Figure 4.13) and total Na_2O+K_2O ranging from 1.5 to 3.75 wt% (Irvine and Baragar, 1971) (Figure 4.14). They are a mixture of tholeiitic and calc-alkalic suites (Figures 4.15 and 4.16). On $FeO_{(T)}/MgO$ vs $FeO_{(T)}$ and $FeO_{(T)}/MgO$ vs SiO_2 (Miyashiro 1974) classification diagrams, five of the twelve samples plot in the tholeiitic field, whilst the other seven plot in the calc-alkalic field (Figure 4.15). On the AFM plot (Figure 4.16), the Kuno (1966) boundary clearly shows that three of the twelve samples plot in the tholeiitic field whilst six samples plot in the calc-alkaline field. The other three samples are not clear in which field they fall as the demarcation line terminates before the part where they plot. On the same plot (Figure 4.16), the Irvine and Baragar model shows that all the samples plot in the calc-alkaline field.

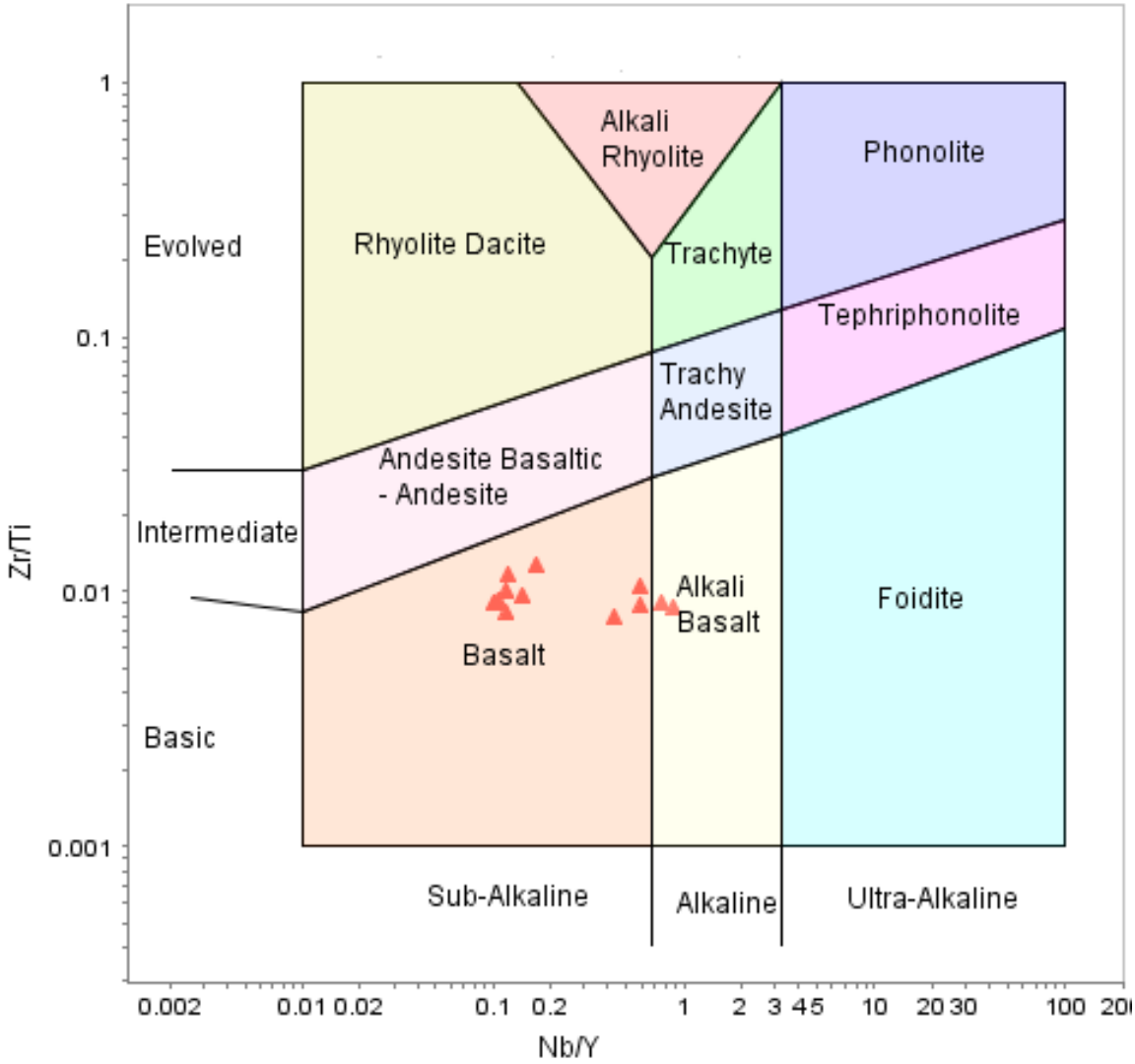

Figure 4.13: Zr/Ti-Nb/Y rock classification diagram plot of the samples of the mafic dykes of the Irumide Belt, Zambia, after Pearce, 1996.

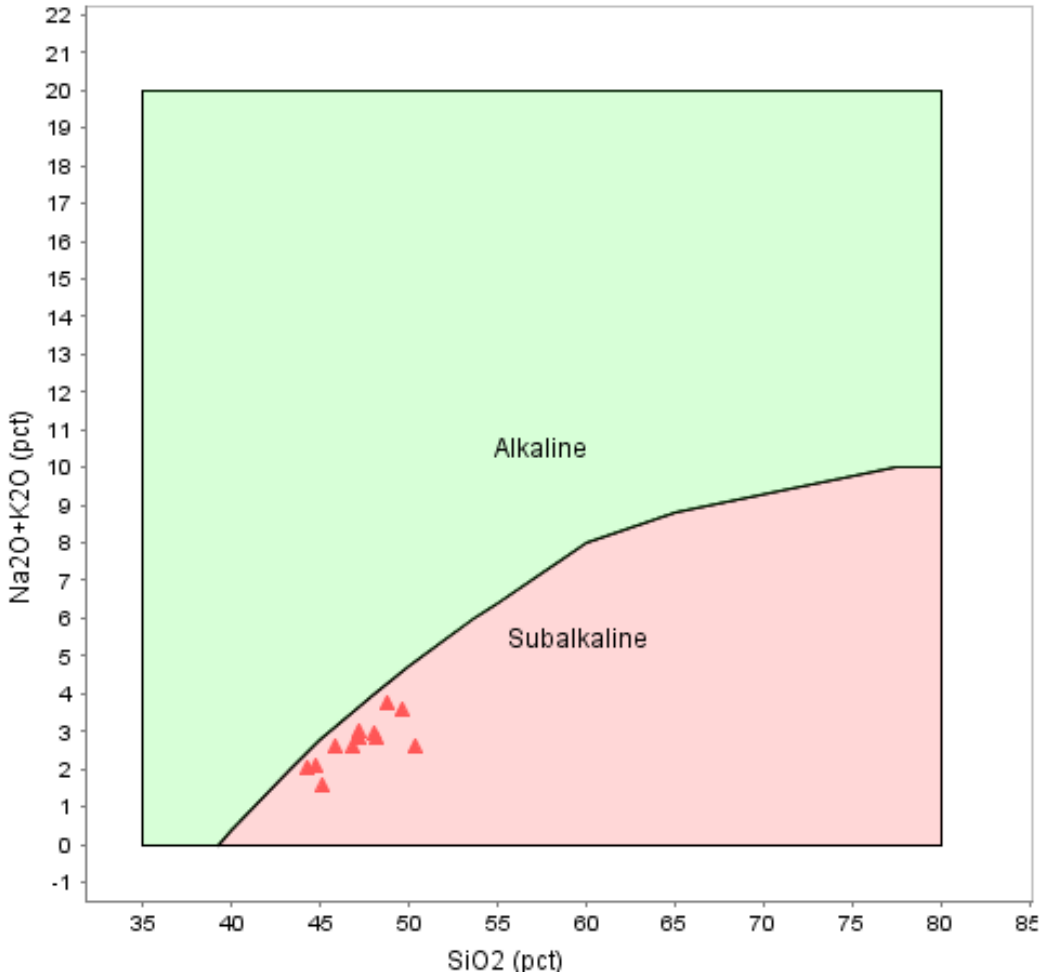

Figure 4.14: Volcanic alkaline – subalkaline curve plot of the samples of the mafic dykes of the Irumide Belt, Zambia (after Irvine and Baragar, 1971).

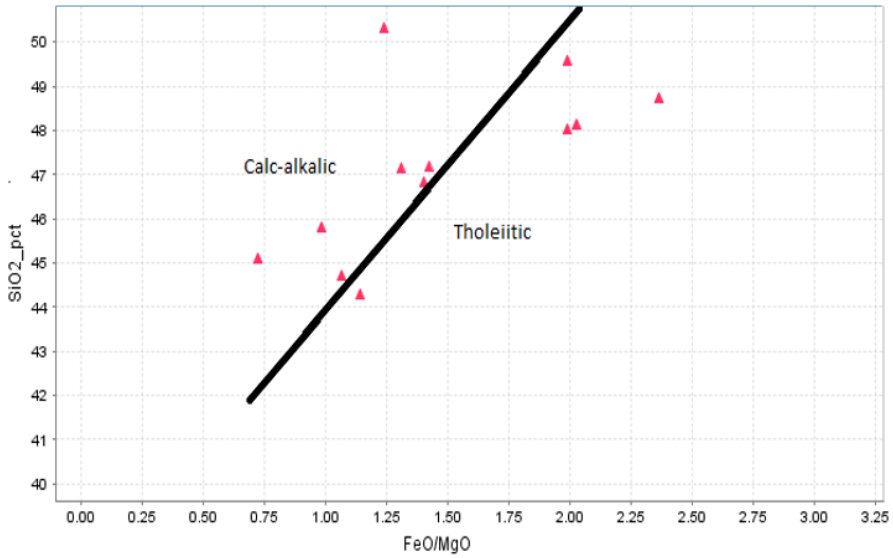

Figure 4.15: SiO_2 vs FeO/MgO plot of the samples of the mafic dykes of the Irumide Belt, Zambia after Miyashiro (1974) in Murphy et al. (2019).

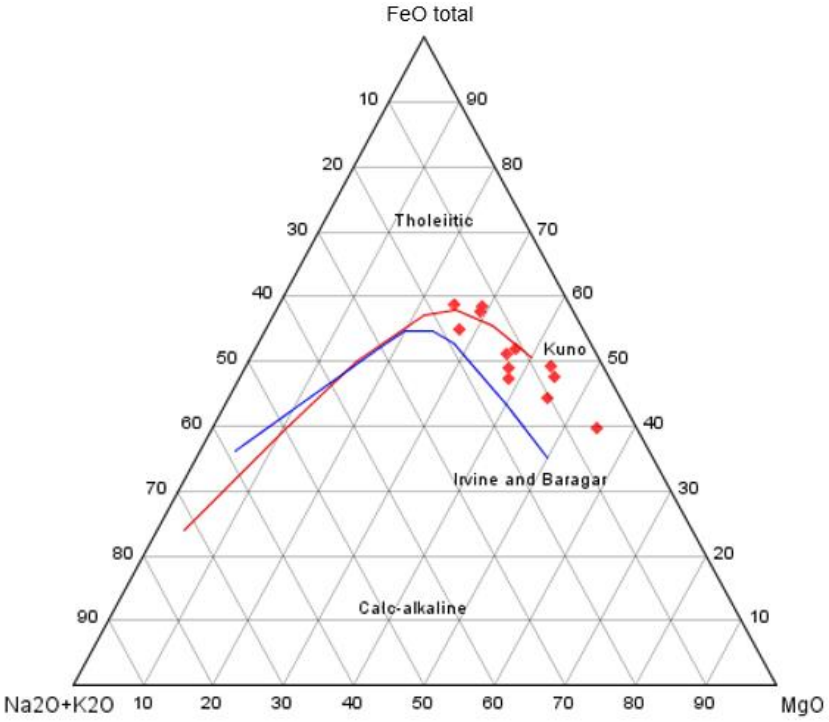

Figure 4.16: AFM plot showing classifications by Irvine and Baragar (1971); and Kuno (1966).

4.3.5 Rare Earth Elements Geochemistry

Several rare earth and multi-element (REE and ME) plots (spider diagrams) are generated from sample results, which are aimed at aiding in petrogenetic interpretations. Normalised variation diagrams for chondrite, MORB, E-MORB, N-MORB and Primitive mantle are generated for both types of dykes, tholeiitics and calc-alkalics. Geochemical trends and patterns are analysed for similarities and differences that would aid in the interpretation of data.

In Figures 4.17 and 4.18, the REE of both types of dykes are plotted in variation diagrams which are chondrite-normalised to values of McDonough and Sun (1995). Chondrite-normalised REE diagram for tholeiitic rocks show sub-parallel trends with elemental concentrations ranging between 8 to 120 times those of chondrite. Calc-alkalic rock samples do not display sub-parallel trends on Chondrite-normalised REE diagram, but have elemental concentrations ranging between about 8 and 48 times those of Chondrite. The Chondrite-normalised REE patterns displayed by the tholeiitic rock samples show close similarity to OIB, whilst the patterns of the calc-alkalic rocks seem to display signatures of between EMORB and continental crust. The diagrams show that both types of mafic rocks, tholeiitics and calc-alkalics, are strongly enriched in the light REE (LREE) over the heavy REE (HREE). In the tholeiitic rocks, LREE enrichment of La, which is the most enriched, ranges between 50-120 times more enriched than the chondrite concentrations whilst Lu, which is the least enriched

of the HREE ranges between 8-18 more enriched than the chondrite concentrations. In the calc-alkalic type of basalts, LREE are moderately enriched with La, the most enriched, ranging between 20 – 48 times more enriched than Chondrite concentrations. The enrichment of the HREE is similar to that of the tholeiitic rocks. The LREE trend has a steeper slope to the right whilst HREE exhibit a relatively flat trend.

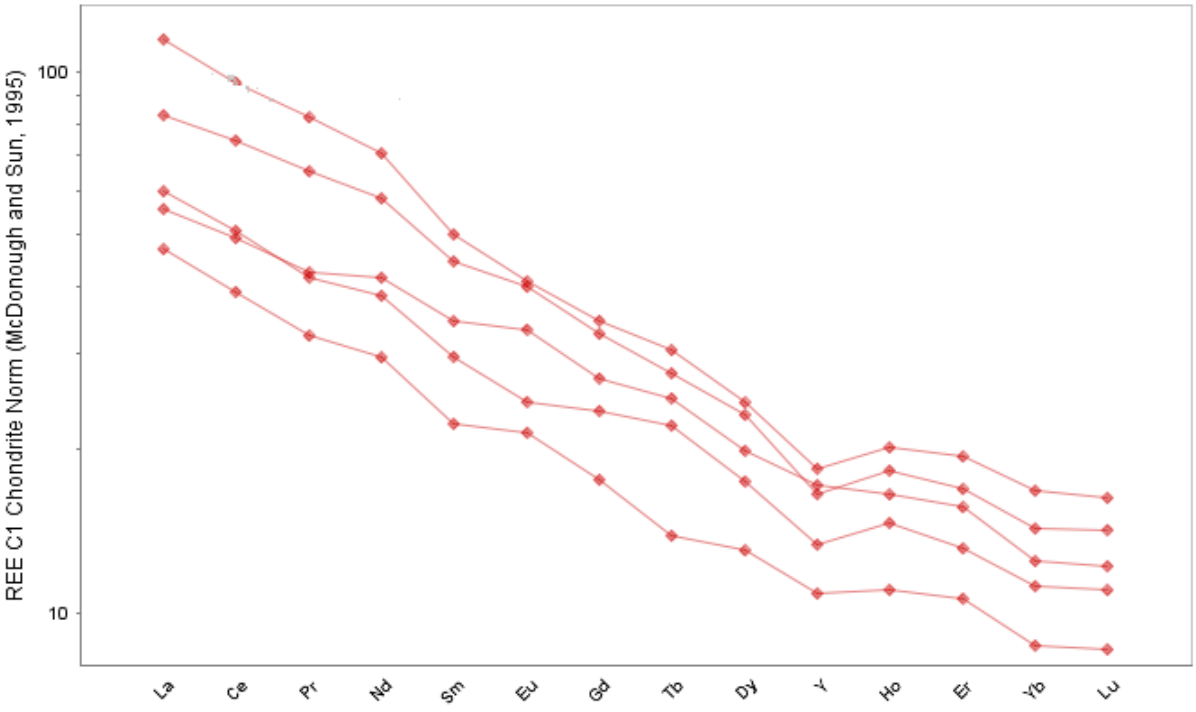

Figure 4.17: Chondrite-normalised REE plot for tholeiitic rocks of the Study area, normalising values from McDonough and Sun, 1995).

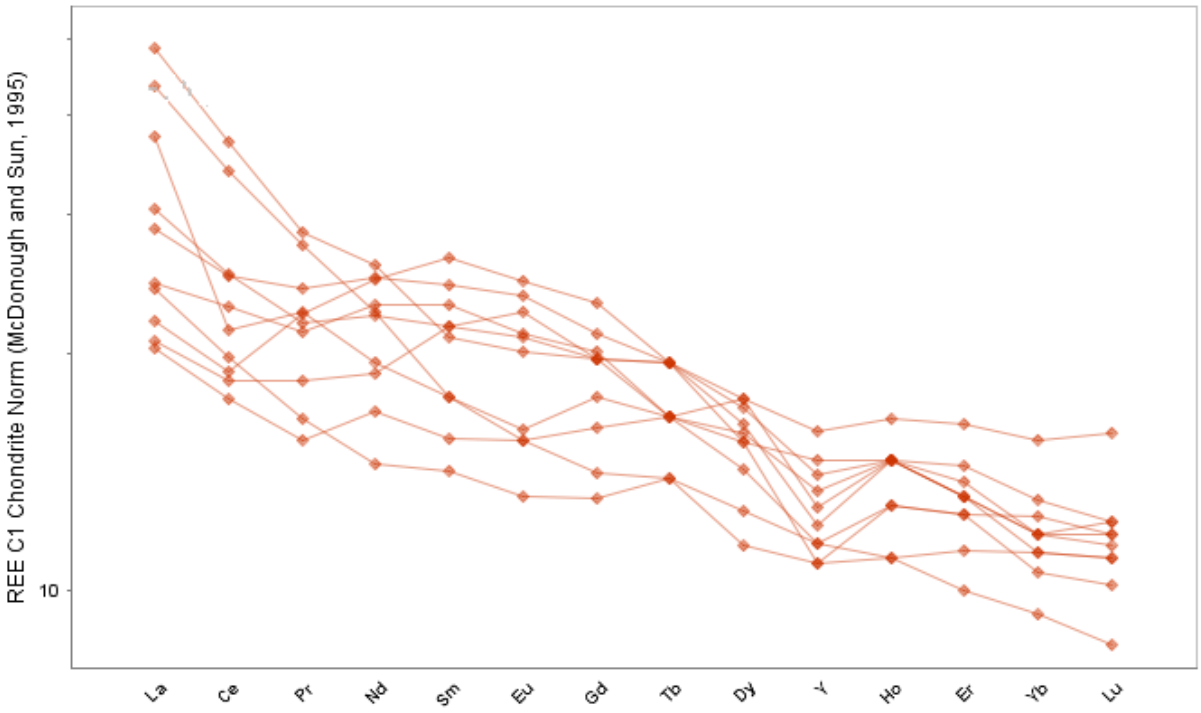

Figure 4.18: Chondrite-normalised REE variation diagram for calc-alkalic rocks of the study area, normalising values from McDonough and Sun, 1995).

On Chondrite-normalized REE diagrams, both tholeiitic and calc-alkalic dykes display a marginal to moderate negative Y anomaly (see Figures 4.17 and 4.18). On the Chondrite-normalised multi-element variation diagrams of McDonough and Sun (1995), both dykes display strong negative anomalies for HFSE that include P, W and Pb; and weakly negative anomalies in the other HFSE such as Nb, Zr and Hf (Figure 4.19). In actual fact, P is depleted relative to Chondrite in both rock types. The LILE display positive Ba and Sr anomalies but negative K anomalies. In both dyke types, there is a general increase in concentrations of the REE with increasing SiO_2 and decreasing MgO (Figure 4.20). A strong positive correlation between Zr and REE is observed, especially the LREE, which are more incompatible (Figure 4.21). This is expected as REE in general are incompatible just like Zr and are enriched in the late crystalising phases in a mafic magma at the the expence of Mg which is used up in the early crystalising phases.

(a)

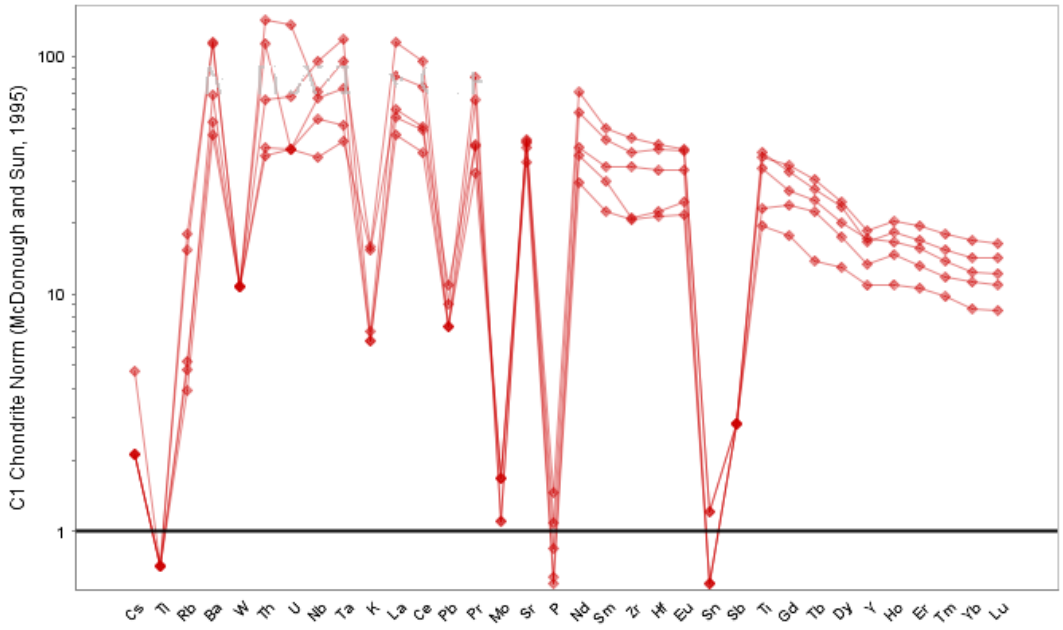

(b)

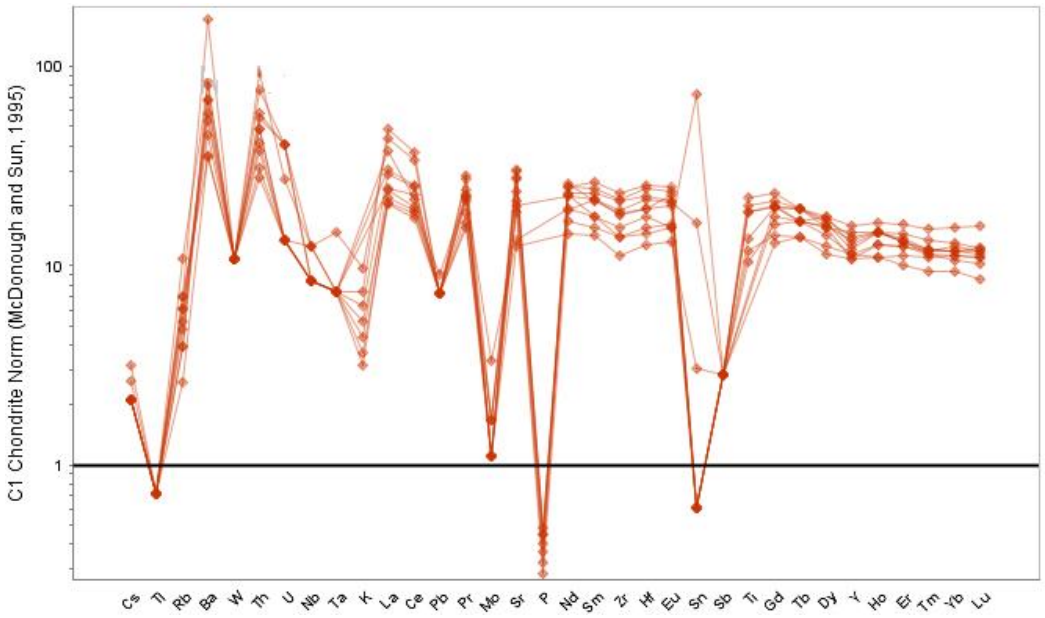

Figure 4.19: Chondrite-normalised ME variation diagram for (a) tholeiitic rocks, and (b) calc-alkalic rocks of the study area, normalising values from McDonough and Sun, 1995).

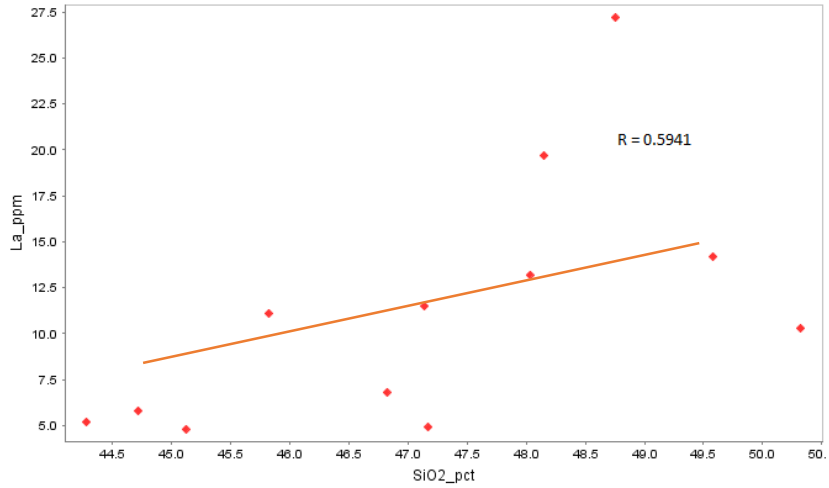
R = 0.5941
La_ppm
SiO2_pct

(a)

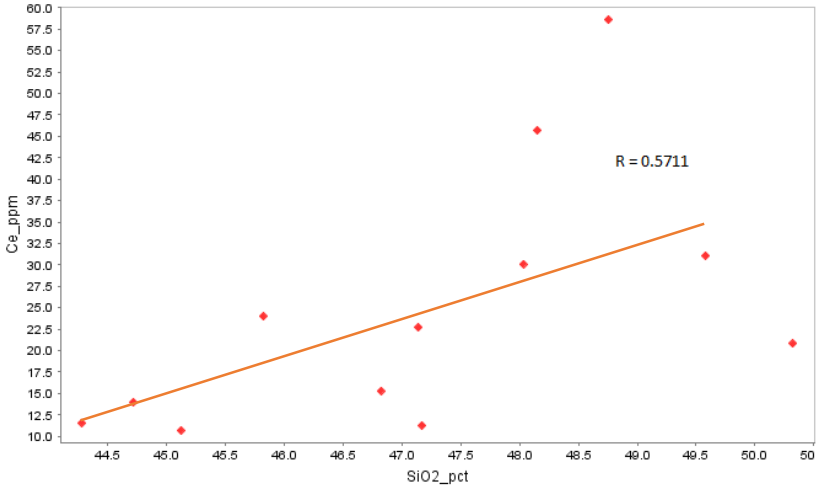
R = 0.5711
Ce_ppm
SiO2_pct

(b)

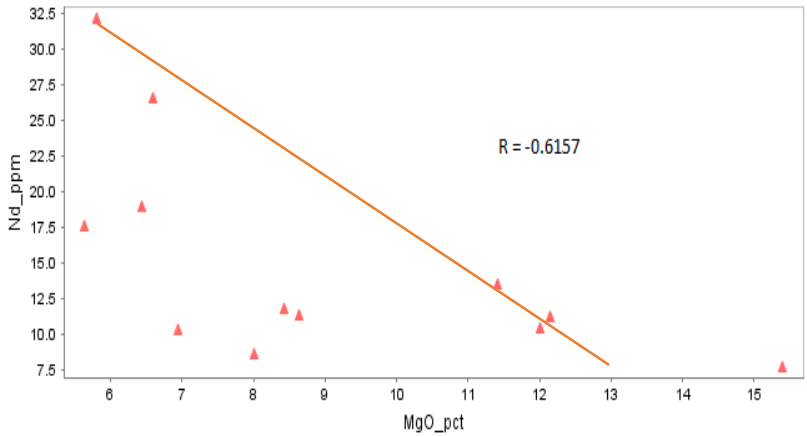
R = -0.6157
Nd_ppm
MgO_pct

(c)

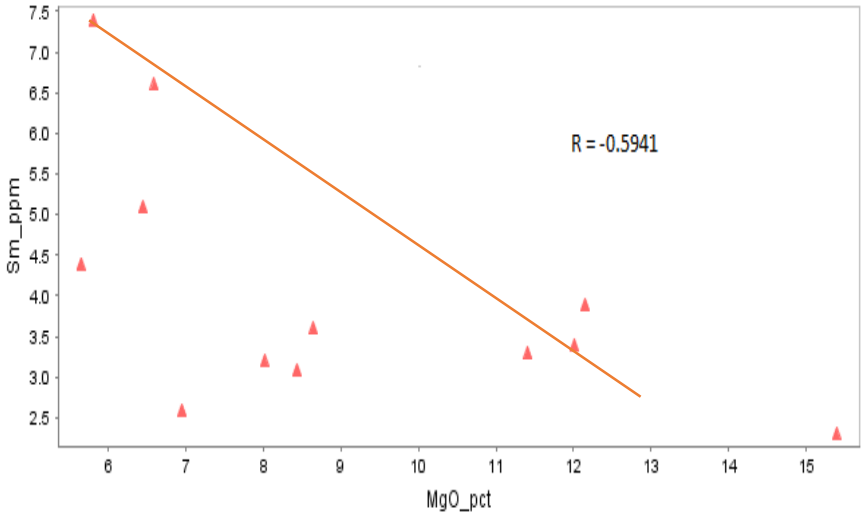

(d)

Figure 4.20: MgO and SiO_2 variatiation plots with some REE (HFSE, immobile elements) where (a) = SiO_2 vs La; (b) = SiO_2 vs Ce; (c) = MgO vs Nd; and (d) =(MgO vs Sm (R = Pearson linear correlation factor).

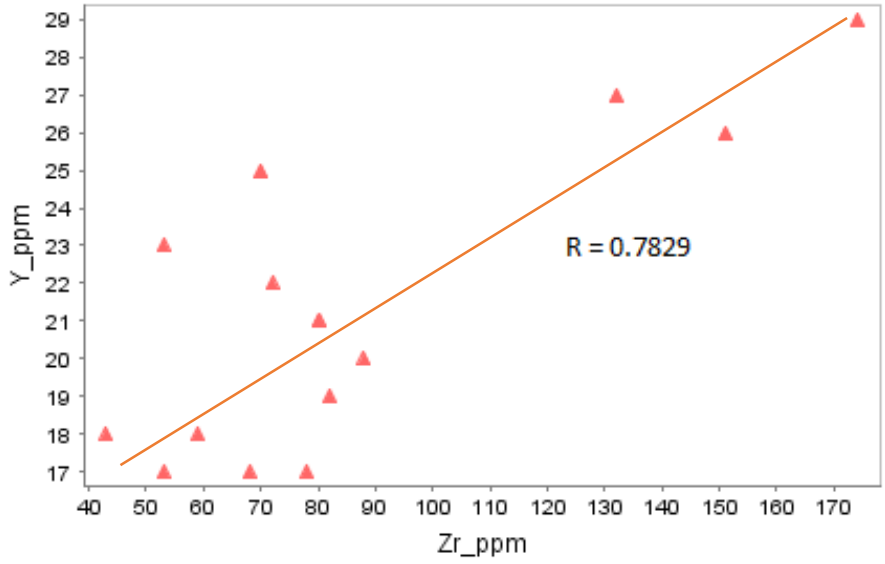

(a)

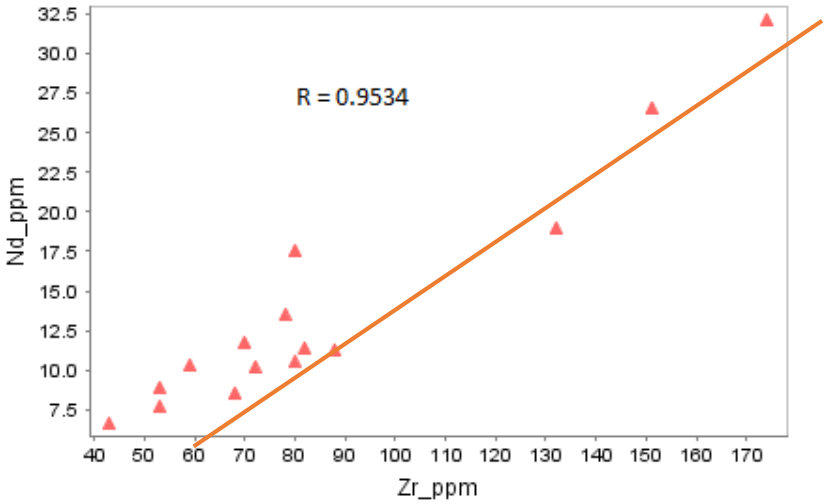

(b)

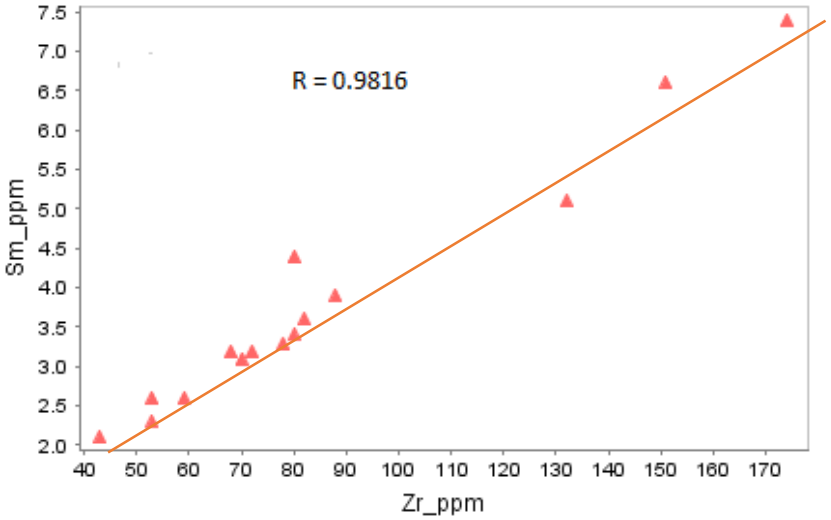

(c)

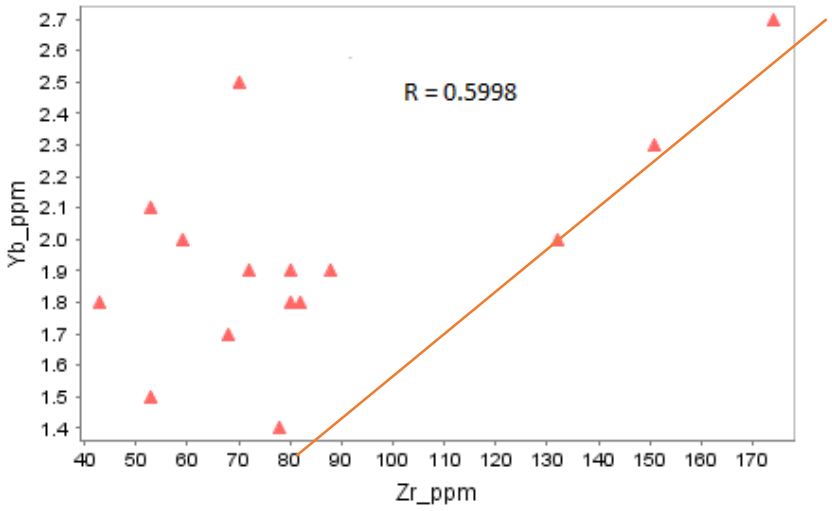

(d)

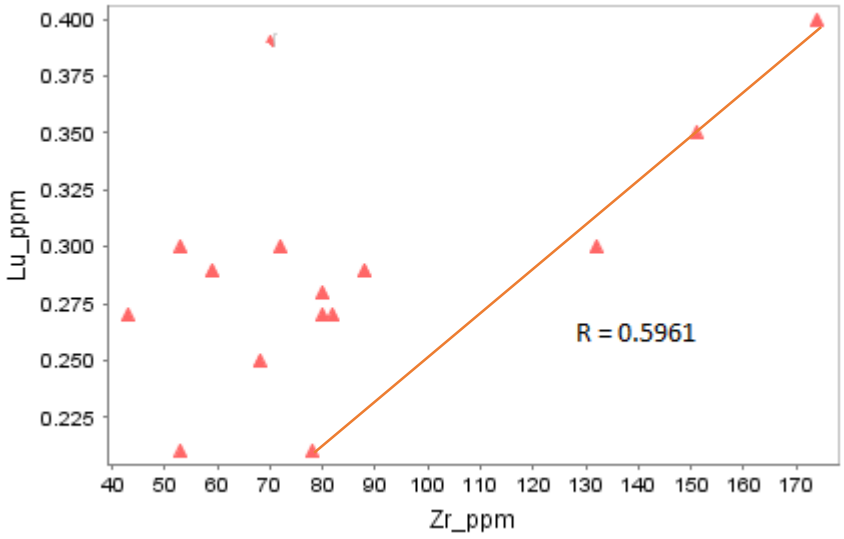

(e)

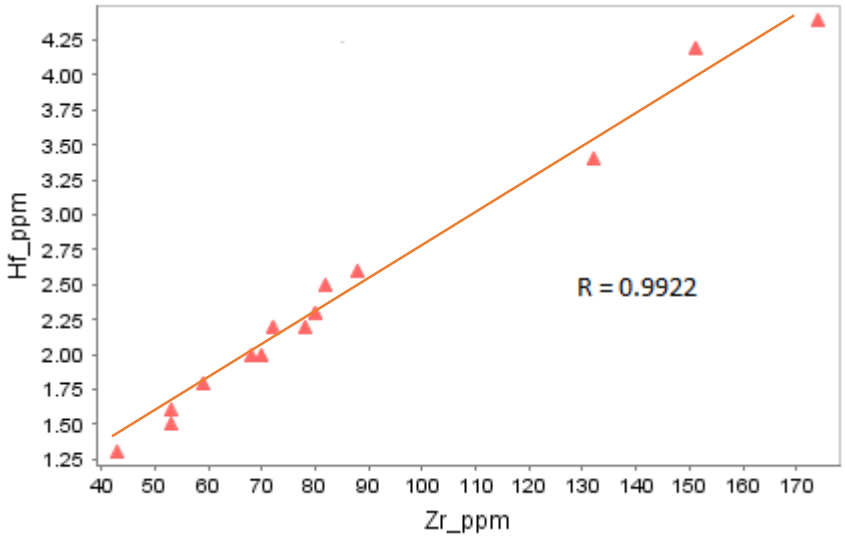

(f)

Figure 4.21: Zr variation plots with some REE where (a) = Zr vs Y; (b) = Zr vs Nd; (c) = Zr vs Sm; (d) = Zr vs Yb; (e) = Zr vs Lu; and (e) = Zr vs Hf (R = Pearson linear correlation factor).

On the primitive mantle-normalised ME spider diagram plot, of the calc-alkalic dyke samples studied (Figure 4.22), Pb shows a positive anomaly whilst Ti, Ta, Nb display troughs. These features, coupled with the enrichment of LREE over the HREE, are typical of calc-alkalic magmatism in active continental margins (Sun and McDonough, 1989). According to Schmidt et al. (2006), marked Nb-Ta trough in primitive-mantle normalized trace element patterns are attributed to the retention of these elements in mineral phases containing Ti (e.g. rutile) during dehydration of subducted oceanic crust or crustal contamination. The primitive mantle-

normalised ME spider diagram plot for the tholeiitic dyke type samples display a typical OIB signature (Figure 4.23).

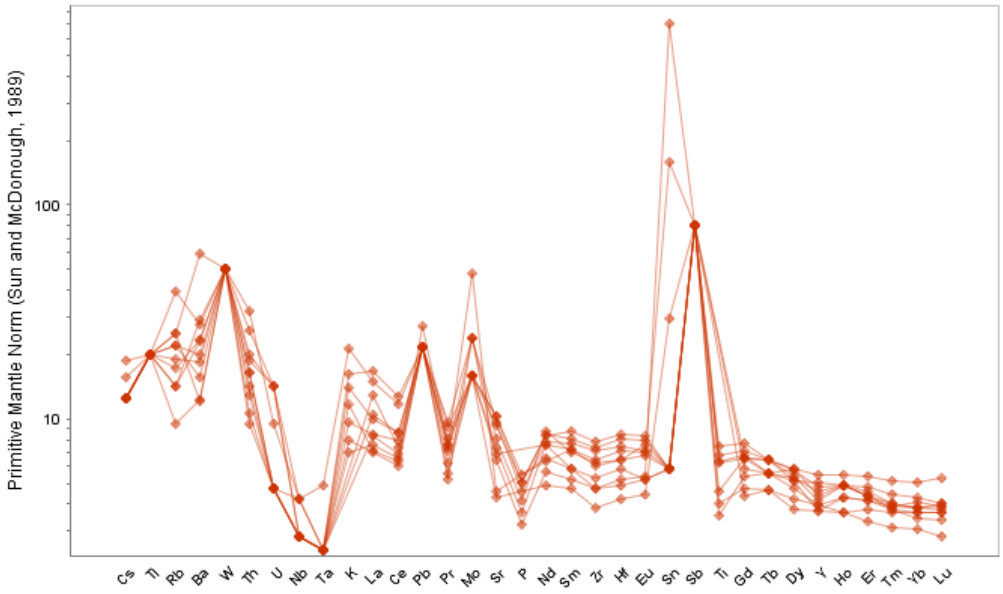

Figure 4.22: Primitive mantle-normalised multi element variation diagram for calc-alkalic rocks of the study area, normalising values from Sun and McDonough (1989).

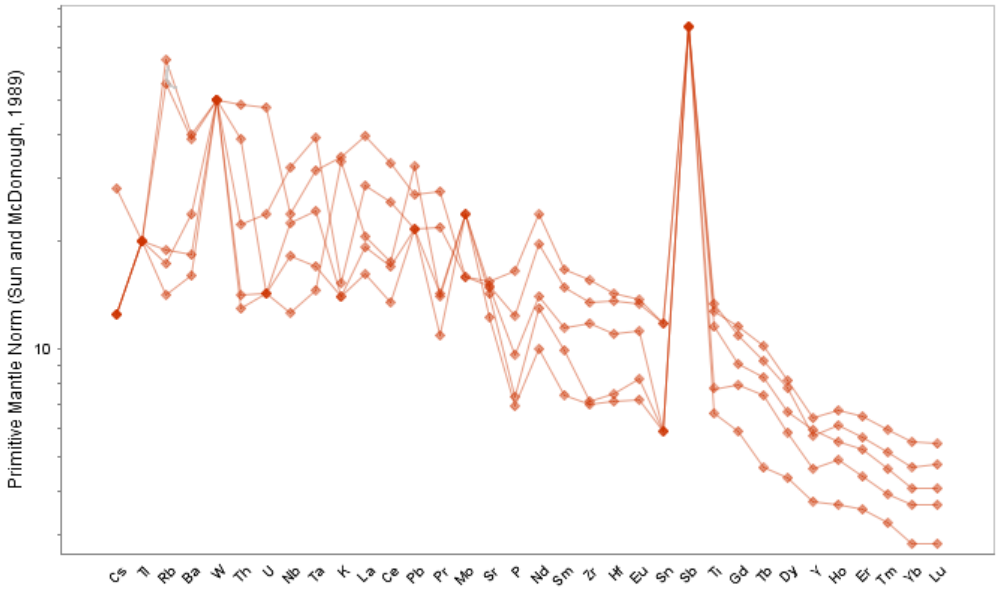

Figure 4.23: Primitive-mantle normalised multi element variation diagram for tholeiitic rocks of the study area, normalising values from Sun and McDonough (1989).

4.3.6 Isotope Geochemistry and Dating

The measured ratios and ages of the analysed samples are shown in Tables 4.3 to 4.5 and the most useful information is summarised in Table 4.6. From these tables, it is observed that measured $^{87}Sr/^{86}Sr$ (which measures the Sr isotopic ratio of a sample at the time of intrusion) ratios fall within the narrow range of 0.710886-0.719612 (Table 4.3), whilst measured

$^{143}Nd/^{144}Nd$ ranges between 0.512139-0.512370 (Table 4.4). The epsilon notation εNd describes the magnitude of deviations in Nd from the Chondritic uniform reservoir (CHUR) line at the time of intrusion or at the present time, and in this study, modern εNd values range between -5.23 and -9.73 (Table 4.4). The ages of the three samples rocks are markedly different, being 608 ± 35 Ma, 1067 ± 55 Ma and 1522 ± 90 Ma (Table 4.5), revealing that the dykes were intruded in at least three phases over a period of about 900 Ma. By sheer coincidence, all the three samples are of the calc-alkalic rock type.

Table 4.3: Rb-Sr isotope ratios

Sample	Rb, ppm	Sr, ppm	$^{87}Rb/^{86}Sr$	±2σ	$^{87}Sr/^{86}Sr$	±2σ
CH-ISO-01	12.9	104	0.3591	0.0017	0.714503	0.000012
CH-ISO-02	16.0	154	0.3006	0.0015	0.710886	0.000010
CH-ISO-03	17.7	99	0.519	0.002	0.719612	0.000011

Table 4.4: Sm-Nd isotope ratios

Sample	Sm, ppm	Nd, ppm	$^{147}Sm/^{144}Nd$	±2σ	$^{143}Nd/^{144}Nd$	±2σ	εNd^*
CH-ISO-01	2.449	8.298	0.1784	0.0005	0.512216	0.000009	-8.23
CH-ISO-02	3.112	9.880	0.1904	0.0005	0.512370	0.000007	-5.23
CH-ISO-03	1.990	6.664	0.1805	0.0005	0.512139	0.000004	-9.73

* - modern values

Table 4.5: K-Ar age dating results

Client's ID	*K, % ± σ*	*^{40}Ar rad, (ng/g)*	*% ^{40}Ar air*	*Age, Ma*	*Error 2σ*
CH-ISO-01	0.240±0.01	39.78±0.12	5.3	**1522**	90
CH-ISO-02	0.276±0.01	27.85±0.09	5.7	**1067**	55
CH-ISO-03	0.348±0.01	17.47±0.05	4.9	**608**	35

Table 4.6: Consolidated summary of isotopic and age data of the three samples of the study area.

Sample No.	$^{87}Sr/^{86}Sr$	$^{143}Nd/^{144}Nd$	εNd	Age (Ma)
CH-ISO-01	0.714503	0.51226	-8.23	1522 ± 90
CH-ISO-02	0.710886	0.51237	-5.23	1067 ± 55
CH-ISO-03	0.719612	0.512139	-9.73	608 ± 35

4.4 Tectonic Classification of the Dykes

4.4.1 Tholeiitic Mafic Dykes

Basaltic and dykes of tholeiitic affinity may occur either in oceanic or continental environments (Pearce et al., 1975; Roberts, 1990). One of the effective ways of discriminating the environments is by the application of the TiO_2-K_2O-P_2O_5 diagram of Pearce et al. (1975) (Figure 4.24). In this diagram, all tholeiitic rock samples of the Study area plot within the oceanic field.

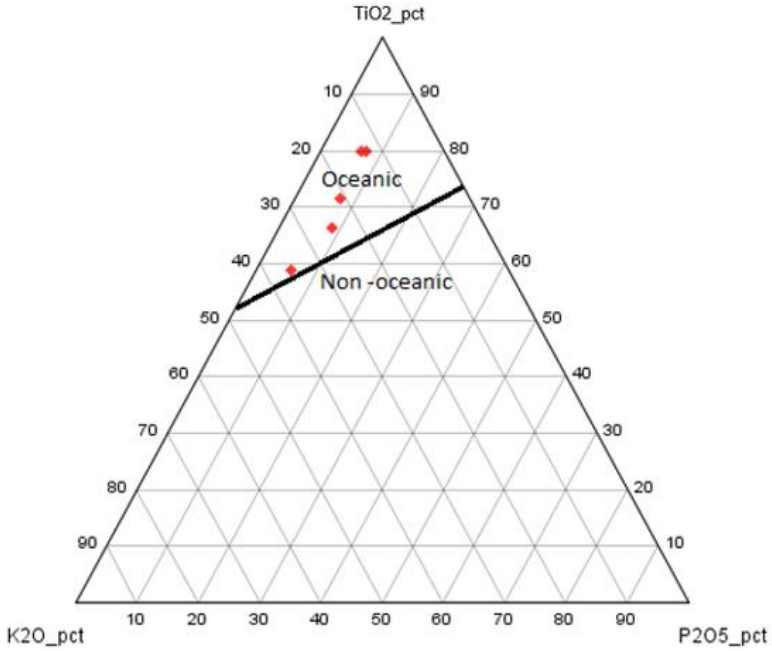

Figure 4.24: TiO_2-K_2O-P_2O_5 discrimination diagram for tholeiitic rocks of the Study area, (Pearce et al., 1975) between tholeiites of oceanic and continental affinity, adapted from Roberts (1990).

On the TiO_2-MnO-P_2O_5 discrimination diagram model of Mullen (1983), for basaltic andesites and basalts of ocean regions (Figure 4.25), three of the rock samples plot in the MORB field whilst the other two plot in the OIT (Oceanic Island Tholeiites) field.

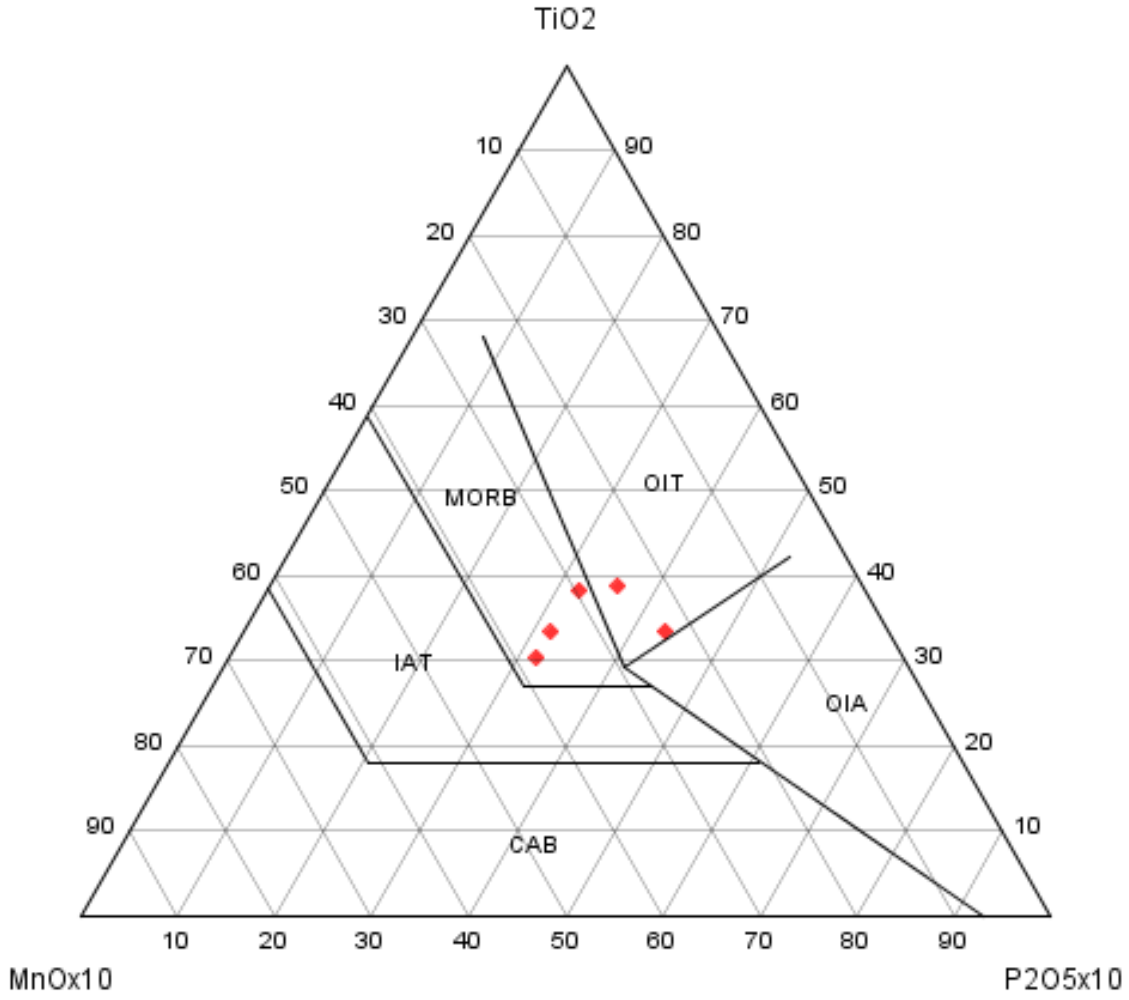

Figure 4.25: TiO_2-MnO-P_2O_5 discrimination diagram, after the model of Mullen (1983) for basaltic andesites and basalts of Ocean Regions, for the tholeiitic rocks of the mafic dykes of the Irumide Fold Belt, Zambia.

On the Th/Yb vs Nb/Yb plot of Pearce (2014; Figure 4.26), three of the five tholeiitic rock samples with the highest Nb/Yb ratio of all the samples, plot in the E-MORB (Enriched Mid-Oceanic Ridge Basalt) field, but moving in the direction of the OIB (Oceanic Island Basalt) field. One sample, with the lowest Nb/Yb ratio, plots in the in the Continental Arcs field, whilst the remaining sample plots at the Continental Arcs margin.

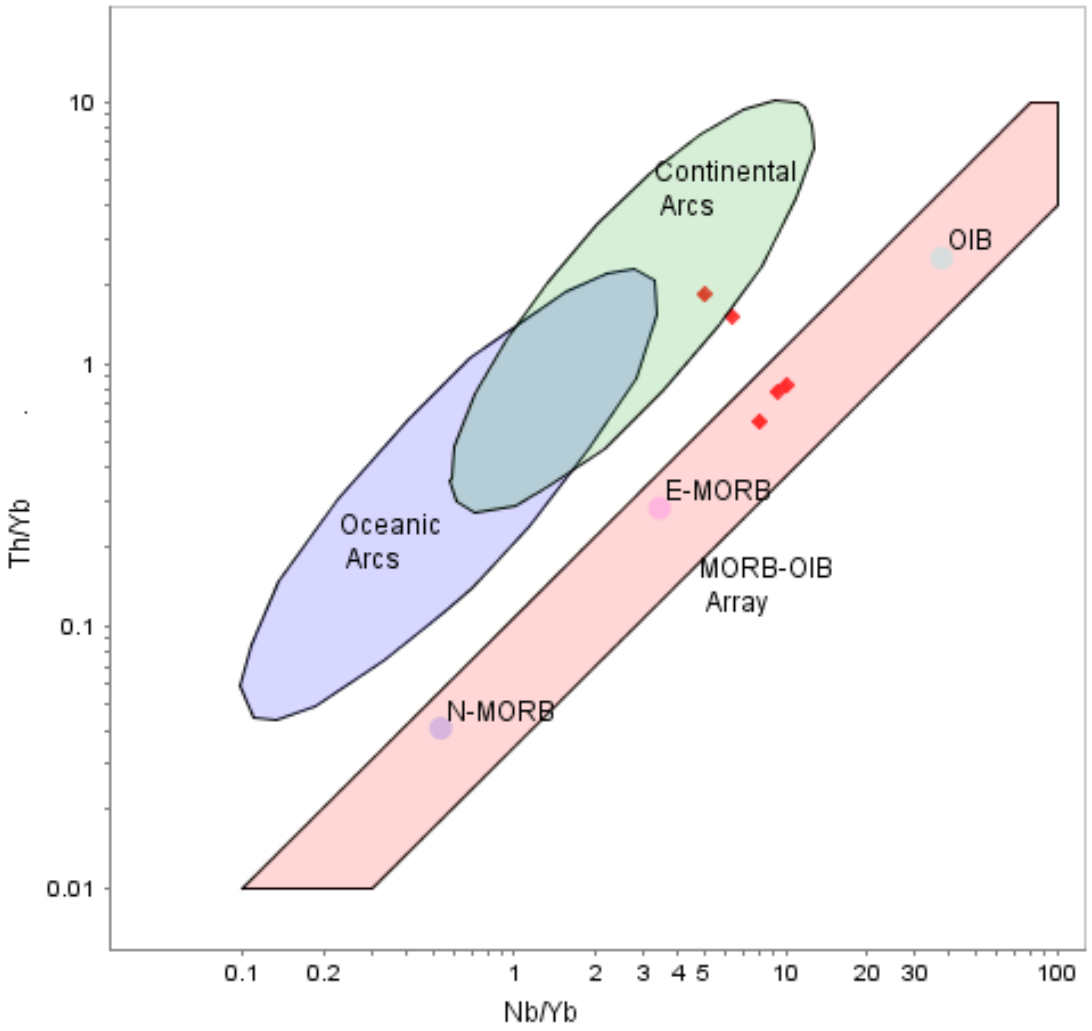

Figure 4.26: Diagram of Basalt plot, Th/Yb vs Nb/Yb (Pearce 2014) geotectonic environment classification, for the tholeiitic rocks of the mafic dykes of the Irumide Fold Belt, Zambia.

On tectonic classification of igneous rocks model diagram of Cabanis and Lecolle (1989), four of the five the tholeiitic rock samples plot in the “Late to post orogenic intra continental domain”, and one sample plots in the E-MORB field (Figure 4.27). On the Th-Hf-Ta classification model (Fgure 4.28) of Wood (1980), three of the tholeiitic samples plot in the E-MORB WPT (Enriched Mid-Oceanic Ridge Basalts Within Plate Basalt) field and one plots in the transit between Alk WPB (Alkaline Within Plate Basalts) and (E-MORB WPT), but much closer to the E-MORB. One sample plots in the VAB CAB (Volcanic Arc Basalt - Calc-alkaline Basalts) field, whilst the remaining one sample does not plot in any specific field.

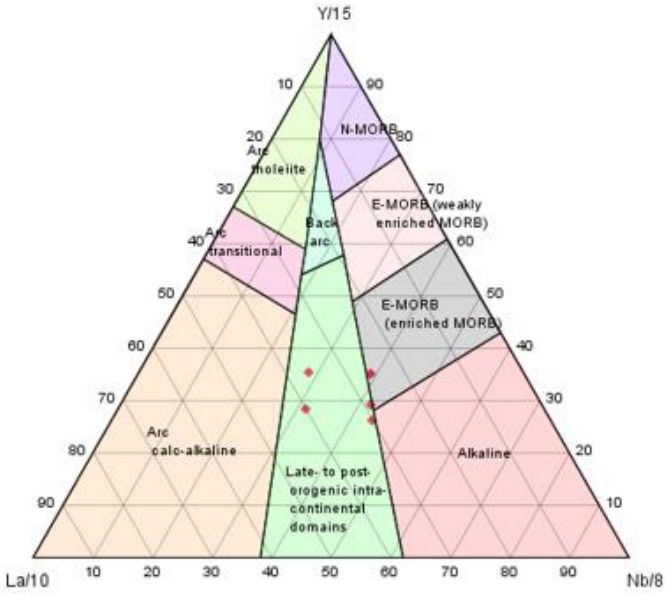

Figure 4.27: La-Y-Nb Tectonic Classification plot of the tholeiitic rocks of the mafic dykes of the Irumide Fold Belt, Zambia (after Cabanis and Lacolle, 1989).

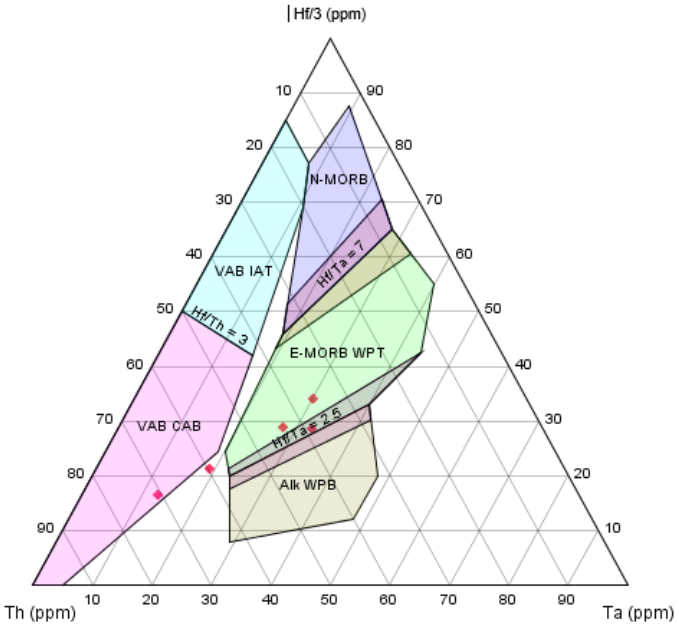

Figure 4.28: Plot of Th-Hf-Ta, classification model of Wood (1980), for the tholeiitic rocks of the mafic dykes of the Irumide Fold Belt, Zambia.

The application of Ti/1000 versus V plots in the identification of paleo-tectonic environments, is based on the variation in the crystal/liquid partition coefficients for vanadium, which range with increasing oxygen fugacity (fO_2) from >1 to <<1 (Kumar and Ahmad, 2007). In this regard, since the partition coefficient for Ti is almost always <<1, the depletion of V relative to Ti is a function of the fO_2 of the magma and its source, the degree of partial melting and subsequent fractional crystallisation (Kumar and Ahmad, 2007). On the Ti/1000 vs V discrimination model diagram of Shervais (1982) (Figure 4.29), all the tholeiitic rock samples plot in the MORB field

although two of them plot very close to the borderline with the IOB field. Kumar and Ahmad (2007) classify the MORB field as “Within Plate Basalt”.

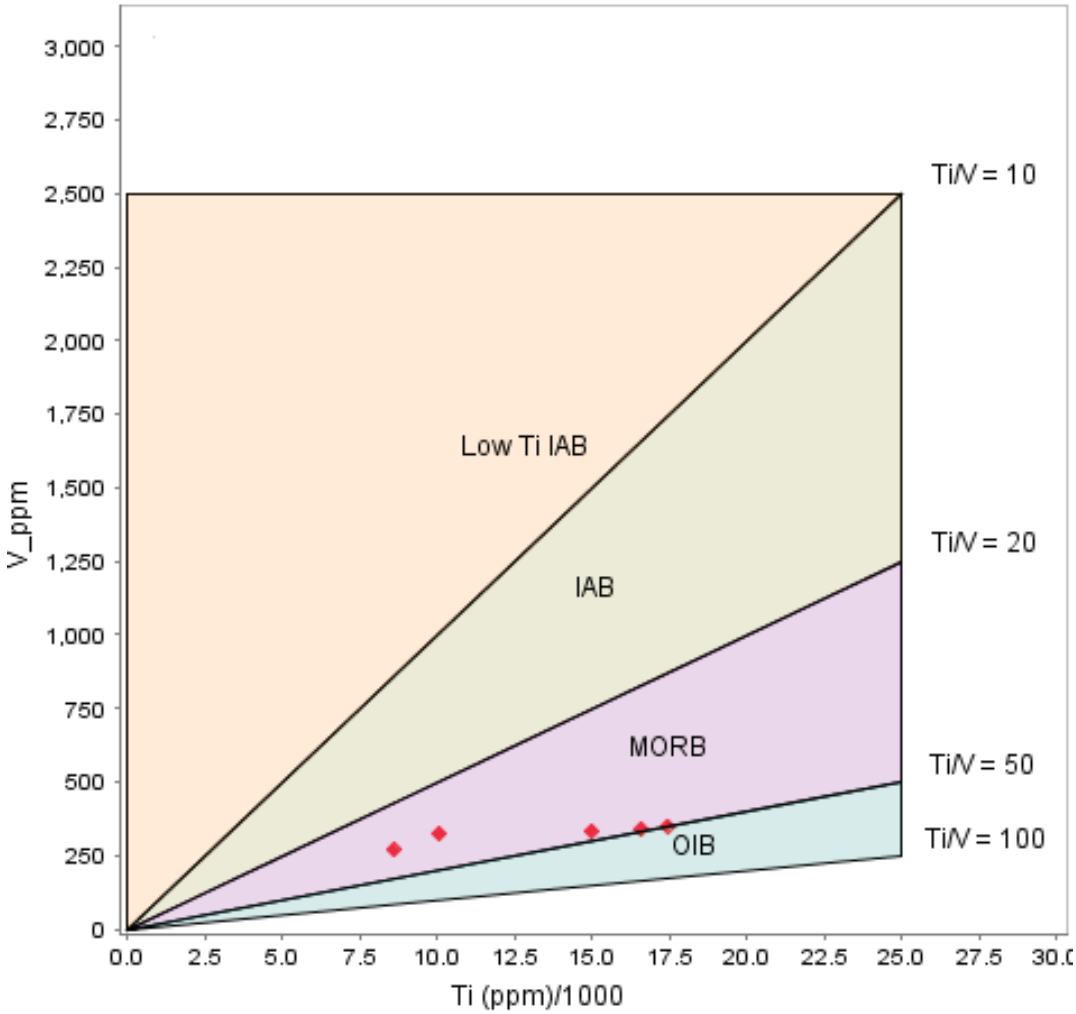

Figure 4.29: Ti vs V discrimination plot, model diagram of Shervais (1982), for the tholeiitic rocks of the mafic dykes of the Irumide Fold Belt, Zambia

On the Nb-Zr-Y discrimination model plot of Meschede (1986) (Figure 4.30), three of the five tholeiitic rock samples plot in the WPB + WPT (Within Plate Basalts + Within Plate Tholeiites) field, whilst the other two samples plot in the E-MORB field. Applying the Ti-Zr-Y discrimination model of Pearce and Cann (1973), all the tholeiitic rock samples of the Study area are positioned in the WPB (Within Plate Basalts) field (Figure 4.31). On the Geotectonic Zr/Y vs Nb/Y discrimination plot (Figure 4.32), adapted from Srivastava et al., (2014), four of the five tholeiitic rock samples of the Study area plot in the N-MORB zone.

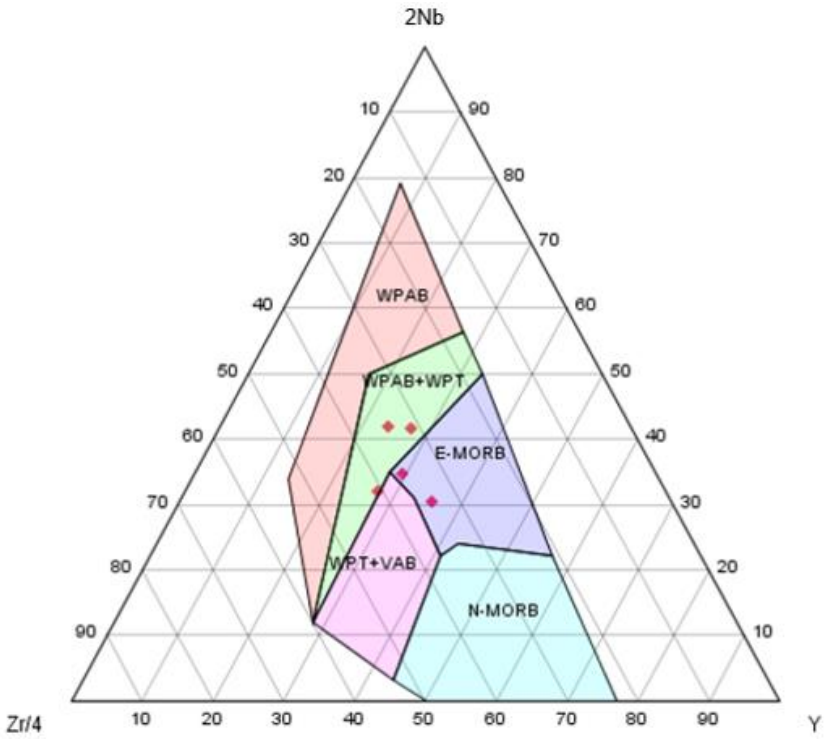

Figure 4.30: Geotectonic Nb-Zr-Y discrimination plot, model diagram of Meschede (1986) for the tholeiitic rocks of the mafic dykes of the Irumide Fold Belt, Zambia.

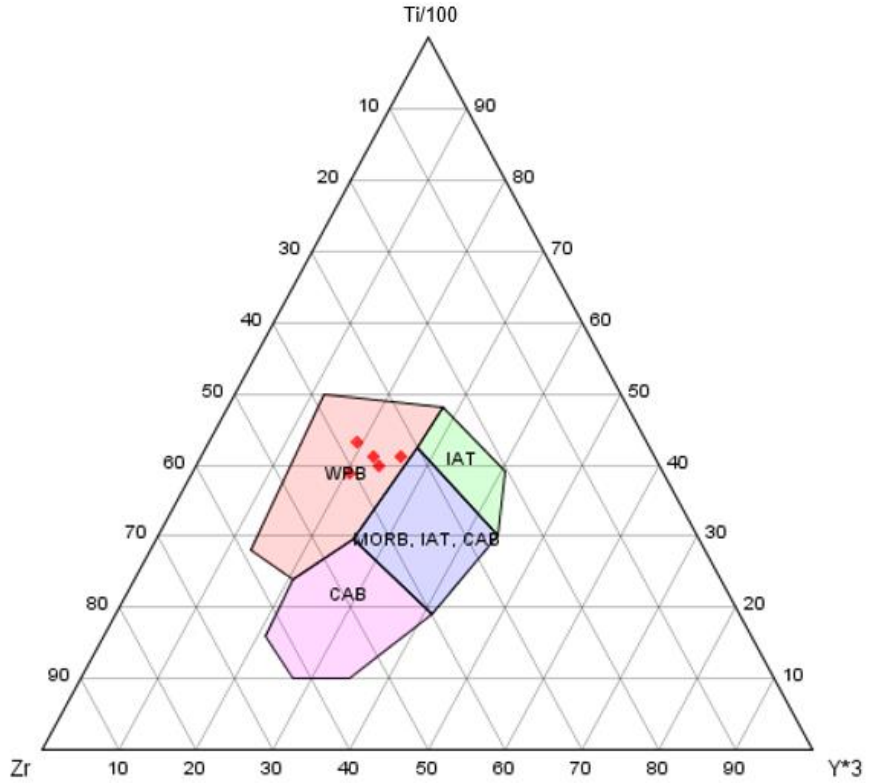

Figure 4.31: Geotectonic Ti-Zr-Y basalt discrimination plot, model diagram of Pearce and Cann (1973) for the tholeiitic rocks of the mafic dykes of the Irumide Fold Belt, Zambia.

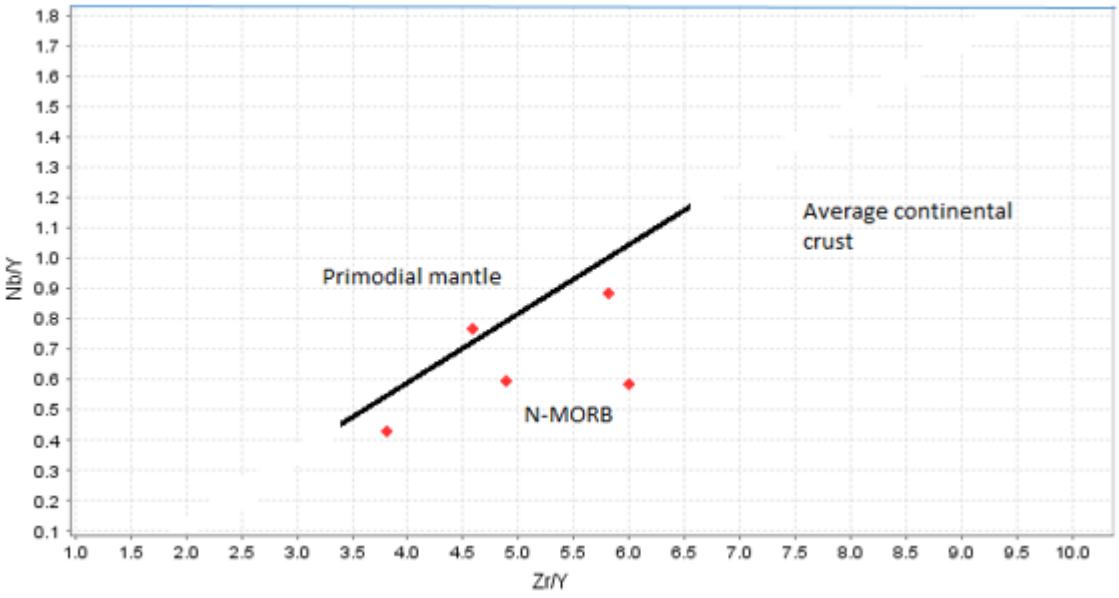

Figure 4.32: Geotectonic Zr/Y vs Nb/Y discrimination plot, adapted from Srivastava et al., (2014) (with fields as follows: N-MORB (Fitton et al., 1997; Baksi, 2000); Primodial mantle (McDonough and Sun, 1995); and Average Continental Crust (Rudnick and Fountain, 1995)) for the tholeiitic rocks of the mafic dykes of the Irumide Fold Belt, Zambia.

4.4.2 Calc-alkalic dykes

On the Th/Yb vs Nb/Yb discrimination plot of Pearce 2014 (Figure 4.33), the calc-alkalic samples plot in the overlap (transition) between Continental Arcs and Oceanic Arcs. On tectonic classification of igneous rocks model diagram of Cabanis and Lecolle (1989), all calc-alkalic samples plot in the transition between Arc Tholeiitic and Arc Calc-alkaline fields; apart from one each, that plot in Arc Tholeiitic and Arc Calc-alkalic fields (Figure 4.34). On the Th-Hf-Ta Basalt classification model of Wood (1980), the calc-alkalic rock samples plot in the VAB CAB (Volcanic Arc Basalts – Calc-alkalic Basalts) field apart from one that plots in VAB IAT (Volcanic Arc Basalts – Island Arc Basalts) field (Figure 4.35). All the calc-alkalic rock samples plot in the VAB CAB field on the Zr-Th-Nb Basalt classification model of Wood (1980), (Figure 4.36).

(a)

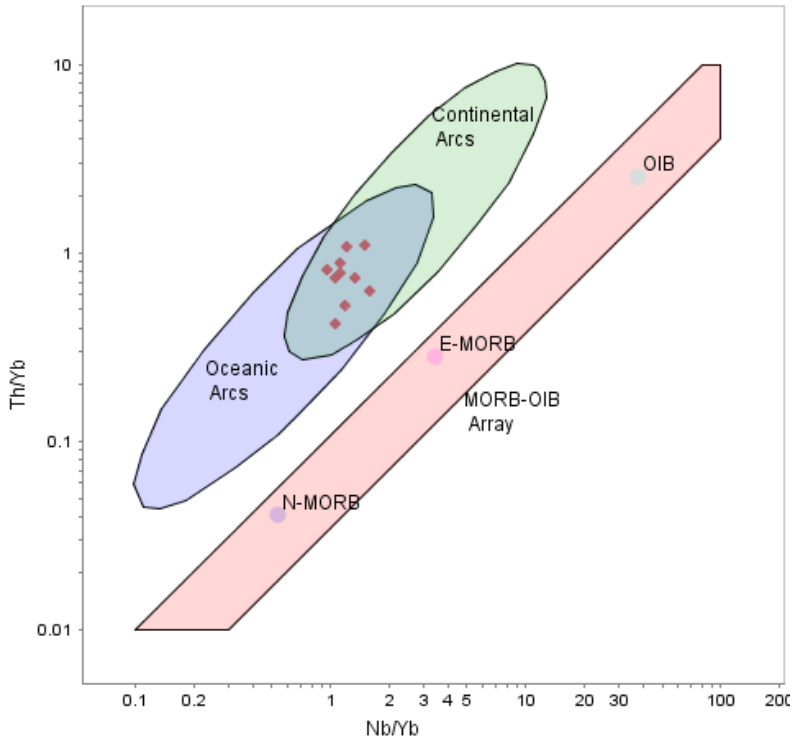

(b)

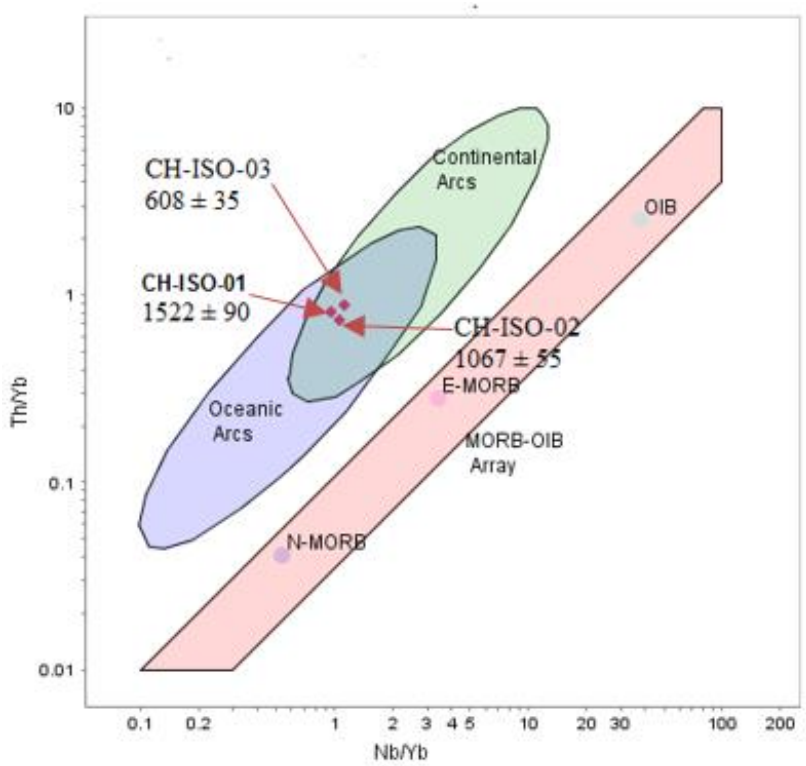

Figure 4.33: Diagram of Basalt plots, Th/Yb vs Nb/Yb (Pearce 2014) geotectonic environment classification, (a) for all the calc-alkalic rock samples, and (b) for the dated three rock samples, of the mafic dykes of the Irumide Fold Belt, Zambia.

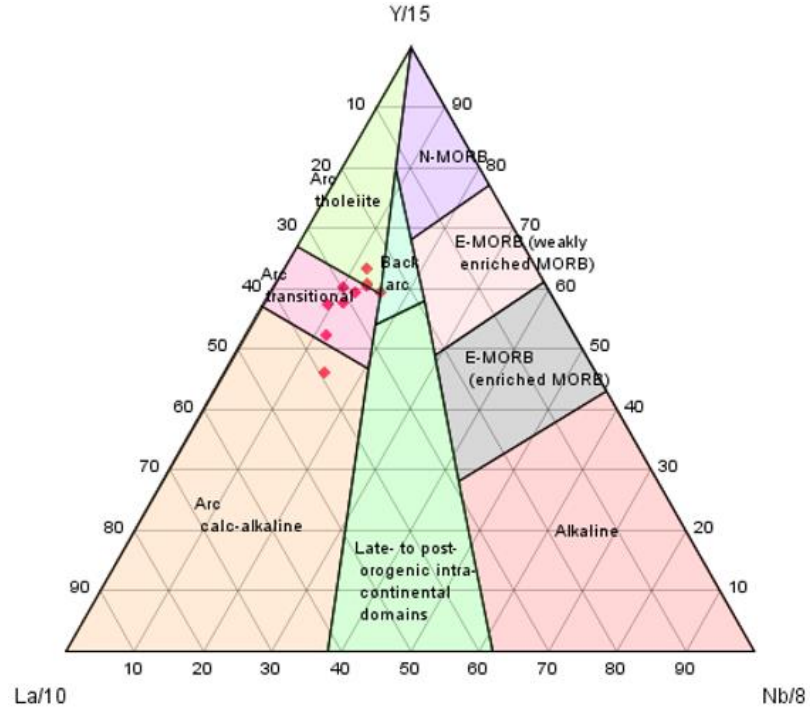

Figure 4.34: La-Y-Nb Tectonic Classification plot of the calc-alkalic rocks of the mafic dykes of the Irumide Fold Belt, Zambia (after Cabanis and Lacolle, 1989).

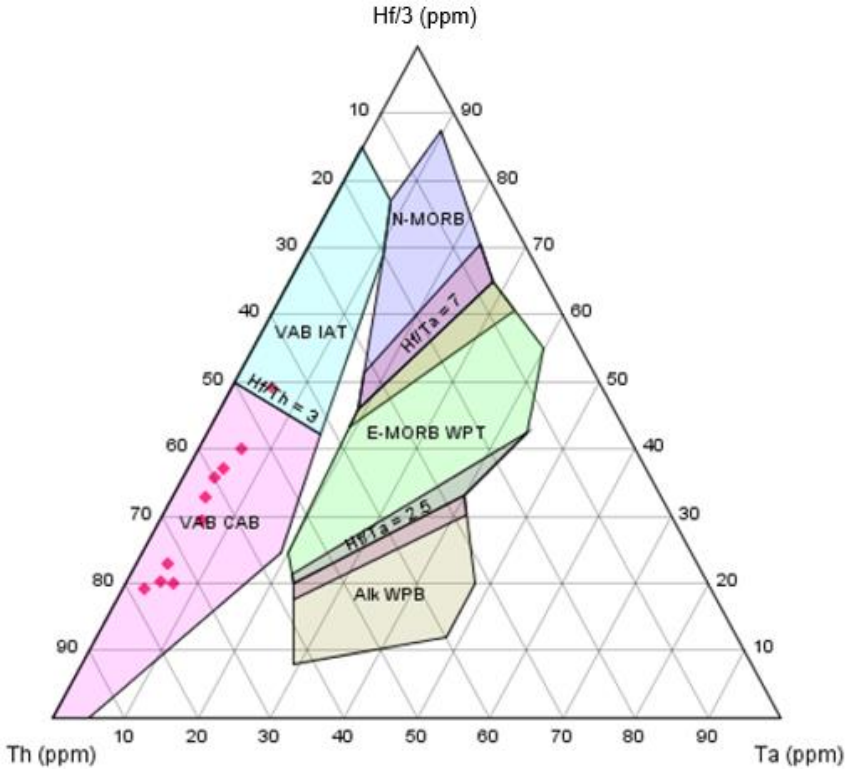

Figure 4.35: Plot of Th-Hf-Ta, classification model of Wood (1980), for the calc-alkalic rocks of the mafic dykes of the Irumide Fold Belt, Zambia.

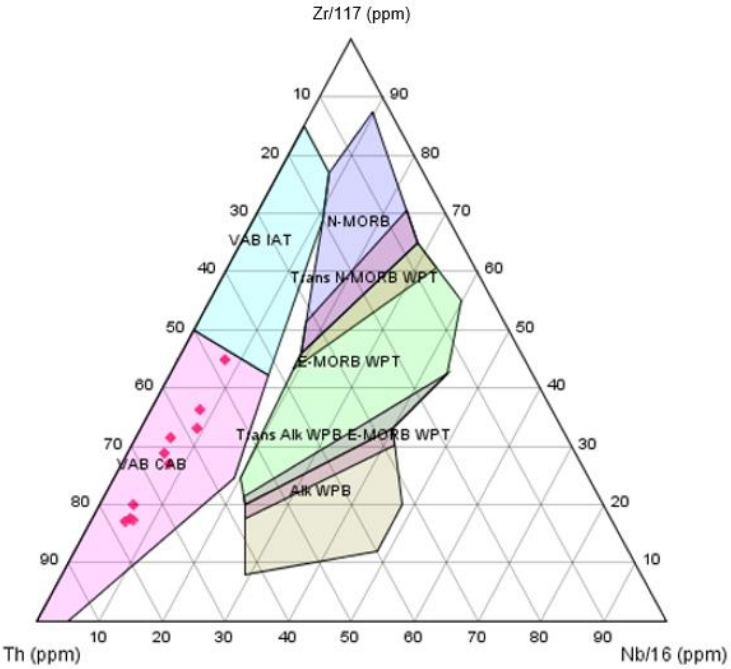

Figure 4.36: Plot of Zr-Th-Nb, classification model of Wood (1980), for the calc-alkalic rocks of the mafic dykes of the Irumide Fold Belt, Zambia.

On the Zr-Ti-Sr, classification model of Pearce and Cann (1973), the calc- alkalic rocks plot in the MORB field apart from two samples which plot in IAT, but just at the border with MORB (Figure 4.37). All the samples plot in the N-MORB on the Zr-Nb-Y, classification model diagram of Meschede (1986) (Figure 4.38), whilst on the Ti vs V classification model of Shervais (1982), all the calc- alkalic rocks plot in the MORB field (Figure 4.39).

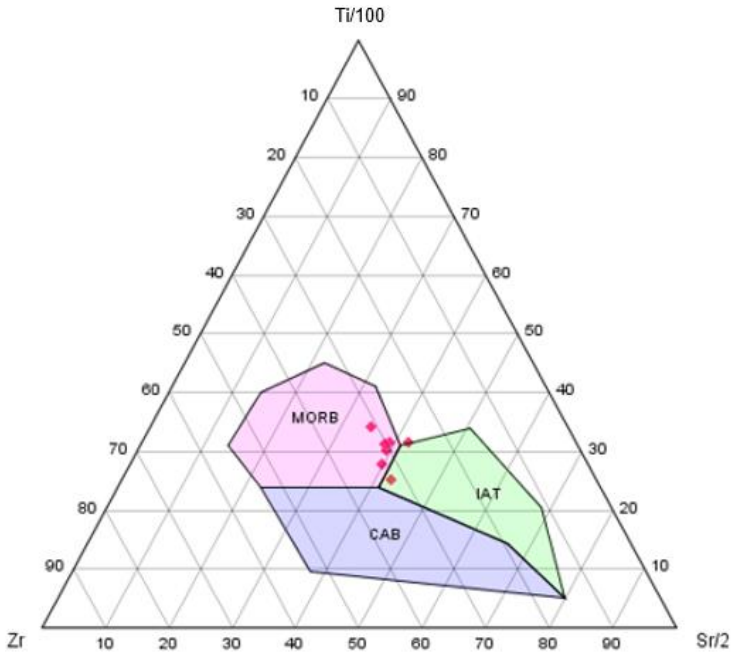

Figure 4.37: Plot of Zr-Ti-Sr, classification model of Pearce and Cann (1973), for the calc-alkalic rocks of the mafic dykes of the Irumide Fold Belt, Zambia.

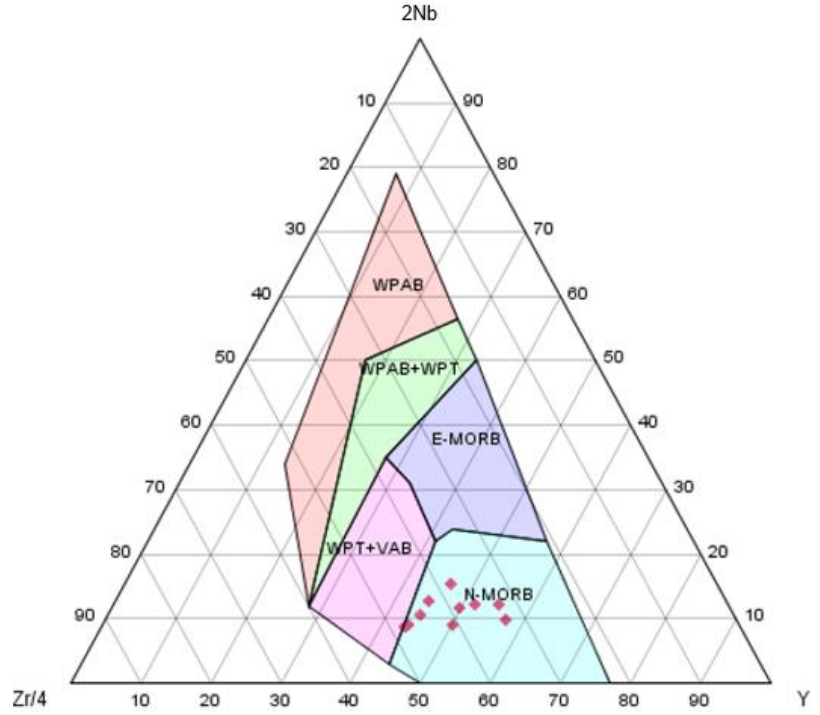

Figure 4.38: Plot of Zr-Nb-Y, classification model of Meschede (1986), for the calc-alkalic rocks of the mafic dykes of the Irumide Fold Belt, Zambia.

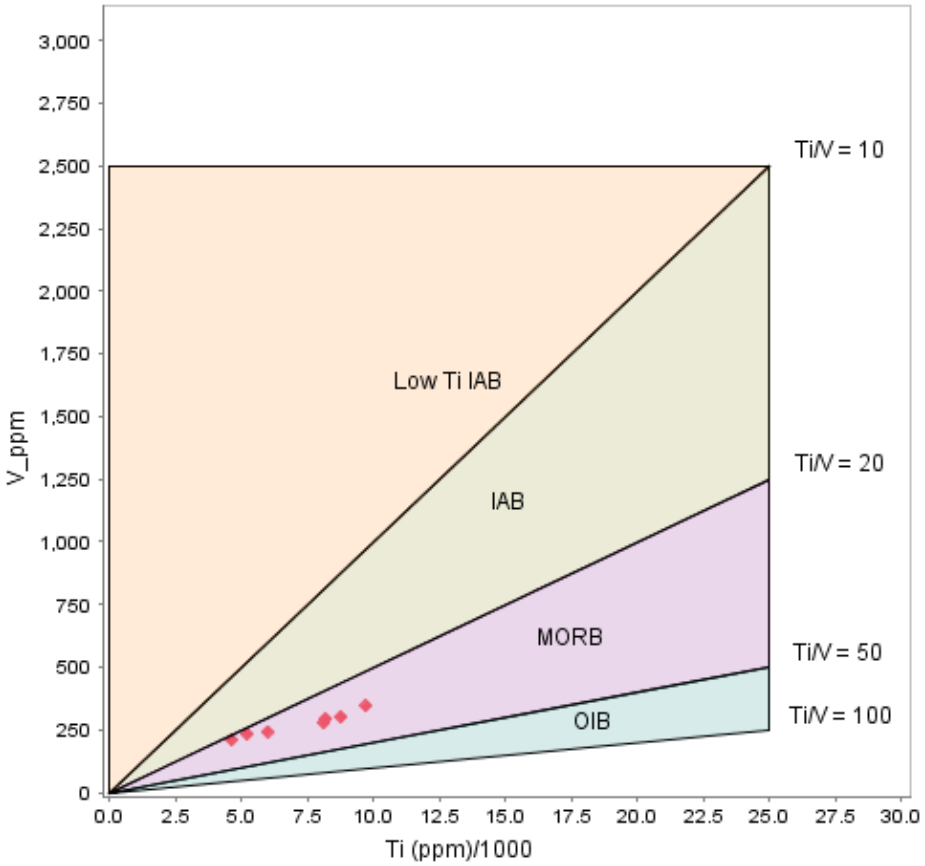

Figure 4.39: Plot of Ti vs V, classification model of Shervais (1982), for the calc-alkalic rocks of the mafic dykes of the Irumide Fold Belt, Zambia.

4.5 Petrogenesis

4.5.1 Crustal contamination

The significance of crustal contamination can be assessed through correlations between indices of fractionation and the other chemical and/or isotope data of the rocks being studied (Zhao and Zhou, 2007; Tang et al., 2012; Srivastava et al., 2014; Sreenivasulu et al., 2014). In this study, for both rock types, variation plots of MgO (as an index of fractionation) versus LILEs (Ba, Rb, Sr and K) and HFSEs (Ti, P, Zr, Y, Ce, Hf, Sm and Nd) are generated and analysed accordingly. The continental crust is largely felsic and any contamination of mafic magma is unlikely to alter the concentration of MgO, but will raise the concentration of most LILEs and HFSEs, which, because of their incompatibility, are more concentrated in these parts of the Earth. Uncontaminated mafic rocks will display more or less linear trends between MgO and the incompatible elements on variation plots, but display scatter if there is significant contamination. A combination of compatible and incompatible trace elements and their ratios, as well as isotope data, are also applied for this purpose (e.g. Rollinson 1993).

Tholeiitic dykes

On the variation plots against MgO (Figure 4.40), the LILEs; Ba, Rb, Sr and K; exhibit moderate to good negative correlation with linear coefficient factor ranging between -0.5717 to -0.9105. The HFSEs are showing similar trends displayed by the LILEs (Figure 4.41). The trace element ratios of Nb/Y versus Zr/Y variation plot (Figure 4.42) yields similar linear trend to those of MgO versus the LILEs and the HFSEs. These trends suggest absence of serious alteration of the chemical composition of the parent magma through crustal contamination (Srivastava et al., 2014). Elemental ratios of the incompatible elements, Zr/Nb = 6.0 - 10.24, Ba/La = 6.54 - 19.59, and Ba/Nb = 5.57 - 30.81, are significantly lower than the continental crust values of Hofmann et al. (1986), which are; Zr/Nb = 16.2, Ba/La = 25 and Ba/Nb = 54 (Cheng et al., 2015). This suggests absence of crustal contamination of the parent magma during magmatic processes.

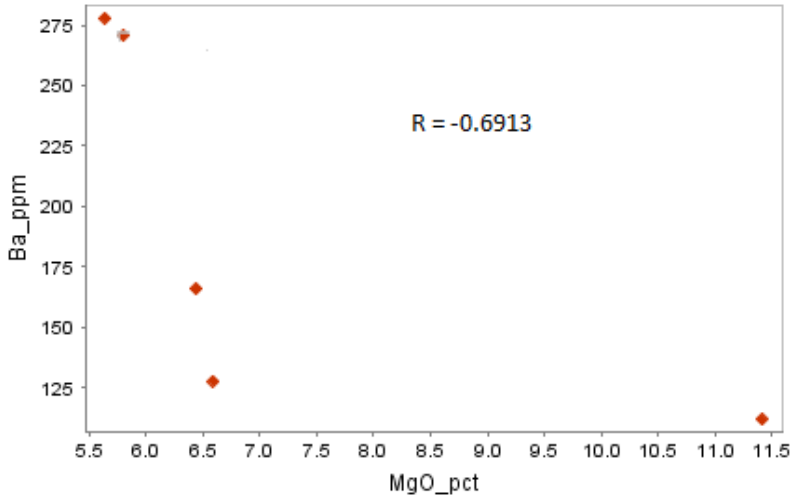
R = -0.6913
Ba_ppm
MgO_pct
275
250
225
200
175
150
125
5.5
6.0
6.5
7.0
7.5
8.0
8.5
9.0
9.5
10.0
10.5
11.0
11.5

(a)

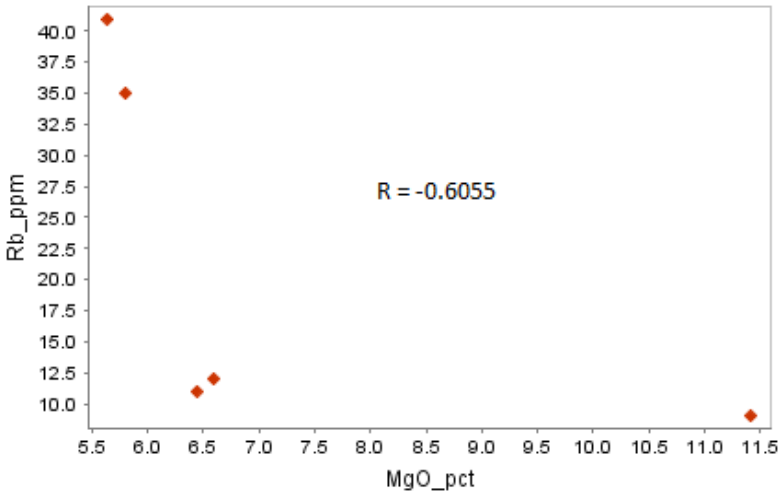
R = -0.6055
Rb_ppm
MgO_pct
40.0
37.5
35.0
32.5
30.0
27.5
25.0
22.5
20.0
17.5
15.0
12.5
10.0
5.5
6.0
6.5
7.0
7.5
8.0
8.5
9.0
9.5
10.0
10.5
11.0
11.5

(b)

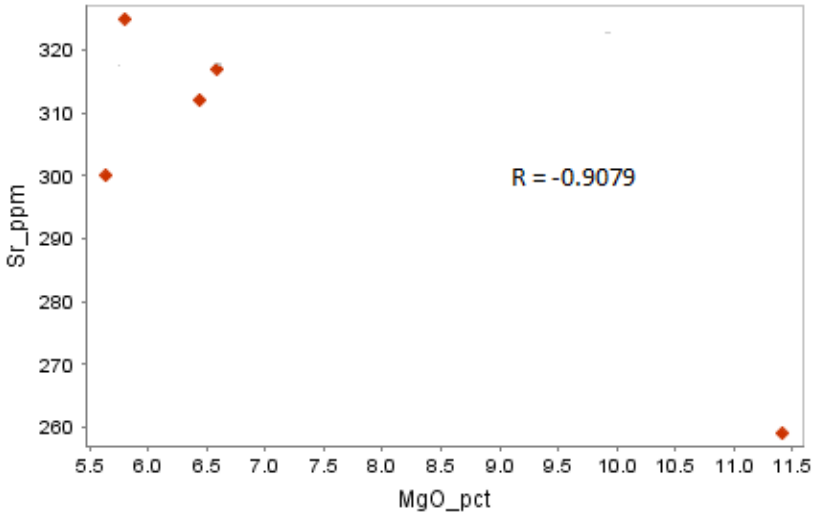
R = -0.9079
Sr_ppm
MgO_pct
320
310
300
290
280
270
260
5.5
6.0
6.5
7.0
7.5
8.0
8.5
9.0
9.5
10.0
10.5
11.0
11.5

(c)

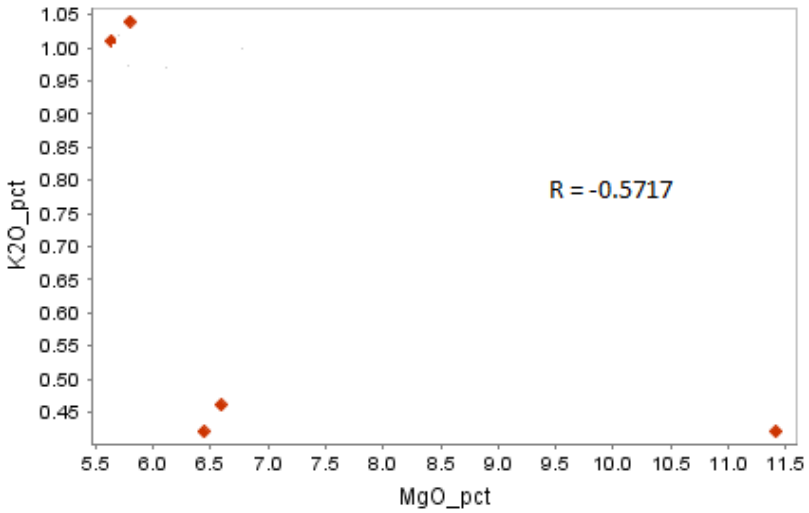

(d)

Figure 4.40: Variation plots of MgO vs some LILEs (incompatible elements), tholeiitic mafic dyke samples, where: (a) = MgO vs Ba; (b) = MgO vs Rb; (c) = MgO vs Sr ; and (d) = MgO vs K_2O, of the Study area.

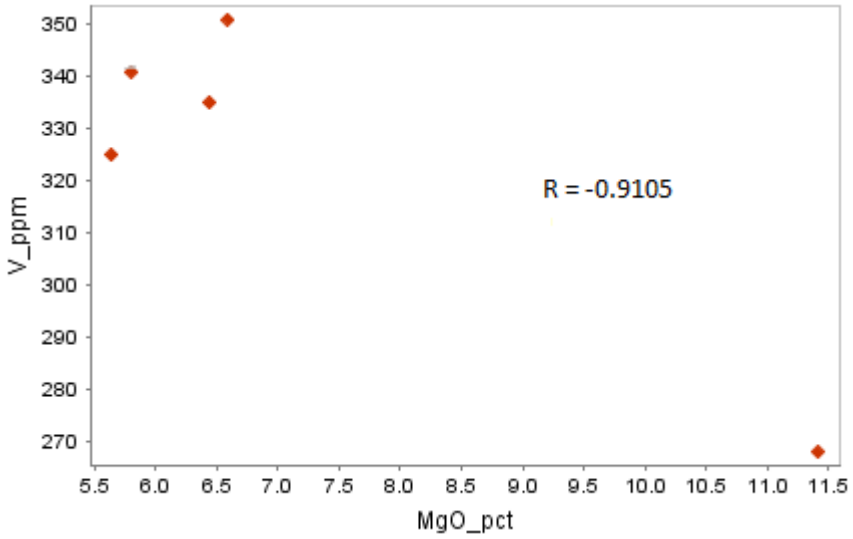

(a)

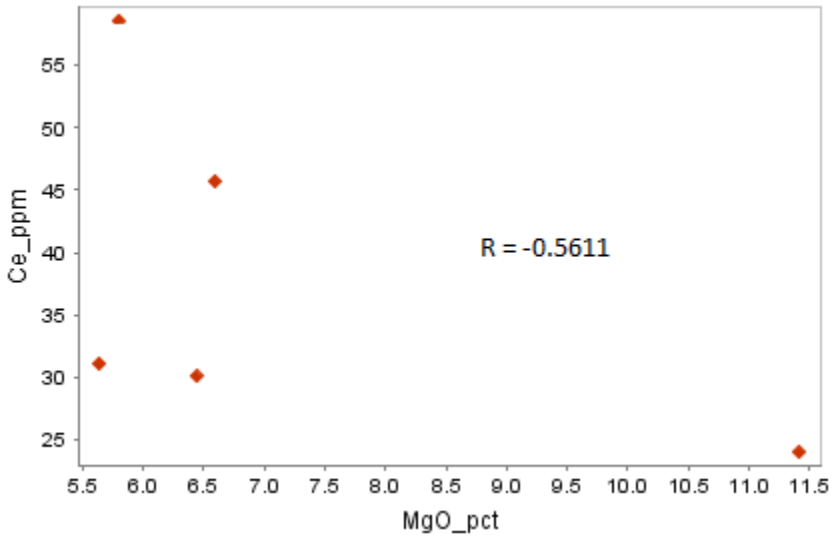

(b)

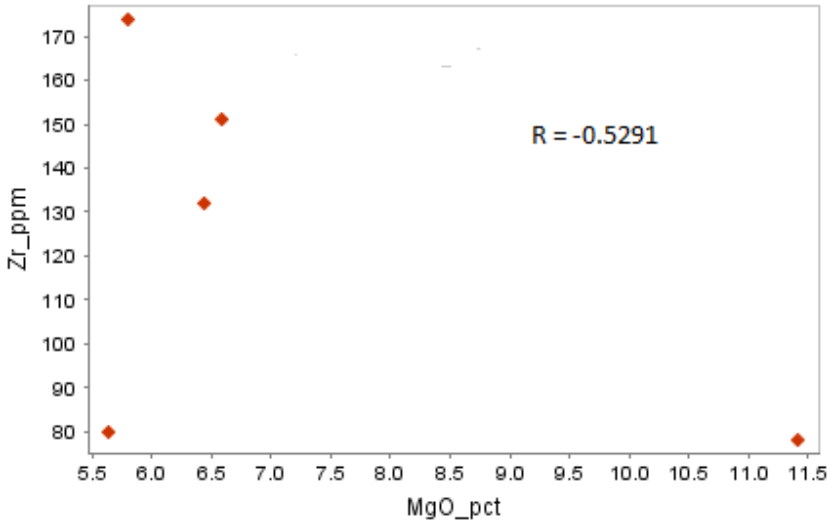

(c)

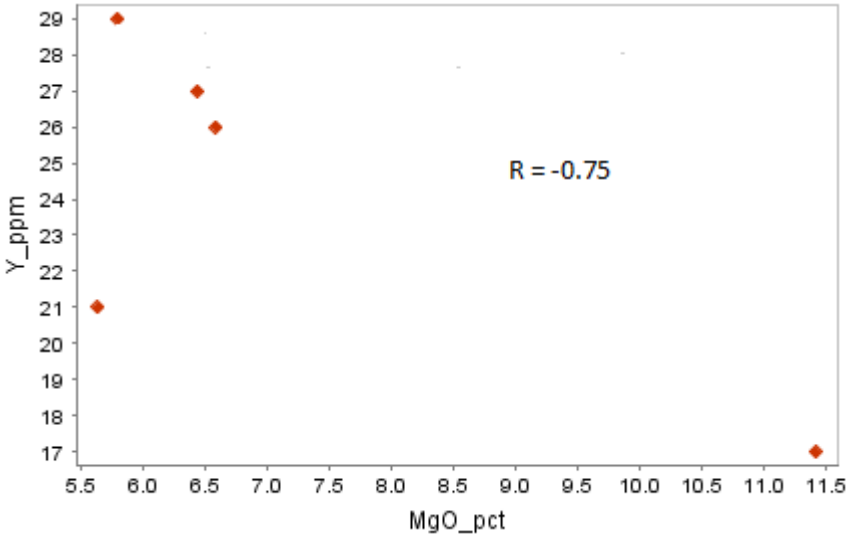

(d)

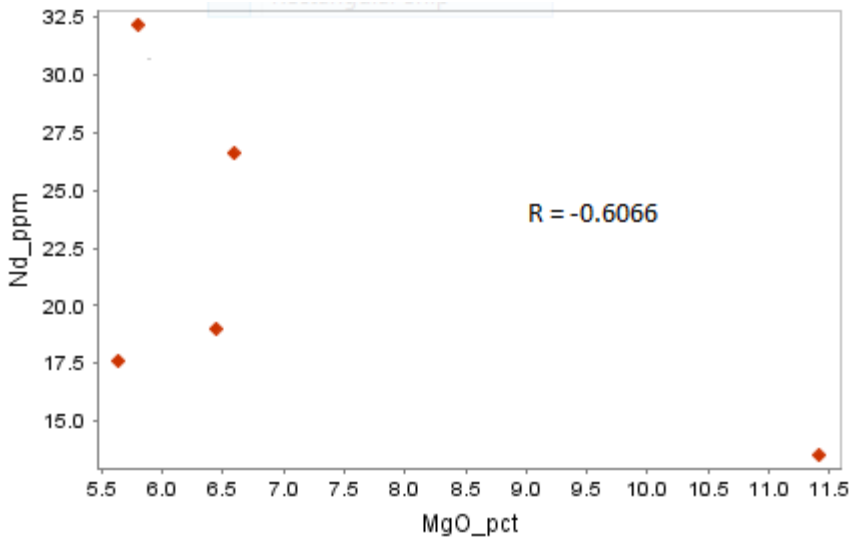
Nd_ppm
MgO_pct
R = -0.6066

(e)

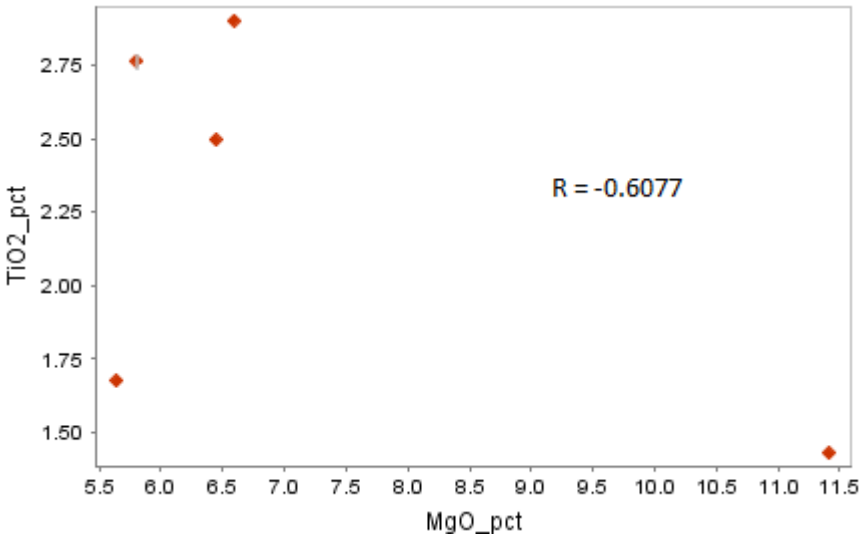
TiO2_pct
MgO_pct
R = -0.6077

(f)

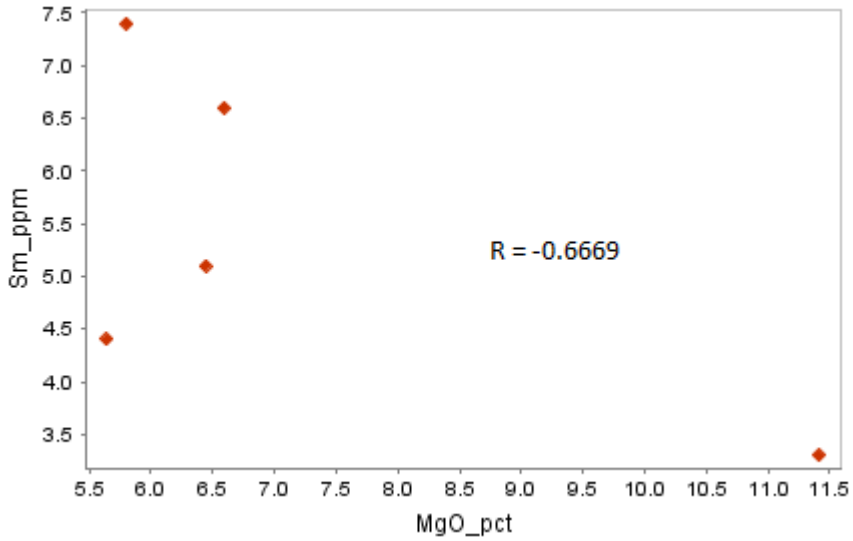
Sm_ppm
MgO_pct
R = -0.6669

(g)

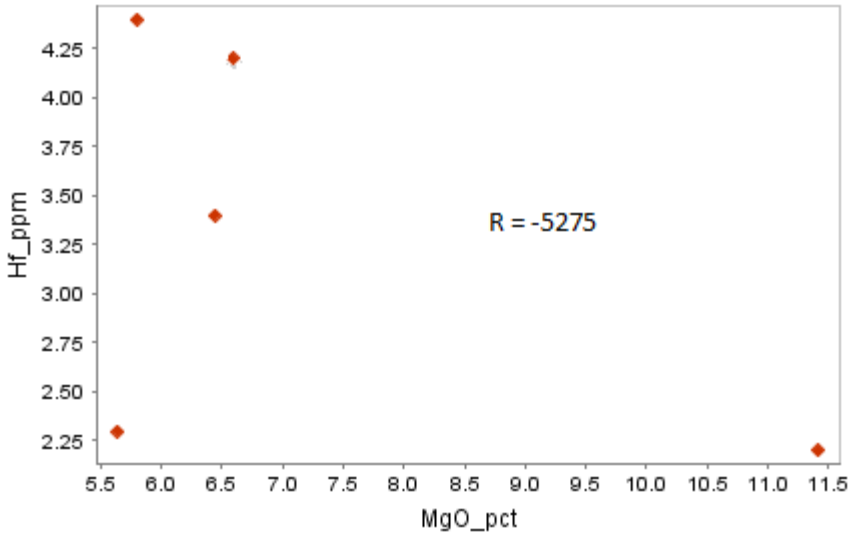

(h)

Figure 4.41: Variation plots of MgO vs some HFSE (incompatible elements), tholeiitic mafic dyke samples, where: (a) = MgO vs V; (b) = MgO vs Ce; (c) = MgO vs Zr; (d) = MgO vs Y; (e) = MgO vs Nd; (f) = MgO vs TiO_2; (g) = MgO vs Sm; and (h) = MgO vs Hf, of the Study area.

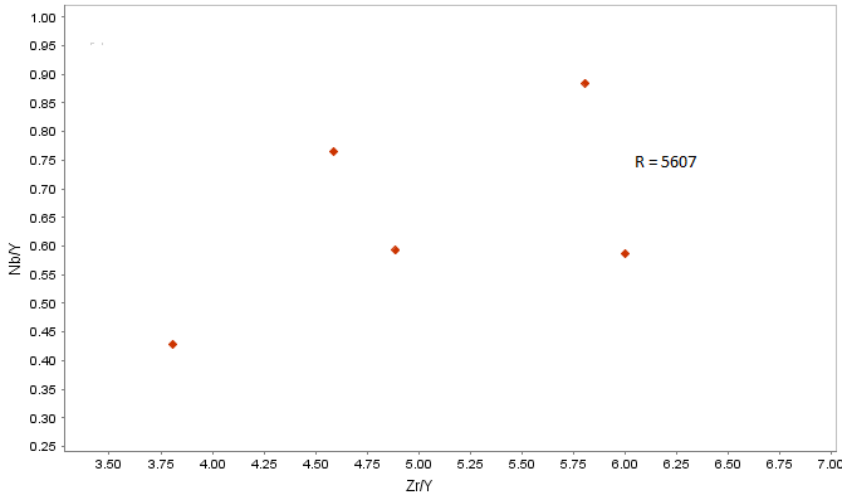

Figure 4.42: Variation plot of the ratios of Zr/Y vs Nb/Y, tholeiitic mafic dyke rock samples of the Study area.

Chemical characteristics and behaviour of Ta-Nb and Hf-Zr can be successfully applied in the assessment and identification of possible of crustal contamination. The release of Nb-Ta depleted fluids from a descending slab, in an oceanic setting, imparts a negative Nb-Ta anomaly to a suite of magmatic rocks and introduces this component into the upper asthenosphere by subduction (Kakar et al., 2014). On a multi element spider diagram of normalised primordial or primitive mantle, both sets of elements, Ta-Nb and Hf-Zr, will show

negative anomalies, to indicate possible crustal contamination (Zhao and Zhou, 2007; Cai et al. 2010; Srivastava et al., 2014).

On the primitive mantle-normalised multi-element spider diagram plot of the tholeiitic rock samples of the Study area (Figure 4.43), no negative anomalies of Ta-Nb and Hf-Zr are noticed. The enrichment in LREE accompanied by flat HREE patterns (Figure 4.44), which is also a characteristic feature of crustally contaminated mafic rocks, are considered by Srivastava et al. (2014) as not being adequate to confirm crustal contamination. In conclusion, the studied samples of the tholeiitic mafic dykes of the Study area, do not show a clear indication of crustal contamination during the processes that led to their emplacement. The conclusion drawn from the chemical characteristics exhibited by the samples under study is that suggestions of crustal contamination involvement during the magmatism of the tholeiitic rocks are clearly eliminated.

Figure 4.43: Primitive mantle-normalised multi-element spider diagram plot for the tholeiitic rock samples of the Study area, after Sun and McDonough (1989).

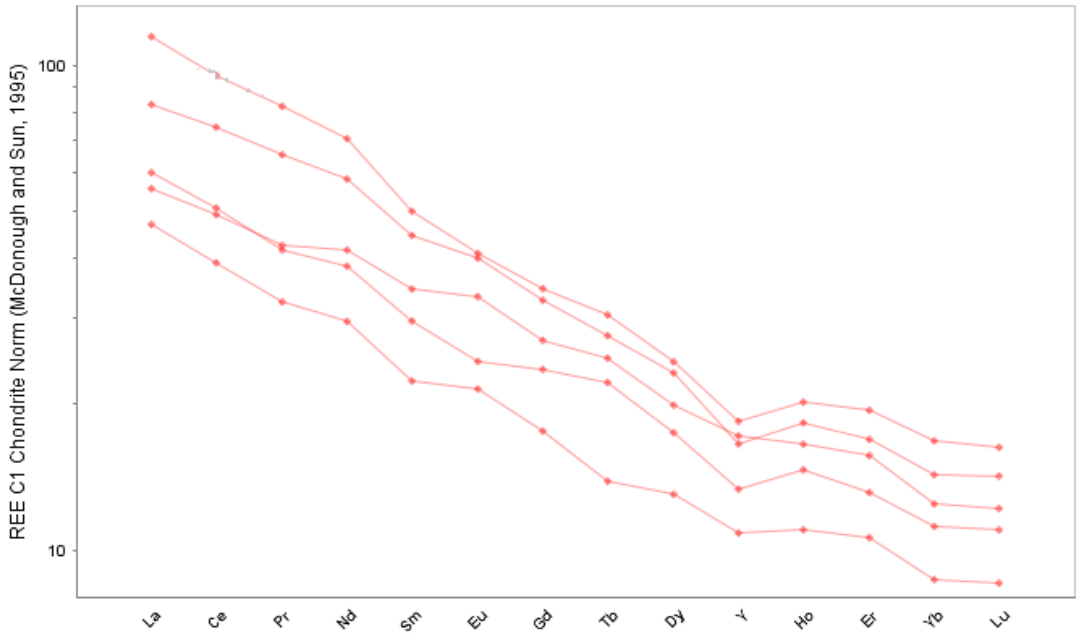

Figure 4.44: Chondrite-normalised REE spider diagram plot of the tholeiitic rocks of Study area, after McDonough and Sun, 1995.

Calc-alkalic dykes

On the variation plots against MgO (Figure 4.45), the LILEs, Rb and K exhibit moderate to good negative linear trends, whilst Ba and Sr show no correlation. The HFSEs (Figure 4.46) all show negative, mostly very poor to no correlation with MgO. The trace element ratios plot of Nb/Y versus Zr/Y variation (Figure 4.47) shows absolute no correlation.

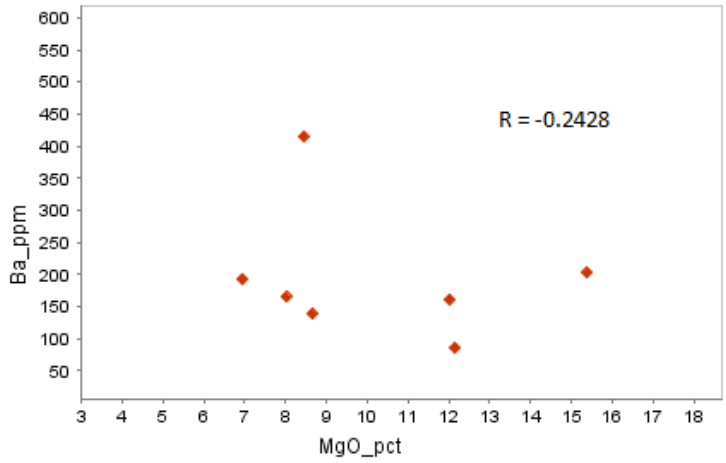

(a)

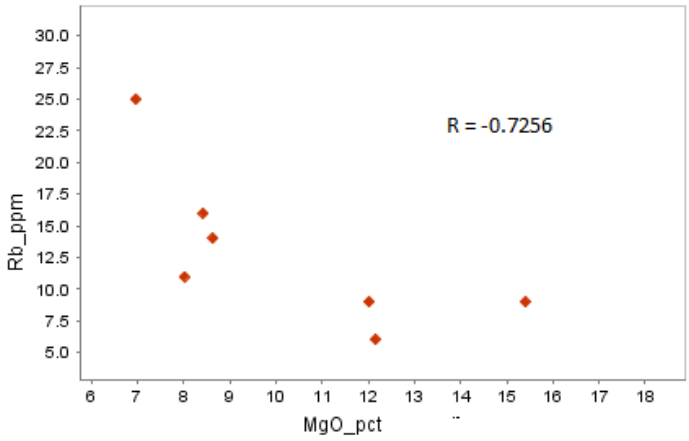

(b)

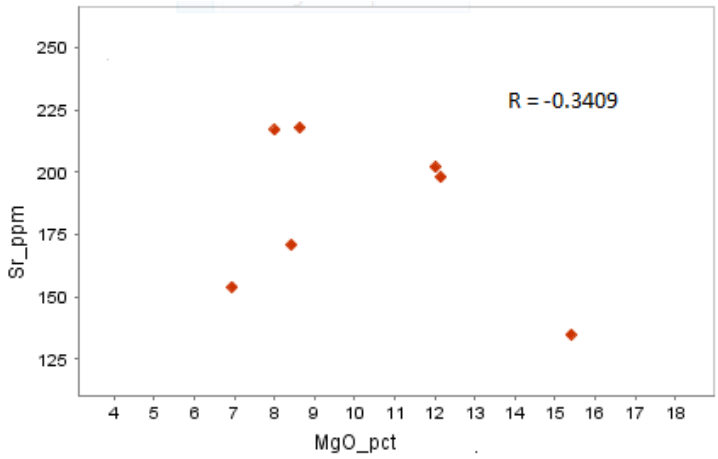

(c)

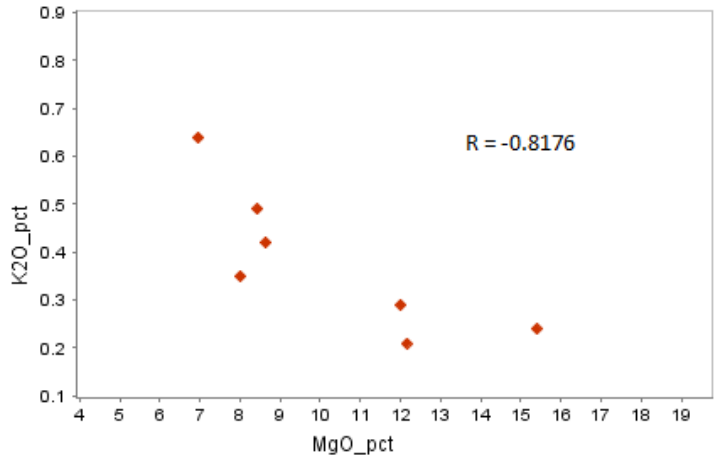

(d)

Figure 4.45: Variation plots of MgO vs LILE (incompatible elements), calc-alkalic mafic dykes samples, where: (a) = MgO vs Ba; (b) = MgO vs Rb; (c) = MgO vs Sr ; and (d) = MgO vs K_2O, of the Study area.

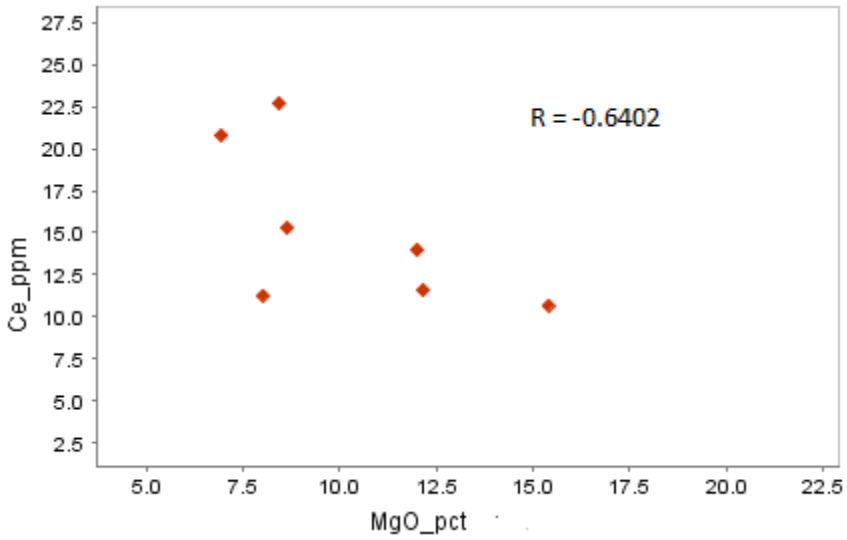
R = -0.6402
Ce_ppm
MgO_pct
27.5
25.0
22.5
20.0
17.5
15.0
12.5
10.0
7.5
5.0
2.5
5.0
7.5
10.0
12.5
15.0
17.5
20.0
22.5

(a)

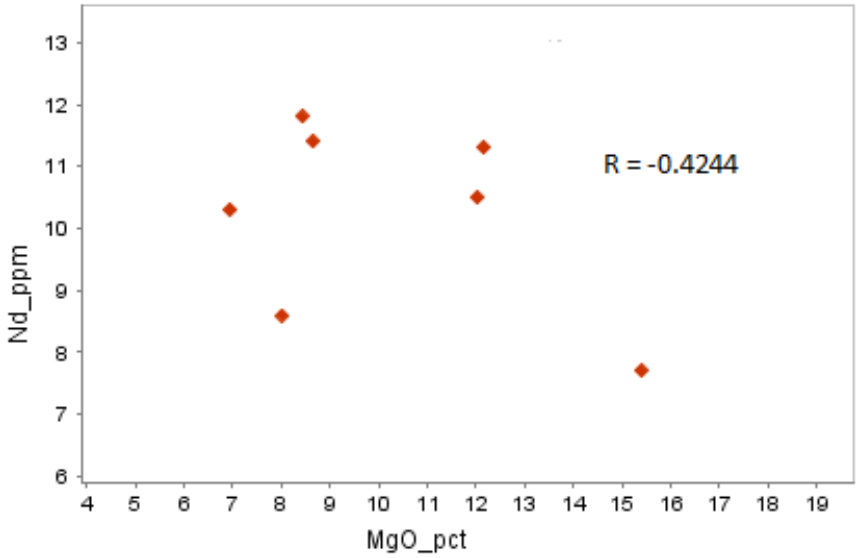
R = -0.4244
Nd_ppm
MgO_pct
13
12
11
10
9
8
7
6
4
5
6
7
8
9
10
11
12
13
14
15
16
17
18
19

(b)

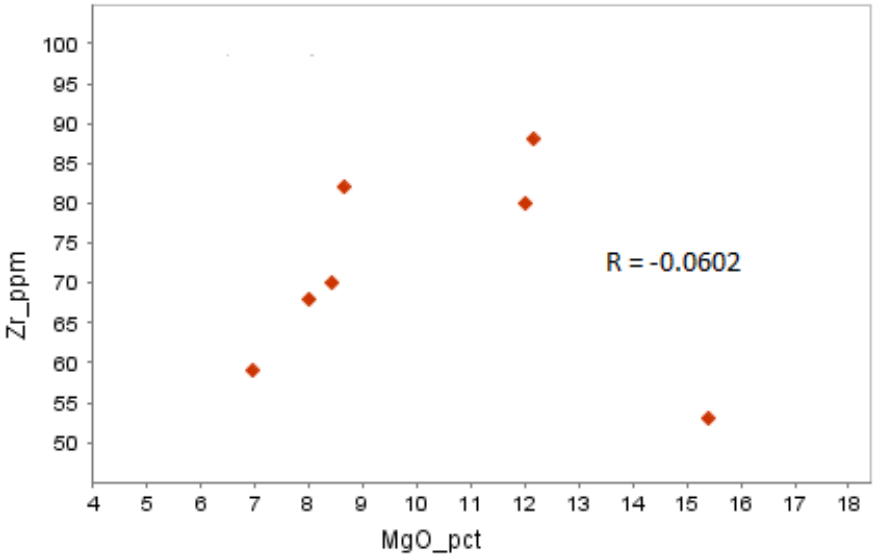
R = -0.0602
Zr_ppm
MgO_pct
100
95
90
85
80
75
70
65
60
55
50
4
5
6
7
8
9
10
11
12
13
14
15
16
17
18

(c)

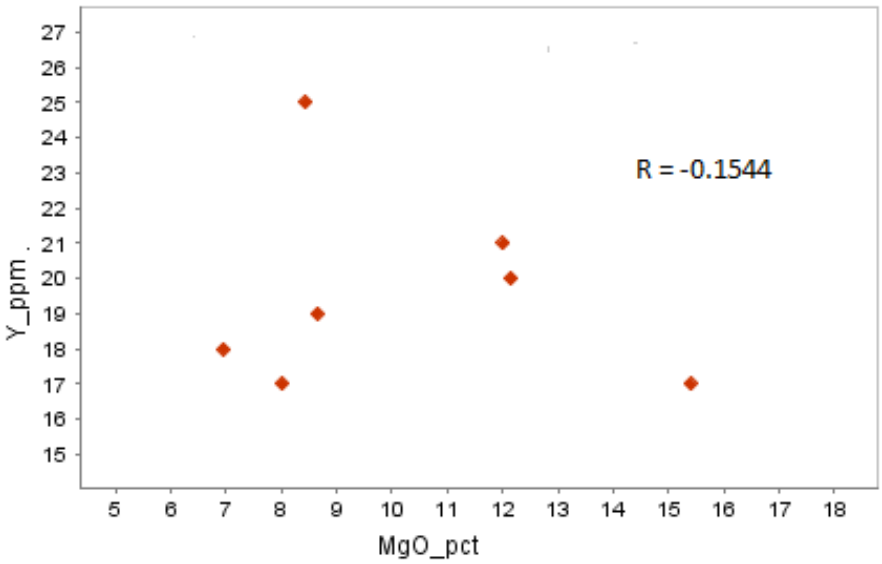

(d)

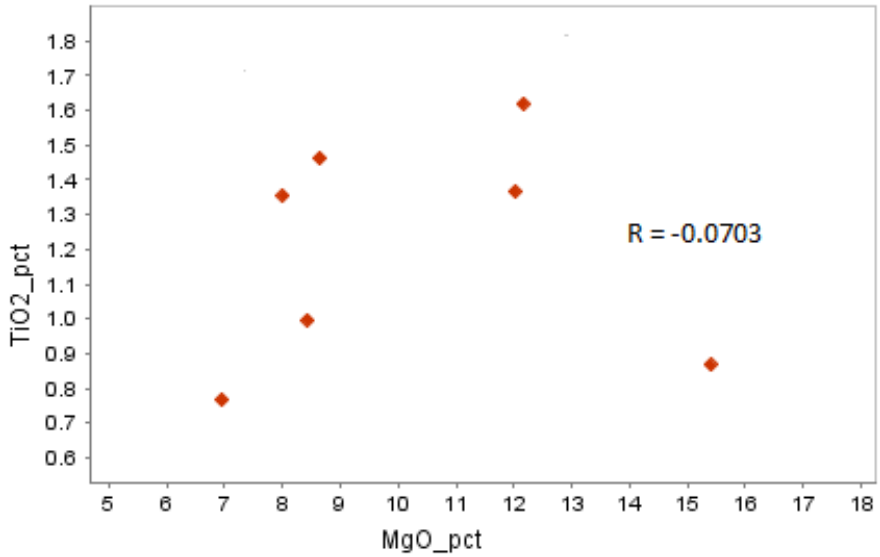

(e)

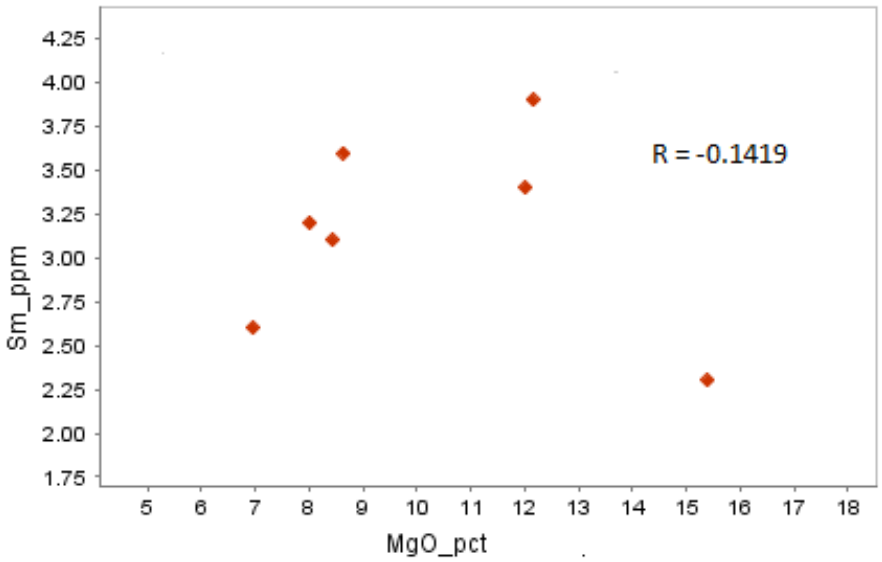

(f)

Figure 4.46: Variation plots of MgO some vs HFSE (incompatible elements), calc-alkalic mafic dykes samples, where: (a) =MgO vs Ce; (b) = MgO vs Nd; (c) = MgO vs Zr; (d) = MgO vs Y; (e) = MgO vs TiO_2; (f) = Mg vs Sm, of the Study area.

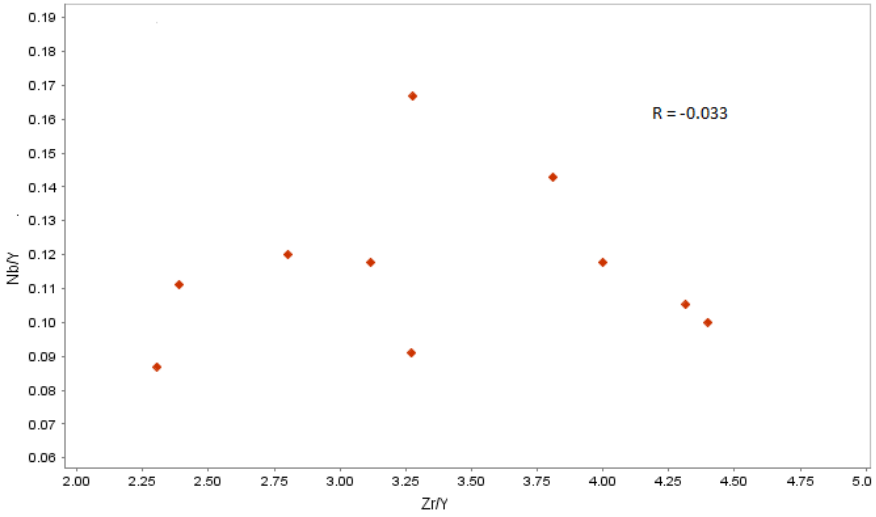

Figure 4.47: Variation plot of the ratios of Zr/Y vs Nb/Y, calc-alkalic mafic dyke rock samples of the Study area.

On the primitive mantle-normalised multi-element spider diagram plot of the calc-alkalic rock samples of the Study area (Figure 4.48), negative anomalies are noticed for Nb-Ta, whilst Hf-Zr show no anomaly at all. On the Chondrite-normalised REE variation diagram (Figure 4.49), the calc-alkalic dykes display a mild negative anomaly for Y. From the isotopic results of the three studied samples from the Study area, which happen to all be calc-alkalic, the negative εNd(t) values (−5.23 to – 9.73) (see section 4.3) suggest contamination by crustal material. From the observed chemical characteristics, the studied samples of the calc-alkalic mafic dykes of the Study area clearly indicate crustal contamination during the processes that led to

their emplacement. There is also a possibility that the parent magma was drawn from a contaminated mantle melt.

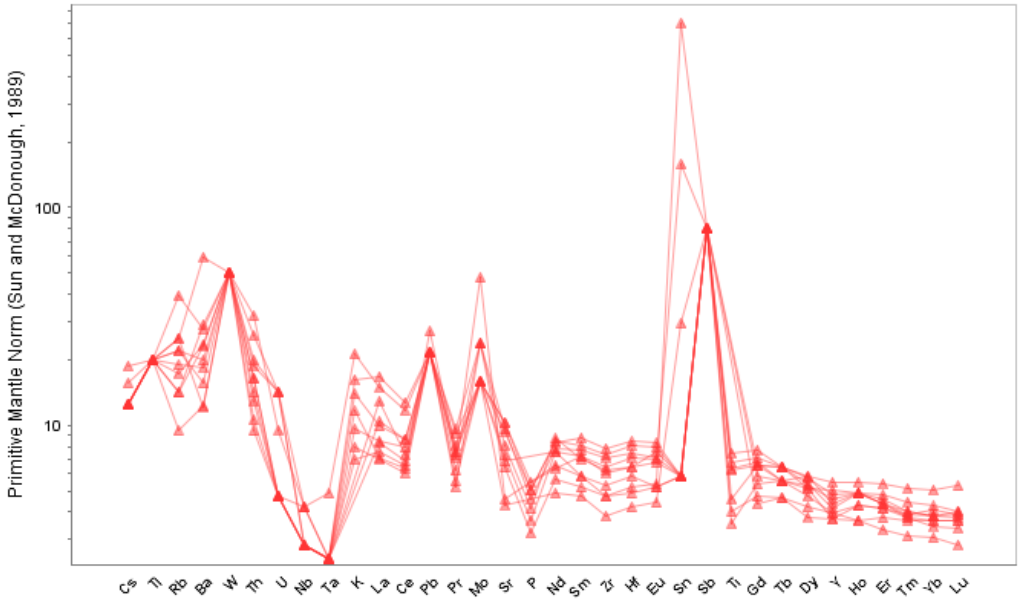

Figure 4.48: Primitive mantle-normalised multi element variation diagram for calc-alkalic rocks of the Study area, normalising values from Sun and Mc Donough (1989).

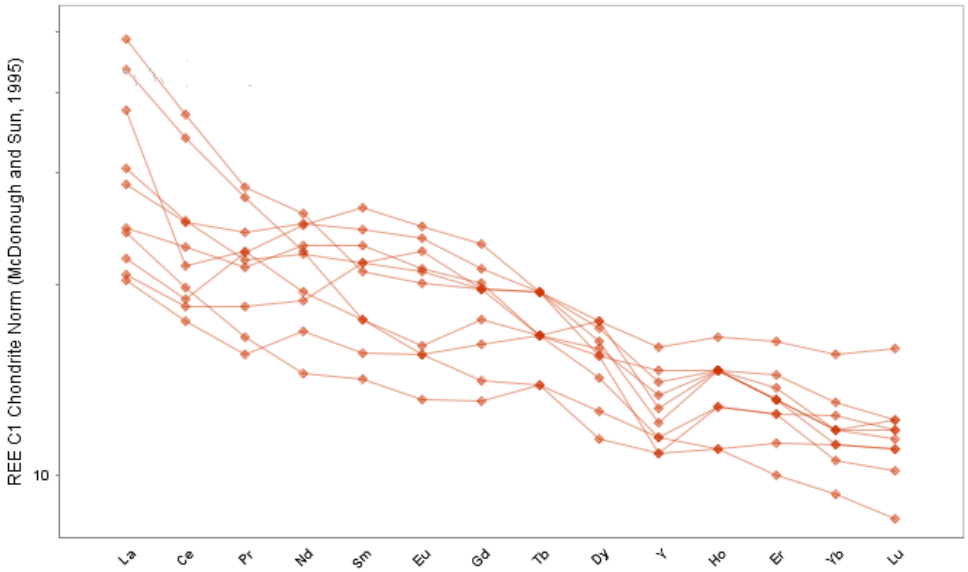

Figure 4.49: Chondrite-normalised REE variation diagram for calc-alkalic rocks of the study area, normalising values from Mc Donough and Sun (1995).

4.5.2 Fractional Crystallisation

Variation diagrams of MgO and Mg# as well as SiO_2, as indices, against major oxides and selected trace elements are useful tools in examining and evaluating possible fractionation crystallisation of mafic igneous rocks (Lightfoot et al., 1991; O'Hara and Herzberg, 2002;

Hamala et al., 2004; Zhang et al., 2011; Srivastava et al., 2014). In this study, MgO and SiO_2 are applied for the same purpose of examining possible crystallisation behaviour of the studied samples of both types of rocks.

Tholeiitic dykes

Almost all the plotted major oxides exhibit increase with decreasing MgO, crystallisation differentiation/fractionation (Figure 4.50). This crystallisation fractionation is also evidenced by some linear correlation variations exhibited in decreasing elemental concentrations of TiO_2, CaO and P_2O_5 with the increase in the concentrations of SiO_2 (Figure 4.51). These observed major element correlations with MgO, are consistent with the fractionation of olivine and clinopyroxene (Cheng et al., 2015).

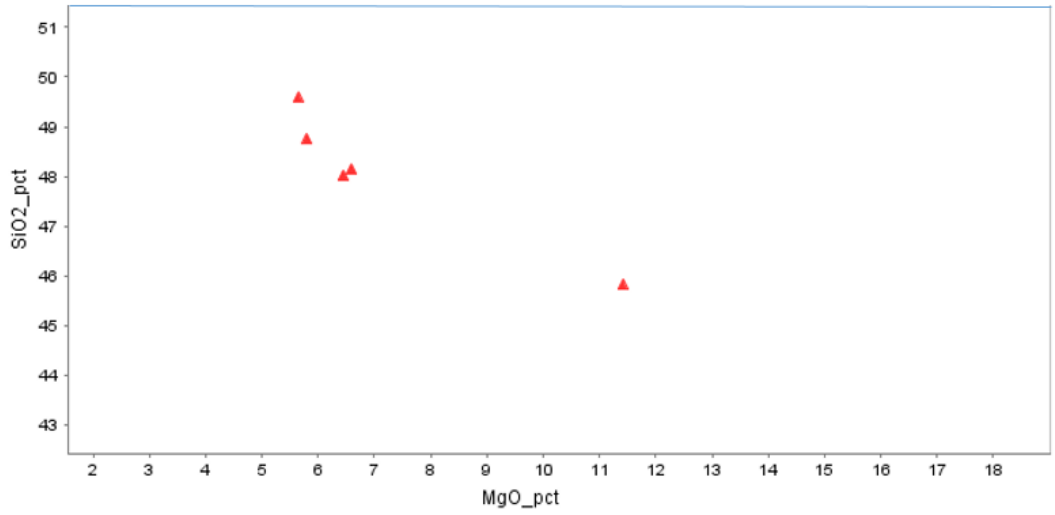

(a)

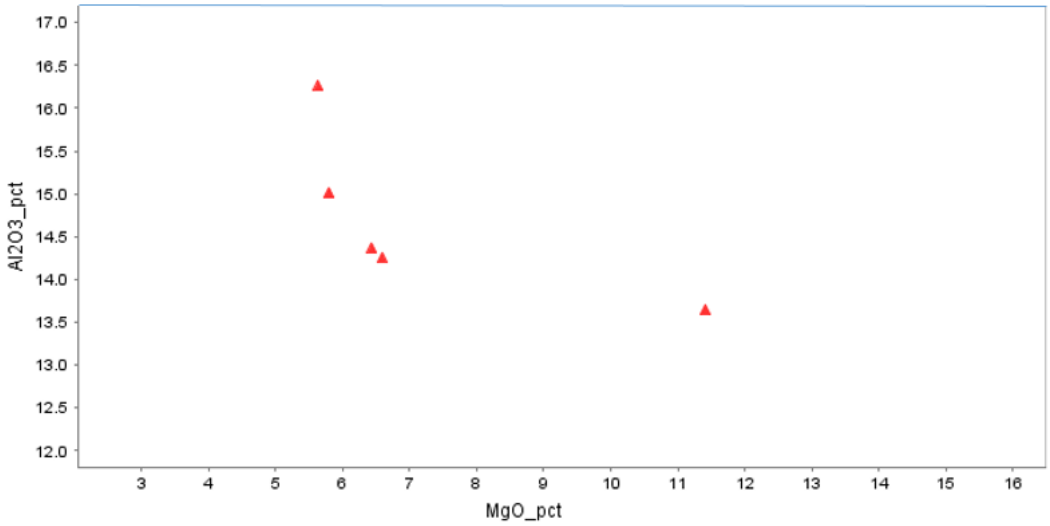

(b)

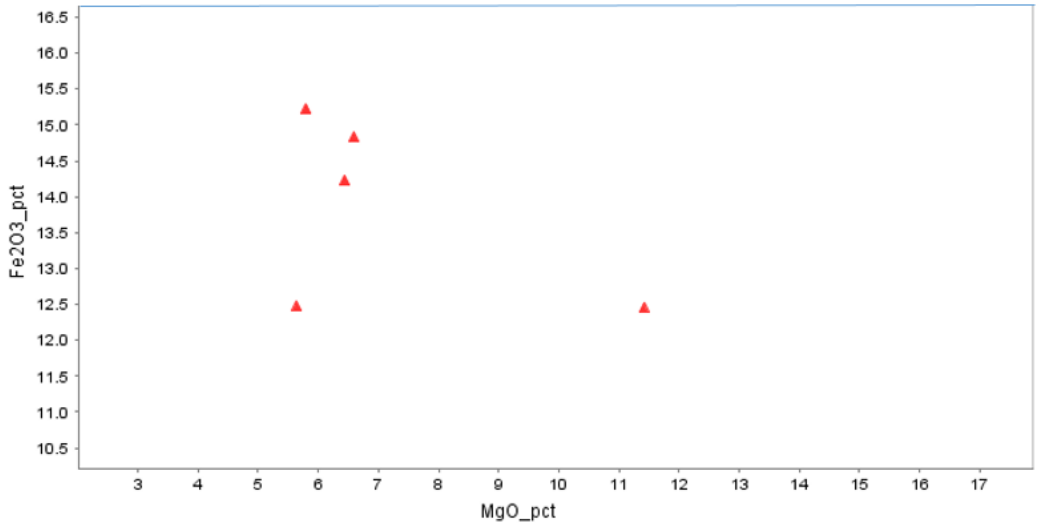
Fe2O3_pct
16.5
16.0
15.5
15.0
14.5
14.0
13.5
13.0
12.5
12.0
11.5
11.0
10.5
3
4
5
6
7
8
9
10
11
12
13
14
15
16
17
MgO_pct

(c)

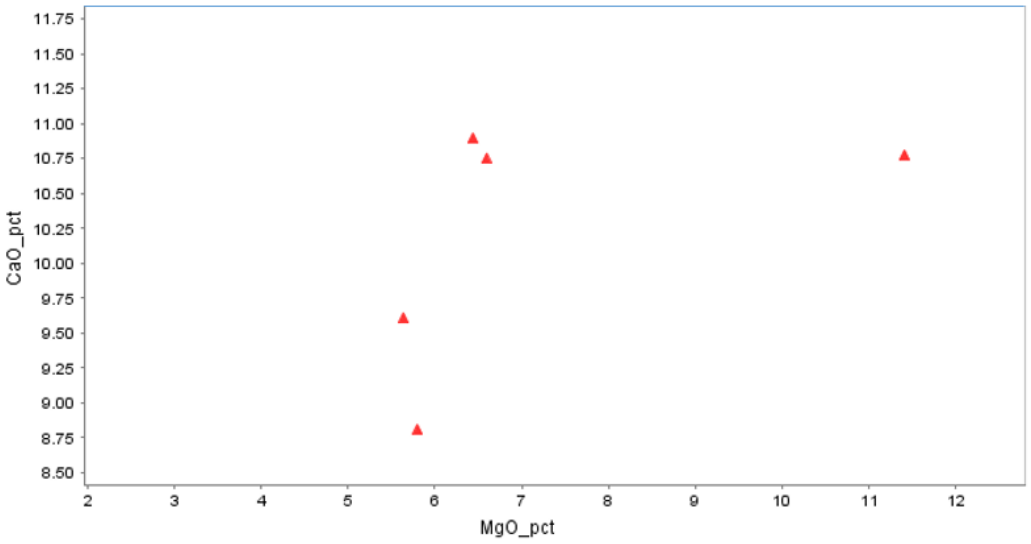
CaO_pct
11.75
11.50
11.25
11.00
10.75
10.50
10.25
10.00
9.75
9.50
9.25
9.00
8.75
8.50
2
3
4
5
6
7
8
9
10
11
12
MgO_pct

(d)

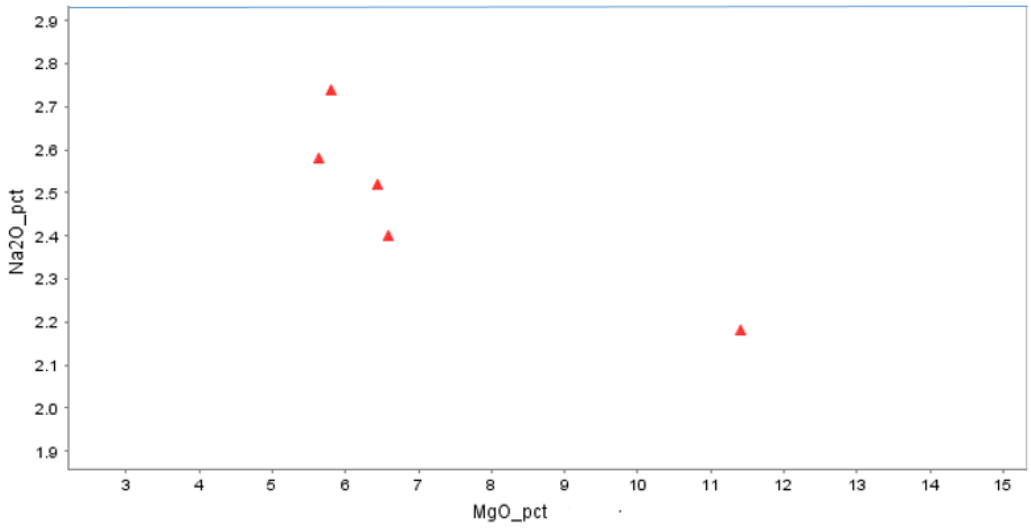
Na2O_pct
2.9
2.8
2.7
2.6
2.5
2.4
2.3
2.2
2.1
2.0
1.9
3
4
5
6
7
8
9
10
11
12
13
14
15
MgO_pct

(e)

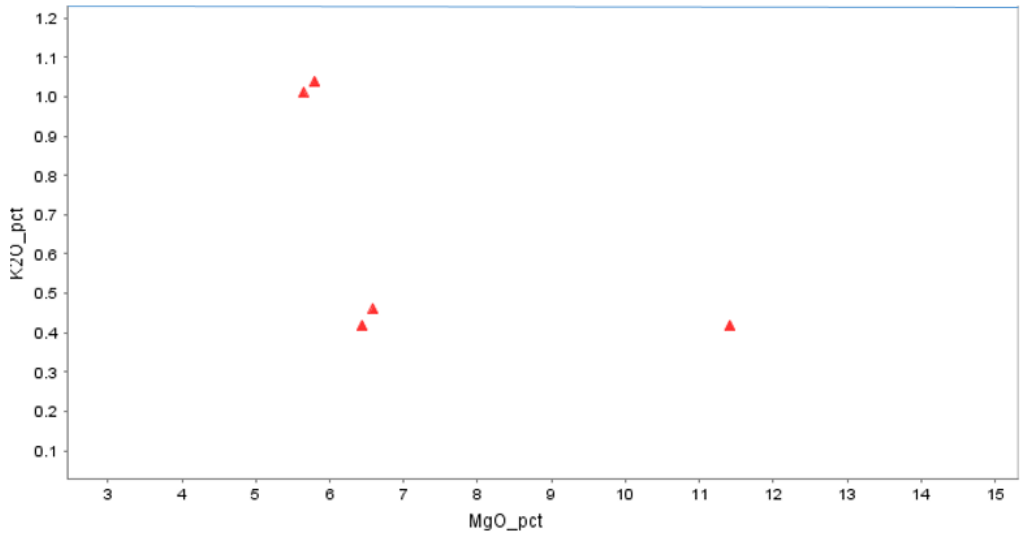

(f)

Figure 4.50: Variation plots of MgO vs some major oxides, tholeiitic mafic dykes samples, where: (a) = MgO vs SiO_2; (b) = MgO vs Al_2O_3; (c) = MgO vs Fe_2O_3; (d) = MgO vs CaO; (e) = MgO vs Na_2O; and (f) = MgO vs K_2O, of the Study area.

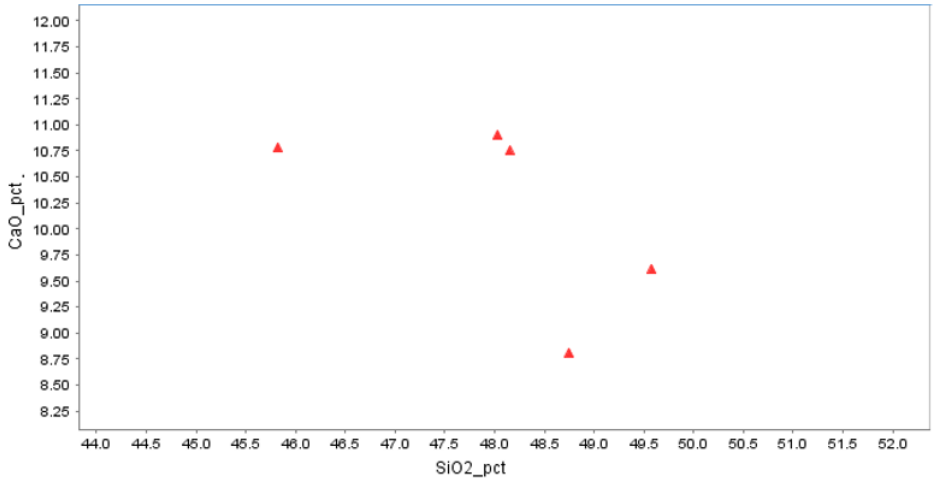

(a)

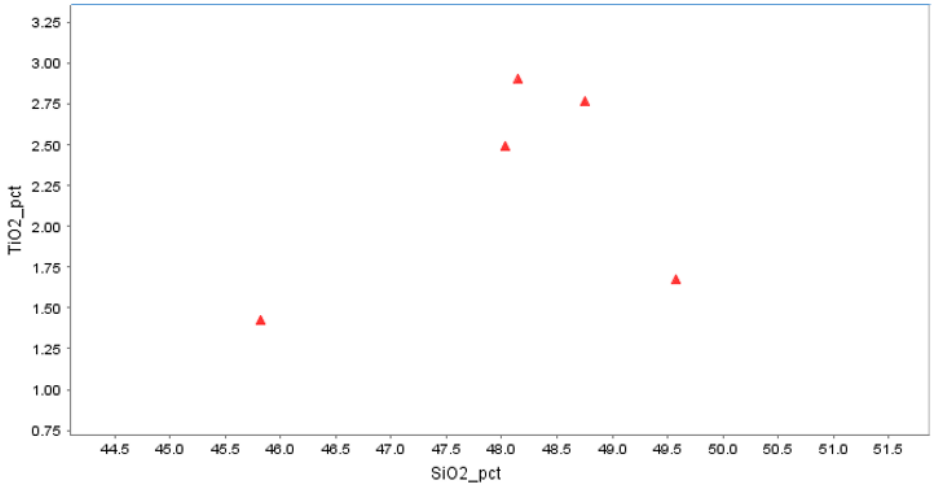

(b)

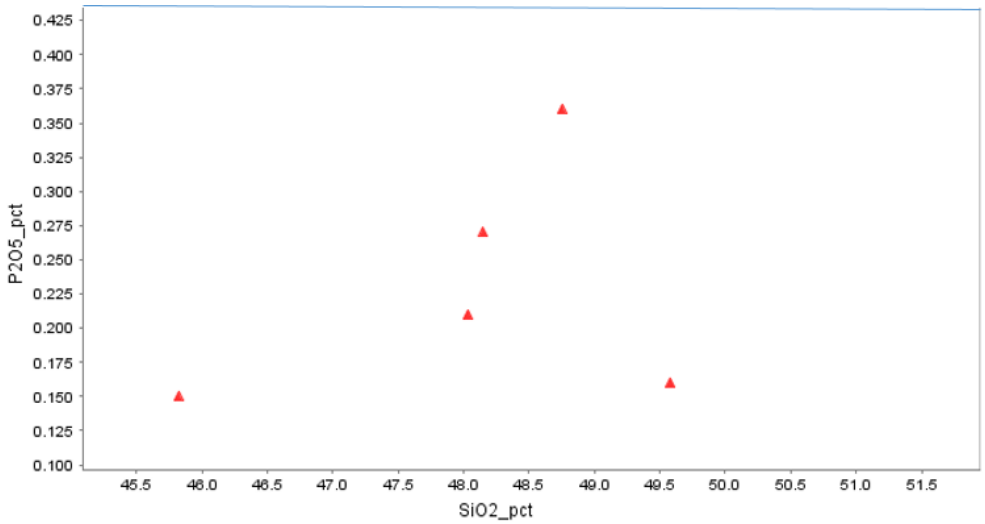

(c)

Figure 4.51: Variation plots of SiO_2 vs (a) CaO, (b) TiO_2, and (c) P_2O_5, tholeiitic mafic dykes samples of the Study area.

The decrease in MgO plus FeO_T concentrations with the increase in SiO_2 (Figure 4.51) indicates the crystallisation fractionation of olivine (Zi et al., 2008), whilst the negative correlation between SiO_2 and CaO/Al_2O_3 (Figure 4.52) suggests the clinopyroxene crystallisation fractionation. The decrease of compatible elements, Cr and Ni, with the decrease in Mg# (magma evolution) (Figure 4.54) is indicative of the fractionation crystallisation of olivine and clinopyroxene (Zi et al., 2008). The positive linear correlation between TiO_2 and P_2O_5 (Figure 4.55) content indicates simultaneous fractionation from least differentiated mafic magma composition, with higher TiO_2-P_2O_5 content, to a more differentiated mafic magma that has lower TiO_2-P_2O_5 concentrations (Karmalkar et al., 2016). The wide ranges of Mg#, MgO, Ni and Cr indicate significant crystallisation fractionation either in magma chambers or during ascent (Zi et al., 2008; Srivastava et al., 2014). The low Mg# (29.7 – 58.0), Ni (80–720 ppm) and Cr (150–1400 ppm) are suggestive of evolved magmas that underwent fractional crystallisation (Cheng et al., 2015).

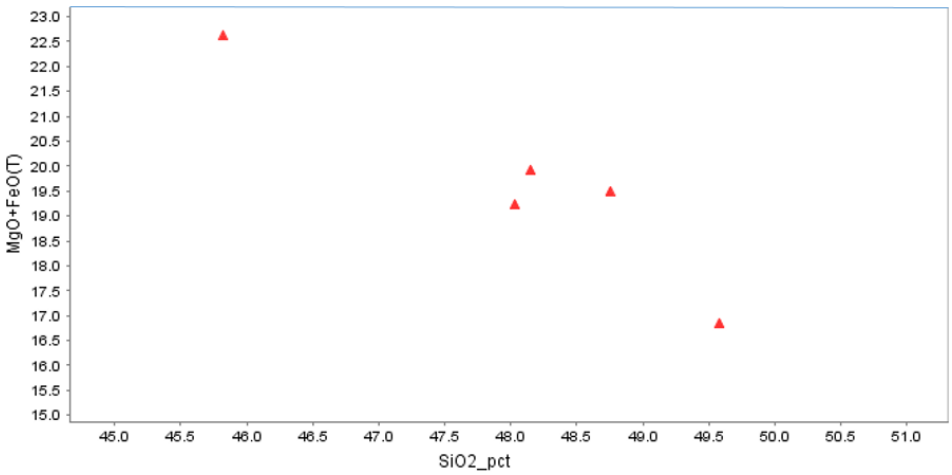

Figure 4.52: Variation plot of SiO_2 vs MgO+FeO(T), tholeiitic mafic dykes samples of the Study area.

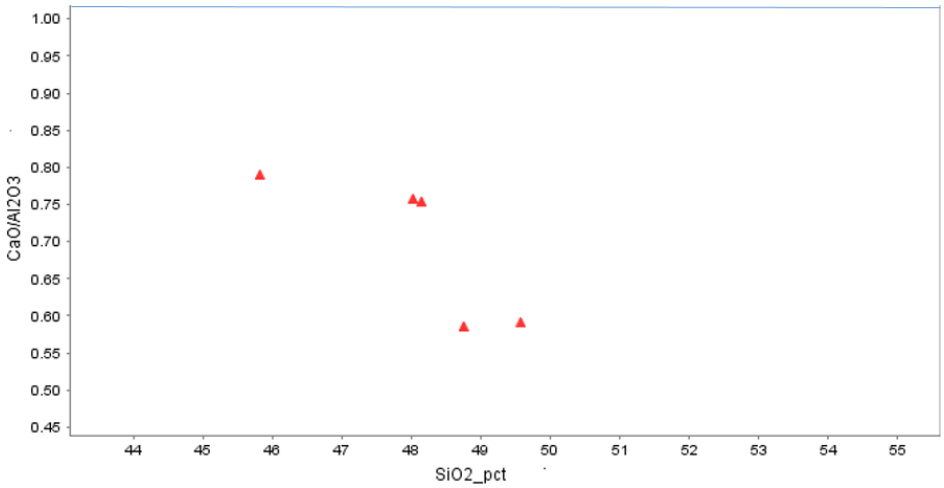

Figure 4.53: Variation plots of SiO_2 vs CaO/Al_2O_3, tholeiitic mafic dykes samples of the Study area.

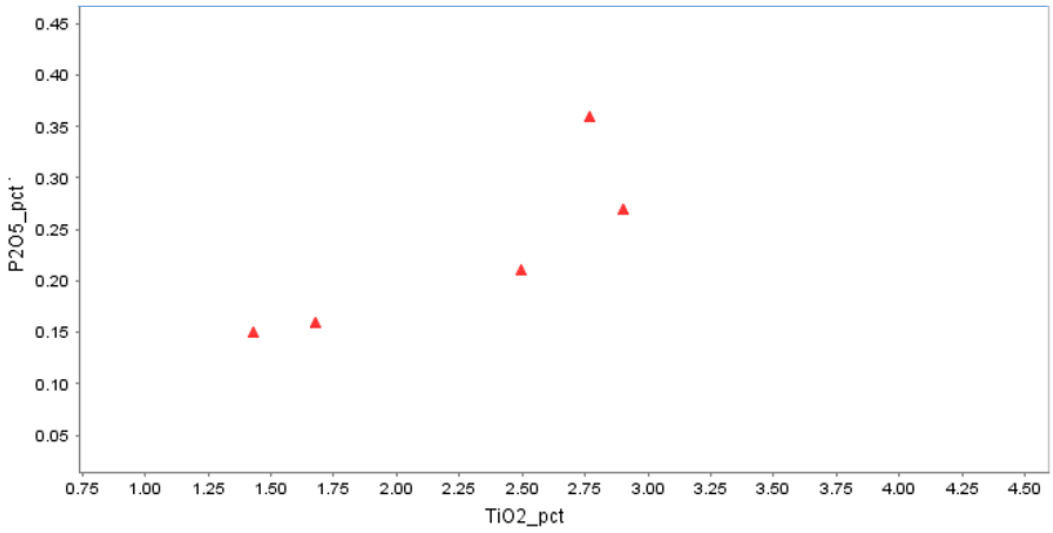

Figure 4.54: Variation plot of TiO_2 vs P_2O_5, tholeiitic mafic dykes samples of the Study area.

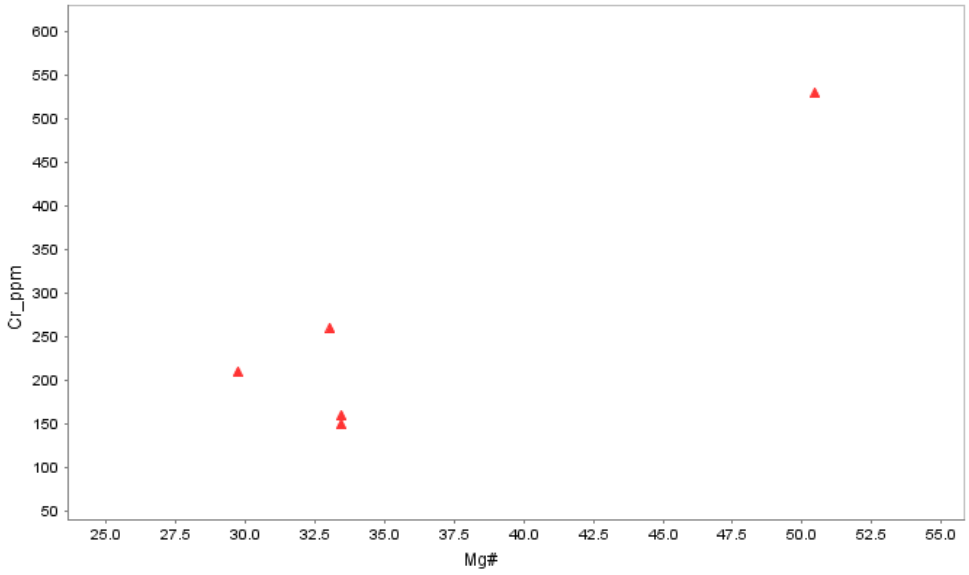

(a)

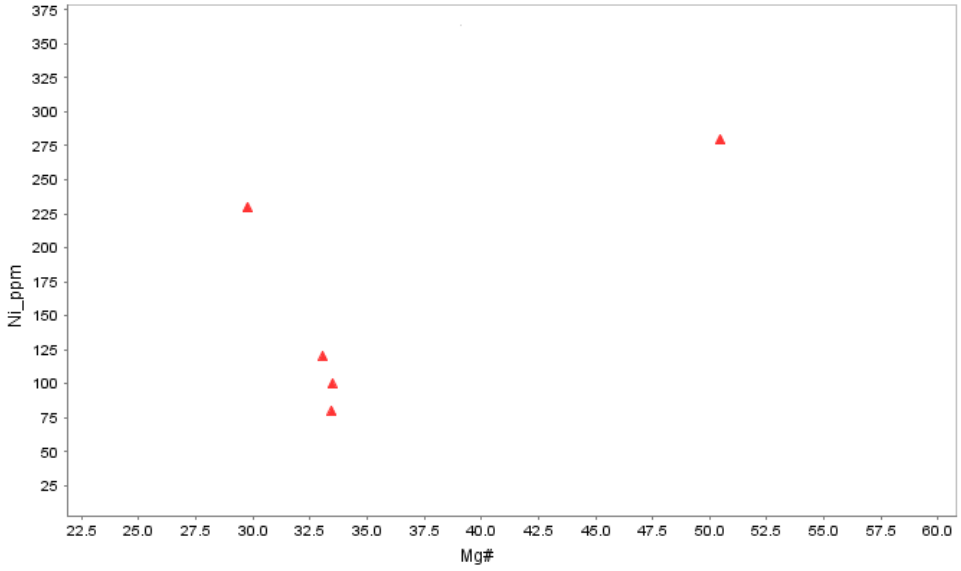

(b)

Figure 4.55: Variation plots of Mg# vs compatible elements, Cr and Ni, tholeiitic mafic dykes samples of the Study area.

Calc-alkalic dykes

The chemical features which are observed in the tholeiitic dyke samples concerning the assessment of crystallisation fractionation, are also displayed in the calc-alkalic dyke samples. Almost all the plotted major oxides exhibit increase with decreasing MgO, crystallisation differentiation/fractionation (Figure 4.56) and decreasing elemental concentrations of TiO_2, CaO, Fe_2O_3 and P_2O_5 with the increase in the concentrations of SiO_2, are also observed (Figure 4.57).

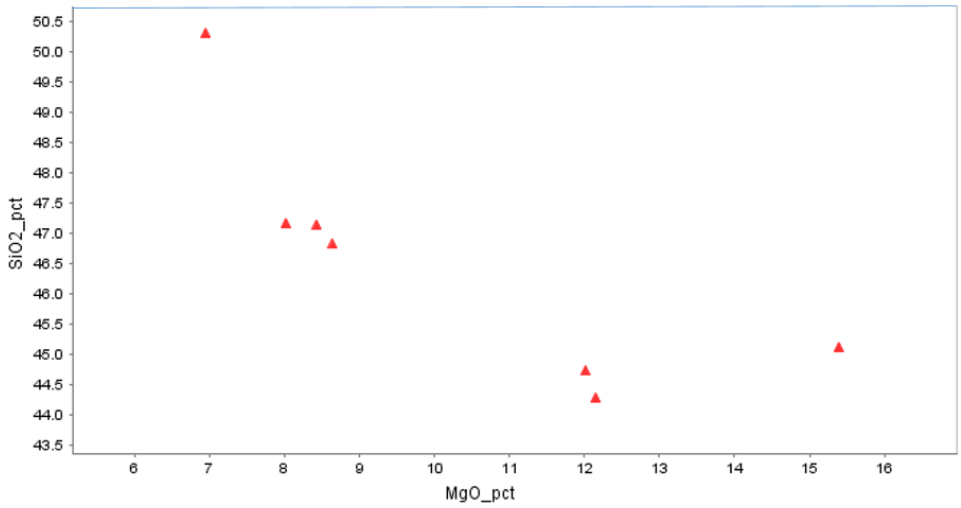
SiO2_pct
MgO_pct

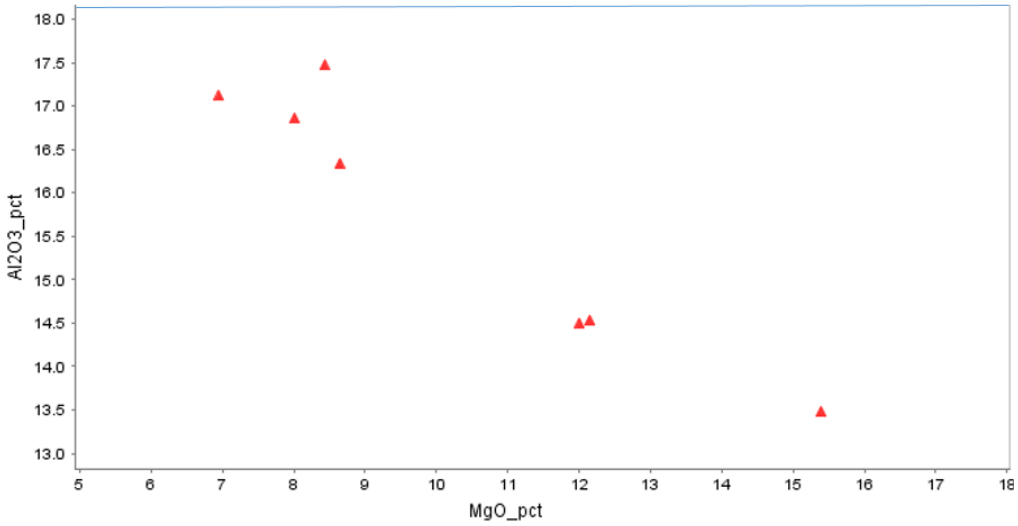
Al2O3_pct
MgO_pct

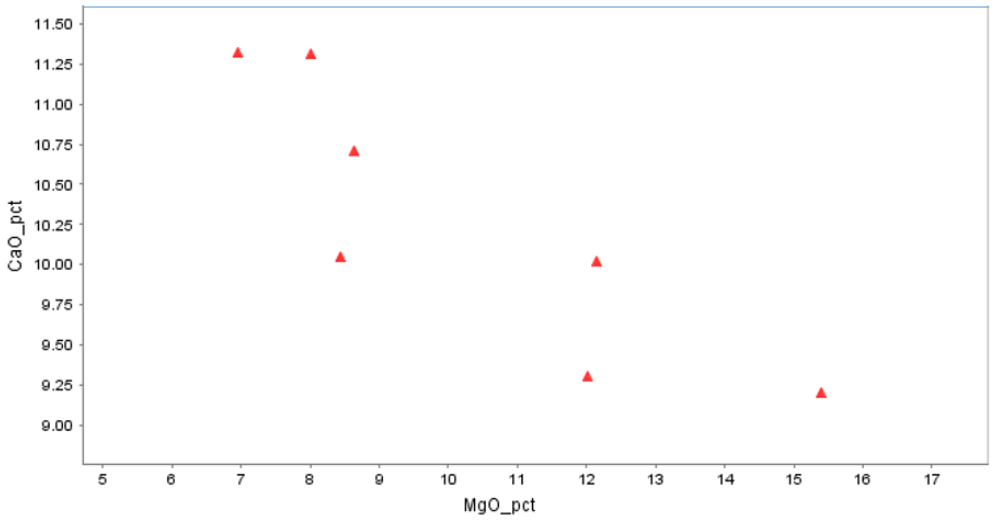
CaO_pct
MgO_pct

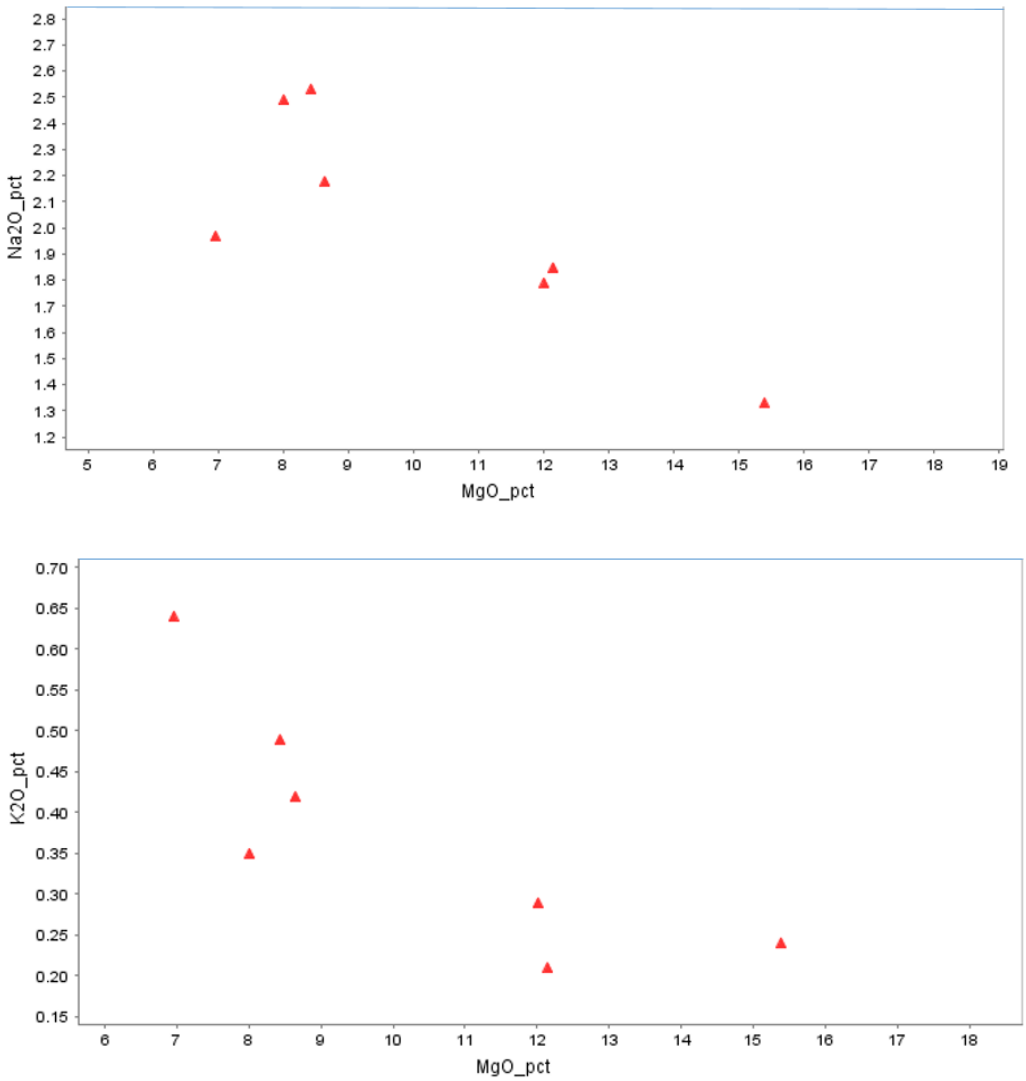

Figure 4.56: Variation plots of MgO vs major oxides, calc-alkalic mafic dykes samples, where: (a) = MgO vs SiO_2; (b) = MgO vs Al_2O_3; (c) = MgO vs CaO; (d) = MgO vs Na_2O; and (e) = MgO vs K_2O, of the Study area.

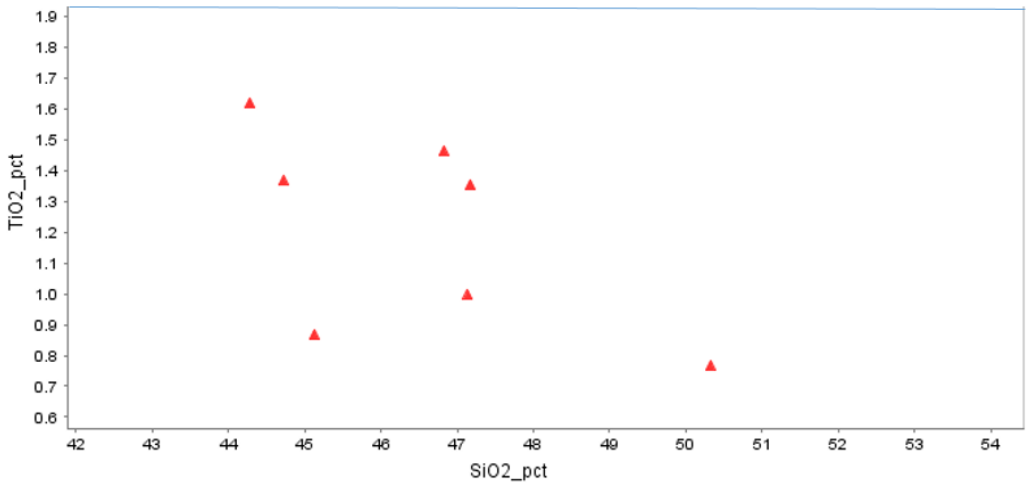

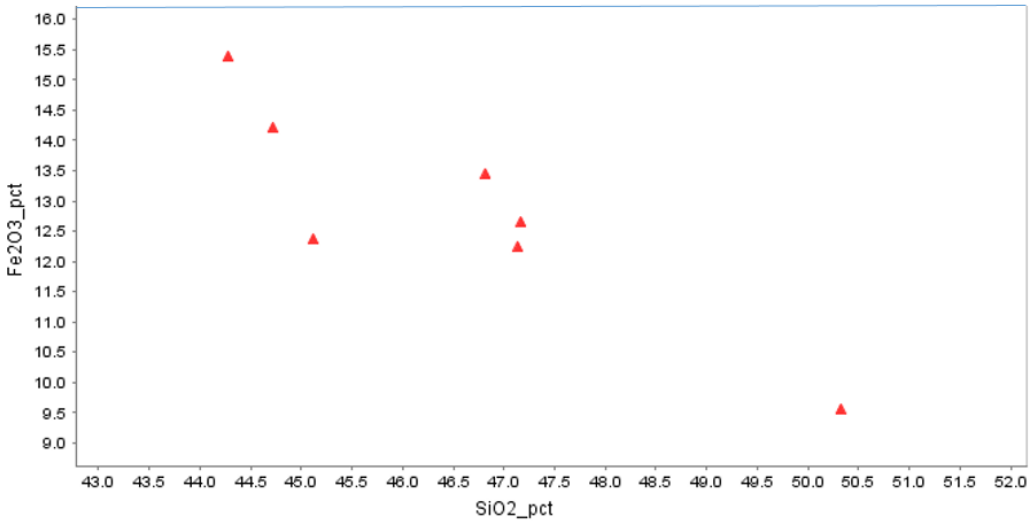

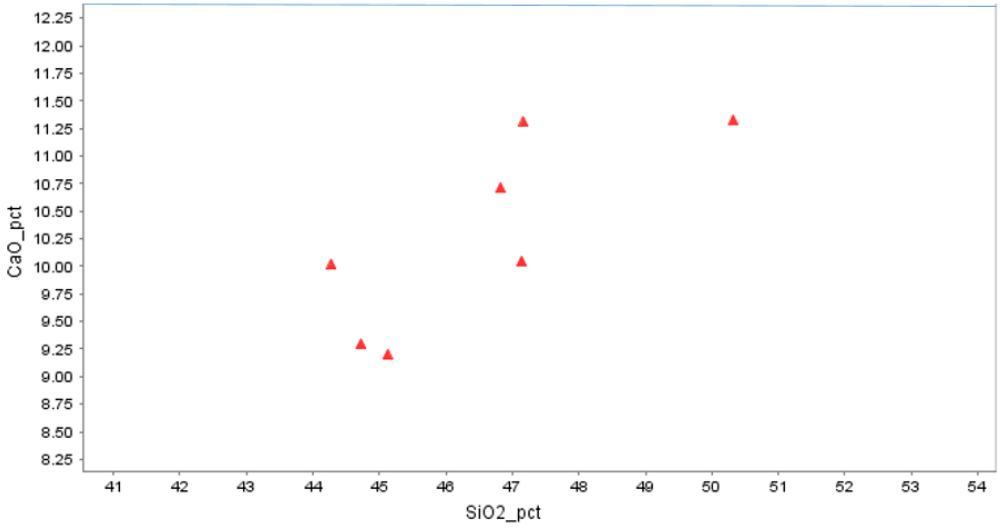

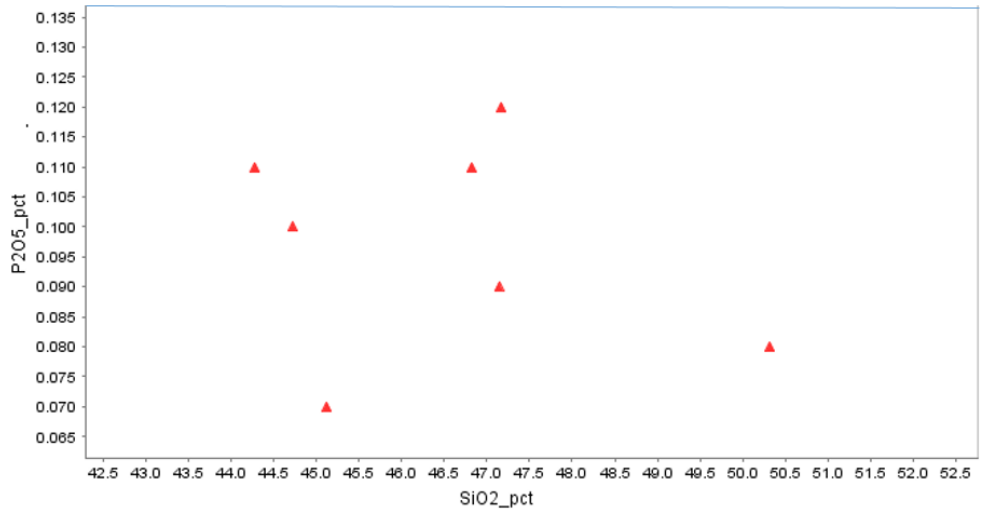

Figure 4.57: Variation plots of SiO_2 vs (a) CaO, (b) TiO_2, (c) Fe_2O_3, and (d) P_2O_5, calc-alkalic mafic dykes samples of the Study area.

The decrease in MgO plus FeO_T concentrations with the increase in SiO_2 (Figure 4.58), which indicates crystallisation fractionation of olivine, and the negative correlation between SiO_2 and CaO/Al_2O_3 (Figure 4.59) that suggests the clinopyroxene crystallisation fractionation are also manifested in the calc-alkalic rock samples. The decrease of compatible elements, Cr and Ni, with the decrease in Mg# (magma evolution) (Figure 4.60), indicative of the fractionation crystallisation of olivine and clinopyroxene, is another feature which is also well exhibited in the calc-alkalic dyke samples. The positive linear correlation between TiO_2 and P_2O_5 content (Figure 4.61), which indicates simultaneous fractionation from least differentiated mafic magma composition, with higher TiO_2-P_2O_5 content, to a more differentiated mafic magma that has lower TiO_2-P_2O_5 concentrations is well displayed.

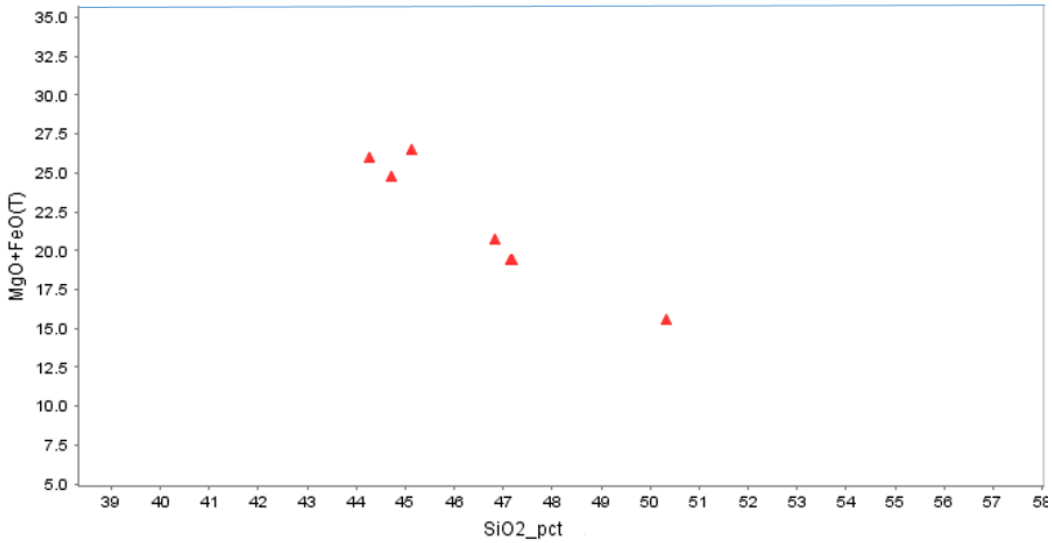

Figure 4.58: Variation plots of SiO_2 vs MgO+FeO(T), calc-alkalic mafic dykes samples of the Study area.

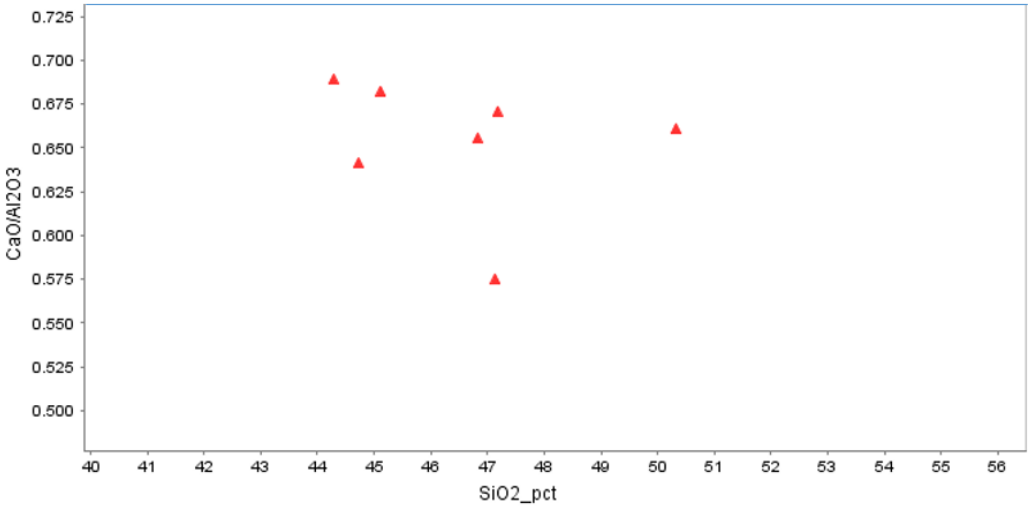

Figure 4.59: Variation plot of SiO_2 vs Cao/Al_2O_3, calc-alkalic mafic dykes samples of the Study area.

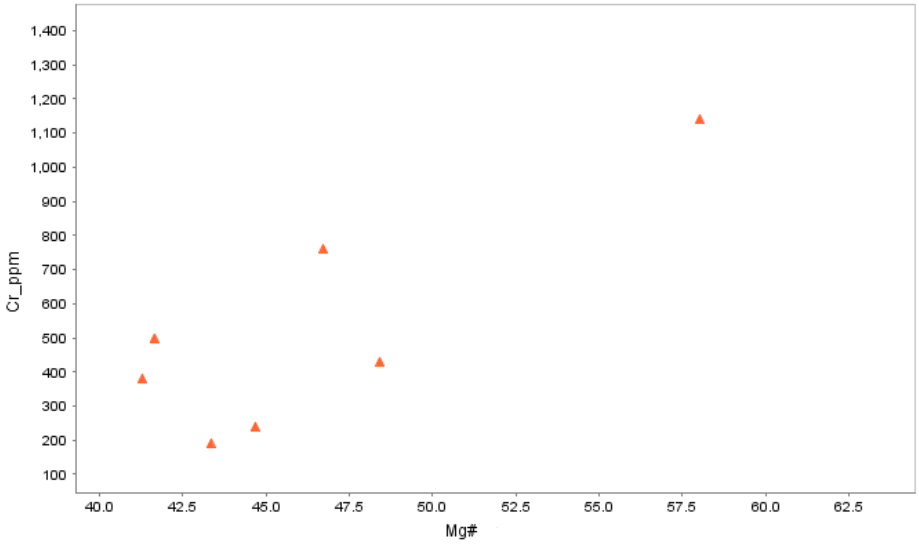

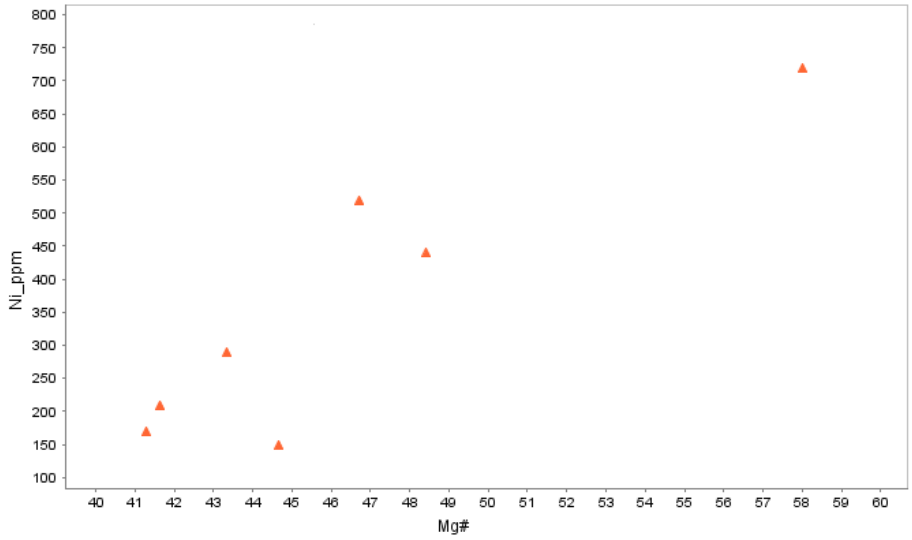

Figure 4.60: Variation plots of Mg# vs compatible elements, (a) Cr, and (b) Ni, calc-alkalic mafic dykes samples of the Study area.

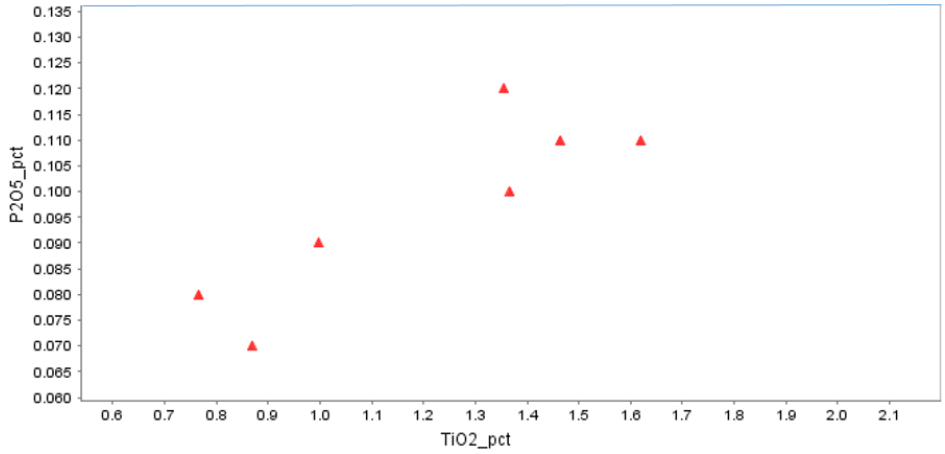

Figure 4.61: Variation plots of TiO_2 vs P_2O_5, calc-alkalic mafic dykes samples of the Study area.

4.5.3 Magma Mantle Source

An important integral part of any petrogenetic studies of basaltic rocks is the evaluation of the source of the magma from which the rocks being studied crystallised, and in almost all cases, the source of the magma is the mantle (Takahashi, 1986; Pearce and Parkinson 1993; Turner and Hawkesworth, 1995; Phinney and Halls, 2001, Pertermann and Hirschmann, 2003a; Tatsumi and Suzuki, 2009; Srivastava et al., 2014; Sreenivasulu et al., 2014; Sayit et al., 2016; Murphy et al., 2019). Basalts, high-MgO picrite melts and komatiites that have erupted on Earth were produced by variable conditions of partial melting of a mantle source and partial crystallisation, assimilation, and mixing during transit to and within the crust (Herzberg and Asimow, 2015). In this study, the magma source of the dykes is evaluated by applying selected chemical information

REE patterns and their element ratios, are useful tools in the evaluation and understanding of melting conditions and nature of mantle compositions (Cullers and Graf 1984; Hirschmann et al. 1998; Srivastava et al., 2014). The chemical patterns of this group of elements, combined with HFSE, represent the original composition of the unaltered parental magma (Srivastava et al., 2014). Plots of Zr/Y vs Nb/Y and La/Yb vs Zr/Nb ratios have been applied to extract useful information related to the possible mantle sources (Aldanmaz et al., 2000; Sayıt et al., 2016). According to Sun and McDonough (1989), N-MORB ratios are as follows: Zr/Y= 2.64; Nb/Y= 0.08; and La/Yb= 0.81; and that lower ratio values would indicate derivation from a depleted mantle source.

The studied dykes are already established to have the following features that determine what they are: 1) petrographically they are classified as gabbroic; 2) chemically there are two types of rocks, tholeiitics and calc-alkalics, both types being of sub-alkalic affinity; 3) major and trace element data for each dyke type suggest a genetic relationship of the samples in the particular type; 4) calculated Mg# for both types of dykes shows a wide variation with values ranging between 29.7 and 58.0; and these Mg-numbers are much lower than the Mg# of 70 which is estimated for primitive mantle-derived basaltic magmas.

Tholeiitic dykes

On plots of Zr/Y vs Nb/Y Geotectonic discrimination plot, adapted from Srivastava et al., (2014), four out of five samples plot on the N-MORB side of the dividing line (Figure 4.62), indicating some N-MORB affinity. On the La/Yb vs Zr/Nb ratios model diagram of Aldanmaz et al. (2008), samples of tholeiitic rocks plot to the left (enriched by melt addition) of the dividing line between enrichment and depletion (Figure 4.63). The samples plot on the “enriched by addition” side of the mantle. The studied samples’ ratio values which are calculated from the

analytical results: Zr/Y= 3.8-6; Nb/Y= 0.4-0.9; La/Yb= 6.6-10.1 and Zr/Nb= 6.0-10.24; are higher than those of Sun and McDonough (1989). These higher ratio values of Zr/Y, Nb/Y and La/Yb suggest derivation from an enriched mantle, OIB. The low Mg# values ranging between 29.7 and 50.5 indicate derivation from an evolved magma, and not primitive magma.

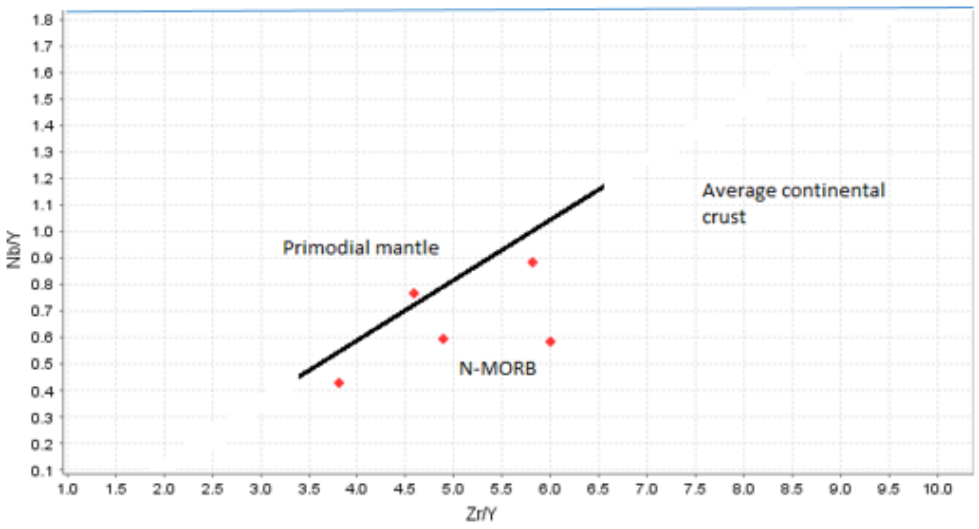

Figure 4.62: Geotectonic Zr/Y vs Nb/Y discrimination plot, adapted from Srivastava et al., (2014) (with fields as follows: N-MORB (Fitton et al., 1997; Baksi, 2000); Primodial mantle (McDonough and Sun, 1995); and Average Continental Crust (Rudnick and Fountain, 1995)) for the tholeiitic rock type of the mafic dykes of the Irumide Fold Belt, Zambia.

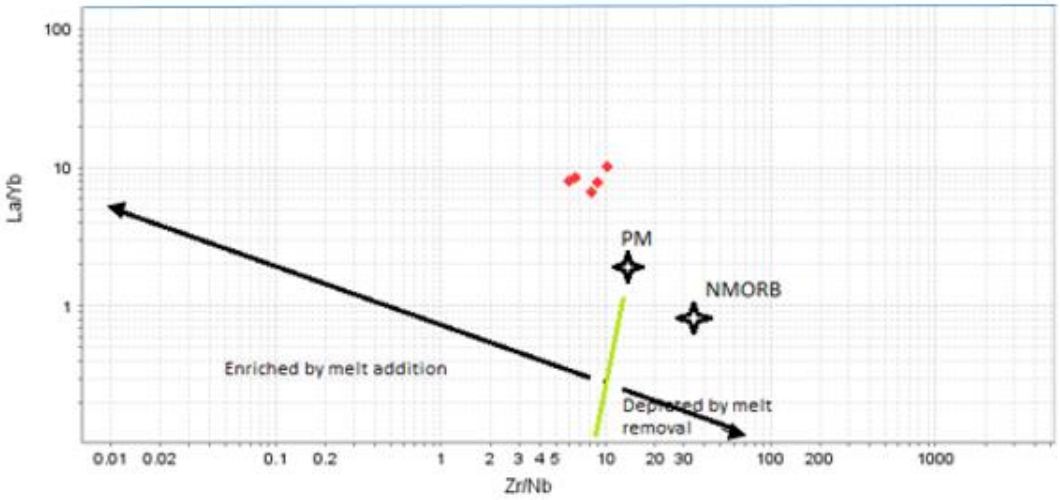

Figure 4.63: La/Yb vs Zr/Nb plot of the tholeiitic rock type of the mafic dykes of the Irumide Fold Belt of Northeastern Zambia, after the model diagram of Aldanmaz et al. (2008).

Calc-alkalic dykes

On the mantle source discrimination diagrams, eNd vs Th/Yb and eNd vs Ce/Yb, both of De Paolo (1988) (Figures 4.64 and 4.65) all the tree samples of the Study area which were analysed for isotopic data, plot in the zone of Paleoproterozoic crust on both diagrams. The

studied samples ratio values which are calculated from the analytical results: Zr/Y= 2.3-4.4; Nb/Y= 0.1-0.2; La/Yb= 2.7-5.2 and Zr/Nb= 21.5-44.0; are higher than those of Sun and McDonough (1989). Like in the case of the tholeiitic dyke samples, these higher ratio values of Zr/Y, Nb/Y and La/Yb suggest derivation from an enriched mantle. The Mg# values ranging between 41.29 and 58.01 are much lower than those of derivation from primitive magma (Mg#=70) and hence indicate derivation from an evolved magma, and not primitive magma.

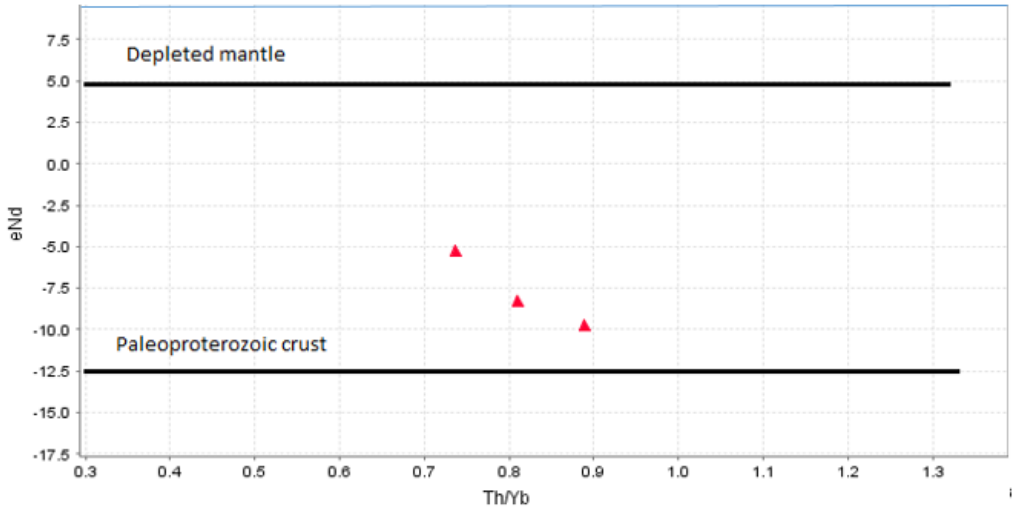

Figure 4.64: Isotope mantle source discrimination diagram, eNd vs Th/Yb for the calc-alkalic rock type of the mafic dykes of the Irumide Fold Belt of Northeastern Zambia, after De Paolo (1988).

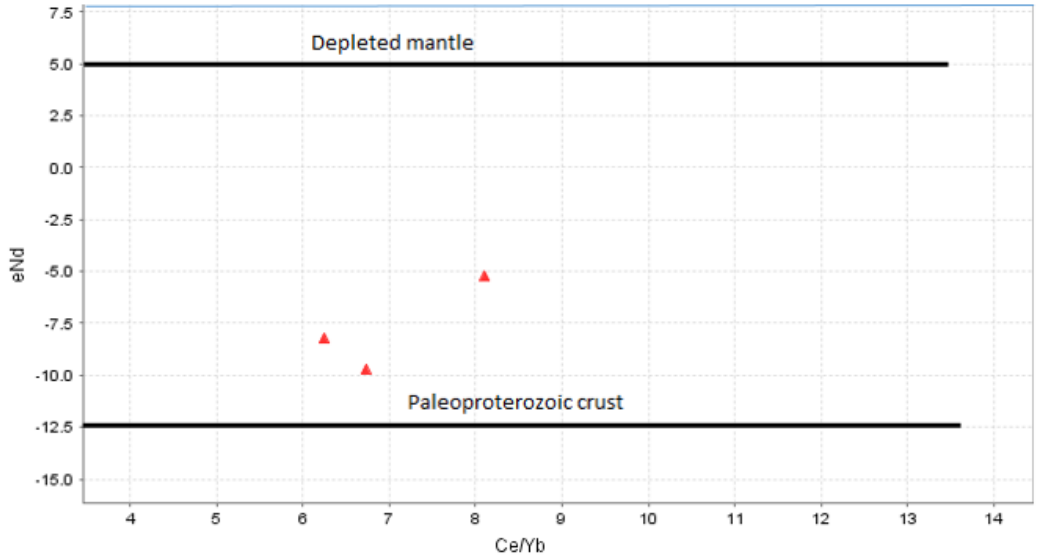

Figure 4.65: Isotope mantle source discrimination diagram, eNd vs Ce/Yb for the calc-alkalic rock type of the mafic dykes of the Irumide Fold Belt of Northeastern Zambia, after De Paolo (1988).

4.5.4 Partial Melting Processes

Studies have established that, melting of 15–30% of upper mantle peridotite may generate subalkaline tholeiitic magma, whereas any melting of less than 10% of peridotitic mantle would yield alkali-rich basaltic melt (Green, 1973; Hirschmann et al. 1998; Srivastava et al., 2014;). It has also been established that melts which are generated at low degree of melting show an enriched LREE (which are more incompatible and easily go in the melt) pattern, whereas their concentration decreases rapidly with increased melting (as more incompatible HREE get in the melt) up to 30% (Cullers and Graf 1984; Hirschmann et al. 1998; Srivastava et al., 2014). Beyond 30% of upper mantle melting, there is no significant change in the REE concentration (Srivastava et al., 2014). In this study, element and chemical combinations of TiO_2, Sm and Yb are applied in generating variation plots for the interpretation exercise. In addition, a computer based programme, PRIMELT3 MEGA.XLSM software is also applied separately for the same purpose.

TiO_2, Sm and Yb evaluation models

The rare earth element ratios and their trends are applied in this study in the evaluation of melting conditions and nature of mantle compositions. Models of Gribble et al., (1998) and Sayıt et al., (2016) of TiO_2 vs Yb and Sm vs Sm/Yb diagrams respectively, as adapted by Cimen (2016), are applied in the interpretation of the melting systematics (Figures 4.66 a & b). The method applied by Cimen (2016), of only using samples with MgO concentrations higher than 8 wt% to avoid effects of fractional crystallisation, is adopted. In this regard, the models could not be applied on the tholeiitic dyke samples as all of them, apart from one, show MgO concentration values which are less than 8 wt%. Consequently, the data used in Figures 4.66 a & b) is for the calc-alkalic dykes samples, which all but one, have MgO values greater than 8 wt%.

> "For the first diagrame (Figure 4.66a), the curve of "spinel lherzolite" is for non-modal batch melting and is labelled with degrees of F (estimates of degree of melting) for "primitive mantle" (PM) source concentrations of 0.217% TiO2 and 0.493 ppm Yb (**Sun and McDonough, 1989**), D_O= 0.117 and 0.127 (modal bulk coefficient) for a lherzolite composition ol: opx: cpx of 54:30:16, and P = 0.325 and 0.397 (non-modal bulk partition coefficient) for ol: opx: cpx melting proportions of 0:30:70. The curve of "garnet lherzolite" is for non-modal batch melting of a garnet lherzolite "primitive mantle" source with ol: opx: cpx: gar composition and melt proportion of 52:29:16:3 and 0:45:45:10, respectively. D_O and P are 0·127 and 0·247 for TiO2, and 0.288 and 0.684 for Yb. Both curves are labelled for from 5 to 40% melting (calculations taken from **Gribble et al., 1998**)".

"In constructing second curve (Figure 4.66b), however, first 25% batch melt is extracted from the spinel peridotite source and the residue is modified by 1% garnet-facies melt. This metasomatised source is assumed to have a mode of 0.700 Ol + 0.220 Opx + 0.065 Cpx + 0.015 Spi, which melts in a fractional fashion with the proportions of 0.20 Ol + 0.15 Opx + 0.55 Cpx + 0.10 Spi (calculations taken from Sayıt et al., 2016)".

(a)

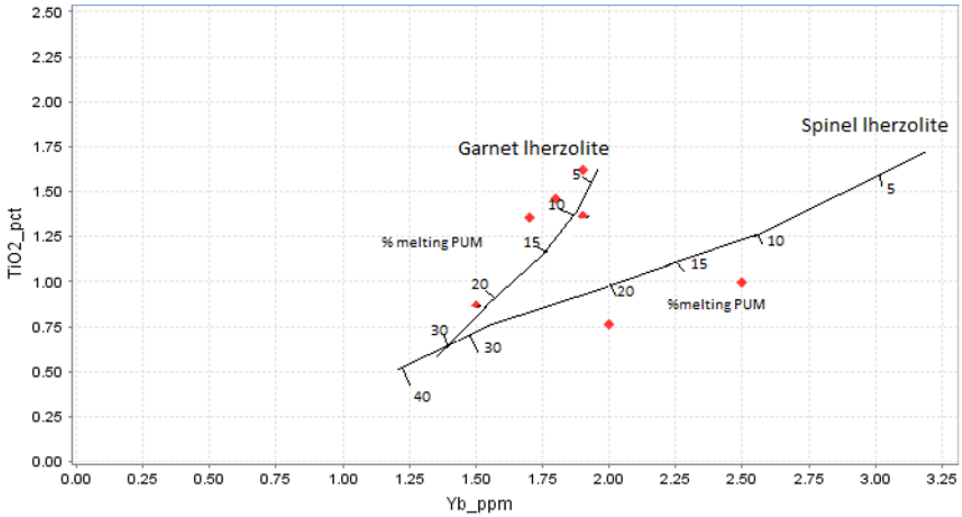

Figure 4.66 (a): Plot of TiO_2 vs Yb, after Gribble et al., (1998), partial melting diagram for the Primitive Mantle calc-alkalic dykes of the Irumide Fold Belt of Northeastern Zambia, adapted from Cimen, (2016).

(b)

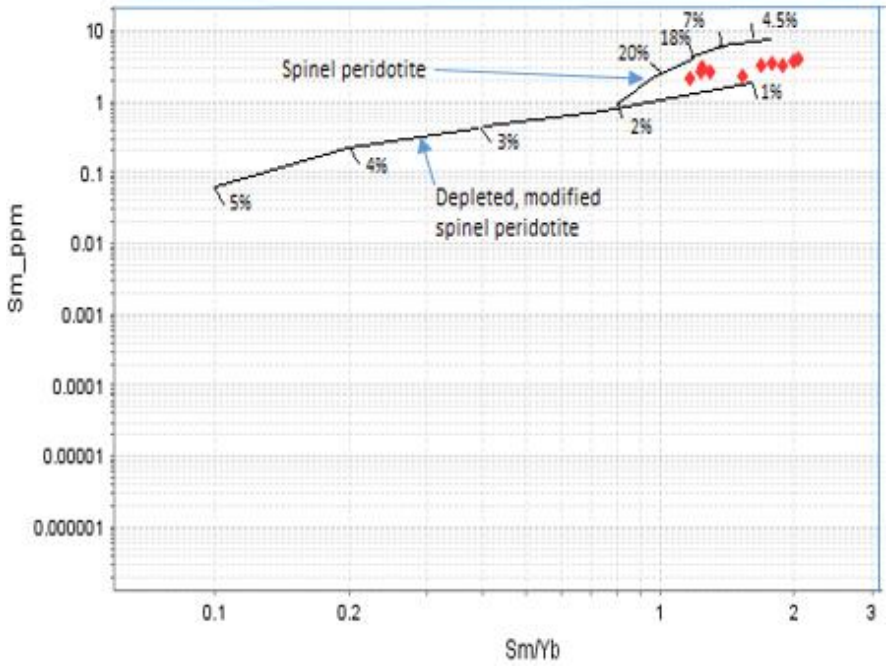

Figure 4.66 (b): Plot of Sm vs Sm/Yb, after Sayıt et al. (2016), partial melting diagram for the Primitive Mantle calc-alkalic dykes of the Irumide Fold Belt of Northeastern Zambia, adapted from Cimen, (2016).

Both plots show that the samples analysed are products of partial melting that ranges about 5 to 20%.

Application of PRIMELT3 MEGA.XLSM

The variable conditions of partial melting of a mantle source, crystallisation, assimilation and mixing during transit within the crust, result in the production of basaltic rocks with a wide chemical composition (Herzberg et al., 2007; Putirka et al., 2007; Lee et al., 2009; Herzberg and Asimow, 2015). According to Herzberg and Asimow (2015), if the effects of partial melting can be isolated, then it is possible to use the compositions of the rocks being studied to distinguish "hot" from "cold" mantle sources, which is important in understanding the thermal characteristics of ambient and anomalous mantle. Herzberg and Asimow (2015), noted that, extracting such information from a lava is not straightforward because primary magmas that form by partial melting of a mantle source are transformed by partial crystallisation, assimilation, and mixing during transit to the crust.

In an effort to solving the petrological problems highlighted above, Herzberg and Asimow (2015), produced a software, whose latest is the 2015 version, which can calculate primary magma compositions for evolved lavas. The software uses forward and inverse models to compute a melt fraction which is capable of; (a) being produced by partial melting of mantle peridotite as derived from parameterisation of experimentally determined partial melt compositions of fertile mantle peridotite (Herzberg and Asimow, 2008), and (b) producing the major element composition of the evolved lava through fractionation or accumulation of olivine. A forward model is a petrological method for computing how the chemistry of melts change from the beginning of melt production at depth in the mantle to solidification in the crust. Melts in the mantle can respond to variations in temperature (T) and pressure (P) of melting, variations in mantle source composition (X), and the extent to which it melts (F), also called melt fraction (Herzberg and Asimow, 2015). However, a primary magma composition also depends on how the mantle melts, whether it is by batch, fractional, accumulated fractional, or some more complex melting process. PRIMELT3 MEGA.XLSM uses the olivine-anorthite-quartz projected compositions of primary magmas to identify the residium mineralogy from which it separated (however, an aggregate fractional melt is not in equilibrium with its residue). Only the final drop of liquid extracted is in equilibrium with the residue deficient in TiO_2 and Na_2O, high in K_2O, and P_2O_5 has not been determined (Herzberg and Asimow, 2015).

A successful PRIMELT3 primary magma solution for a basalt provides the user the following information:

- primary magma composition, melt fraction (F);
- mantle potential temperature TP;

- olivine liquidus temperatures at 1 atmosphere;
- olivine phenocryst composition at the liquidus, residuum mineralogy, and;
- residuum composition (Herzberg and Asimow, 2015).

The geochemical results for the mafic dykes being studied, both calc-alkalic and tholeiitic, were analysed using PRIMELT3 MEGA.XLSM, and the results are presented here below. Table 4.7 shows the major element compositions, degrees of partial melting and potential temperatures (TP) of all of the primary magmas produced in this study for each mafic dyke sample.

Table 4.7: Primary magma compositions for (a) calc-alkalic rock samples, and (b) tholeiitic rock samples, of the mafic dykes of the northeastern part of the Irumide Fold Belt, Northeastern Zambia as calculated by PRIMELT3 MEGA.XLSM. BP – batch melting; AF – accumulated fractional melting; T (^{O}C) – melting temperature; TP – mantle potential temperature; F (Fe/Mg) – degree of melting; Xfo – forsterite content of olivine in equilibrium with the melt; % ol ad'n– percentage of olivine added to sample composition needed to obtain primary magma composition.

(a)

Sample ID	CH-WHR-01		CH-WHR-02		CH-WHR-04		CH-WHR-05		CH-WHR-08		CH-WHR-09		CH-WHR-11	
	BP	AF	BP	AF	BP	AF	BP	AF	BP	AF	BP	AF	BP	AF
SiO2 %	42.91	42.94	44.59	44.70	44.24	44.39	47.56	48.05	43.75	43.89	44.89	45.08	44.84	45.06
TiO2 %	1.11	1.13	0.89	0.91	0.91	0.96	0.53	0.57	0.93	0.98	0.66	0.69	0.71	0.75
Al2O3 %	9.90	10.08	10.92	11.28	10.11	10.58	11.85	12.72	9.85	10.33	11.47	12.01	10.94	11.58
Fe2O3 %	1.16	1.18	0.91	0.94	0.92	0.96	0.73	0.79	1.07	1.12	0.89	0.93	1.11	1.18
FeO %	12.78	12.87	11.36	11.48	11.69	11.88	9.34	9.46	11.99	12.22	11.01	11.17	10.78	10.97
MnO %	0.18	0.18	0.16	0.16	0.17	0.17	0.15	0.15	0.17	0.17	0.15	0.16	0.17	0.17
MgO %	23.66	23.16	21.89	20.95	23.64	22.35	20.09	17.81	24.43	23.10	22.26	20.89	22.64	20.96
CaO %	6.85	6.97	7.37	7.61	6.67	6.97	7.89	8.46	6.34	6.65	6.64	6.95	7.48	7.92
Na2O %	1.25	1.27	1.60	1.66	1.34	1.40	1.36	1.46	1.21	1.27	1.65	1.73	1.08	1.14
K2O %	0.14	0.14	0.23	0.23	0.26	0.27	0.44	0.47	0.20	0.21	0.32	0.34	0.19	0.21
P2O5 %	0.07	0.08	0.08	0.08	0.07	0.07	0.06	0.06	0.07	0.07	0.06	0.06	0.06	0.06
T (°C)	1511.91	1504.29	1479.03	1464.26	1506.23	1486.67	1437.35	1399.46	1519.66	1499.87	1485.88	1464.79	1483.61	1457.20
TP	1640.88	1631.75	1608.39	1590.39	1640.44	1616.83	1573.42	1525.66	1654.60	1630.80	1615.17	1589.20	1622.36	1590.60
TP new	1654.70	1642.24	1610.92	1587.38	1654.10	1622.14	1565.69	1507.64	1673.63	1640.96	1619.92	1585.84	1629.56	1587.65
%ol ad'n	38.75	36.88	43.53	40.28	48.49	43.81	38.39	31.14	41.00	36.07	43.09	38.38	23.00	17.18
KD	0.28	0.28	0.29	0.29	0.29	0.29	0.31	0.31	0.29	0.29	0.29	0.30	0.29	0.29
Xfo	0.92	0.92	0.92	0.92	0.93	0.92	0.93	0.92	0.93	0.92	0.92	0.92	0.93	0.92
F (Fe/Mg)	0.10	0.10	0.15	0.15	0.19	0.19	0.31	0.30	0.19	0.19	0.20	0.21	0.24	0.25
Residual lithology	Garnet Peridotite		Garnet Peridotite		Garnet Peridotite		Harzburgite		Garnet Peridotite		Garnet Peridotite		Garnet Peridotite	

(b)

Sample ID	CH-WHR-03		CH-WHR-06		CH-WHR-07		CH-WHR-010		CH-WHR-012	
	BP	AF	BP	AF	BP	AF	BP	AF	BP	AF
SIO2	48.29	48.29	47.66	47.66	48.01	44.55	49.89	45.72	45.12	45.24
TIO2	2.74	2.74	2.87	2.87	2.49	1.41	1.69	0.97	1.13	1.16
Al2O3	14.88	14.88	14.10	14.10	14.36	8.06	16.36	9.35	10.74	11.03
Fe2O3	2.45	2.45	2.39	2.39	2.31	1.29	2.04	1.16	1.59	1.63
FeO	12.89	12.89	12.54	12.54	12.15	12.18	10.72	11.32	10.61	10.68
MnO	0.19	0.19	0.19	0.19	0.19	0.17	0.18	0.17	0.17	0.17
MgO	5.74	5.74	6.52	6.52	6.44	24.43	5.67	23.60	19.96	19.14
CaO	8.73	8.73	10.64	10.64	10.89	6.16	9.67	5.57	8.51	8.74
Na2O	2.71	2.71	2.38	2.38	2.52	1.40	2.60	1.47	1.71	1.76
K2O	1.03	1.03	0.46	0.46	0.42	0.23	1.02	0.58	0.33	0.34
P2O5	0.36	0.36	0.27	0.27	0.21	0.12	0.16	0.09	0.12	0.12
T (°C)	1163.81	1163.81	1170.05	1170.05	1166.69	1521.90	1148.77	1509.09	1449.09	1435.51
TP	1026.91	1026.91	1097.62	1097.62	1090.60	1654.54	1019.86	1639.71	1570.84	1553.99
TP new	1186.45	1186.45	1207.91	1207.91	1205.56	1673.55	1184.55	1653.11	1562.45	1541.53
%ol ad'n	No solution	No solution	No solution	No solution	No solution	58.99	No solution	57.01	25.77	23.07
KD	0.31	0.31	0.31	0.31	0.31	0.29	0.31	0.30	0.29	0.30
Xfo	0.72	0.72	0.75	0.75	0.75	0.92	0.75	0.93	0.92	0.92
F (Fe/Mg)	No solution	No solution	No solution	No solution	No solution	0.27	No solution	0.36	0.15	0.15
Residual lithology	No solution		No solution		Garnet Peridotite		Garnet Peridotite		Garnet Peridotite	

PRIMELT3 MEGA.XLSM was applied successfully in calculating primary magma compositions for all the seven calc-alkalic mafic dyke samples studied. It was possible to calculate melt fractions using both batch and accumulated fractional melting of fertile peridotite for all the seven samples. The results are summarised in Table 4.8 (a) . As regards the tholeiitic mafic dyke samples studied, PRIMELT3 MEGA.XLSM was able to successfully calculate the primary magma compositions of the five samples using both batch and accumulated fraction melting. However it was not able to calculate the melt fractions. The ensuing information is summarised in Table 4.8 (b).

Table 4.8: Summary of the calculations by PRIMELT3 MEGA.XLSM. BP for, (b) calc-alkalic rock samples, and (b) tholeiitic rock samples.

(a)

Sample ID	Batch melting				Accumulated fraction melting			
	MgO content %	Olivine Forsterite content (Fo_x)	Degree of partial melting of source (%)	Melting temperature ^oC	MgO content %	Olivine Forsterite content (Fo_x)	Degree of partial melting of source %	Melting temperature ^oC
CH-WHR-01	23.66	Fo_{92}	10	1511	23.16	Fo_{92}	10	1504
CH-WHR-02	21.89	Fo_{92}	15	1479	20.95.	Fo_{93}	15	1464
CH-WHR-04	23.65	Fo_{93}	19	1506	22.35	Fo_{92}	19	1486
CH-WHR-05	20.09	Fo_{92}	31	1437	17.81	Fo_{92}	30	1399
CH-WHR-08	24.43	Fo_{93}	19	1519	23.10	Fo_{92}	19	1499
CH-WHR-09	22.26	Fo_{92}	20	1485	20.89	Fo_{92}	21	1464
CH-WHR-11	22.64	Fo_{93}	24	1463	20.96	Fo_{92}	25	1457

(b)

Sample ID	Batch melting				Accumulated fraction melting			
	MgO content %	Olivine Forsterite content (Fo_x)	Degree of partial melting of source (%)	Melting temperature ^oC	MgO content %	Olivine Forsterite content (Fo_x)	Degree of partial melting of source %	Melting temperature ^oC
CH-WHR-03	5.74	Fo_{72}	No solution	1163	5.74	Fo_{72}	No solution	1163
CH-WHR-06	6.52	Fo_{75}	No solution	1170	6.52	Fo_{75}	No solution	1170
CH-WHR-07	6.44	Fo_{75}	No solution	1166	24.43	Fo_{92}	27	1521
CH-WHR-10	5.67	Fo_{75}	No solution	1148	23.60	Fo_{93}	36	1509
CH-WHR-12	19.96	Fo_{92}	15	1499	19.14	Fo_{92}	15	1435

The residual lithology indicated by PRIMELT3 MEGA.XLSM for all the samples of the calc-alkalic type of the mafic dykes is garnet peridotite apart from sample ID CH-WHR-05 which is indicated as hazerbugite. The sample shows the lowest melting temperatures for batch and accumulated fraction melting. It also has the lowest MgO content of all the calc-alkalic dykes samples, but has the highest degree of melting. The tholeiitic dykes samples with low MgO content show no lithology solutions and degree of melting.

4.6 Magmatic Mineralisation Potential Assessment

4.6.1 Exploration historical data

Exploration carried out by Zawar Natural Resources Limited that culminated in the drilling of a few bore holes over target areas delineated from anomalous soil surveys results (Cu-Ni), did not discover any sulphide mineralisation (Musiwa and Shanzambwa, 2014). The drilling revealed that the dykes are almost vertical. There were no features indicative of possible mineralisation observed in the exploration exercise.

4.6.2 Analysis of whole rock geochemistry data

Geochemical signatures, behaviour of Cu with sulphide fractionation, plotted against MgO, should show scatter if there is sulphide fractionation but show negative linear correlation if there is no sulphide fractionation. Similarly, when Cu is plotted against Zr, there should be a positive linear trend if there is no sulphide fractionation.

On the plot of Zr versus Cu for calc-alkalic mafic dykes (Figure 4.67), a moderately positive linear correlation (R=0.6584) is displayed. A similar plot for the tholeiitic mafic dykes (Figure 4.68) also shows a positive linear correlation, although lower (R=0.5343). On the plot of MgO versus Cu for tholeiitic mafic dykes (Figure 4.69), there is no correlation that is exhibited (R=-0.3845), whilst a similar plot for the calc-alkalic mafic dykes (Figure 4.70) displays strong negative linear correlation (R=0.794).

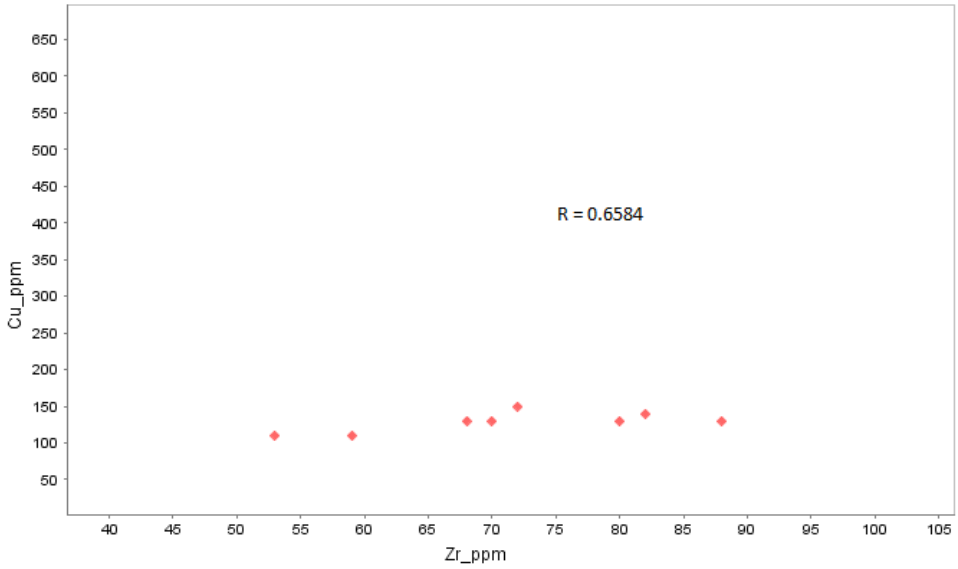

Figure 4.67: Zr versus Cu variation diagram plot of the calc-alkalic mafic dykes of the northeastern part of the Irumide Fold Belt, Northeastern Zambia (R = Pearson's linear correlation factor).

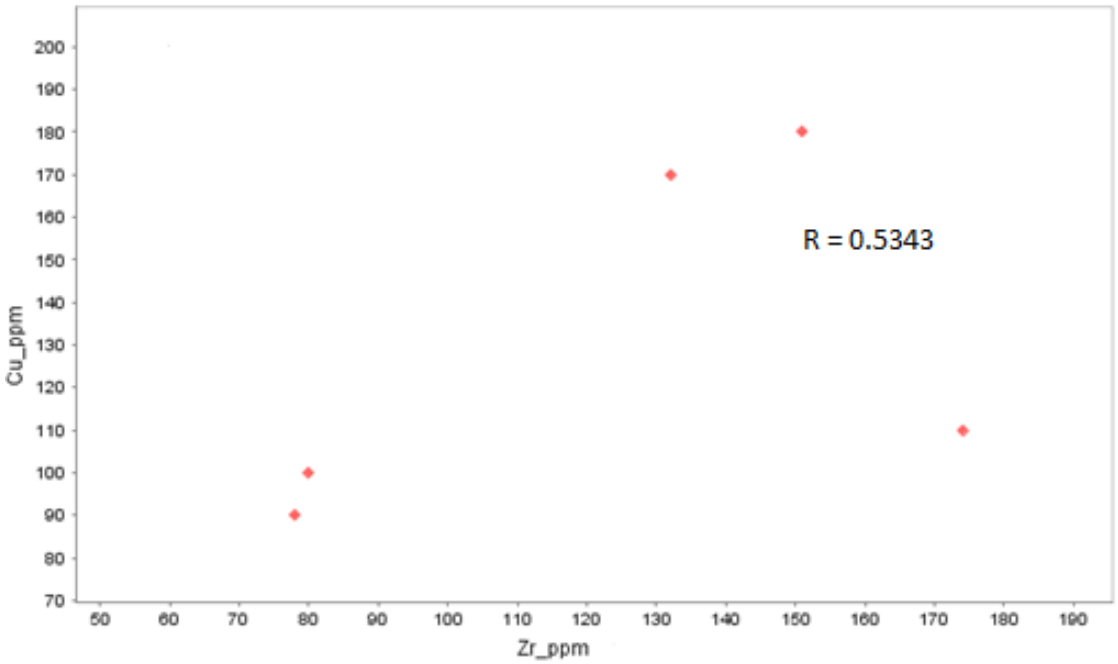

Figure 4.68: Zr versus Cu variation diagram plot of the tholeiitic mafic dykes of the northeastern part of the Irumide Fold Belt, Northeastern Zambia (R = Pearson's linear correlation factor).

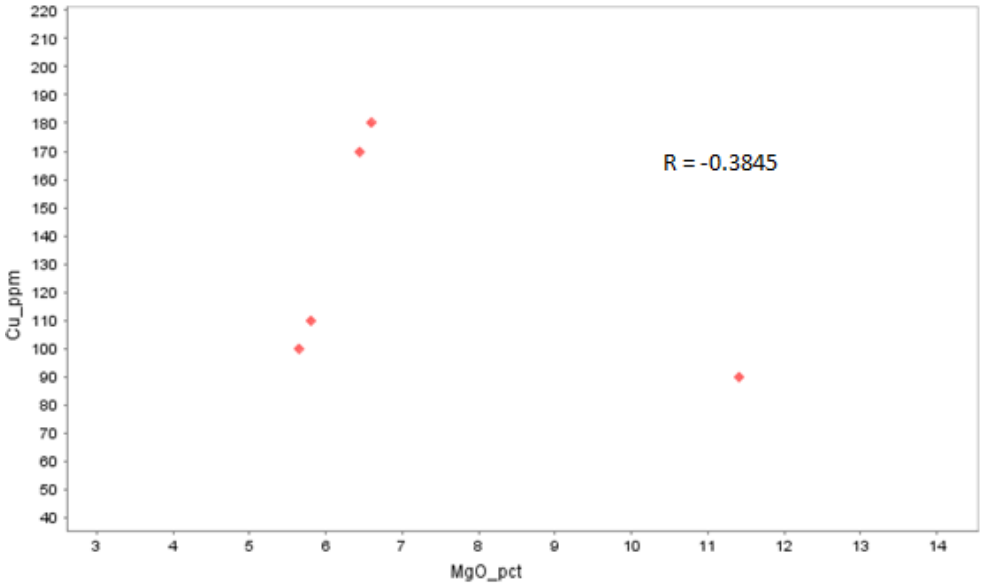

Figure 4.69: MgO versus Cu variation diagram plot of the tholeiitic mafic dykes of the northeastern part of the Irumide Fold Belt, Northeastern Zambia (R = Pearson's linear correlation factor).

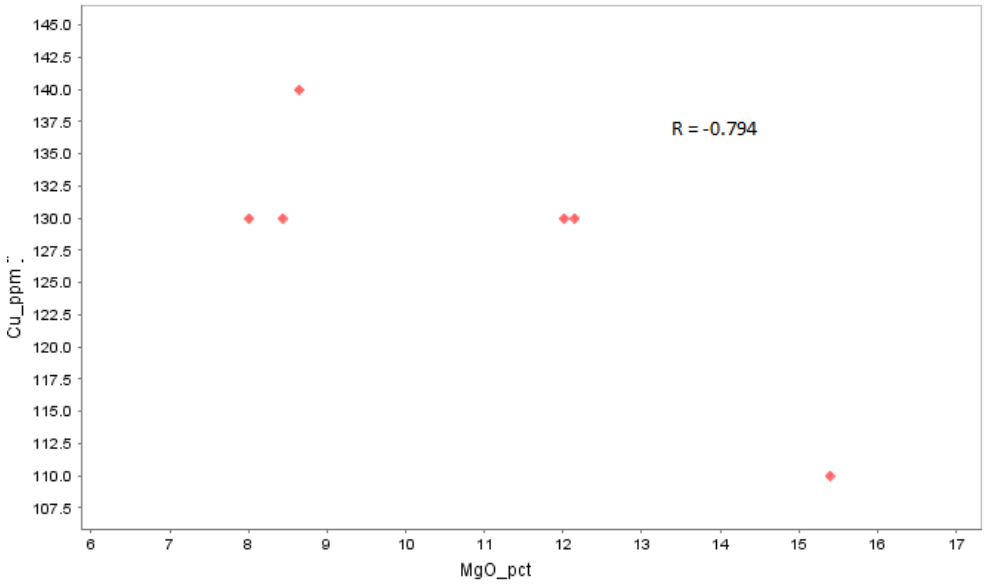

Figure 4.70: MgO versus Cu variation diagram plot of the calc-alkalic mafic dykes of the northeastern part of the Irumide Fold Belt, Northeastern Zambia (R = Pearson's linear correlation factor).

4.6.3 Possible source of sulphur

From the observed chemical characteristics, the studied samples of the calc-alkalic mafic dykes of the Study area clearly indicate crustal contamination during the processes that led to their emplacement (see section 4.4.1). Crustal contamination is considered to be a primary source of sulphur required for sulphide mineralisation (Lesher and Groves, 1986; Keays and Lightfoot, 2010).

4.6.4 Tectonic setting, geometries and sizes of intrusions

The northeastern part of the Irumide Fold Belt in northeastern Zambia is located in tectonic setting of continental subduction environment (see section 4.3.2). The geometries of the dykes being studied, which may have a bearing on sulphide mineralisation, are not established. The known morphologies of the dykes are limited to their spatial extent as observed on the surface. The sizes of the intrusions vary in dimensions from a few hundreds of metres to about 4.5 km long and a few metres to hundreds of metres wide (see section 2.2).

5 DISCUSSION

5.1 Petrography

Information extracted from the examination of thin sections of any rocks being studied; igneous, metamorphic or sedimentary, complement hand-specimen observations. Microscopic analyses of thin sections provide a more complete package of information from the description of the rock samples being studied because of the method's ability to bring out features and detail which cannot be observed through inspection of hand specimens.

In this study, detailed petrographic thin section descriptions of twelve dyke swarm samples were made to aid in identification and characterisation of metamorphic and vein mineral assemblages, if any, in the rock samples. Stable mineral parageneses were noted, as well as textural features of minerals indicating overprinting events. Secondary mineral assemblages and replacement relations to primary phases were described. Particular emphasis was therefore placed on the identification and description of minor and traces phases. The modal estimates allowed characterisation of the intensity of metamorphism and aided in establishing the accuracy of the macroscopic and microscopic visual estimates of the extent of alteration. The description of the thin sections also included extraction of microtextural information of all the minerals identified. The distinction between pseudomorphic, non-pseudomorphic, and transitional serpentinisation provided useful information, as only pseudomorphic textures are primary alteration features (see Figure 4.2C), whereas the latter two represent recrystallisation phenomena (see Figure 4.3D).

Formation of strong planar fabrics (foliation) may occur during serpentinisation by development of closely spaced subparallel veins termed ribbon textures (O'Hanley, 1996). The texture is characterised by anastomosing, often cross-fibre, replacement serpentine veins. In general, the veins wrap around relict or pseudomorphed pyroxene grains with little evidence of shear offset (see Figure 4.3C). These create a strongly foliated serpentinite that is actually a variant of hourglass serpentine texture and largely represents in situ replacement of the primary olivine (O'Hanley, 1996). This texture may parallel pre-existing crystal-plastic foliation, and its intensity may reflect stress state or the presence of a pre-existing fabric in the rock.

Some of the fine and medium grained dykes samples show large phenocrysts of olivine and hornblende in a matrix of more hornblende, sericite, quartz and some opaque phase. The matrix is made of polycrystalline aggregates of anhedral crystals of the minerals which have clear grain boundaries. The large crystals of olivine and hornblende occur as either single crystals or aggregates of several crystals, especially hornblende. These phenocrysts suggest

that they formed during fractional crystallisation of a magma in a deeper chamber and were transported with the melt during periodic tapping of the chamber and finally incorporated in the dykes. The large olivine crystals are characteristically altered to clinopyroxene at the rims, giving them ragged edges (see Figure 4.2A). Epidote is markedly more in the two of the four medium grained samples and exhibits subhedral to euhedral crystals, where it appears to have totally replaced hornblende (see Figures 4.2C and D). In the same samples, hornblende also displays subhedral crystal texture. The crystal contacts of the two minerals are sharp, giving the impression that epidote was not replacing hornblende from the edges.

Hornblende replacing olivine and augite indicates that some of the portions of the dykes could be classified as an alkaline olivine gabbro. The primary magmatic minerals include plagioclase, olivine, augite, and late brown hornblende (see Figure 4.1A). Probably very close to solidus temperatures, olivine and augite reacted with the hydrous residual liquid to grow hornblende rims on both of them (see Figure 4.3E). Imperfections in the augite, possibly trapped liquid inclusions or exsolution lamellae (see Figure 4.3E), also reacted to grow hornblende within augite crystals. It is well observed that the hornblende rims are brown on augite and green on parts of the olivine (see Figure 4.2D). The green hornblende may be low in titanium, contrasting with the brown high-titanium hornblende. Clinopyroxene is possibly inverted subcalcic augite.

Cleavage, exsolution lamellae and minor alteration along cracks are prominent features of the clinopyroxene. It is the coarsest-grained mineral in the rocks, but there is some recrystallisation (see Figure 4.2A). In some samples, plagioclase grains are subhedral, but olivine and clinopyroxene are anhedral. In Figure 4.3F, plagioclase grain shape is generally subhedral with sharp and straight to very curvilinear and muted boundaries with other plagioclase/microline grains. However, olivine is less than 3% medium grained, subhedral granoblastic, in the same sample (see Figure 4.3F), and clinopyroxene is less than 10%, medium grained, subhedral, some contain stringers at a very reddish-brown phase, oxide of some sort may be. Anhedral opaques may be included in clinopyroxene, whilst brown hornblende as anhedral grains, form in cracks of olivine, also as anhedral blebs in talc aggregates (see Figure 4.3F).

Orthocumulate texture, with cumulate plagioclase and olivine crystals enclosing quenched gabbroic liquid, is not present in the dykes of Northeastern Zambia. If this was present in the more slowly-cooled gabbro, the trapped liquid pockets would have crystallized into overgrowths on adjacent plagioclase and olivine, plus a few relatively large grains of clinopyroxene, apatite, and other interstitial phases. What is present is the mesocumulate texture, in which liquid trapped between cumulate crystals was able to exchange material with

the nearby magma, allowing more extensive overgrowths of cumulate minerals and a smaller volume of ultimately trapped liquid (see Figure 4.3E). Small grains of olivine, clinopyroxene, and apatite indicate the original trapped liquid.

Ophitic texture, in which large pyroxene crystals enclose randomly-oriented plagioclase and commonly other minerals, forms where there are few pyroxene nuclei, so those few grow quite large, enclosing the other minerals. Igneous subophitic texture in photomicrograph see Figure 4.2D, is still well preserved. Original texture is probably plagioclase with interstitial clinopyroxene and olivine, in which randomly-oriented plagioclase crystals touch one another, generally enclosing clinopyroxene and other minerals. Poikilitic texture, in which one large crystal encloses many smaller crystals (see Figure 4.3E), is similar to ophitic textures, but the enclosing mineral need not be pyroxene. Plagioclase is dominant but there are also some poikilitic inclusions by clinopyroxene and olivine. Maximum grain size is probably about 2 cm in Figure 4.3D.

5.2 Geochemistry

Igneous rocks vary in composition from gabbro-diorite to granite (Arndt et al., 1987; Arndt and Goldstein, 1989; Clemens et al., 2010, Chen et al., 2017). Many factors lead to this wide range in composition and these include, but not limited to, crystal fractionation, multiphase or pulse intrusions in which the magmas of different phases have different compositions, even if they come from the same source, magma mixing, restite separation and contamination by assimilation (Roberts and Clemens, 1993; Karmalkar et al., 2016). Whilst the nature of magma's genesis in subduction zone settings can be determined by whole rock geochemistry and isotopic compositions, complicated differentiation processes stated above render whole-rock geochemistry and isotopic compositions not to always be indicative of actual magma source characteristics. Furthermore, the geochemical variations of the mantle wedge, subducted oceanic crust, subducted sediments or melts and slab configuration also play an important role in magma genesis (Abdurrachman et al., 2018). This brings in the aspects of closed systems on one hand, and open systems on the other.

A closed system has no communication with the rocks outside the magma. The open system is where the magma is contaminated by the country or intruded rock in many different ways during the ascent and emplacement or by mingling with magmas of different compositions. The only way to confidently distinguish between an open and a closed system is by means of isotope ratios (e.g. $^{87}Sr/^{86}Sr$ and $^{143}Nd/^{144}Nd$) (Verma, 2001; Verma et al., 2002; Lassen et al., 2004). Whilst in closed system there is no much change in these ratios, there is significant change where there was interaction of magmas from different sources or where there was

interaction with the intruded rock. In this study, Rb-Sr and Sm-Nd isotopic numerical data and plots are applied in deducing possible crustal contamination. REE and trace element data are further used in the interpretation and establishment of processes like levels of partial melting and fractional crystallisation.

Crystal fractionation is more effective at fractionating compatible elements and the discrimination between the two mechanisms may be based on the behaviour of the trace elements in the logarithimic plot of an incompatible element against a compatible element, where they have very different bulk partitioning coefficients. In such a diagram, liquids produced by crystal fractionation give a straight line with strong decrease in compatible elements, whereas the incompatible elements increase slowly. The opposite relationship applies to liquids produced by partial melting (Cocheries, 1986).

The geochemical results of the dykes of northeastern Zambia, show a range of SiO_2 (44. 24-50.32 wt%) over the ratio of $FeO_{(T)}$/MgO. This is considered to be quite narrow and a feature that is typical of tholeiitic differentiation (Atherton and Ghani, 2002; Murphy et al., 2019). The medium to high concentrations of Mg (5.64 -15. 39 wt%), Ni (80 -720 ppm), Cr (160 – 1400 ppm), V (206 – 344 ppm) and Ba (85 – 415 ppm) are indicative of a mantle source (Atherton and Ghani 2002). The high average values of Na_2O/K_2O (5.2) and $Na_2O + K_2O$ (2.71) indicate further that the rocks are sodic. The ratio of $Al_2O_3/(CaO+Na_2O+K_2O)$ ranges between 1.02 and 1.34, and this is an exhibition of marginal peraluminous characteristics ($Al_2O_3 > (CaO + Na_2O + K_2O)$). The low $FeO_{(T)}$/MgO ratio (0.7 – 2.4) exhibited by the dyke mafic samples is typical of calc-alkaline suites (Murphy et al., 2019). The samples that plot in the tholeiitic field generally exhibit comparatively lower MgO and Mg#, but higher SiO_2, TiO_2 and P_2O_5, than the samples that plot in the calc-alkali field, an indication that they are more evolved. They also exhibit higher contents of Sr, Zr, Sm, Nd, La, Hf and Th. The same samples that plot in the tholeiitic field, further show higher Ce/Yb and Nb/Yb ratios with a clear separation of the two types of rocks observed from Nb content, which is much higher in the tholeiitics. The calc-alkalic rocks are richer in compatible elements of Ni and Cr. Talusani (2010) observed that the relationship between tholeiitic and alkalic magmatic series is a key problem in igneous petrology, particularly in situations where both types occur in association. This association regarding the two types of rocks occurring together is typical of the study area.

The Zr content in the two types of dykes is so markedly distinguishable, averaging 123 ppm for tholeiitic samples and 71 ppm for calc-alkalic samples, a feature that provides strong evidence in favour of their genetic relationship through different degrees of partial melting of a common mantle source (Talusani, 2010). However, this feature may also indicate that the two types of dykes are no cogenetic. The marked difference in content of Zr regarding the two

types of rocks is clearly noticeable on the variation diagram plots (see Figure 4.4) of Zr versus other elements. In most of these plots, the calk-alkalic rocks are clearly separated from the tholeiitic rocks, especially the three samples with the highest content of Zr. The increase in Zr content in calc-alkalic and tholeiitic rocks is characteristically accompanied by the general increase in the content of; Hf, Ce, Nb, Y, La, P_2O_5, V, Nd, Sm and Yb. However, whilst the increase in content of Ce, Lu, Yb, Th and La is so well correlated with the increase in Zr in tholeiitic rocks, the same elements show significant scatter in calc-alkalic rocks. On the other hand, V exhibits good positive correlation with Zr in the calc-alkalic rocks, but fairly poor in the tholeiitic rocks. The calc-alkalic rocks show strong increase in Sr content with the increase in Zr content but the same element has very little content variation with the increase in Zr in tholeiitic rocks. The patterns of K_2O and Rb are very similar on the variation plots, very poor in the calc-alkalic rocks, but better positive correlation in the tholeiitic rocks.

The increase of MgO content in both the calc-alkalic and the tholeiitic dykes shows a good general increase in the content of compatible elements Cr, and Ni. There is a general decrease in major element oxides of SiO_2, K_2O, Al_2O_3, Na_2O, TiO_2 and P_2O_5, with the increase in the content of MgO in both types of rocks. Similarly, there is also a general decrease in the element concentrations of Rb, Sr, Zr, Nb, Y, Nd, and Sm with the increase in the concentration of MgO in both calc-alkalic and tholeiitic rocks. These are expected evolutionary trends where there is crystal fractionation.

5.3 Alteration and element mobility

Petrogenesis of igneous rocks is interpreted from the overall information that is kept by the rock, which relates to the processes of its origin, all that happened to the magma until the solidification of the rock. Any changes which are post emplacement due to secondary alteration are likely to alter the element combinations and ratios on which the interpretation would be based. For this reason, any elemental and isotopic data that is targeted for petrogenetic interpretations, must be assessed for possible post solidification or sub solidus alterations that might lead to element mobility which subsequently will lead to incorrect conclusions. Elements which are interpreted to have remobilised under alteration levels of the rocks being studied, are not suitable for petrogenetic interpretations.

The assessment for possible post magmatic alteration and subsequent element mobility can be done by plotting a highly incompatible and immobile element, as an index mineral, against selected other incompatible but highly soluble and mobile elements, under alteration and fluid environments. The best candidates for such plots are HFSE and LILE. Both HFSE and LILE behave the same, incompatible during mantle partitioning (partial melting) and fractionation.

However, their responses to sub-solidus alterations and post magmatic changes differ, and it is this difference in behaviour that is useful to petrogenetic studies. HFSE are immobile in low to medium grade metamorphism, and hydrothermal alterations are highly unlikely to change their content in the residual rock (e.g. Pearce and Cann 1973; Floyd and Winchester 1978; Jochum and Verma 1996, Wong et al., 2010). These elements which include Zr, P, Nb, Ti, Hf, Th, U, Y and Lu, have characteristically very small ionic radii compared to their large cation charge (z/r). This aspect gives them a very high electrical field strength that makes them have very strong bonds with nearby anions. The LILE, on the other hand, are larger than other cations, and these include Eu, Sr, Pb, Ba, K, Rb, and Cs. Their large ionic radii make them incompatible and therefore, they end up being enriched in the crust (lithosphere). These elements are easily remobilised during secondary alteration and enter the solution as either hydrated cations or hydrated oxyanions (Pearce, 1996; Hastie et al., 2007).

Because of their resistance to change in content and proportions to each other due to post magmatic (sub-solidus) alteration, HFSE contents are perceived to be representative of the original rock. Consequently, relative proportions of selected elements can be used in the interpretation of a number of magmatic processes and environments of emplacement. As seen above, one of the HFSE which is found in many igneous rocks and which is very immobile is Zr. Zr is incompatible during basalt fractionation and considered to be immobile at low to medium metamorphic levels (Pearce, 1996; Kumar and Ahmad, 2007). Hence, Zr can be used as a parameter for evaluating the elemental mobility and also to understand the differentiation of magma (Kumar and Ahmad, 2007). Other incompatible elements that tend to remain in the solid product during alteration include REE, (excluding Eu and La), Hf, Nb, Ta, Y, Ti, Th, Sc, and Ge (Pearce, 1996, Hastie et al 2007). In this regard, when other incompatible, but easily mobile elements (LILE), from co-magmatic suites are plotted against Zr, there should be linear correlation if there has been no remobilisation as a result of alteration. A significant degree of scatter will be observed if there was some remobilisation of the element plotted against Zr. However, some loss of correlation may also be as a result of different degrees of contamination or partial melting of heterogeneous mantle source (Cannon, 1970; Ciborowski, 2013). Plotting Zr against some LILE should reveal, to some extent, whether the rocks under study have been altered or not.

5.4 Isotope geochemistry and age dating

Isotopic ratios are useful in the characterisation of the mantle source regions from which the mafic rocks being studied were derived. This is because, owing to the negligible mass difference between the isotopes of an element, isotopic ratios are unaffected by partial melting and fractional crystallisation (Ciborowski, 2013). In this regard, the initial isotopic ratios of

the mafic rock, when the parent magma was extracted from the mantle, will be the same as the isotopic ratio of the source region at the time of extraction (Hanson, 1980). Further, the isotopic ratios measured in a sample are a function of the initial isotopic ratios and the rock's age (Ciborowski, 2013). In these studied samples, there is no observed relationship between the initial $^{87}Sr/^{86}Sr$ and $^{143}Nd/^{144}Nd$ with ages of the dykes. The negative εNd and $^{87}Sr/^{86}Sr$ values shown in table 4.4 indicate a continental or contaminated magma (De Paolo 1988; Kerr, 2015).

5.5 Classification of geotectonic environment

5.5.1 Introduction

Classification or discrimination of tectonic settings can be achieved from the geochemistry of the basaltic rocks being studied from that particular area (Halls, 1982; Pearce, 1983; Schandl and Gorton, 2002; Duggen et al., 2005; Harangi et al., 2007). Basaltic rocks are formed in almost every tectonic environment and they are believed to be geochemically sensitive to the changes in plate tectonic frameworks (Holm, 1985). Multi-element and REE patterns are applied extensively to understand and make these classifications (Pearce, 1983).

This study has revealed that, the mafic dyke swarm of the Study area occurs as a mixed suite of tholeiitic and the calc-alkalic gabbroic rocks. The two types of rocks occur as individual dykes that display no clear distinguishing characteristics from each other in the field. In order to understand the tectonic and magmatic processes that led to the emplacement of the dykes, chemical signatures are applied on the results of the studied samples. Discrimination diagrams, using some major element oxides, rare earth and trace elements, are applied. Trace and rare earth elements that include; Th, Hf, Ta, Yb, Y, Nb, La and Zr are applied in the evaluation due to their particular usefulness in the studies of arc magmatism (e.g. Pearce and Peate, 1995; Schandl and Gorton, 2002; Cimen, 2016). Nb and Ta are particularly useful in that the two elements are depleted in continental crust relative to other highly incompatible elements such as cesium, rubidium, thorium, and uranium, and the light REEs, including cerium and lanthanum (Kelemen et al., 1993).

Continental crustal rocks are typically characterised by high lanthanum to niobium (La:Nb) ratios-the average crustal ratio is about 2.5 (Rudnick and Gao, 2003). The depletion of niobium and tantalum in continental crust is attributed to the formation of crustal rocks at convergent margins above subduction zones where titanium-rich minerals that host niobium and tantalum, may remain as residual phases in the source region during generation of the magmas (Kelemen et al., 2003). Consequently, the relative depletion of Nb and Ta to the

aforementioned elements is characteristic of lavas in subduction-related magmatic arcs, and are distinct from mid-ocean ridge basalts (Kelemen et al., 1993).

5.5.2 General characteristics of tholeiitic and calc-alkalic basaltic rocks

Chemically, tholeiitic series rocks are distinguished from rocks in the calc-alkalic magma series by redox state of the magma they crystallised from. Tholeiitic magmas are in a reducing environment, whilst calc-alkalic magmas are in an oxidising environment. From the onset, as the tholeiitic parent magmas of basalts crystallise, the preference is of the more Mg-rich and Fe-poor forms of the silicate minerals, olivines and pyroxenes, to crystallise earlier, depleting the melt of Mg and increasing the concentration of Fe. This effectively reduces the ratio of Mg to Fe drastically as the magma cools and differentiating progresses. However, in the case of a calc-alkalic magma, as Mg-rich silicate minerals crystallise, significant amounts of Fe-rich (magnetite) also crystallises because of the oxidising nature of the magma. In calc-alkalic magmas therefore, the ratios of Fe-Mg remains relatively steady as the magma cools and as differentiation takes place.

Geologically, tholeiitic rocks are the most common igneous rocks on Earth, and these are mainly produced by submarine volcanism at the Mid-Oceanic Ridges and make up much of the ocean crust (e.g. Baker, 1974; Gill, 1981; Pearce, 1982; Fujinawa, 1988; Fujinawa, 1990). These basalts that form the ocean crust are collectively termed as MORBs – Mid-Oceanic Ridge Basalts. Tholeiitic basaltic magmas are initially generated as partial melts of peridotite (olivine and pyroxene) produced by decompression melting of the Earth's mantle (e.g. Hooper et al., 1995; Cameron et al., 2003; Harangi et al., 2007). Calc-alkalic basalts, in contrast, are not typical of ocean ridges, but are erupted on some oceanic islands and on continents, as also are some tholeiitic basalts. Calc-alkalic basalts occur mainly in volcanic arcs that are above subduction zones, especially in those arcs on continental crust (Miyashiro, 1971; Gill, 1981; Duggen et al., 2005; Tatsumi and Suzuki, 2009).

Whilst calc-alkalic series magmas are clearly dominant in continental arcs and mature arcs with thicker crust (Miyashiro, 1971; Baker, 1974; Gill, 1981), and tholeiitic series magmas characterise magmatism in intra-oceanic arcs, both types of rocks have been found to coexist in some mature arcs. Some of the examples of this coexistence are reported by Yatsumi et al. (2009 and references therein) as: Mt. Shasta, USA; Chichontepec, El Salvador; Aso in SW Japan; and Myoko-Kurohime in Central Japan.

During tectonic activities, mass and energy exchange between the crust and the mantle takes place at the subduction zones (Ikemoto and Iwamori, 2014). Calc-alkalic basaltic rocks are the typical products of convergent plate margin tectonic settings and are characterised by

enrichment of large ion lithophile elements (LILE) and Pb, whilst showing depletion in high field strength elements (HFSE) (Pearce, 1982; Tatsumi, 1989; Harangi et al., 2007). This typical geochemical signature characteristic of calc-alkalic basalts, is attributed to the addition of hydrous fluids from subducting oceanic lithosphere, dehydration of the subducting slab and the melts from subducted sediments, which have a fluxing effect, to the mantle wedge (Elliot et al., 1997; Harangi et al., 2007). Essentially, during subduction, the down going oceanic crust will progressively experience prograde dehydration reactions as it sinks deeper, which will result in the transportation of fluid-mobile elements (LILEs) from the subducted oceanic crust to the overlying mantle and then to the continental crust via arc magmatism (Hawkesworth et al., 1997; Savov et al., 2007; Zhang et al., 2017) (see Figure 5.1). This, effectively, lowers the mantle solidus, leading to partial melting and magma generation (Gill, 1981; Harangi et al., 2007).

Studies have shown that extension will cause calc-alkalic-dominated magmatism in areas of continental crust with a history of previous subduction (Davis and Hawkesworth, 1993; Ewart et al., 1992). Calc-alkalic magmatism may occur in an extensional tectonic setting by decompression melting in addition to occurring above, and as a direct consequence of, active subduction (Defant and Drummond, 1990). Whilst lithospheric extension controls the magma generation, the geochemical signature of the magmas is inherited from the older subduction imprint (Fujinawa, 1990; Ferns et al., 1993; Harangi et al., 2007). Consequently, calc-alkalic magmatism can also occur without contemporaneous subduction or following cessation of active subduction (post-collisional magmatism) (Hooper et al., 1995; Harangi et al., 2007). Whilst calc-alkalic magmatism is typically formed in the subduction process, it may also result from decompression melting accompanying lithospheric extension (Hooper et al., 1995). In either case, the ensuing rocks will carry similar chemical signature typical of subduction environments. In a continental margin arc environment, the magmatic products are derived from the partial melting of a subcontinental lithospheric mantle which is enriched by the dehydration process accompanying subduction, either immediately during subduction magmatism, or at a subsequent date by decompression melting (Fujinawa, 1990; Ferns et al., 1993; Hooper et al., 1995; Harangi et al., 2007).

The aqueous solutions, driven off the descending slab as the temperature increases (dehydration), are enriched in the most soluble components, silica and the LIL incompatible elements, and rise into the overlying mantle wedge (Harangi et al., 2007). During the process of mantle enrichment, the more soluble LILE are separated from the insoluble HFS incompatible elements because of their different solubilities in hydrous fluids (Fujinawa, 1990; Gaetani et al., 1993; Castillo and NewHalls, 2004; Harangi et al., 2007; Zhang et al., 2017). The subcontinental mantle, so enriched, provides the source for the basaltic partial melts

entering the crust as the more mafic end members of the subduction-related calc-alkalic suite (Pearce, 1983; Hooper et al., 1995; Harangi et al., 2007). Partial melts of the enriched mantle, resulting from the release of pressure accompanying extension, would carry the same chemical signature as those melts created at the time of subduction (Hooper et al., 1995; Harangi et al., 2007). The only difference would be the time-related changes in isotope ratios resulting from the geochemical changes.

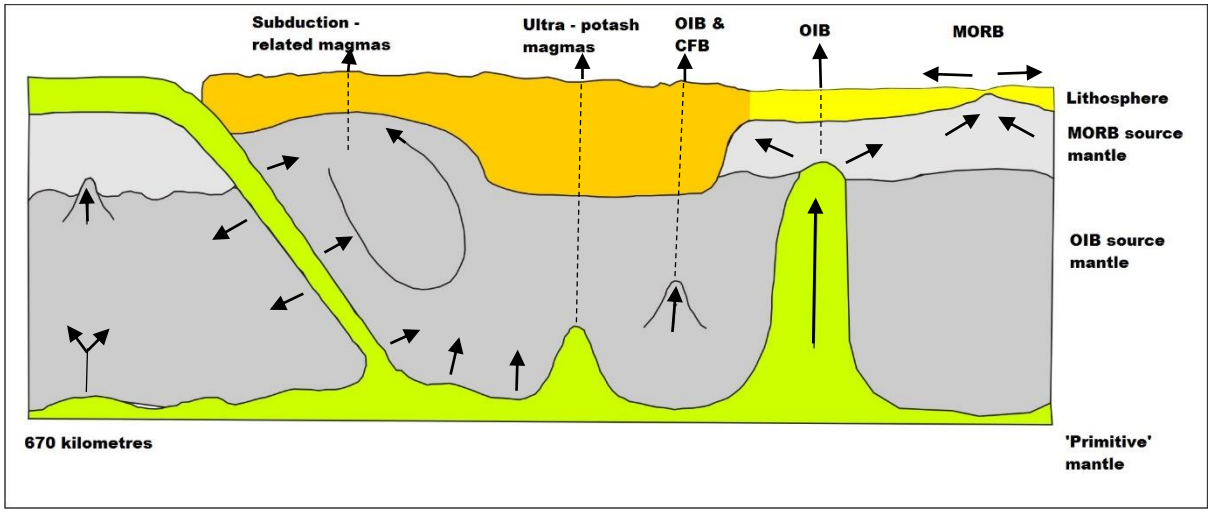

Figure 5.1: Sketch of model Upper Mantle circulation and magma genesis, modified from Thompson et al., (1984).

5.6 Petrogenesis

Igneous rocks seen on the Earth's surface originated by partial melting of a solid source in the mantle or sub-continent to produce primary magma and residual solid rock (de Paulo, 1981; Pearce, 1983; Turner et al., 1997; Kelemen et al., 2004; Esory et al., 2010; Herzberg and Asimow, 2015). Once the magma is solidified, the rocks formed carry a chemical signature, similar to DNA in humans, of their source, processes of partial melting and all the other materials which interacted with them before solidification (Hanson, 1980). The chemical signature is preserved in their compositions for as long as there has been no significant post solidification alteration. By examining the chemical compositions of the specific unaltered rocks of interest, particularly trace element (which include REE) concentrations and their ratios, it is possible to determine the nature of the source region and the processes that took place during partial melting and ascend to place of emplacement.

Hanson (1980) summarised petrogenetic studies of igneous rocks as a process that involves determining the history of the sources of melts, the conditions of melting, the mineralogical and chemical composition of the source during melting, the extent of the melting process involved and how the melt is modified by assimilation, metasomatism, differentiation and

fluids. In modern days, isotopes and trace elements, which include Rare Earth Elements, have been extensively researched and applied in petrogenetic studies of igneous rocks, with great success (Kay and Gast, 1973; Lugmair and Scheinin, 1975; De Paolo and Wasserburg, 1976; De Paolo, 1988; Kerr and Fryer, 1993; Zi et al., 2008; Kerr, 2015). Petrogenetic studies of igneous bodies in general and dykes in particular, bring out information that is useful in mineral exploration and interpretation of geodynamic evolution of respective geological environments (Halls, 1982).

The samples used in this study are all fresh and therefore considered to carry the chemical signatures of the parent magma. To interpret the evolution of the mafic dykes of the northeastern part of the Irumide Fold Belt of northeastern Zambia, all the chemical data presented and deduced are applied. The classified two different types of dykes, the tholeiitics and the calc-alkalics, are in some cases analysed separately although they spatially occur together. The lack of age dates on the tholeiitic dykes has made correlating them to the calc-alkalic ones, geochronologically, impossible. The discussion in this section addresses crustal contamination, fractional crystallisation, magma source and partial melting, in that order.

5.6.1 Crustal contamination

In a situation where the mafic dyke rocks being studied are emplaced in a continental setting, like the Study area, it is necessary to make an assessment of possible crustal contamination of the magma, before petrogenetic evaluations are carried out (e.g. Xiao et al., 2004; Srivastava et al., 2014; Kamalkar et al., 2016). It is generally considered that when continental basaltic magmas rise from their sources in the mantle, through the continental crust, they often experience contamination during ascent and/or residence in crustal magma chambers (Watson, 1982, Halama et al., 2004). The crust is understood to be a source of incompatible elements and a density filter in continental mafic magmatism (Lightfoot et al., 1991), although Halama et al. (2004) indicated that there is still significant debate on whether the trace element and isotopic characteristics of intracontinental basalts are mantle-derived or due to crustal contamination. The crust also acts as a site of extensive partial crystallisation of primitive melts (O'Hara and Herzberg, 2002). Crustal contamination has been shown to be important in the petrogenesis of flood basalts. However, it is possible that a mantle sourced magma enriched in incompatible trace elements may not experience much crustal input of similar elements (Halama et al., 2004), as observed in some Proterozoic dyke swarms and flood basalts (Molzahn et al., 1996).

The significance of crustal contamination can be assessed through correlations between indices of fractionation and the other chemical and/or isotope data of the rocks being studied

(Tang et al., 2012 and the references therein). In this study, for both dyke types, variation plots of MgO (as an index of fractionation) versus LILEs (Ba, Rb, Sr and K) and HFSEs (Ti, P, Zr, Y, Ce, Hf, Sm and Nd) are generated and analysed accordingly. The continental crust is largely felsic and any contamination of mafic magma is unlikely to alter the concentration of MgO, but will raise the concentration of most LILEs and HFSEs, which, because of their incompatibility, are more concentrated in these parts of the Earth. Uncontaminated mafic rocks will display more or less linear trends between MgO and the incompatible elements on variation plots, but display scatter if there is significant contamination. A combination of compatible and incompatible trace elements and their ratios, as well as isotope data, are also applied for this purpose (e.g. Rollinson 1993).

5.6.2 Fractional crystallisation

The features observed in the results of the plots of different combinations of elements (section 4.4.2) indicate specific information in fractional crystallisation processes. The observed decrease in MgO plus $FeO_{(T)}$ concentrations with the increase in SiO_2 indicates the crystallisation fractionation of olivine (Zi et al., 2008), whilst the negative correlation between SiO_2 and CaO/Al_2O_3 suggests the clinopyroxene crystallisation fractionation. The decrease of compatible elements, Cr and Ni, with the decrease in Mg# (magma evolution) is indicative of the fractionation crystallisation of olivine and clinopyroxene (Zi et al., 2008). The positive linear correlation between TiO_2 and P_2O_5 content indicates simultaneous fractionation from least differentiated mafic magma composition, with higher TiO_2-P_2O_5 content, to a more differentiated mafic magma that has lower TiO_2-P_2O_5 concentrations (Karmalkar et al., 2016). The wide ranges of Mg#, MgO, Ni and Cr indicate significant crystallisation fractionation either in magma chambers or during ascent (Zi et al., 2008; Srivastava et al., 2014). The low Mg# (29.7 – 58.0), Ni (80–720 ppm) and Cr (150– 1400 ppm) are suggestive of evolved magmas that underwent fractional crystallization olivine and pyroxene (Cheng et al., 2015).

5.6.3 Magma source

An important integral part of any petrogetic studies of basaltic rocks is the evaluation of the source of the magma from which the rocks being studied crystallised, and in almost all cases, the source of the magma is the mantle (Takahashi, 1986; Pearce and Parkinson 1993; Turner and Hawkesworth, 1995; Phinney and Halls, 2001, Pertermann and Hirschmann, 2003a; Tatsumi and Suzuki, 2009; Srivastava et al., 2014; Sreenivasulu et al., 2014; Sayit et al., 2016; Murphy et al., 2019). Basaltic magmas posses inherent critical information about their mantle source chemical compositions, and continental basaltic magmas in particular, posses a record of critical information regarding the chemical composition of the sub-continental mantle and regional tectonic evolution (Wager and Brown, 1968; Thompson et al., 1984; de Paulo, 1988;

Deyhle et al., 2001; Caro and Bourdon, 2010; Tang et al., 2012; Kerr, 2015). Continental basalts have several possible distinct mantle sources which include: 1) subcontinental lithospheric mantle (SCLM); 2) plume-related OIB (oceanic island basalt)-type mantle sources; and 3) depleted MORB (middle oceanic ridge basalt)-type asthenospheric mantle (Thompson et al., 1984; Garfunkel, 2008; Tang et al., 2012) (see Figure 5.1). Causes of continental magmatism are considered to include: a) decompressional melting as a result of lithospheric mantle detachment and upwelling of the asthenospheric mantle; b) lithosphere extension induced by continental rifting and breakup; c) high temperature melting of mantle owing to elevated mantle temperature by deep-seated mantle plume head impinging on the lithosphere; and d) the roll-back and/or foundering of flat-subducted oceanic plateaus or aseismic ridges (Tang et al., 2012 and references therein; Li et al., 2014).

Anorogenic continental basaltic alkalic magmatic suites from diverse localities are isotopically indistinguishable from OIB (Thompson et al., 1984). Thompson et al. (1984) indicated that, all continental anorogenic magmatism (distant from subduction zones in space and time) seems to be related ultimately to the OIB-source mantle reservoir, which therefore must extend beneath the lithospheric roots of continents (figure 5.1). The minor sodic-alkalic magmatism of continents is effectively identical in composition to OIB, Thompson et al. (1984) observed. Some continental flood basalts are similar to OIB but the majority contain minor contamination (rarely more than 15%) from fusible sialic rocks. Thompson et al. (1984) were of the opinion that continental flood basalts, range in silica saturation from quartz tholeiite to basanite and that most of the largest provinces are almost exclusively tholeiitic. From their studies, Thompson et al., (1984) observed that most of their samples on continental flood basalts indicated modification from primary mantle-derived magma and that, these may have equilibrated within or at the base of the continental crust before extrusion.

Subduction-related magmas are generally considered MORB-OIB (generated within converting mantle wedges behind subduction zones) with complexities introduced by added components brought into the system through subduction (Thompson et al., 1984; Stern, 2002; Manning, 2004; Savov et al., 2007; Carlson et al., 2018). Zhao et al. (2013) suggested that the subduction of oceanic crust is an important mechanism for exchanging mass and energy between the mantle and the crust and that the recycling of the oceanic crust into the asthenospheric mantle is accepted as the basic mechanism for mantle heterogeneity. Zhao et al. (2013) further stated that the subduction of oceanic crust and subsequent crust-mantle interaction produce the mantle source of arc volcanics at convergent plate margins. In this process, subduction-zone fluids have played a substantial role in transferring typical slab-derived signatures from oceanic basalt and seafloor sediment to the mantle wedge (Yang et

al., 2012; Zhao et al., 2013). In their view, these mantle-derived liquids are subduction-related before continental collisions and then change to OIB, several million years after subduction ceases.

According to Thompson et al. (1984), only a small proportion of subducted sediments re-appears in products of island arc and Cordillera magmatism and that the much larger portion of sediment fractions enter the ultrapotassic magmatism that occurs far behind some subcontinental subduction zones. They suggested that the remaining subducted terrigenous sediments, which are sialic fractions, rich in incompatible HFS and LIL elements, finally pass into the OIB-mantle source reservoir, effectively enriching it by addition. Accordingly, the subduction of increasingly large quantities of terrigenous sediments during the final stages of ocean closure leads to the large subducted sialic fractions which re-emerge in the ultrapotassic mafic magmas that characteristically appear immediately after a continental collision (Thompson et al., 1984). Thompson et al. (1984) were of the view that, the heat that leads to the production of batholithic intermediate and acid magmas in deep crustal levels may come directly or indirectly from mantle derived ultra mafic to mafic magmas.

5.6.4 Partial melting

The marked difference between calc-alkalic and tholeiitic magmas is the distinction in their major element contents and this has been suggested to be a product of both conditions of melting and variability in the composition of the sources of the two magma types (Takahashi & Kushiro, 1983; Takahashi, 1986; Kinzler & Grove, 1992; Gaetani & Grove, 1998; Grove et al., 2003; Munker et al., 2004; Carlson et al., 2018). Tholeiitic primary magmas are produced by the partial melting of dry peridotites (Jaques and Green, 1980; Fuji and Scarfe, 1985; Kinzler and Grove, 1992; Carlson et al., 2018). Calc-alkalic primary magmas, on the hand, show evidence of melting of peridotites with high water contents (Carlson et al, 2018 and references therein). The high water concentrations, and distinctive trace element signatures that often include enrichment in fluid-mobile elements and depletion in high-field-strength (HFSE) trace elements, of primary calc-alkalic magmas, are often attributed to the melting of sources that experienced some degree of metasomatism by fluids/melts released from subducting oceanic plates (Carlson et al, 2018 and references therein). A distinction in major element concentrations and the different degrees of enrichment or depletion in incompatible trace elements are quite evident in the studied dyke samples of the northeastern part of the Irumide Fold Belt, Northeastern Zambia.

The clear difference in compatible element concentrations and Mg# as well as the marked difference in the concentrations of fluid mobile elements in the two types of dykes are

suggestive of different degrees of partial melting of mantle peridotites and sources of magma. The trace element data of the incompatible elements exhibited by the tholeiitic dykes, showing enrichment in HFSE, suggest both low degree and shallow depths of melting, with magma generated within the spinel peridotite stability field (e.g. Carlson et al., 2018).

The large difference in LILE/HFSE ratios between the tholeiitic and calc-alkalic dykes may reflect the difference in the abundances of these elements in the source regions rather than the degree of melting or processes of melting of compositionally similar sources (Carlson et al., 2018). Therefore, the pattern observed from comparing the enrichment of LILE elements of the two types of dykes of the northeastern part of the Irumide Fold Belt, northeastern Zambia, is likely to represent both the pattern and degree of incompatible element compositional difference between their sources.

5.7 Magmatic mineral potential

5.7.1 Critical factors required for magmatic mineralisation

The most important factors that govern Cu-Ni magmatic sulphide mineralisation include: a) temperature (> 1600^{o}C); b) viscosity; c) volatile content; and d) mode of emplacement of the magma (Lesher and Groves, 1986; Arndt et al., 2005; Zhou et al., 2008; Godel et al., 2011, Barnes et al., 2016). The magma interacts with its wall rocks, losing heat, forming a hybrid or contaminated magma, and commonly incorporating crustal sulphur, processes that result in the generation or segregation of an immiscible sulphide melt. Ore formation, on the other hand, is directly linked to the incorporation of sulphur-rich country rocks and indirectly through contamination by felsic crust. There are mechanisms required to enhance reaction between sulphides and sufficient amount of magma to concentrate chalcophile elements to an economic level. Among them is magma dynamics and physical traps to concentrate magmatic sulphides in a restricted locality where their abundance is sufficient to constitute an ore (e.g. Barnes et al., 2016).

Barnes et al. (2016) reported that magma sources are generally held to be sub-lithospheric and derived from deep seated mantle plumes. According to Barnes et al. (2016), available evidence indicates that most mineral provinces are commonly associated with magmas that are higher in MgO, and hence hotter, than typical ambient mantle melting products such as MORBs. Consequently, where multiple magma suites are found within the same province, Ni–Cu–PGE ores are characteristically associated with the suite formed by the highest degree of partial melting, which are higher in MgO and low Ti (Zhou et al., 2008; Godel et al., 2011, Barnes et al., 2016). Barnes et al. (2016) noted that in most cases, including komatiites, host rocks are predominantly cumulates: rocks formed by accumulation of liquidus crystallisation

products. In this regard, the composition of cumulates differs significantly from the composition of the parent magma itself, having higher MgO and lower contents of incompatible elements.

5.7.2 Mineralisation potential - Factors observed on the mafic dykes of northeastern part of the Irumide Fold Belt of northeastern Zambia

Source of sulphur

From the observed chemical characteristics, the studied samples of the calc-alkalic mafic dykes of the Study area clearly indicate crustal contamination during the processes that led to their emplacement (section 4.4.1). Crustal contamination is considered to be a primary source of sulphur required for sulphide mineralisation (Lesher and Groves, 1986; Keays and Lightfoot, 2010). There is also a possibility that the parent magma was drawn from a contaminated mantle melt. Crustal contamination of the calc-alkalic mafic dykes of the Study area is deduced, from the chemical signature (section 4.4.1), to have taken place at the source, mantle wedge. It is not evident that there was enough crustal contamination to supply enough sulphur for sulphur saturation that would allow sulphide mineralisation. There is also no evidence of residence chambers for more crustal rock assimilation. The tholeiitic mafic dykes of the Study area, do not show a clear indication of crustal contamination during the processes that led to their emplacement. The chemical characteristics exhibited by the samples under study, eliminate clear suggestions of crustal contamination involvement during the magmatism of the tholeiitic dykes (section 4.4.1). The tholeiitic dykes, thus, are less likely to have had enough sulphur to reach sulphur saturation.

Tectonic setting

The northeastern part of the Irumide Fold Belt in northeastern Zambia is located in tectonic setting of continental subduction environment (see section 4.3.2). Thakurta et al. (2008), stated that magmatic Cu-Ni-PGE sulphide mineralisation associated with mafic to ultramafic igneous rocks is rare in convergent plate settings, but Barnes et al. (2016) pointed out that this picture is too restrictive, and does not account for the tectonic settings of many of the world's major camps and deposits, described by others as unlikely to form sulphide deposits although there are a few exceptions.

Geometries and sizes of intrusions

The geometries of the dykes being studied which may have a bearing on sulphide mineralisation are not established. The known morphologies of the dykes are limited to their spatial extent as observed on the surface. There are no traps that have been identified in the present study or reported in the previous studies, which are required for magma residence that would allow for sulphur saturation. Traps allow for prolonged time of interaction between

the magma and the wall rock, leading to hybridisation of the resultant melt that may have significant concentrations of sulphur from crustal rocks. The sizes of the intrusions are large enough for magmatic sulphide mineralisation (see section 4.5.1).

Magma partial melting

The partial melting temperatures of the different types pf magma that led to the emplacement of the mafic dykes are obtained from the evaluation of the geochemical data using PRIMELT3 MEGA.XLSM (see section 4.4.4). PRIMELT3 MEGA.XLSM computations clearly show a separation in the evaluated melting temperatures of the two types pf dykes with calc-alkalic dykes averaging 1450^{o}C and the tholeiitic dykes averaging 1160^{o}C. Four of the five tholeiitic dykes samples do not show results on the degree of partial melting in batch melting computations, only one sample gave a result. It can be speculated that the degree of melting of the tholeiitic rock samples that cannot be estimated by the formulary, may be quite low and this may also be suggested by the low calculated MgO %. In fact, the only sample, CH-WHR-12, whose degree of melting is estimated by the formulary, has a calculated MgO value of 19% in batch melting, compared to the average of about 6% for the other four samples. It may then, be concluded that the tholeiitic magma was generated from partial melting of a low degree at about 1160^{o}C giving rise to a melt rich in the incompatible elements, HFSE, and lower in Mg. The calc-alkalic rocks, on the other hand, are generated from partial melting at about 1450^{o}C, with about 25% degree of melting that led to higher concentration of Mg in the melt.

The mafic rocks of the Study area have very similar geochemical signatures in each dyke type, tholeiitic and calc-alkalic. Each dyke type shows low to moderate chemical variations. They also exhibit almost parallel ME and REE patterns on chondrite normalised spider diagrams (see Figures 4.43. 4.44, 4.48 and 4.49). These features point to co-genetic relationships of the magma for each dyke type. The trends displayed by HFSE when plotted against MgO (see Figures 4.41 and 4.46) also are suggestive of the rocks, especially the tholeiitics, to have been derived from a single magma batch (Srivastava et al., 2014).

6 CONCLUSIONS AND RECOMMENDATIONS

6.1 Conclusions

6.1.1 Petrology

From the study of the thin sections and photomicrographs, it has been concluded that the dykes studied are gabbroic in composition and exhibit differences in composition, textures, alteration and microstructures. They are composed mainly of plagioclase, clinopyroxene, hornblende with subordinate olivine, quartz, sericite, epidote and opaque phase minerals. The dyke rocks occur mainly in coarse and medium grained varieties as only two of the twelve samples examined, are fine grained. Relect igneous textures indicate that plagioclase is preferentially Subhedral in some thin sections, with grain boundaries between plagioclase and clinopyroxene usually being cuspate.

High temperatures deformation is minimal, but deformation is predominantly brittle in some samples. Plagioclase is more cracked than clinopyroxene. Late cracks in plagioclase and a few pyroxenes are filled with sericite, chlorite and lesser amphibole in some samples. Cracks appear to be crystallographic ally controlled in many plagioclase grains.

Alteration in most of the dyke samples was observed to primarily occur along cracks and was observed in plagioclase grains and perimeter of mafic phase groups in thin section. Only minor alteration occurs within a cluster of mafic minerals, and that which exists is usually confined to a crack or vein originating in the plagioclase. Alteration of olivine is predominantly serpentinisation, primarily localized along fractures. Alteration minerals may account for about 15% of the rock volumes. Patches of fibrous amphibole mimic pyroxene cleavage, are usually pale and cloudy. Some patches suggest alteration after recrystallisation and some of these patches are of serpentine pseudomorph orthopyroxenes. Kinking of some of fibrous material indicates some deformation after alteration. Alteration of olivine is considered to be essentially static, but other minerals recrystallised with substantial reduction in grain size. Most likely, alteration was exclusively high temperature. Blue-green hornblende and may be chlorite probably indicate greenschist facies.

Alteration of plagioclase is also considered to be reasonably static and postdates deformation that destroyed most of original mineral's textures, creating subgranoblastic texture and mechanical twins to be observed in some samples. There was little apparent deformation after alteration. In general, most of the alteration zones are composed of quartz and sericite. Sericite occurs as fine grains as well as widespread dustings. Opaques may rim grains and

their alteration are also present in cracks within the mineral mafic mineral grains. There is a weak foliation defined by the shape of the relict mineral grains.

From the petrographic studies, it is speculated that the examined rocks were most likely originally coarse grained and consisted of mainly pyroxenes, olivine and plagioclase. Plagioclase, apparently slightly elongate, is very clearly the dominant mineral. Much of the plagioclase texture is still discernible occurring in euhedral to subhedral mineral crystals, especially near pyroxene. Deformation of plagioclase is predominantly cataclastic with no evidence of recrystallisation in certain samples. Internal slip in plagioclase and olivine also occurred. Relict igneous textures suggest that the mafic phase may have been interstitial to plagioclase and that the interstitial textures of mafic minerals is fairly well preserved. Pyroxene is considerably more resistance to deformation than plagioclase, preserving some primary texture. Most prominent, however, are the zones of fine grained, recrystallised or broken mineral grains and large rounded pyroxenes.

6.1.2 Geochemistry and geodynamic evolution

1. The geochemical data obtained from the calc-alkalic dykes of the dyke swarm of the northeastern part of the Irumide Fold Belt, northeastern Zambia, have confirmed that this part of the Fold Belt was deposited in a back arc rift basin of a continental subduction environment. The back arc depositional environmental was reported, among others, by Daly (1986); De Waele et al. (2006). The movement of the continental mass was in the NW towards the Bangweulu Block, which was the fore land. The subducted mantle slab was sinking to the SE and the volcanic arc developed on the continent part of the continental margin, with a NE-SW trend. The sinking subducted oceanic slab dragged the SCLM above it, behind the subduction magmatic arc, creating an extensional regime that led to the initial back arc Irumide rifting. The rift basin was parallel to the volcanic-plutonic arc.

2. The rifting induced decompression in the upper mantle above the mantle wedge that led to partial melting of the metasomatised mantle, enriched in LILEs from dehydration processes of the terrigenous sediments and water dragged down with the oceanic crust slab at the mantle wedge.

3. The dyke swarm of the northeastern part of the Irumide Fold Belt, northeastern Zambia, occurs as a suite of a mixture of sub-alkaline tholeiitic and calc-alkalic individual dykes of variable dimensions.

4. Geochronological K-Ar dating has revealed that the calc-alkalic mafic dykes were intruded in at least three pulses, 1522 ± 90 Ma, 1067 ± 55 Ma and 608 ± 35 Ma. The first phase of intrusion may be the group that was described by Page (1973) as the syn-rifting and deposition

of the rift sediments in the Irumide Rift Basin. The second pulse that is given by the results happened during the breaking up of the Rodinia Super Continent, around 1000 Ma, that led to global mafic magmatism. The third recorded pulse obtained from the age dating results happened during the Neoproterozoic Pan African Orogeny, which was responsible for the rifting and deposition of the Katanga Supergroup.

5. The tholeiitic dykes' intrusion post date the Karoo sedimentation and these are related to the Batoka Basalts, which are the youngest in the Karroo stratigraphy. The age of the tholeiitic dykes are obtained from Page (1973), who described some of the dykes he mapped to be cutting through the Karroo sediments. The tholeiitic dykes are as a result of continental rifting and are not cogenetic to the calc-alkalic dykes.

6. Coexistence of calc-alkalic and tholeiitic mafic dykes is common in mature subduction environments (e.g. Yatsumi et al., 2009). Hence the occurrence of the two types of mafic dyke rocks together in the Study area indicates that this part of the Irumide Fold Belt is a mature subduction continental arc environment.

7. The tholeiitic source magma had a shallower source above the contaminated metasomatised deeper parts of the mantle affected by dehydration of depositional waters and felsic sediments. The lower temperature and lower degree of melting meant that the magma would be rich in the incompatible HFSE and lower Mg content. This is observed in the analytical results, element variation plots and spider diagrams of both REE and ME. Compared to the calc-alkalic magma, the tholeiitic magma has higher HFSE:LILE ratio.

8. From the several chemical classification models applied above, it is evident that the studied calc-alkalic mafic dyke rocks were emplaced in a continental arc subduction environment. The continental margin signature is strongly suggested by the model of Pearce (2014) on which all the samples plotted in the overlap between continental and island arcs. The volcanic arc signature is affirmed on the models by Wood (1980), Figures 5.32 and 5.33, where in both cases the samples cluster in the VAB CAB field. Arc magmas are enriched in Th and depleted in Ta and Nb and consequently plot nearer to the Hf-Th and Zr-Th joining lines, far removed from WPB and MORB. The depletion in Nb is also exhibited in figure 5.35. The magma affinity of MORB/N-MORB is strongly positioned on models by Pearce and Cann (1973), Meschede (1986) and Shervais (1982), Figures 5.34, 5.35 and 5.36 respectively.

9. As regards tholeiitic dykes, the element combinations used and the plots which have resulted from the combinations indicate strongly that this type of dykes of the Study area were emplaced in a WPB "Within Plate Basalt" tectonic environment. This feature is especially exhibited on the diagram plots based on the models of: Pearce and Cann (1973) (Figure 5.28);

Meschede (1986) (Figure 5.27); Shervais (1982) (Figure 5.26); and Mullen (1983) (Figure 5.22). The rocks further exhibit MORB to E-MORB affinity with an oceanic signature (Figure 5.21). The basalts are not related to any orogenic activity (Figure 5.24), and may be related to rift tectonics.

10. Samples of calc-alkalic mafic dykes display similar chemical characteristics and trends on variation diagrams and spider diagrams, all carrying chemical signatures of continental arc – subduction environment.

11. The several diagrams which have been applied in the evaluation of crystallisation fractionation of both types of rocks have revealed fractional crystallisation affected the magma of both types of rocks studied, tholeiitics and calc-alkalics. This is further supported by the wide ranges of Mg#, MgO, Ni and Cr in both rock types, which indicate significant crystallisation fractionation either in magma chambers or during ascent (Zi et al., 2008; Srivastava et al., 2014). The low Mg# (29.7-58.0), Ni (80-720 ppm) and Cr (150-1400 ppm) are suggestive of evolved magmas that underwent fractional crystallisation (Cheng et al., 2015). Since no two samples came from the same dyke, it can also be concluded that all the mafic dykes in the Study area experienced various levels of fractional crystallisation of olivine, clinopyroxenes, plagioclase feldspars, hornblende and titanomagnetite. These are the main minerals identified in petrographic studies of the same samples.

12. Both types of dykes show enrichment of the source magma by addition. The enrichment must principally have come from the terrigenous felsic sediments rich in HFSE and LILE which were subducted at the mantle wedge.

13. The tectonic and geodynamic evolution of the studied mafic dykes of the northeastern part of the Irumide Fold Belt of northeastern Zambia are summarised in the illustration model below (Figure 6.1).

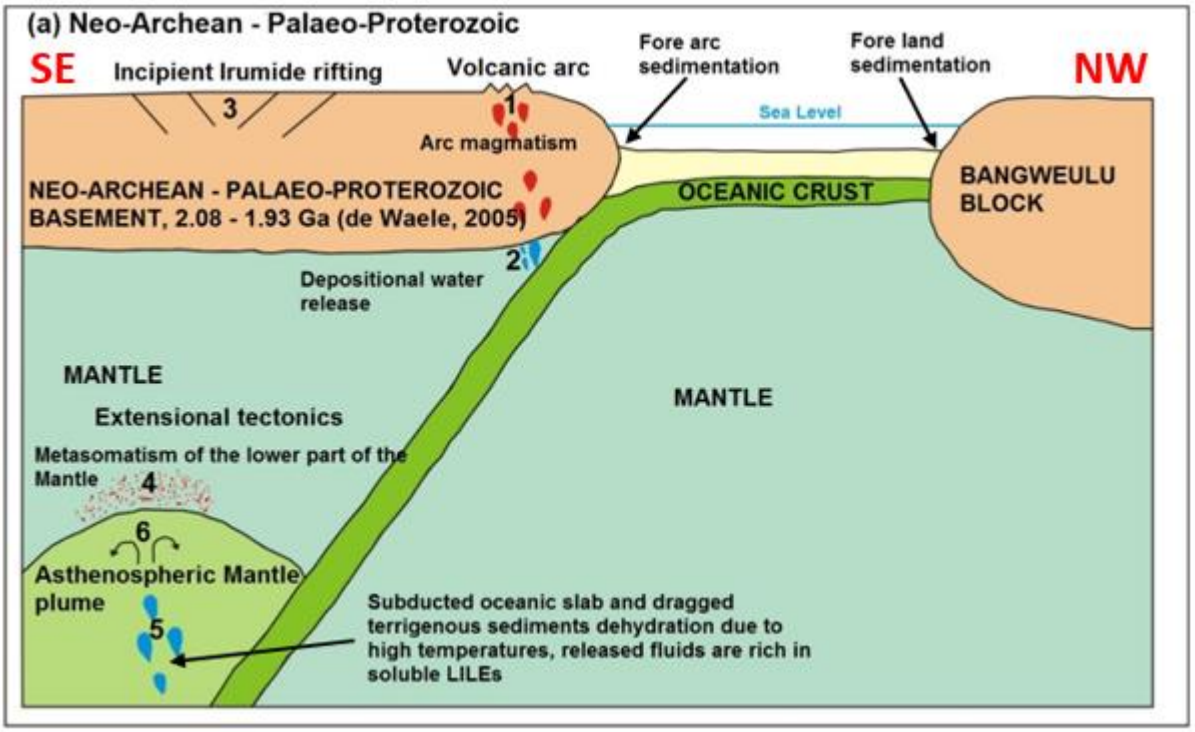
(a) Neo-Archean - Palaeo-Proterozoic
SE
Incipient Irumide rifting
Volcanic arc
Fore arc sedimentation
Fore land sedimentation
NW
Sea Level
3
1
Arc magmatism
NEO-ARCHEAN - PALAEO-PROTEROZOIC BASEMENT, 2.08 - 1.93 Ga (de Waele, 2005)
OCEANIC CRUST
BANGWEULU BLOCK
2
Depositional water release
MANTLE
Extensional tectonics
MANTLE
Metasomatism of the lower part of the Mantle
4
6
Asthenospheric Mantle plume
5
Subducted oceanic slab and dragged terrigenous sediments dehydration due to high temperatures, released fluids are rich in soluble LILEs

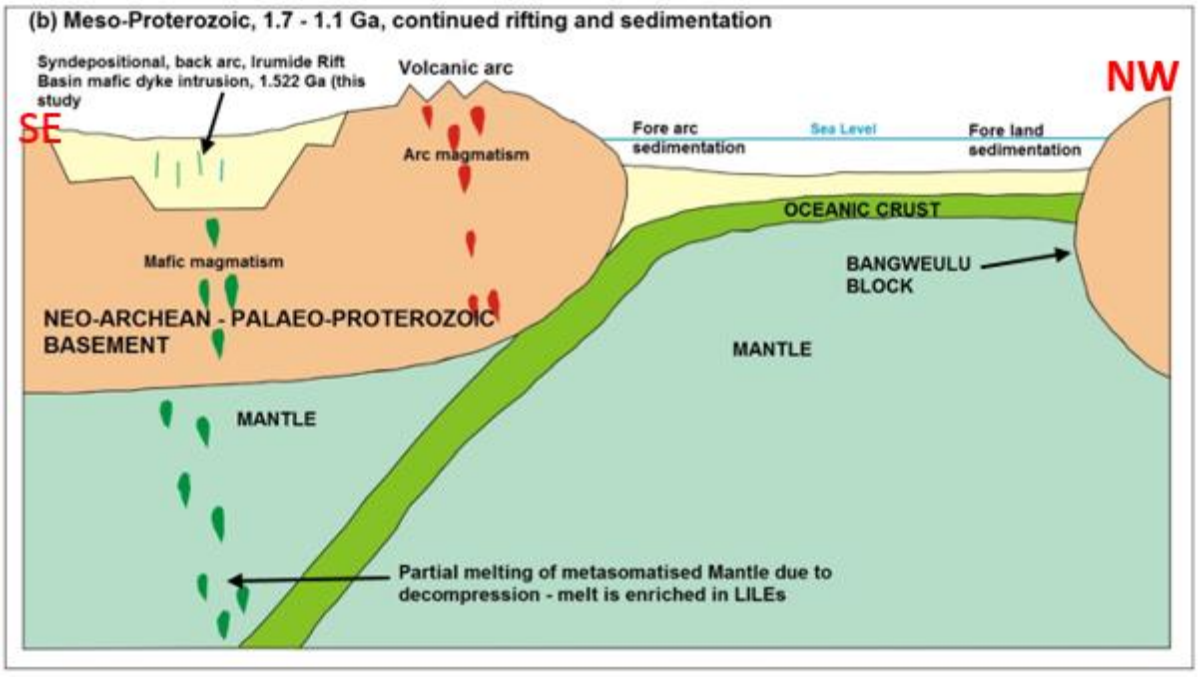
(b) Meso-Proterozoic, 1.7 - 1.1 Ga, continued rifting and sedimentation
Syndepositional, back arc, Irumide Rift Basin mafic dyke intrusion, 1.522 Ga (this study
Volcanic arc
NW
SE
Fore arc sedimentation
Sea Level
Fore land sedimentation
Arc magmatism
OCEANIC CRUST
Mafic magmatism
BANGWEULU BLOCK
NEO-ARCHEAN - PALAEO-PROTEROZOIC BASEMENT
MANTLE
MANTLE
Partial melting of metasomatised Mantle due to decompression - melt is enriched in LILEs

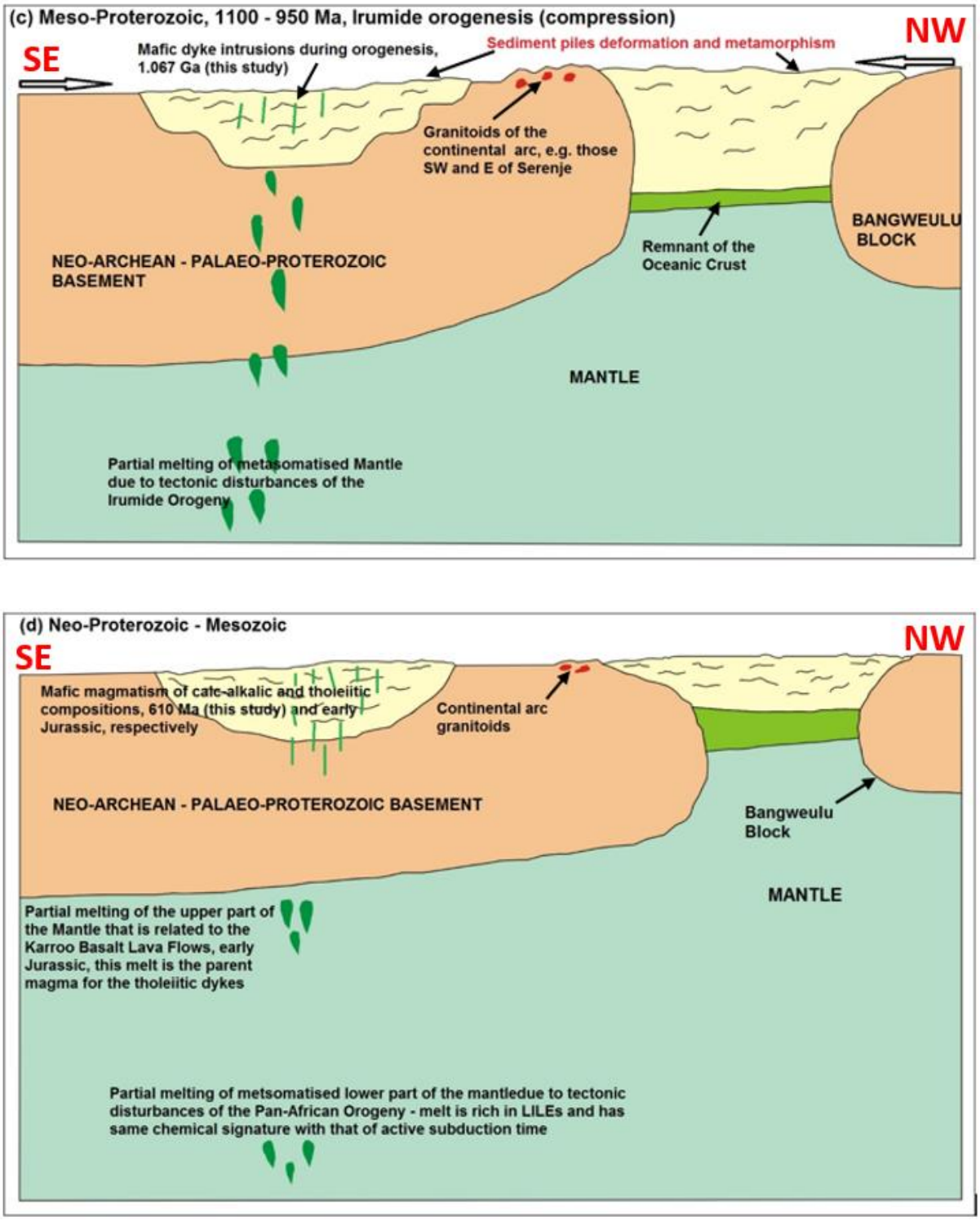

Figure 6.1: The tectonic and geodynamic model illustrating the development of the Irumide Rift Basin and emplacement of the mafic dykes:

(a) Neo-Archean – Palaeo-Proterozoic; 1. Continental magmatic arc rocks established at 1.87 and 1.82 Ga (De Waele and Fritzsimmons, 2007); 2. Release of depositional water from terrigenous sediments dragged down by the subducted Oceanic slab, hot fluids lower the melting temperature in the Continental Crust as it moves up, triggering partial melting resulting

in Continental Arc magmatism; 3. Incipient back arc Irumide rifting induced by Asthenospheric Mantle plume which caused extensional tectonics – started probably about the same time with the oldest magmatic arc rocks emplacement at about 1.85 Ga; 4. Metasomatism of the lower parts of the Mantle by hot fluids derived from dehydration of the Oceanic slab and dragged terrigenous sediments due to very high temperatures. The fluids are rich in soluble LILEs and poor in insoluble HFSEs; 5. Oceanic slab and terrigenous sediments dehydration; and 6. Development of Asthenospheric Mantle plume due to interaction of the Mantle material with dehydration fluids;

(b) Meso-Proterozoic period of extensional tectonics and sediment filling of the Irumide back arc rift basin followed by rifting induced decompression resulting in partial melting of the metasomatised Mantle thereby generating magma of the calc-alkalic dykes intruded at about 1.522 Ga (this study);

(c) Meso-Proterozoic, 1100 – 950 Ma, Irumide deformation and metamorphism (Daly, 2007), partial melting of the metasomatised lower parts of the Mantle due to tectonic disturbances (instigated by the break-up of the Pangea Super continent) leading to the intrusion of calc-alkalic mafic dykes dated at about 1.067 Ga (this study); and

(d) Neo-Proterozoic – Mesozoic, partial melting of metasomatised lower parts of the Mantle due to tectonic disturbances of the Pan African Orogeny, giving rise to intrusion of calc-alkalic dykes dated at about 610 Ma (this study), whilst the upper parts of the Mantle, below the Irumide Rift fill, experienced partial melting associated with the Karoo continental flood basalts resulting in the intrusion of the tholeiitic dykes in early Jurassic (Mesozoic) (tholeiitic dykes have not been dated in this study).

6.1.3 Potential for CU-Ni-PGE magmatic mineralisation

From the analysis of all the available information that would be critical to sulphide mineralisation and possible occurrence of deposits of Cu-Ni in the mafic dykes of the study area, it is concluded that the dykes exhibit no parameters that would have allowed such mineralisation to take place. This conclusion is drawn from the following direct and deduced information:

1. There is no evidence of enough interaction between the magmas of the two types of dykes and crustal rocks that would have allowed introduction of sulphur from the wall into the magma which would lead to sulphur saturation;

2. The melting partial melting temperatures for both calc-alkalic magma and tholeiitic magma given by the PRIMELT3 MEGA.XLSM, averaging about 1400^{o}C and 1140^{o}C respectively, are too low for the melting temperatures of >1600^{o}C of magmas that lead to Cu-Ni (Lesher and Groves, 1986; Arndt et al., 2005; Zhou et al., 2008; Godel et al., 2011, Barnes et al., 2016);

3. The negative linear correlation observed in the plots of Cu versus MgO indicates that there was no crystallisation fractionation of Cu during the ascent of the magma. Crystallisation fractionation of Cu in a mafic melt can only take place if there is enough sulphur saturation that would lead to Cu to fractionate into sulphides;

4. Similarly, the positive correlation display in the plots of Cu versus Zr, two incompatible elements, is an indication that there was general enrichment in the two elements as the magmas evolved. This trend would not have been there if there was fractionation crystallisation of Cu into sulphides;

5. There are no traps which have been reported in the previous studies or observed in the present study that would have allowed for enough residence time of the magma to interact with wall rock, a process that would have led to possible sulphur saturation; and

6. The previous works, which include the mineral exploration activities over a part of the Study area, have not reported any magmatic sulphide mineralisation.

6.2 Recommendations

Whilst the study has revealed, from age dating perfomed on three samples, that the mafic dykes of the northeastern part of the Irumide Fold Belt of northeastern Zambia were emplaced in at least three pulses, it is still recommended that high precision and more expensive age dating methods such as U-Pb Zr are carried out. The dating that was applied in the current research, based on whole rock K-Ar, is considered to be of low precision and this was dictated by budget constraints. Since none of the dated samples came from tholeiitic dykes, it is recommended that in the high precision dating exercise, these dykes should be deliberately targeted now that some of their localities have been established. At the time of sampling for this study, there was no prior knowledge of the differences in the types of dykes between calc-alkalic and tholeiitic and their spatial distribution.

REFERENCES

Abdurrachman, M., Widiyantoro, S., Pradi, B. and Ismail, T., 2018. Geochemistry and structure of Krakatoa Volcano in Sunda Strait, Indonesia. Geosciences 2018, vol. 8(4), pp. 1-10.

Activation Laboratories Limited, 2020. Analytical report on 3 samples for K-Ar age dating; and Sm-Nd and Rb-Sr isotopes from northeastern Zambia, for the University of Zambia (Unpublished).

Aldanmaz, E., Yalınız, M. K., Guctekin, A., and Goncuoglu, M. C., 2008. Geochemical characteristics of mafic lavas from the Tethyan ophiolites in western Turkey: implications for heterogeneous source contribution during variable stages of ocean crust generation, Geological Magazine, 145, pp. 37-54.

Allegre, C. J., Minster, J F., 1978. Quantitative models of trace element behaviour in magmatic processes. Earth Planet, Sci. Lett. 38, pp. 1 -25.

Allgre, C. J., Treuil, M., Minster, J. F., Minster, B., Albarede, F. 1977. Systematic use of trace elements in igneous processes. Part 1: Fractional crystallisation processes in volcanic suites. Contrib. Mineral. Petrol. 62, pp. 57-75.

ArC Minerals Limited, 2020. Large Scale Copper Exploration in Zambia. Unpublished Company Report.

Arndt N. T., and Goldstein, S. L., 1987. Use and abuse of crustal information ages. Geology, v. 15, pp 893-895.

Arndt. N.T., Goldstein, S.L. 1989. An open boundary between lower continental crust and the mantle: its role in crust formation and crustal recycling. Tecronophysics 161, pp. 201-212.

Arndt N. T., Lesher C. M., Czamanske G. K., 2005. Mantle-derived magmas and magmatic Ni-Cu-(PGE) deposits. Economic Geology, 100th Anniversary volume, pp. 5-24.

Arndt, N. T., Czamanske, G. K., Walker, R.J., Chauvel, C., and V. A. Fedorenko, 2003. Geochemistry and origin of the intrusive hosts of the Noril'sk-Talnakh Cu-Ni-PGE deposits. Economic Geology 98, pp. 495-515.

Atherton, M. P. and Ghani, A. A. (2002). Slab Breakoff: A Model for Caledonian, Late Granite Syncollisional Magmatism in the Orthotectonic (Metamorphic) Zone of Scotland and Donegal, Ireland. Lithos, 62, pp. 65-85.

Banno, S., Matsui, Y., 1973. On the formulation of partition coefficients for trace elements distribution between minerals and magma. Chem. Geol. 11, pp. 1-15.

Baker, M. C. W., 1974. Volcano spacing, fractures, and thickness of the lithosphere - discussion. Earth and Planetary Science Letters 23, pp. 161-163.

Barnes, S. J., Cruden, A. R., Arndt, N. T. and Saumur, B. M., 2016. The mineral system approach applied to magmatic Ni‐Cu‐PGE sulphide deposits. Ore Geology Reviews 76 (2016), pp. 296‐316.

Barnes, S. J. and Lightfoot, P. C., 2005. Formation of magmatic nickel sulphide ore deposits and processes affecting their copper and platinum group element contents: Economic Geology 100th Anniversary Volume, pp. 179–214.

Baumgartner, R. J., Fiorentini, M. L., Baratoux, D., Micklethwaite, S., Sener, A. K., Lorand, J. P. and McCuaig, T. C., 2015. Magmatic controls on the genesis of Ni‐Cu±(PGE) sulphide mineralisation on Mars. Ore Geology Reviews 65 (2015), pp. 400‐412.

Bekker, A., Barley, M. E., Fiorentini, M. L., Rouxel, O. J., Rumble, D. and Beresford, S. W., 2009. Atmospheric sulphur in Archean komatiite-hosted nickel deposits. Science 326, pp. 1086-1089.

Bennett, V. C., Nutman, A. P., and McCulloch, M. T., 1993. Nd isotopic evidence for transient, highly depleted mantle reservoirs in the early history of the Earth. Earth and Planetary Sci. Lett. 119 (1993), pp. 299-317.

Cabanis, B. and Lecolle, M., 1989. The La/10-Y/15-Nb/8 Diagram: A Tool for Discrimination Volcanic Series and Evidencing Continental Crust Magmatic Mixtures and/or Contamination. Compte Rendus de l'Academie des Sciences, Seris II, Mécanique, Physique, Chimie, Sciences de l'univers, Sciences de la Terre 309(20), pp. 2023–2029.

Cai, K., Sun, M., Yuan, C., Zhao, G., Xiao, W., Long, X., Wu, F., 2010. Geochronological and geochemical study of mafic dykes from the northwest Chinese Altai: Implications for petrogenesis and tectonic evolution. Gondwana Research 18, pp. 638–652.

Cameron, B. I., Walker, J. A., Carr, M. J., Patino, L. C., Matias, O. and Feigenson, M. D., 2003. Flux versus decompression melting at stratovolcanoes in southeastern Guatemala. Journal of Volcanology and Geothermal Research 119, pp. 21-50.

Campbell, I. H. and Naldrett, A. J., 1979. The influence of silicate:sulphide ratios on the geochemistry of magmatic sulphides. Econ. Geol. 74, pp. 1503-1506.

Carlson, R. W., Grove, T. L., and Donnelly-Nolan, J. M., 2018. Origin of primitive tholeiitic and calc-alkaline basalts at Newberry Volcano, Oregon. Geochemistry, Geophysics, Geosystems, 19, pp. 1360-1377.

Caro, G. and Bourdon, B., 2010. Non-chondritic Sm/Nd ratio in the terrestrial planets: Consequences for the geochemical evolution of the mantle-crust system. Geochimica et Cosmochimica Acta, Volume 74, Issue 11, pp. 3333-3349.

Castillo, P. R. and NewHalls, C. G., 2004. Geochemical Constraints on Possible Subduction Components in Lavas of Mayon and Taal Volcanoes, Southern Luzon, Philippines. Journal of Petrology, vol. 45, No. 6, pp. 1089–1108.

Chai, G. and Naldrett, A. J., 1992. Characteristics of Ni-Cu-PGE mineralization and genesis of the Jinchuan Deposit, Northwest China. Economic Geology 87, 1475-1495.

Chiarenzelli, J., Lupulescu, M., Cousens, B., Thern, E., Coffin, L., and Regan, S., 2010. Enriched Grenvillian lithospheric mantle as a consequence of longlived subduction beneath Laurentia. Geological Society of America, Geology February 2010, v. 38; no. 2, pp. 151–154.

Chen, J. Y., Yang, J. H. and Ji, W. Q., 2017. Ages and petrogenesis of Jurassic and Cretaceous rocks in the Matsu Island: implications of the lower crust modification beneath southeast China. Journal of Asian Earth Sciences 150 (2017), pp. 14-24.

Cheng, Z., Zhang, Z., Hou, T., Santosh, M., Zhang, D. and Ke, S., 2015. Petrogenesis of nephelinites from the Tarim Large Igneous Province, NW China: Implications for mantle source characteristics and plume–lithosphere interaction. Lithos 220-223 (2015), pp. 164-178.

Christie, A. B. and Barker, R. G., 2016. Regional mineral resource assessments to promote recognition of mineral resource potential. In: Christie, A. B. (editor). Mineral deposits of New Zealand: exploration and research. Carlton (AU): Australasian Institute of Mining and Metallurgy (Monograph series; 31), pp. 45-,52.

Ciborowski T. J. R., 2013. The Geochemistry and Petrogenesis of the Early Proterozoic Matachewan Large Igneous Province, unpublished PhD Thesis, Cardiff University, 461 pp.

Cimen, O., 2016. Petrology and geochronology of the igneous rocks from Cangaldag Metamorphic Complex and the Cangaldag Pluton (Central Pontides, Turkey). Unpublished PhD thesis, Middle East Technical University, 282 pp.

Clemens, J. D., Blecher, R. W. and Kisters, A. F. M., 2010. Heerenveen Batholith, Barberton Mountain Land, South Africa: Mesoarchean, Potassic, Felsic Magmas formed by melting of an ancient subduction complex. Journal of Petrology, April 8, 2010, pp. 1-22.

Cline, J. S., Hofstra, A. H., Muntean, J. L., Tosdal, R. M., and Hickey, K. A., 2005. Carlin-type gold deposits in Nevada: Critical geologic characteristics and viable models: Economic Geology 100th Anniversary Volume, pp. 451-484.

Costa, A., Melnik, O. and Sparks, R. S. J., 2007. Controls of conduit geometry and wallrock elasticity on lava dome eruptions. Earth and Planetary Science Letters 260, pp. 137-151.

Cox, K.G., Bell, J.D., Pankhurst, R.J., 1979. The Interpretation of Igneous Rocks. George Allen & Unwin, London, 445 pp.

Cucciniello, C., Choudhary, A.K., Zanetti, A., Sheth, H. C., Vichare, S. and Pereira, R., 2013. Mineralogy, geochemistry and petrogenesis of the Khopoli mafic intrusion, Deccan Traps, India. Mineralogy and Petrology (2013), vol. 108, pp. 333-351.

Cullers, R. L and Graf, J. L., 1984. Rare earth elements in igneous rocks of the continental crust: predominantly basic and ultrabasic rocks. In: Henderson, P. (editor), Rare Earth Element Geochemistry. Elsevier, Amsterdam, pp. 237-274.

Daly, M. C., 2007. Geometry and evolution of the Mesoproterozoic Irumide Belt of Zambia. Geological Society, London, Special Publications, 272, pp. 223-230.

Daly, M.C., 1988. Crustal shear zones in central Africa. A kinematic approach to Proterozoic tectonics. Episodes 11, pp. 5-11.

Daly, M. C., 1986. The tectonic and thermal evolution of the Irumide belt, Zambia. PhD Thesis, University of Leeds, Leeds, 326 pp.

Davies, G. F., 2011. Solid Earth Dynamical geochemistry of the mantle. Solid Earth, 2, 2011, pp. 159–189.

Davis, J., and Hawkesworth, C. J., 1993. The petrogenesis of 30-20 Ma basic and intermediate volcanics from the Mogollon-Datil volcanic field, New Mexico, USA, Contrib. Mineral. Petrol., 115, pp. 165-183.

Defant, M. J., and Drummond, M. S., 1990. Derivation of some modem arc magmas by melting of young subducted lithosphere, Nature, 347, pp. 662-665.

De Paolo, D. J. and Wasserburg, G. J., 1976. Nd variations and petrogenetic models. Geophysical Research Letters vol.3, No. 5, pp 249-252.

De Paolo, D. J., 1988. Neodymium Isotope Geochemistry. An Introduction. Springer-Verlag, Berlin, 187 pp.

De Waele, B. and Mapani, B. S. E., 2002. Geology and correlation of the central Irumide belt. Journal of African Earth Sciences, 35(3): pp. 385-397.

De Waele, B., Kampunzu, A. B., Mapani, B. S. E., and Tembo, F., 2006. The Mesoproterozoic Irumide belt of Zambia: Journal of African Earth Sciences, v. 46, pp. 36-70.

De Waele, B. and Fitzsimons, I. C. W., 2007. The nature and timing of Palaeoproterozoic sedimentation at the southeastern margin of the Congo Craton; zircon U–Pb geochronology of plutonic, volcanic and clastic units in northern Zambia. Precambrian Research 159 (2007), pp. 95-116.

Deyhle, A., Kopf, A. and Eisenhauer, A., 2001. Boron systematics of authigenic carbonates: A new approach to identify fluid processes in accretionary prisms, Earth Planet. Sci. Lett., 187, pp. 191-205.

Drake, M. J., Weill, D. F., 1975. Partition of Sr, Ba, Ca, Y, Eu^{+2}, Eu^{+3} and other REE between plagioclase, feldspar and magmatic liquid: an experimental study. Geochim. Cosmochim. Acta 39, pp 689-712.

Drury, S. A., 1993. Image Interpretation in Geology. Chapman and Halls, London, 283 pp.

Eden , J. G. and Binda P. C., 1972 Scope of stratigraphic and sedimentologic analysis of the Katanga Sequence, Zambia. Geologie en Mijnbouw, 51, pp. 321-328.

Ewart, A., Schon, R.W. and Chappell, B.W., 1992. The Cretaceous volcanic plutonic province of the central Queensland (Australia) coast - A rift-related 'calc-alkaline' province, in The

Second Hutton Symposium: The Origin of Granites and Related Rocks , edited by P.E. Brown and B .W. Chappell, Special Paper, Geological Society of America, 272, pp. 327-346.

Fahrig, W.F., Christie, K.W., Chown, E.H., Janes, D., Machado, N., 1986. The tectonic significance of some basic dyke swarms in the Canadian Superior-Province with special reference to the geochemistry and paleomagnetism of the Mistassini Swarm, Quebec, Canada. Canadian Journal of Earth Sciences 23 (2), pp. 238–253.

Faure, G., 1986. Principles of Isotope Geology, 2nd Edition, John Wiley and Sons, New York, 589 pp.

Ferns, M. L., Brookes, H. C., Evans, J. G. and Cummings, M .L., 1993. Geologic map of the Vale 30 x 60 minute quadrangle, Malheur County, Oregon and Owyhee County, Idaho, scale1 :100,000, Oreg. Dep. of Geol. Miner. Ind., GMS-77.

Floyd, P. A. and Winchester, J. A., 1978. Identification and discrimination of altered and metamorphosed volcanic rocks using immobile elements. Chem. Geol. 21, pp. 291-306.

Frimmel, H. E., Groves, D. I., Kirk, J., Ruiz, J., Chesley, J., and Minter, W. E. L., 2005. The formation and preservation of the Witwatersrand goldfields, the world's largest gold province: Economic Geology 100th Anniversary Volume, pp. 769-788.

Fujinawa, A., 1988. Tholeiitic and calc-alkaline magma series at Adatara Volcano, Northeast Japan: 1. Geochemical constraints on their origin. Lithos 22, pp. 135-158.

Fujinawa, A., 1990. Tholeiitic and calc-alkaline magma series at Adatara Volcano, Northeast Japan: 2. Mineralogy and phase relations. Lithos 24, pp. 217-236.

Fyfe, W. S. and Kerrich, R., 1976. Geochemical prospecting: extensive versus intensive factors. Journal of Geochemical Exploration. 6(1), pp. 177-192.

Gaetani, G. A., and Grove, T. L.,1998. The influence of water on melting of mantle peridotite. Contributions to Mineralogy and Petrology, 131(4), pp. 323-346.

Gaetani, G. A.; Grove, T. L. and Bryan, W. B., 1993. The influence of water on the petrogenesis of subduction-related igneous rocks. Nature 365, pp. 332-334.

Galer, S. J. G., Goldstein, S. L. and O'Nions, R. K., 1989. Limits on chemical and convective isolation in the Earth's interior. Chemical Geology, 75, pp. 257-290.

Garfunkel, Z., 2008. Formation of continental flood volcanism - the perspective of setting of melting. Lithos 100, pp. 49-65.

Gill, R. 2011., Igneous Rocks and Processes: A Practical Guide. Wiley, 438 pp.

Godel, B., Seat, Z., Maier, W. D. and Barnes, S. -J., 2011. The Nebo‑Babel Ni‑Cu‑PGE sulphide deposit (West Musgrave Block, Australia); Pt. 2, constraints on parental magma and processes, with implications for mineral exploration. Econ. Geol. Bull. Soc. Econ. Geol. 106, 557 pp.

Gonzalez-Guzman, R., 2016. NORRRM: A free software to calculate the CIPW Norm. Open Journal of Geology, 2016, pp. 30-38.

Green, D. H., 1973. Experimental mantle studies on a model upper mantle composition under water-saturated and water-unsaturated conditions. Earth Planet Science Letters 19, pp. 37-53.

Gresham, J. J. and Loftus-Hills, G. D., 1981. The geology of the Kambalda nickel field, Western Australia: Economic Geology, v. 76, pp. 1373-1416.

Gribble, R. F., Stern, R. J., Newman, S., Bloomer, S. H., and O'Hearn, T., 1998. Chemical and isotopic composition of lavas from the northern Mariana Trough; implications for magma genesis in back-arc basins. Journal of Petrology, 39, pp. 125-154.

Grove, T. L., Elkins-Tanton, L. T., Parman, S. W., Chatterjee, N., Meuntener, O. and Gaetani, G. A., 2003. Fractional crystallization and mantle melting controls on calc-alkaline differentiation trends. Contributions to Mineralogy and Petrology, 145(5), 515-533.

Guilbert, J. M. and Park, G. F. Jr., 1986. The Geology of Ore Deposits. W. H. Freeman and Company, New York. 985pp.

Hagemann, S. G., Lisitsin, V. and Huston, D. L., 2016. Mineral system analysis: Quo vadis. Ore Geology Reviews 76, pp. 504-522.

Halama, R., Marks, M., Brugmann, G., Siebel, W., Wenzel, T., and Mark, G., 2004. Crustal contamination of mafic magmas: evidence from a petrological, geochemical and Sr-Nd-Os-O isotopic study of the Proterozoic Isortoq dike swarm, South Greenland. Lithos 74 (2004), pp. 199-232.

Halls, H. C., 1982. The importance and potential of mafic dyke swarms in studies of geodynamic processes. Geological Society of Canada 9, pp.145-154.

Hanson, G. N., 1980. Rare Earth Elements in petrogenetic studies of igneous systems. Ann. Rev. Earth Planet. Sci. 1980, 8, pp. 371-406.

Hanson, G. N., Langmuir, C. H. 1978. Modelling of major elements in mantle melt systems using trace element approaches. Geocim, Cosmochim. Acta, 42, pp. 725-741.

Harangi, S., Downes, H., Thirlwall, M. and Ling, K. G. M. E., 2007. Geochemistry, Petrogenesis and Geodynamic Relationships of Miocene Calc-alkaline Volcanic Rocks in the Western Carpathian Arc, Eastern Central Europe. Journal of Petrology Volume 48 Number 12, pp. 2261-2287.

Herzberg, C. and Asimow, P. D., 2015. PRIMELT3 MEGA.XLSM software for primary magma calculation: Peridotite primary magma MgO contents from the liquidus to the solidus. Geochem., Geophys., Geosyst., 16, pp. 563-578.

Hirschmann, M. M., GhiorsoM, S., Wasylenki, L. E., Asimow, P. D. and Stolper, E. M., 1998. Calculation of peridotite partial melting from thermodynamic models of minerals and melts. I Method and composition to experiments, Journal of Petrology 39, pp. 1,091-1,115.

Hitzman, M. W., 2000. Source basins for sediment-hosted stratiform Cu deposits: implications for the structure of the Zambian Copperbelt. Journal of African Earth Sciences, 30, pp. 855-863.

Hoefs, J., 1987. Stable Isotope Geochemistry, 3rd Edition, Springer-Verlag, Berlin, 241 pp.

Hofmann, A. W., 1997. Mantle Geochemistry: the message from ocean volcanism. Nature, vol. 385, pp. 219-229.

Holm, P. E., 1985. The geochemical fingerprints of different tectonornagmatic environments using hygromagmatophile element abundances of tholeiitic basalts and basaltic andesites – Chem. Geol., 51, pp. 303-323.

Hooper, P. R.; Bailey, D. G. and McCarley Holdeft, G. A., 1995. Tertiary calc-alkaline magmatism associated with lithospheric extension in the Pacific Northwest. Journal of Geophysical Research, vol 100, No. B7, pp. 10,303-10,319.

Ikemoto, A., and Iwamori, H., 2014. Numerical modelling of trace element transportation in subduction zones: Implications for geofluid processes. Earth Planets Space, 66(1), pp. 1-10.

Irvine, T. N. and Baragar, W. R. A., 1971. A guide to the chemical classification of the common volcanic rocks. Canadian Journal of Earth Science, 8, pp. 523-548.

Jochum, K. P. and Verma, S. P., 1996. Extreme enrichment of Sb, Tl, and other trace elements in altered MORB. Chem. Geol. 130, pp. 289-299.

Johnson, S. P, Rivers, T. and De Waele, B., 2005. A review of the Mesoproterozoic to early Palaeozoic magmatic and tectonothermal history of south–central Africa: implications for Rodinia and Gondwana. Journal of the Geological Society, London, Vol. 162, 2005, pp. 433-450.

Lewington, G. L. D., 1987. The Geology of the Chikwa and Lake Beu Area; Explanation of Degree Sheets 1132, SE Quarter and 1133, part of SW Quarter. Geological Survey of Zambia Report No. 62, 25 pp.

Kakar, M. I., Kerr, A. C., Mahmood, K.,. Collins, A. S., Khan, M. and McDonald, I., 2014. Supra-subduction zone tectonic setting of the Muslim Bagh Ophiolite, northwestern Pakistan: Insights from geochemistry and petrology. Lithos 202–203 (2014), pp. 190–206.

Karmalkar, N. R., Duraiswami, R. A., Jonnalagadda, M. K., Griffin, W. L., Gregoire, M., Benoit, M. and Delpech, G., 2016. Magma Types and Source Characterization of the Early Deccan Magmatism, Kutch Region, NW India: Insights from Geochemistry of Igneous Intrusions. Special Publication of the Geological Society of India No. 6, 2016, pp. 193-208.

Kamona, A. F., 1993. The carbonate-hosted Kabwe Pb-Zn Deposit, Central Zambia. PhD Thesis, Mitteilungen zur Mineralogie und Lagerstattenlehre, 207 pp.

Kay, R. W., Gast, P. W. 1973. The rare earth content and origin of alkali-rich basalts. J. Geol. 81, pp. 653-682.

Kelemen, P. B., Shimizu, N. and Dunn, T., 1993. Relative depletion of niobium in some arc magmas and the continental crust: partitioning of K, Nb, La and Ce during melt/rock reaction in the upper mantle. Earth and Planetary Science Letters 120 (1993), pp. 111-134.

Kelemen, P. B., Hanghoj, K. and Greene, A. R., 2004. One view of the geochemistry of subduction-related magmatic arcs, with an emphasis on primitive andesite and lower crust. In: Treatise on Geochemistry, Vol. 3: The Crust, ed. R. L. Rudnick, pp. 593–659.

Kerr, A. and Fryer, B.J., 1993. Neodymium isotopic evidence for crust-mantle interaction in the genesis of 'A-type' granitoid suites in Labrador, Canada. Chemical Geology, Volume 103, pp. 39-60.

Kerr, A., 2015. Sm-Nd isotopic geochemistry of rare earth element mineralisation and associated peralkaline granites of the Strange Lake Intrusion, Labrador. Current Research (2015), Newfoundland and Labrador Department of Natural Resources; Geological Survey, 15-1, pp. 63-83.

Kinzler, R. J. and Grove, T. L., 1992. Primary magmas of mid-ocean ridge basalts: 1. Experiments and methods. Journal of Geophysical Research, 97(B5), pp. 6885-6906.

Kumar, A. and Ahmad, T., 2007. Geochemistry of mafic dykes in part of Chotanagpur gneissic complex: Petrogenetic and tectonic implications. Geochemical Journal, Vol. 41, pp. 173-186.

Kuno, H., 1966. Lateral variation of basalt magma type across continental margins and island arcs. Bull. Volcanol. 29, pp. 195-222.

Lamberg, P., 2005. From Genetic Concepts to Practice-Lithogeochemical Identification of Ni-Cu Mineralised Intrusions and Localisation of the Ore. Geological Survey of Finland, Bulletin 402, 264 pp.

Lassen, B., Bridgwater, D., Bernsrein, S., Rosing, M., 2004. Assimilation and highpressure fractional crystallisation (AFC) recorded by Paleo-proterozoic mafic dykes, Southeast Greenland. Lithos 72, pp. 1-18.

Lesher, C. M. and Keays, R. R., 2002, Komatiite-Associated Ni-Cu-(PGE) Deposits: Mineralogy, Geochemistry, and Genesis, in L. J. Cabri (Editor), The Geology, Geochemistry, Mineralogy, and Mineral Beneficiation of the Platinum-Group Elements, Canadian Institute of Mining, Metallurgy and Petroleum, Special Volume54, pp. 579-617.

Lesher, C. M. and Groves, D. I., 1986. Controls on the formation of komatiite associated nickel-copper sulphide deposits. In: Genkin, A. D., Naldrett, A. J., Ridge, J. D., Sillitoe, R. H. and

Vokes, F. M. (eds), Geology and metallogeny of copper deposits. Springer-Verlag, Heidelberg, pp. 43-62.

Lightfoot, P. C., 2007. Advances in Ni-Cu-PGE Sulphide Deposit Models and Implications for Exploration Technologies: in “Proceedings of exploration 7: Fifth Decennial International Conference on Mineral Exploration”, edited by B. Milkereit, 2007, pp. 629-646.

Lightfoot, P. C. and Zotov, I. A., 2007, Ni-Cu-PGE sulphide deposits at Noril'sk, Russia. Short Course; International Polar Year; Prospectors and Developers Association of Canada. Short Course Notes.

Lightfoot, P. C., Sutcliffe, R. H. and Doherty, W., 1991. Crustal contamination identified in Keweenawan Osler Group Tholeiites, Ontario: a trace element perspective. Journal of Geology 99, pp. 739-760.

Li, J., Wang, X. C., Ren, Z. Y., Xu, J. F., He. B, Xu, Y. G., 2014. Chemical heterogeneity of the Emeishan mantle plume: Evidence from highly siderophile element abundances in picrites. Journal of Asian Earth Sciences 79 (2014), pp. 191-205.

Li, X. H., Su, L., Chung, S. L., Li, Z. X., Liu, Y., Song, B. and Liu, D. Y., 2005. Formation of the Jinchuan ultramafic intrusion and the world's third largest Ni–Cu sulphide deposit: associated with the ~825 Ma south China mantle plume? Geochemistry Geophysics Geosystems 6, pp. 1-16.

Lugmair, G. W. and Scheinin, N. B., 1975. Sm-Nd Systematics of the Stannem Meteorite. Meteorics 10, 1975, pp 447-448.

Maier, W. D., Barnes, S. –J., Chinyepi, G., Barton, J. M., Eglington, B. and Setshedi, I., 2008. The composition of magmatic Ni-Cu-(PGE) sulphide deposits in the Tati and Selebi Phikwe belts of eastern Botswana. Mineral Deposita 43, pp. 37-60.

Manning, C. E., 2004. The chemistry of subduction-zone fluids, Earth Planet. Sci. Lett., 223, pp. 1-16.

Mapani, B. S. E., Rivers, T., Tembo, F., and Katongo, C., 2001. Terrane Mapping in the eastern Irumide and Mozambique belts: Implications for the assembly and dispersal of Rodinia, *in* McCourt, S., editor, IGCP 418 4th fieldmeeting: Durban, South Africa, University of Durban-Westville, pp. 10-11.

Master, S., C., Rainaud, Armstrong, A., Phillips, D. and Robb, L. J., 2005. Provenance Ages of the Neoproterozoic Katanga Supergroup (Central African Copperbelt), with Implications for Basin Evolution. Journal of African Earth Sciences, Vol. 42, pp. 41-60.

Maurice, C., David, J., O’Neil J. and Francis, D., 2009. Age and tectonic implications of Paleoproterozoic mafic dyke swarms for the origin of 2.2 Ga enriched lithosphere beneath the Ungava Peninsula, Canada. Precambrian Research 174, pp. 163-180.

McCuaig, T. C. and Hronsky, J. M. A., 2014. The Mineral System Concept: The Key to Exploration Targeting, Society of Economic Geologists, Inc. Special Publication 18, pp. 153-175.

McCuaig, T. C., Beresford, S. and Hronsky J., 2010. Translating the mineral systems approach into an effective exploration targeting system. Ore Geology Reviews. 38(3), pp. 128-138.

McNutt, M. K. and Fischer, K. M., 1987. The South Pacific superswell. In: B.H. Keating, P. Fryer, R. Batiza and G. W. Boehlert (eds.). Seamounts, Islands and Atolls. American Geophysical Union, Washington D.C., pp. 25-34.

Meschede, M., 1986. A method of discriminating between different types of mid-ocean ridge basalts and continental tholeiites with the Nb-Zr-Y diagram. Chemical Geology, 56, pp. 207-218.

Minister, J. and Jordan, T. H., 1978. Present-day plate motions. Journal of Geophysical Research, vol. 83, pp. 5331-5354.

Miyashiro, A., 1971. Processes and patterns of metamorphism in a plate tectonic framework. Geological Society of America, Abstracts with Programs 3, 648 pp.

Molzahn, M., Reisberg, L. and Worner, G., 1996. Os, Sr, Nd, Pb, O isotope and trace element data from the Ferrar flood basalts, Antarctica: evidence for an enriched subcontinental lithospheric source. Earth and Planetary Science Letters 144, pp. 529-546.

Morgan, W. J., 1972. Plate motions and deep mantle convection. Geological Society of America, Memoirs, vol. 132, pp. 7-22.

Mullen, E. D., 1983. $MnO/TiO_2/P_2O_5$ a minor element discriminate for basaltic rocks of oceanic environment and its implication for petrogenesis. Earth and Planetary Science Letters, 62, pp. 53-62.

Munker, C., Worner, G., Yogodzinski, G., and Churikova, T., 2004. Behavior of high elements in subduction zones: Constraints from Kamachatka-Aleutian arc lavas. Earth and Planetary Science Letters, 224(3-4), pp. 275-293.

Munteanu, M., Wilson, A. H., Costin, G., Yao, Y., Lum, J. E., Jiang, S. Y., Jourdan, F., Chunnett, G., and Cioac, M. E., 2017. The Mafic–Ultramafic Dykes in the Yanbian Terrane (Sichuan Province, SW China): Record of Magma Differentiation and Emplacement in the Emeishan Large Igneous Province. Journal of Petrology, 2017, vol. 58, No. 3, pp. 513-538.

Musiwa, S., 1996. Determining geological controls on the mineralisation in area west of Mumbwa, Central Zambia. Unpublished M Sc Thesis, ITC, Delft.

Musiwa, S. and Shanzambwa A. S., 2016. Unpublished Zawar Natural Resources Limited First Phase Exploration Report of tenement 20009-HQ-LPL, Northeastern Zambia.

Murphy, J. B., Nance, R. D., Gabbler, L. B., Martell, A., and Archbald, D. A., 2019. Age, Geochemistry and origin of the Ardara Appinite Plutons, Northwest Donegal, Ireland.

Geoscience Canada Vol. 46 (2019), pp 31- 48.Nagler, T. M. and Stille, P., 1993. Remarks on the mantle evolution models used for Nd model age calculation. Schweiz. Mineral. Petrogr. Mitt. 73, pp.375-381.

Naldrett, A. J., 2004, Magmatic Sulphide Deposits: Geology, Geochemistry and Exploration, Springer Verlag, Heidelberg, Berlin, 728 p.

O'Connor, E. A., 1976. Geology of the Lumezi River and Lundazi areas; Explanation of Degree Sheets 1232 NE Quarter and parts of 1233 NW and NE Quarters. Geological Survey of Zambia Report No.71, 29 pp.

O'hanley, D. S., 1996. Serpentinites. Records of Tectonic and Petrological History. Oxford Monographs on Geology and Geophysics Volume 34, Xiii, Oxford University Press, 277 pp.

O'Hara, M. J., Herzberg, C., 2002. Interpretation of trace element and isotope features of basalts: relevance of field relations, petrology, major element data, phase equilibria, and magma chamber modelling in basalt petrogenesis. Geochimica et Cosmochimica Acta 66, pp. 2167-2191.

Page, T. C., 1973. The Geology of the Chama Area; Explanation of Degree Sheet 1133, NW Quarter. Geological Survey of Zambia Report No.57, 25 pp.

Pearce, J. A., Peate, D. W., 1995. Tectonic implications of the composition of volcanic arc magmas. Annual Review of Earth and Planetary Sciences 23, pp. 251–285.

Pearce, J. A. and Parkinson, I. J., 1993. Trace element models for mantle melting: application to volcanic arc petrogenesis. In: Prichard, H. M., Alabaster, T., Harris, N. B. W. and Neary, C. R. (eds): Magmatic Processes and Plate Tectonics, Geological Society, London, Special Publications 76, pp. 373-403.

Pearce, J. A., 1983. Role of the subcontinental lithosphere in magma genesis at active continental margins. In: Hawkesworth, C. J., and Norry, M. J. (eds), Continental basalts and mantle xenoliths. Shiva, Nantwich, England, pp. 230-249.

Pearce, T. H., Gorman, B. E. and Birkett, T. C., 1975. The TiO_2-K_2O-P_2O_5 diagram a method of discriminating between oceanic and non-oceanic basalts, Earth and Planetary Sciences Letters, 24, pp. 419-426.

Pearce, J. A. and Cann, J. R., 1973. Tectonic setting of basic volcanic rocks determined using trace element analysis. Earth Planet Sci. Lett. 19: pp. 290-300.

Pertermann, M. and Hirschmann, M. M., 2003a. Partial melting experiments on a MORB-like pyroxenite between 2 and 3 GPa: constraints on the presence of pyroxenite in basalt source regions from the solidus location and melting rate. Journal of Geophysical Research 108(B2), pp. 2125-2137.

Petersson, A., Schersten, A., Bingen, B., Gerdes, A. and Whitehouse, M. J., 2015. Mesoproterozoic Continental growth: U-Pb-Hf-O zircon record in the Idenfjorden Terrane, Svenconorwegian Orogen. Precambrian Research 261, pp. 75-95.

Petersson, A., Bjarnborg, K., Gerdes, A. and Naeraa, T., 2017. Tracing Proterozoic arc mantle Hf isotope depletion of south Fennoscandia through coupled U-Pb and Lu-Hf isotopes. Lithos 284-285 (2017), pp. 122-131.

Petersson, A., Schersten, A. and Gerdes, A., 2017. Extensive reworking of Archaean crust within the Birimian terrane in Ghana as revealed by combined zircon U-Pb and Lu-Hf isotopes. Geoscience Frontiers xxx (2017), pp. 1-17.

Phinney, W. C. and Halls, H. C., 2001. Petrogenesis of the Early Proterozoic Matachewan Dyke Swarm, Canada,, and implications for magma emplacement and subsequent deformation. Canadian Journal of Earth Sciences, 38, pp 1541-1563.

Pirajno, F., Ernst, R. E., Borisenko, A. S., Fedoseev, G. and Naumov, E. A., 2009. Intraplate magmatism in Central Asia and China and associated metallogeny. Ore Geology Reviews 35 (2009), pp. 114–136.

Porada, H., 1989. Pan-African rifting and orogenesis in southern equatorial Africa and eastern Brazil. Precambrian Research 44, pp. 103-136.

Ringwood, A. E., 1975. Composition and Petrology of the Earth's Mantle, McGraw-Hill, 618 pp.

Roberts, D. 1990.Geochemistry of mafic dykes in the Corrovarre Nappe, Troms, North Norway. Nor. geol. unders. Bull. 419, pp. 45-53.

Roberts, M. P. and Clemens, J. D.1993.Origin of high potassium, calc-alkaline, I type granitoids. Geology, vol. 2, (1993), pp. 825-828.

Rudnick, R. L. and Gao, S., 2004. Composition of the Upper Crust. In: Treatise on Geochemistry, Vol. 3: The Crust, ed. R. L. Rudnick, pp. 1-64.

Salters, V. J. M., and Stracke, A., 2004. Composition of the depleted mantle, Geochem. Geophys. Geosyst., 5, 27p.

Savov, I. P., Ryan, J. G., D'Antonio, M., and Fryer, P., 2007. Shallow slab fluid release across and along the Mariana arc-basin system: Insights from geochemistry of serpentinized peridotites from the Mariana fore arc. J. Geophys. Res., 112 pp.

Sayit, K., Marroni, M., Goncuoglu, M.C., Pandolfi, L., Ellero, A., Ottria, G. and Frassi, C., 2016. Geological setting and geochemical signatures of the mafic rocks from the Intra-Pontide Suture Zone: implications for the geodynamic reconstruction of the Mesozoic Neotethys. International Journal of Earth Science, 105, pp. 39-64.

Schandl, E. S., and Gorton, M. P., 2002. Application of high field strength elements to discriminate tectonic settings in VMS environments. Economic Geology 97, pp. 629-642.

Severson, M., 2009. Field Trip 2: Cu-Ni-PGE mineralisation along the footwall contact of the Duluth Complex in Drill Core: Precambrian Research Centre Professional Workshop Series; Field, Petrographic and Mineralisation of Mafic Layered Intrusions.

Sheraton, J. W. and Sun, S. S., 1997. Mafic dyke swarms of the western Musgrave Block, central Australia: theirgeochemistry, origin, and relationships to the Giles Complex. Journal of Australian Geology &Geophysics. 16(5), pp. 621-636.

Shervais, J. W., 1982. Ti-V plots and the petrogenesis of modern and ophiolitic lavas. Earth and Planetary Science Letters, 59, pp. 101-118.

Sial, A. N., Oliveira, E. P. and Choudhuri, A., 1987. Mafic Dyke Swarms of Brazil; in Mafic Dyke Swarms; Editors: Halls, H. C. and Fahrig, W. F. Geological Association of Canada Special Paper 34, pp. 467- 481.

Sikamo, J., Mwanza, A. and Mweemba, C., 2016. Copper mining in Zambia - history and future. The Journal of Southern African Institute of Mining and Metallurgy, vol. 116, number 6, pp. 491-496.

Sillitoe, R. H., 2004. Musings on future exploration targets and strategies in the Andes: Society of Economic Geologists Special Publication 11, pp. 1–14.

Sreenivasulu, P., Padmasree, P., and Vijayakumar, K. S., 2014. Petrology, geochemistry and tectonic setting of mafic dyke swarms of Kadiri Schist Belt, Eastern Dharwar Craton, South India. International Journal of Basic and Applied Chemical Sciences, vol. 3, July-September, pp. 34 – 43.

Srivastava, R. K., Jayananda, M., Gautam, G. C. and Samal, A. K., 2014. Geochemical studies and petrogenesis of 2.21 – 2.22 Ga Kunigal mafic dyke swarm (trending N-S to NNW-SSE) from eastern Dharwar craton, India: implications for Paleo Proterozoic large igneous province and supercratonic superia. Miner Petrol (2014): 108, pp. 695 – 711.

Stern, C. R., and Kilian, R., 1996. Role of the subducted slab, mantle wedge and continental crust in the generation of adakites from the Andean Austral Volcanic Zone, Contrib. Mineral. Petrol., 123, pp. 263-281.

Streckeisen, A. L., 1976. Classification and Nomenclature of Igneous Rocks. N. Jahrb. Miner. Abh., 107, pp. 144-240.

Sun, S. S. and McDonough, W. F., 1989. Chemical and Isotopic Systematics of Oceanic Basalts: Implications for Mantle Composition and Processes. In: Saunders, A.D. and Norry M.J., Eds., Magmatism in the Ocean Basins, Vol. 42, Geological Society, London, Special Publications, pp. 313-345.

Sweeney, M. A. and Binda, P. L., 1989. The role of diagenesis in the formation of the Konkola Cu-Co orebody of the Zambian Copperbelt. Geological Association of Canada, Special Paper, 36, pp. 499-518.

Takahashi, E., 1986. Melting of dry peridotite KLB-1 up to 14 GPa: implications on the origin of peridotitic upper mantle. Journal of Geophysical Research 91(B9), pp. 9367-9382.

Takahashi, E. and Kushiro, I., 1983. Melting of a dry peridotite at high pressures and basalt magma genesis. American Mineralogist, 68, pp. 859-879.

Talusani, R. V. R., 2010. Bimodal tholeiitic and mildly alkalic basalts from Bhir area, central Deccan Volcanic Province, India: Geochemistry and petrogenesis. Journal of Volcanology and Geothermal Research 189 (2010), pp. 278–290.

Tang, G. J., Wang, Q., Wyman, D. A., Li, Z. X., Xu, Y. G. and Zhao, Z. H., 2012. Metasomatized lithosphere-asthenosphere interaction during slab roll-back: Evidence from Late Carboniferous gabbros in the Luotuogou area, Central Tianshan. Lithos 140-141, pp. 86‑102.

Tang, Z., 1991. The metallogenetic model of the Jinchuan platinum-bearing copper‑nickel sulphide deposit. International Symposium on Sulfide Deposits, Academic Papers on Special Subjects, Jinchang, Gansu, China, pp. 17-43.

Tanimoto, T. and Lay, T., 2000. Mantle dynamics and seismic tomography. PNAS, November 7, 2000, vol. 97 (23), pp. 12409-12410.

Tatsumi, Y. and Suzuki, T., 2009. Tholeiitic vs Calc-alkalic Differentiation and Evolution of Arc Crust: Constraints from Melting Experiments on a Basalt from the Izu Bonin Mariana Arc. Journal of Petrology, volume 50 Number 8, pp. 1575-1603.

Thompson, G. M., 1998. The Geochemistry and Petrogenesis of Rarotonga, an Ocean Island in the Soutb Pacific. Upublished PhD thesis for the Memorial University of Newfoundland, 338 pp.

Thompson, R. N ., Morrison, M . A., Hendry, G. L. and Parry, S. J., 1984. An assessment of the relative roles of crust and mantle in magma genesis: an elemental approach. Phil. Trans. R. Soc. Lond. A 310, pp. 549-590.

Turner, S. and Hawkesworth, C., 1995. The nature of the subcontinental mantle: constraints from the major-element compositions of continental flood basalts. Chemical Geology 120, pp. 295-314.

Unrug, R., 1988. Mineralization controls and source of metals in the Lufilian Fold Belt, Shaba (DRC), Zambia, and Angola. Economic Geology, 83, pp. 1247-1258.

Verma, S. P., 2001. Geochemical evidence for a lithospheric source for magmas from Acoculco caldera, Eastern Mexican Volcanic Belt. Int Geol. Rev 43, pp. 31-51.

Verma, S. P., Torres-Alvarado, I. S. and Sotelo-Rodriguez, Z. T., 2002. Standard igneous norm and volcanic rock classification system. Computers and Geosciences 28, pp. 711-715.

Wager, L. and Brown, G., 1968. Layered Igneous Rocks. Oliver and Boyd, Edinburgh, 588 pp.

Watson, E. B., 1982. Basalt contamination by continental crust: some experiments and models. Contributions to Mineralogy and Petrology 80, pp. 73-87.

White, R. S. and McKenzie, D., 1995. Mantle plumes and flood basalts. Journal of Geophysical Research: Solid Earth, vol. 100 (B9), pp. 17543-17585.

Wong, K., Sun, M., Zhao, G., Yuan, C. and Xiao, W., 2010. Geochemical and geochronological studies of the Alegedayi Ophiolitic Complex and its implication for the evolution of the Chinese Altai. Gondwana Research 18 (2010), pp. 438-454.

Wyborn, L. A. I., Heinrich, C. A. and Jaques, A. L., 1994. Australian Proterozoic mineral systems: essential ingredients and mappable criteria. In: Hallsenstein, C. P., editor. 1994 AusIMM Annual Conference: Australian mining looks north: the cHallsenges and choices; 1994 Aug 5-9; Darwin, Australia, pp. 109-115. (Australian Institute of Mining and Metallurgy publication series; 94).

Yang, Q. L., Zhao, Z. F. and Zheng, Y. F., 2012. Slab-mantle interaction in continental subduction channel: Geochemical evidence from Mesozoic gabbroic intrusives in southeastern North China. Lithos 155, pp. 442-460. Zambia Chamber of Mines, Media Statement, 9th September, 2020.

Zawar Natural Resources Limited, 2016. Unpublished Ground magnetics report of Musolomoka Prospect, Northeastern Zambia. Tenement 20009-HQ-LPL.

Zhang, Y., Yuan, C., Sun, M., Long, X., Wang, Y., Jiang, Y. and Lin, Z., 2017. Arc magmatism associated with steep subduction: Insights from trace element and Sr–Nd–Hf–B isotope systematics, J. Geophys. Res. Solid Earth, 122, pp. 1816-1834.

Zhang, Y., Dostal, J., Zhao, Z., Liu, C. and Guo, Z., 2011. Geochronology, geochemistry and petrogenesis of mafic and ultramafic rocks from Southern Beishan area, NW China: Implications for crust-mantle interaction. Gondwana Research 20 (2011), pp. 816-830.

Zhao, Z. F., Dai L. Q. and Zheng, Y. F., 2013. Postcollisional mafic igneous rocks record crust-mantle interaction during continental deep subduction. Scientific Reports vol. 3: 3413, pp. 1-6.

Zhao, J. H. and Zhou, M. F., 2007. Geochemistry of Neoproterozoic mafic intrusions in the Anzhihua District (sichuan province, SW China): implications for subduction-related metasomatism in the upper mantle. Precambria Research 152, pp. 27–47.

Zhou, M. F., Arndt, N. T., Malpas, J., Wang, C.Y. and Kennedy, A.K., 2008. Two magma series and associated ore deposit types in the Permian Emeishan large igneous province, SW China. Lithos 103, pp. 352-368.

Zi, J., Fan, W., Wang, Y., Peng, T. and Guo, F., 2008. Geochemistry and petrogenesis of the Permian mafic dykes in the Panxi region, SW China. Gondwana Research 14 (2008), pp. 368-382.